



**HAL**  
open science

**Study of micro- and nanoplastic pollution in the environment : sampling in the atmosphere, development of a labelled environmentally relevant model, interaction with living organisms**

Nadiia Yakovenko

► **To cite this version:**

Nadiia Yakovenko. Study of micro- and nanoplastic pollution in the environment : sampling in the atmosphere, development of a labelled environmentally relevant model, interaction with living organisms. Organic chemistry. Université Paul Sabatier - Toulouse III, 2021. English. NNT : 2021TOU30232 . tel-04213521

**HAL Id: tel-04213521**

**<https://theses.hal.science/tel-04213521>**

Submitted on 21 Sep 2023

**HAL** is a multi-disciplinary open access archive for the deposit and dissemination of scientific research documents, whether they are published or not. The documents may come from teaching and research institutions in France or abroad, or from public or private research centers.

L'archive ouverte pluridisciplinaire **HAL**, est destinée au dépôt et à la diffusion de documents scientifiques de niveau recherche, publiés ou non, émanant des établissements d'enseignement et de recherche français ou étrangers, des laboratoires publics ou privés.



# THÈSE

En vue de l'obtention du  
**DOCTORAT DE L'UNIVERSITÉ DE TOULOUSE**  
Délivré par l'Université Toulouse 3 - Paul Sabatier

---

Présentée et soutenue par  
**Nadiia YAKOVENKO**

Le 9 décembre 2021

**Etude de la pollution environnementale par les micro- et nanoplastiques : échantillonnage atmosphérique, développement d'un modèle de plastique marqué, interaction avec des organismes vivants**

---

Ecole doctorale : **SDM - SCIENCES DE LA MATIERE - Toulouse**

Spécialité : **Chimie Moléculaire**

Unité de recherche :

**IMRCP - Laboratoire des Interactions Moléculaires et Réactivité Chimique et Photochimique**

Thèse dirigée par

**Alexandra TER HALLE et Fabrice COLLIN**

Jury

M. Bruno GRASSL, Rapporteur

M. Jean-François GHIGLIONE, Rapporteur

Mme Messika REVEL, Examinatrice

Mme Alexandra TER HALLE, Directrice de thèse

M. Fabrice COLLIN, Co-directeur de thèse

Mme Christel CAUSSERAND, Présidente



## Acknowledgements

In the first place, I would like to thank the Director of the IMRCP laboratory, Christophe Mingotaud, for welcoming me to the laboratory, supporting and advising me throughout my stay there. My sincere thanks to Eric Benoist, director of the SDM doctoral school, for his invaluable help and support with any difficulties a young PhD student may have.

I must also thank Alexandra ter Halle and Emile Perez for approving my candidacy for this PhD position. Especially, I would like to thank my supervisor Alexandra who gave me the opportunity to work on very original and creative projects. I really appreciated the freedom and encouragement to try new techniques that Alexandra gave me. This allowed me to acquire a diverse knowledge and skill in many advanced analytical techniques such as Py-GC-MS/MS,  $\mu$ -FTIR, NTA, DLS, etc.

I am extremely grateful to my supervisor Fabrice Collin for his understanding, support, and constant help throughout my thesis. Especially for all the revisions, feedback, and help during the writing of my manuscript. Thank you for listening, for respecting my opinion, for supporting my choices, for your patience, humanity, and kindness.

I would like to extend my deepest gratitude to the members of my jury Jean-François Ghiglione, Bruno Grassl, Christel Causserand and Messika Revel, who gave me the honour of accepting to read my manuscript and judge my work. I highly appreciate the discussion that were opened. You made it a rich and exciting scientific exchange, and it was a great pleasure for me.

My research would have been impossible without the aid and support of Christophe Coudret and Clément Roux. I'm afraid there are no words to express all my gratitude to both of you. If someone had told me 3 years ago that I will be working with UCNPs, 2-photon microscopy, deep tissue imaging, etc., I would never have believed it. You made the impossible, possible! Your encouragement and motivation kept me in the darkest moment of my PhD! Thank you for always taking the time to explain, teach, and help to find a solution to any problem. Christophe, you are one of the most brilliant person I have ever met. I will miss those long and always interesting conversations about science, life, and whatever! Clément, I am sure, if we were in a chocolate eating contest, we would win for sure. I will miss your jokes about my Ukrainian accent and poker face.

I would like to express my warmest thanks to Cécile Formosa-Dague and Irem Demir-Yilmaz thanks to whom I had the opportunity to experience amazing AFM technique. I highly appreciate all your help, interest, and motivation that you expressed during our collaboration. It was a pleasure to work with you and learn things from you. My dear Irem, thank you for your support and the beautiful moments and joy you have brought into my life. You were not only the best partner for the lab experiments, but also became a very close person to me.

I would also like to thank Magali Albignac for her assistance with experiments and protocols development of particles grinding, filtration, etc. I am very grateful to Charles-Louis Serpentini for always helping to find or fix things. Especially, I would like to thank Lucie Perquis for always providing us with petit matériel and with a good mood and a smile. Lucie you are a beautiful ray of sunshine in the IMRCP laboratory. I would also like to acknowledge the help of Anne-Françoise Mingotaud with NTA analysis.

I would like to recognize the assistance of various technical platforms, without whom all this work would not have been possible:

- Antonio Peixoto and Eve Pitot (IPBS) for amazing two-photon microscopy experience and the beautiful images we got together.
- Robert Mauricot (CEMES) for trying to help with deep tissue imaging.
- Pierre Roblin for impressive SAXS measurements.
- Bruno Payré, Dominique Goudounèche, and Isabelle Fourquaux (CMEAB) who were helping with TEM images.
- Christine Rey Rouch for the granulometry analysis.
- Corinne Routaboul for constant help and advice on infrared spectroscopy.
- Teresa Hungria (CASTAING) for TEM/EDX analysis of my model nanoplastic.
- Rodica Chiriac (Thermal Analysis Platform (PLAT) at LMI) for TGA analysis of my samples.
- Catherine Claparols and Eric Leroy for invaluable help, support, and always good mood during work on Py-GC-MS/MS method development. It was a challenging time for all of us!

I'm deeply indebted to GDR Polymères et Océans – AAP for the financing my internship at the Biocatalysis and Metabolism laboratory (Institute of Chemistry of Claremont Ferrand) where, thanks to Pierre Amato and Boris Eyheraguibel I had amazing training which allowed me to acquire unique skills on the techniques and methods for collecting samples from the atmosphere.

I would like to give special thanks to my Master program (SMaP, ISA Lille) and especially to my coordinators Bertrand Pourrut and Julien Castelin without whom this adventure could not have happened. Thank you for giving me a chance and opening the door to a new life. Your patience, guidance and encouragement helped me to grow up from a young and shy student to a PhD.

My deepest appreciation goes to my previous internship supervisors (M1 and M2) Boris Eyheraguibel and Messika Revel. I must admit that these two internships with you have forever changed my interests, changed my goals, inspired my research, and most importantly, working with you, I found my favorite topic “Global problem of plastic pollution” that I would like to pursue throughout my career.

During these three years, I was lucky to meet many friends in the lab. My «bureau psychiatrique» Vivien, Aline and Aurélie you will always stay in my heart. My dear Marjorie, Hélène, Camille, Sara, Orélia, Fang, Ranime, Izabela, Barbara, Hai Yen, Sacha, Maksym, Alexis, Vincent, Qilin... I am very happy to have met all of you. I hope that we will meet many more times in the future.

I am grateful to every person I have met during my PhD. Whatever our relationship, you have all contributed to bring something to my life that has forever changed me for the better!

I would like to offer my special thanks to Baptiste Amouroux for introducing UCNPs to the world of plastic. Thank you for providing us with these amazing particles and for helping us to synthesize and characterize model micro- and nanoplastic. I really appreciate you being with me all these years in my hardest and happiest moments. Thank you for unlimited support and love.

Finally, I would like to thank my family for supporting me over all these years. My two grandmothers who encouraged me and motivated me with their love.

Je voudrais aussi exprimer ma grande gratitude à Françoise et Noël Amouroux qui se sont particulièrement occupés de moi pendant ma rédaction et pour leur soutien constant. Je vous remercie pour m'avoir aidée à corriger la partie en français de mon manuscrit et pour m'avoir toujours soutenue et motivée à parler français.



## List of abbreviations

### A

a.s.l.: Above sea level  
ABS: Acrylonitrile butadiene styrene  
AFM: Atomic force microscopy  
ALK: Alkyd resin  
AOM: Algal organic matter  
Ar: Argon  
ASTM: American Society for Testing and Materials

### B

BD: Bas débit  
BHT: Butylated hydroxytoluene  
Blank-PE: bulk HDPE material  
BPA: Bisphenol A

### C

*C. vulgaris*: *Chlorella vulgaris*  
CO-PDD: Atmospheric monitoring station  
Cézeaux-Opme-Puy de Dôme  
CW (laser): Continuous wave (laser)

### D

D: Diffusion coefficient  
Da: Dalton  
DAF: Dissolved air flotation  
DC: Direct current  
DDT: Dichlorodiphenyltrichloroethane  
D<sub>f</sub>: Fractal dimension  
DGTS: Deuterated triglycine sulfate  
DLS: Dynamic light scattering  
DSC: Differential Scanning Calorimetry

### E

E: Flotation efficiency  
EDX: Energy dispersive X-ray spectroscopy  
EP: Epoxy resin  
EPS: Extracellular polymeric substances  
Er: Erbium  
EVA: Ethylene-vinyl acetate copolymer

### F

F: Fluor  
Fluid FM: Fluidic force microscopy  
FWHM: Full Width at Half-Maximum

### G

g: Gram  
G: Green emission of UCNP  
Gd: Gadolinium

### H

HAADF: High-Angle Annular Dark-Field imaging  
HALS: Hindered Amine Light Stabilizers  
HD: Haut débit  
HDPE: High-density polyethylene  
HF: High flow

### I

I<sub>c</sub>: Confirmation Ion, (for SIM)  
ICCF: Institut de Chimie de Clermont-Ferrand  
ICP-MS: Inductively Coupled Plasma – Mass Spectrometry  
I<sub>q</sub>: Quantification Ion (for SIM)  
ISO: International Organization for Standardization

### J

J: Joule

### L

L: Liter  
LC-MS: Liquid chromatography coupled to mass spectrometry  
LD: Low density  
LDPE: Low-density polyethylene  
LF: Low flow  
LOD: Limit of detection

### M

m/z: Mass to charge ratio  
MCT detector: Mercury-Cadmium-Telluride (HgCdTe) detector



min: Minute  
MNPs: Micro- and Nanoplastics  
MPs: Microplastics  
Model-MPs: Model of microplastics  
Model-NPs: Model of nanoplastics

## N

N: Newton  
Na: Sodium  
Nano-Blank-PE: UCNP-free HDPE nanoparticle(s)  
Nano-Upcon-PE: HDPE nanoparticle(s) labelled with UCNPs  
NIR: Near-infrared  
NIST: National Institute of Science and Technology  
NP: Nanoparticles  
NPs: Nanoplastics  
NTA: Nanoparticle tracking analysis

## O

OA: Oleic acid  
OD: Optical density  
ODE: 1-octadecene  
OM: Optical microscopy

## P

PA: Polyamide (Nylon)  
PAHs: Polyaromatic hydrocarbons  
PAN-AA: Poly(acrylonitrile-co-acrylic acid)  
PBS: Phosphate Buffer Saline  
PC: Polycarbonate  
PCBs: Polychlorinated biphenyls  
Pd: Palladium  
PDD: Puy-de-Dôme  
PDMS: Polydimethylsiloxane  
PE: Polyethylene  
PEP: Poly(ethylene-co-propylene)  
PETE / PET: Polyethylene Terephthalate  
PEVA: Poly(ethylene-co-vinyl acetate)  
PLA: Polylactic acid  
POPs: Persistent organic pollutants  
PP: Polypropylene

PPC: Polypropylene carbonate  
PR: Phenoxy resin  
PS: Polystyrene  
PSA: Particle Size Analyzer  
PTFE: Polytetrafluoroethylene  
PUR / PU: Polyurethane  
PVC: Polyvinyl chloride  
PVP: Polyvinylpyrrolidone  
Py-GC-MS: Pyrolysis coupled with gas chromatography and mass spectrometry  
Py-GC-MS/MS: Pyrolysis coupled with gas chromatography and tandem mass spectrometry

## Q

QI: Quantitative imaging

## R

R: Red emission of UCNP  
RE: Rare-earth  
Rg: Gyration radius  
RT: Retention time

## S

SAXS: Small-Angle X-ray Scattering  
SD: Standard deviation  
SEM: Scanning electron microscopy  
SIM: Selected ion monitoring  
SMPs: Small microplastics  
SPI: Society of the Plastics Industry  
SRM: Selected-reaction monitoring

## T

T<sub>c</sub>: Confirmation transition (for SRM)  
TD-PTR-MS: Thermal Desorption - Proton Transfer Reaction - Mass Spectrometry  
TED-GC-MS: Thermal extraction desorption-gas chromatography-mass spectrometry  
TEM: Transmission Electron Microscopy  
TEM-EDX: High resolution Transmission Electron Microscopy coupled to Energy-Dispersive X-ray elemental analysis  
TFF: Tangential Flow Filtration

TGA: Thermogravimetric analysis  
TIC: Total ion current chromatogram  
TMAH: Tetramethylammonium hydroxide  
T<sub>onset</sub>: Onset temperature  
T<sub>peak</sub>: Exothermic peak temperature  
T<sub>q</sub>: Quantification transition (for SRM)

μ-(Upcon)-PE: UCNP-free Microparticles of HDPE and Microparticles of HDPE labelled with UCNP

## U

UCA: Université Clermont Auvergne  
UCNPs: Rare-Earth (or lanthanide) based Upconverting nanophosphors  
Upcon-PE: bulk HDPE material labelled with UCNP

## W

WC medium: Wright's cryptophyte medium  
WCA: Water contact angle measurement  
WWTPs: Wastewater treatment plants

## X

X<sub>c</sub>: Degree of crystallinity  
XRD: X-ray diffraction

## Y

Y: Yttrium  
Yb: Ytterbium

## Z

ZB: Zirconium beads  
ZY-E: Yttrium stabilized Zirconium oxide

## Greek letters

ΔH<sub>m</sub>: Melting enthalpy  
μFTIR / μFTIR-ATR: Micro-Fourier Transform Infrared spectroscopy coupled with an Attenuated Total Reflectance accessory  
μ-PE / μ-Blank-PE: Microparticles of HDPE  
μRaman: Micro-Raman spectroscopy  
μ-Upcon-PE: Microparticles of HDPE labelled with UCNP



# Table of Contents



## Table of Contents

<b>List of abbreviations</b> .....	1
<b>General Introduction</b> .....	9
<b>Chapter I. Plastic as an integral part of our lives, which has become a global environmental threat: a bibliographic review</b> .....	15
I.1. Definition of plastic, its types, and applications .....	18
I.2. History and Global plastic production .....	20
I.3. Plastic fate and behaviour in the environment.....	22
I.3.1. Why plastics are persistent pollutants? .....	22
I.3.2. Plastic degradation .....	24
I.3.3. Size classification of plastic debris .....	24
I.3.4. Occurrence and transport of plastic in the environment .....	26
I.4. Interaction of MPs and NPs with living organisms .....	33
I.4.1. Inclusion in the trophic chain.....	33
I.4.2. Toxicity of chemicals related to plastic .....	34
I.4.3. Physical effect and toxicity of MPs and NPs.....	35
I.4.4. Particular interaction of MPs and NPs in the aquatic environment .....	35
I.5. Study of plastic pollution in the environment.....	36
I.5.1. Sampling and preparation of MPs and NPs prior to analysis .....	36
I.5.2. Characterization of MPs and NPs from environment samples .....	36
I.5.3. Relevance of MPs and NPs models in laboratory study .....	38
Conclusion.....	40
References .....	41
<b>Chapter II. Development of an environmentally relevant luminescent model of Micro- and Nanoplastic for environmental assessment</b> .....	51
II.1. French summary .....	54

II.2. Article .....	59
II.3. Supplementary information .....	78
<b>Chapter III. Study of the mechanism of interaction between microplastic and microalgae .....</b>	<b>87</b>
III.1. French summary .....	90
III.2. Article .....	98
<b>Chapter IV. Development of the sampling and preparation protocol for atmospheric Micro- and Nanoplastics .....</b>	<b>123</b>
IV.1. French summary .....	126
IV.2. Introduction .....	131
IV.2.1. Scientific problematic .....	131
IV.2.2. Context and objectives of the study .....	132
IV.3. Materials and methods .....	135
IV.3.1. Areas of investigation .....	135
IV.3.2. Sampling of the atmosphere .....	137
IV.3.3. Sampling campaigns .....	141
IV.4. GF/F samples .....	144
IV.5. Samples of aqueous dispersion .....	144
IV.5.1. Protocol 1 (2019) .....	144
IV.5.2. Protocol 2 (2020) .....	152
Conclusions and perspectives .....	160
References .....	161
<b>General Conclusion .....</b>	<b>163</b>

# General Introduction





La découverte de la matière plastique a été l'une des découvertes révolutionnaires du début du vingtième siècle. Sa facilité de fabrication, son faible coût de production et sa durabilité ont fait du plastique un substitut compétitif de nombreux matériaux tels que le verre, le métal ou le bois. En conséquence, le plastique est devenu omniprésent dans tous les biens de consommation tels que les emballages, les vêtements, l'électronique, les médicaments, etc. Cependant, la forte demande, la production de masse, l'utilisation généralisée et la mauvaise gestion des déchets plastiques ont contribué à l'émission et à l'accumulation de plastique dans l'environnement, jusqu'à devenir un problème environnemental majeur de notre époque.

Depuis plusieurs années, la pollution plastique et son impact sur l'environnement sont devenus des sujets d'étude de plus en plus répandus dans la communauté scientifique. La production massive de plastique et leurs rejets sont ainsi scrutés, mais également leur devenir dans l'environnement, leur dégradation et leur interaction avec des organismes vivants. Dans ce dernier cas, c'est l'occurrence de micro et nanoparticules de plastique qui est au centre des attentions, puisqu'elle est responsable de l'introduction des matières plastiques dans la chaîne trophique. Si la connaissance croît constamment ces dernières années, de nombreuses questions demeurent. La caractérisation physique et chimique des particules de plastique est rendue difficile par leur grande variabilité, provenant à la fois du type de polymères qui les constituent mais également du processus ayant conduit à leur génération dans l'environnement (usure mécanique, dégradation chimique par oxydation, ...). La composition chimique des particules – type de polymère et état de surface – aura *in fine* une influence importante sur leur impact vis-à-vis des organismes vivant à leur contact. Le développement de modèles particuliers de plastique apparaît dans ce cadre comme un outil qui permettrait d'accroître la connaissance sur le devenir de ces particules dans l'environnement et leur interaction avec des organismes vivants.

C'est dans ce contexte global que ce travail a été réalisé. Il a eu pour objectif de mettre en place et d'optimiser un modèle, environnementalement pertinent, de micro- et de nanoparticules de plastique qui soient facilement détectables et traçables par des techniques analytiques non destructrices. Le polyéthylène haute densité (HDPE) a été choisi comme matrice et les particules ont été produites par une approche top-down en y incorporant des nanoparticules upconverting (UCNPs) à base d'ions lanthanides. Cette approche est originale car elle combine l'utilisation d'un matériau plastique très répandu (HDPE), une méthode de fabrication permettant l'obtention de particules polydisperses ayant une grande disparité de formes, et une détection par luminescence après excitation par un rayonnement infrarouge.

Ce manuscrit de thèse est organisé en 4 chapitres. Le premier présente une revue bibliographique sur le problème général de la pollution plastique. Après une définition de ce qu'est le plastique, de ce que sont ses types et ses applications, un bref historique et des statistiques sur sa production massive sont donnés, ainsi que des informations quant au rejet des déchets plastiques dans l'environnement. Une description plus fine des micro- et nanoplastiques (MPs et NPs) en tant que polluants environnementaux persistants omniprésents est également proposée, sans oublier une attention particulière portée sur l'interaction de ces particules avec les organismes vivants, leur incorporation dans la chaîne trophique et leurs effets toxiques et physiques négatifs. Enfin, un résumé de l'état de l'art concernant les approches et méthodes pour l'étude et le suivi de la pollution plastique sera donné, en mettant en évidence les limites de ces méthodes.

Le chapitre suivant est consacré à la méthodologie de mise en œuvre du modèle de MPs et de NPs. Elle comprend la synthèse du HDPE marqué par des UCNPs et la production du modèle de MPs et NPs de ce matériau en utilisant une approche top-down. Les propriétés chimiques et physiques de ces particules ont ensuite été étudiées à l'aide de plusieurs méthodes analytiques : analyse de suivi de nanoparticules (NTA) et de diffusion dynamique de la lumière (DLS), potentiel zêta, spectroscopie de rayons X à dispersion d'énergie par microscopie électronique à transmission (TEM/EDX), analyse par diffusion des rayons X aux petits angles (SAXS), analyse thermogravimétrique (TGA), calorimétrie différentielle à balayage (DSC), mesures de fluorescence, imagerie sur microscope à deux photons, etc...

Le modèle ainsi développé et caractérisé a ensuite été utilisé pour étudier son interaction avec des microalgues. Le chapitre III présente les résultats obtenus lors de cette étude. Dans un premier temps, les modèles de MPs ont été caractérisés à l'aide d'un microscope à force atomique (AFM) et d'un microscope à force fluide pour visualiser les particules et obtenir des informations quant à leur rugosité et au caractère hydrophobe de leur surface. L'AFM a ensuite été utilisé pour sonder l'interaction des modèles de MPs avec les cellules de microalgues *Chlorella vulgaris*. La combinaison des résultats obtenus par AFM et par des expériences de floculation ont permis de mieux comprendre les mécanismes à l'origine de l'interaction entre les MPs et les microalgues.

Enfin, dans un dernier chapitre, nous exposons l'élaboration d'une méthodologie pour la collecte de MPs et de NPs dans l'atmosphère. Elle inclut la prise en compte des zones géographiques en lien avec le niveau d'activité humaine, la collecte de données

météorologiques, et l'échantillonnage de matières atmosphériques, y compris les aérosols (particules en suspension dans l'atmosphère) et les dépôts (pluie, neige, grésil, etc.). Nous avons également proposé une méthodologie de préparation des échantillons et d'analyse qualitative et quantitative, réalisée par la combinaison de méthodes analytiques comprenant  $\mu$ -FTIR (microscopie infrarouge à transformée de Fourier), Py-GC-MS (pyrolyse couplée à la chromatographie en phase gazeuse et spectrométrie de masse), DLS (diffusion dynamique de la lumière), et NTA (analyse de suivi de nanoparticules).



## Chapter I.

Plastic as an integral part of our lives, which has become a global environmental threat: a bibliographic review



## **Table of content**

I.1. Definition of plastic, its types, and applications .....	18
I.2. History and Global plastic production .....	20
I.3. Plastic fate and behaviour in the environment .....	22
I.3.1. Why plastics are persistent pollutants? .....	22
I.3.2. Plastic degradation .....	24
I.3.3. Size classification of plastic debris .....	24
I.3.4. Occurrence and transport of plastic in the environment .....	26
I.4. Interaction of MPs and NPs with living organisms .....	33
I.4.1. Inclusion in the trophic chain.....	33
I.4.2. Toxicity of chemicals related to plastic .....	34
I.4.3. Physical effect and toxicity of MPs and NPs.....	35
I.4.4. Particular interaction of MPs and NPs in the aquatic environment .....	35
I.5. Study of plastic pollution in the environment.....	36
I.5.1. Sampling and preparation of MPs and NPs prior to analysis .....	36
I.5.2. Characterization of MPs and NPs from environment samples .....	36
I.5.3. Relevance of MPs and NPs models in laboratory study .....	38
Conclusion.....	40
References .....	41



## **I.1. Definition of plastic, its types, and applications**

“Plastic” is a generic term that refers to various polymers whose chemical structures and properties can be very different. The word "plastic" comes from the Greek word "plastikos" which means suitable for moulding into different shapes (Millet *et al.*, 2018). Plastic is a material made from synthetic and semi-synthetic organic compounds. According to Ghosh *et al.*, the term plastic refers to “a long hydrocarbon chain polymer having high molecular weight”. Organic, but mostly inorganic sources are used to produce plastics. The most common basis of plastic is hydrocarbons, unprocessed products, crude oil, natural gas and coal (Shah *et al.*, 2008).

According to raw materials and the processes of production, plastic materials are characterized by a wide variety of properties. Several factors to classify plastics include chemical structure and physical properties (Ghosh *et al.*, 2013). Based on their thermal properties, plastic can be divided into two main groups: thermoplastic and thermosetting polymers (Fried, 2014).








Thermoplastic includes a group of polymers that have unique properties. They are able to deform under the action of heat and pressure without undergoing any chemical change in their structure. Examples of such polymers are polyethylene (PE), polypropylene (PP), polystyrene (PS), polyvinyl chloride (PVC), and polytetrafluoroethylene (PTFE) (Fried, 2014). Plastics of this group can be deformed many times, making them suitable for reuse as raw materials (Ghosh *et al.*, 2013).

Unlike thermoplastic, thermosetting polymers (e.g., phenol-formaldehyde, polyurethanes, etc.) subjected to high heating temperatures undergo irreversible chemical changes, thus preventing a potential reuse of such kind of polymers (Fried, 2014).

Plastic can also be classified by its designing properties including characteristics such as strength, conductivity, thermal stability, or degradability (Ghosh *et al.*, 2013).

In 1988, the Society of the Plastics Industry (SPI) created a classification system for the different types of plastic based on their properties and applications. According to this classification, all types of plastic can be divided into seven major groups, which are represented in Table 1 (Industry Canada, 2012).

**Table 1: Classification of plastic types by the Society of the Plastics Industry (SPI).**

Type of plastic	Industry Symbol	Chemical formula	Main properties	Major uses
<b>Polyethylene Terephthalate (PETE or PET)</b>		$(C_{10}H_8O_4)_n$	<ul style="list-style-type: none"> <li>• Good moisture barrier properties</li> <li>• High heat resistance</li> <li>• Transparency</li> <li>• Solvent resistant</li> </ul>	<ul style="list-style-type: none"> <li>• Soft drink bottles</li> <li>• Food dishes</li> <li>• Packages for baking or boiling</li> <li>• Fibers for sewing and carpet</li> <li>• Shampoo and mouthwash bottles</li> </ul>
<b>High-density polyethylene (HDPE)</b>		$(C_2H_4)_n$	<ul style="list-style-type: none"> <li>• Impermeability</li> <li>• Chemical resistance</li> <li>• Hardness and resistance to bending</li> <li>• Smooth waxy surface</li> </ul>	<ul style="list-style-type: none"> <li>• Milk bottles</li> <li>• Cartons of ice cream and juice,</li> <li>• Packs of shampoo and detergents</li> <li>• Irrigation pipes</li> <li>• Covers for mineral water</li> </ul>
<b>Polyvinyl chloride (PVC)</b>		$(C_2H_3Cl)_n$	<ul style="list-style-type: none"> <li>• High transparency</li> <li>• Chemical resistance</li> <li>• Long-term stability</li> <li>• Stable electrical properties</li> <li>• Low gas permeability</li> </ul>	<ul style="list-style-type: none"> <li>• Food packaging</li> <li>• Cosmetics</li> <li>• Wire/cable insulation</li> <li>• Pipes/fittings</li> <li>• Toys</li> </ul>
<b>Low-density polyethylene (LDPE)</b>		$(C_2H_4)_n$	<ul style="list-style-type: none"> <li>• Softness</li> <li>• Transparency</li> <li>• Lightness</li> <li>• Stable electrical properties</li> <li>• Good moisture barrier properties</li> </ul>	<ul style="list-style-type: none"> <li>• Disposable bags and containers</li> <li>• Liquid soap, shampoos, detergents</li> <li>• Laboratory equipment</li> </ul>
<b>Polypropylene (PP)</b>		$(C_3H_6)_n$	<ul style="list-style-type: none"> <li>• High chemical resistance</li> <li>• High melting point</li> <li>• Hardness but flexible</li> <li>• Translucency</li> <li>• Strength</li> </ul>	<ul style="list-style-type: none"> <li>• Microwave ovens</li> <li>• Plastic cups</li> <li>• Food containers</li> <li>• Utensils</li> <li>• Food packaging</li> </ul>
<b>Polystyrene (PS)</b>		$(C_8H_8)_n$	<ul style="list-style-type: none"> <li>• Rigid or foamed</li> <li>• Brittle</li> <li>• High clarity</li> <li>• Affected by fats and solvents</li> </ul>	<ul style="list-style-type: none"> <li>• Disposable food containers</li> <li>• Cups and disposable cutlery</li> <li>• Toys</li> <li>• Ventilation pipes</li> <li>• Boxes CD / DVD</li> </ul>
<b>Others</b>		$(C_{12}H_{22}N_2O_2)_n$ $(C_8H_8 \cdot C_4H_6 \cdot C_3H_3N)_n$ $C_{15}H_{16}O_2$ $C_{27}H_{36}N_2O_{10}$	<ul style="list-style-type: none"> <li>• Nylon (PA)</li> <li>• Acrylonitrile butadiene styrene (ABS)</li> <li>• Polycarbonate (PC)</li> <li>• Polyurethane (PUR and PU)</li> <li>• Layered or multi-material mixed polymers</li> </ul>	

Widespread application of plastics is related to the variety of inherent polymers properties. In addition, some properties are provided to plastic by introducing into its composition different types of chemical additives (Andrady and Neal, 2009). The main groups of plastic additives and the purpose of their application are presented in Table 2.

**Table 2: Plastic additives and their role.**

<b>Group</b>	<b>Example of additive</b>	<b>Main purpose of addition</b>
Inorganic fillers	Carbon, silica	Strengthening of plastic material
Organic synthetic compound	Bisphenol A (BPA)	Clarity and hardness
Thermal stabilizers	Organophosphites and phenolic antioxidants	Prevent degradation caused by heat exposure, and allow the plastics to be processed at high temperatures
Plasticizers	Polymeric, trimellitates, 1,2 cyclohexanedicarboxylic acid diisononyl ester, citrates, phthalates, etc.	Increasing flexibility and pliability
Antioxidants	Phosphites, thioethers Butylated hydroxytoluene (BHT)	Prevent degradation caused by oxidation
Fire retardants	Polybrominated diphenyl ethers	Protection against ignition and burning
UV stabilizers	Benzophenones, Benzotriazoles, Hindered Amine Light Stabilizers (HALS)	Preventing degradation caused by exposure of sunlight
Pigment	Colorants, matting agents, opacifiers and lustre additives	Improvement the appearance of a plastic product

The wide range of versatile properties inherent in plastic has made it a highly competitive substitute for materials such as glass, metal, or wood. Plastic has become a revolutionary product that forever changed our lifestyle and history, as it is currently one of the most common consumer goods (Andrady and Neal, 2009).

## **I.2. History and Global plastic production**

In 1870, people began looking for materials that could replace ivory. At that time, billiards was rapidly gaining popularity which complicated the supply of ivory obtained by the slaughter of wild elephants because billiard balls were made of ivory. Thus, a New York firm offered 10 000\$ for anyone who will find a substitute for ivory. Inspired by this offer John Wesley Hyatt invented the first synthetic polymer, called “Celluloid”. It was material obtained by treating nitrocellulose extracted from cotton with camphor (that played role of additive). Celluloid became a revolutionary material that was easy shaped in different forms and became a competitive substitute for natural materials such as ivory, horn, tortoiseshell, etc.

Then in 1907, Leo Baekeland invented the first fully synthetic plastic “Bakelite”. This plastic was also called “the material of a thousand uses,” because of its wide range of applications and properties (easily shaped in any form, good insulator, heat resistant, etc). These inventions have shown people that a lot of natural material can be replaced by something that does not depend on natural sources and can prevent the depletion of natural resources.

Companies began to invest in the production of other types of plastic. The production of alternative synthetic materials has become a priority over the use of scarce natural resources (Chalmin, 2019).

World War II was a period called the "Age of the Plastic Industry". After War, massive production of plastic was growing, as it was not expensive, the material was sanitary safe, multifunctional, and adopted for people needs. Annual production of plastic from 1950 to 2019 increased from 1.5 to 368 million tons per year (Figure 1) (Plastics Europe, 2020).

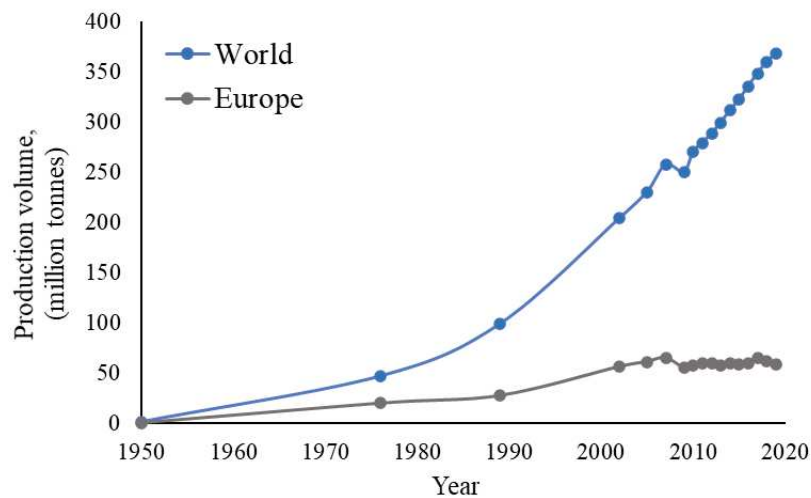


Figure 1: Worldwide production of plastics from 1950 to 2019.

During this period, PE and PP have been the most demanded materials worldwide (Figure 2) (Crawford and Quinn, 2017b).

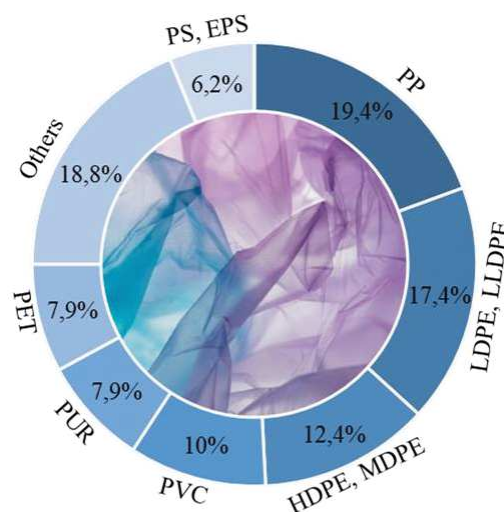
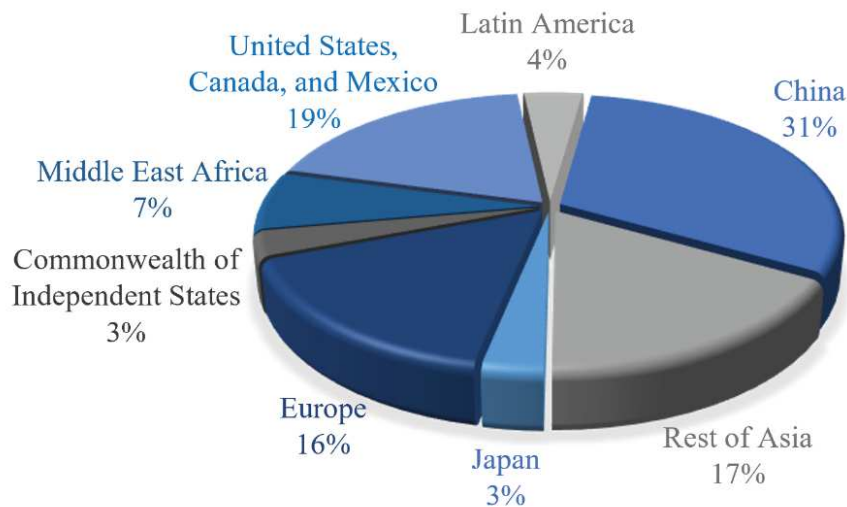


Figure 2: Distribution of demand for plastic by type in 2019. Adapted from (PlasticsEurope 2020).

China, Europe, and North America are the world's production leaders of plastic since 1950 (Figure 3).



**Figure 3: World leaders in the production of plastic in 2019. Adapted from (PlasticsEurope, 2020).**

A large proportion of plastic materials are disposable products consumption with a short lifetime. Fifty percent of plastics are single-use items (e.g. packaging, agricultural films, disposable consumer items, etc.), 20-25% have long-term uses (e.g. pipes, cable coatings, structural materials), and the remaining materials have an intermediate lifetime (electronic appliances, furniture, cars, etc.) (Hopewell *et al.*, 2009). At the end of their life cycle, all plastics are transformed into millions of tons of debris since only a short percentage of it can be recycled (mainly packaging and disposable consumer items). As a result, plastic is transported into the environment (accidentally or voluntarily) and could have detrimental effects on a variety of species.

### **I.3. Plastic fate and behaviour in the environment**

#### **I.3.1. Why plastics are persistent pollutants?**

High demand for the use of plastic products contributes to its accumulation in the environment. Annually, millions of tons of plastic debris are thrown away. The proportion of plastic in the global world volume of solid waste is about 12 % (Figure 4) (Kaza *et al.*, 2018).

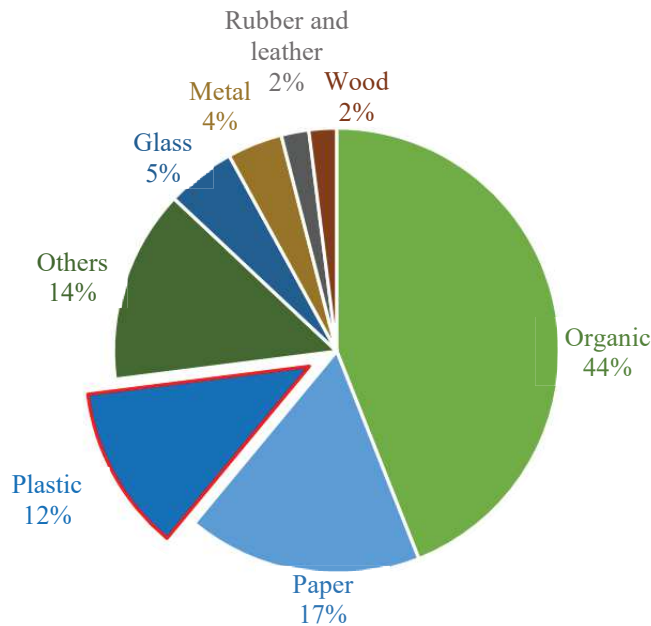


**Figure 4: Global solid waste composition. Redrawn from (Koza et al., 2018).**

Even though the plastic industry is developing extremely fast, the management of plastic waste remains poorly developed. This is due to the variety of plastic material composition and to the recycling procedures which are usually expensive. Thus, among the main solid waste management methods such as recycling, incineration, and dumping on the landfills, the last one is the most implemented for plastic waste. This method is the cheapest and easiest to manage but contributes to the major dissemination of plastic in the environment. In 2015, the amount of plastic waste generated reached up to 6 300 million tons, about 9 % of which was recycled, 12 % was incinerated and 79 % was accumulated in landfills or natural environments (Geyer *et al.*, 2017).

Due to their low weight, plastics are easily transported in the environment by wind, diffused by rain, surface and ground waters (Akdogan and Guven, 2019). Now plastic is a persistent ubiquitous pollutant that is found in all environmental compartments across the whole planet, from highly industrial places to remote pristine areas. This very useful and convenient material of our daily lives has become a threat to the environment and humanity.

Due to its chemical composition and synthetic nature, plastic requires hundreds of years to decompose. Thus, all discarded plastic debris persists and accumulates in the environment. However, getting to the environment plastic waste is continuously exposed to various abiotic and biotic factors such as light, moisture, heat, biological activity, etc. The influence of these factors causes changes in the mechanical and physicochemical properties of plastics that leads to plastic degradation.

### **I.3.2. Plastic degradation**

There are several types of plastic degradation occurring in the environment, which include thermal degradation, photo-oxidative degradation, mechanical degradation, and biodegradation.

Thermal degradation is a process of decomposition of plastic polymers in simple units by heat (Ghosh *et al.*, 2013). Photodegradation mechanisms involve the absorption of UV light which leads to the formation of free radicals and autooxidation process, responsible for the degradation of plastic (Ammala *et al.*, 2011). In addition, in waters, plastic debris move and interact with each other, or with other solid matter, thus inducing a mechanical stress that can cause disturbances in the morphology of the polymer and can contribute to an accelerated degradation process (Ammala *et al.*, 2011). Unlike previously cited degradation processes, biodegradation of plastic is usually a secondary step after partial degradation under the influence of abiotic factors (Bahl *et al.*, 2021). Plastic biodegradation is induced by microorganisms which are able to secrete biologically active enzymes that degrade the long polymers (Ghosh *et al.*, 2013).

More generally, degradation of plastic results in the fragility of plastic materials, which leads to the fragmentation of large objects into small pieces down to the nanoscale (Ter Halle *et al.*, 2017). Thus, plastics of all sizes have been found everywhere on our planet (Akdogan and Guven, 2019).

### **I.3.3. Size classification of plastic debris**

The size of plastics presented in the environment can be classified as mega-, macro-, meso-, micro-, and nanoplastic (Laender *et al.*, 2011; GESAMP, 2015). Detail on the different size of the plastic debris is presented in Figure 5.

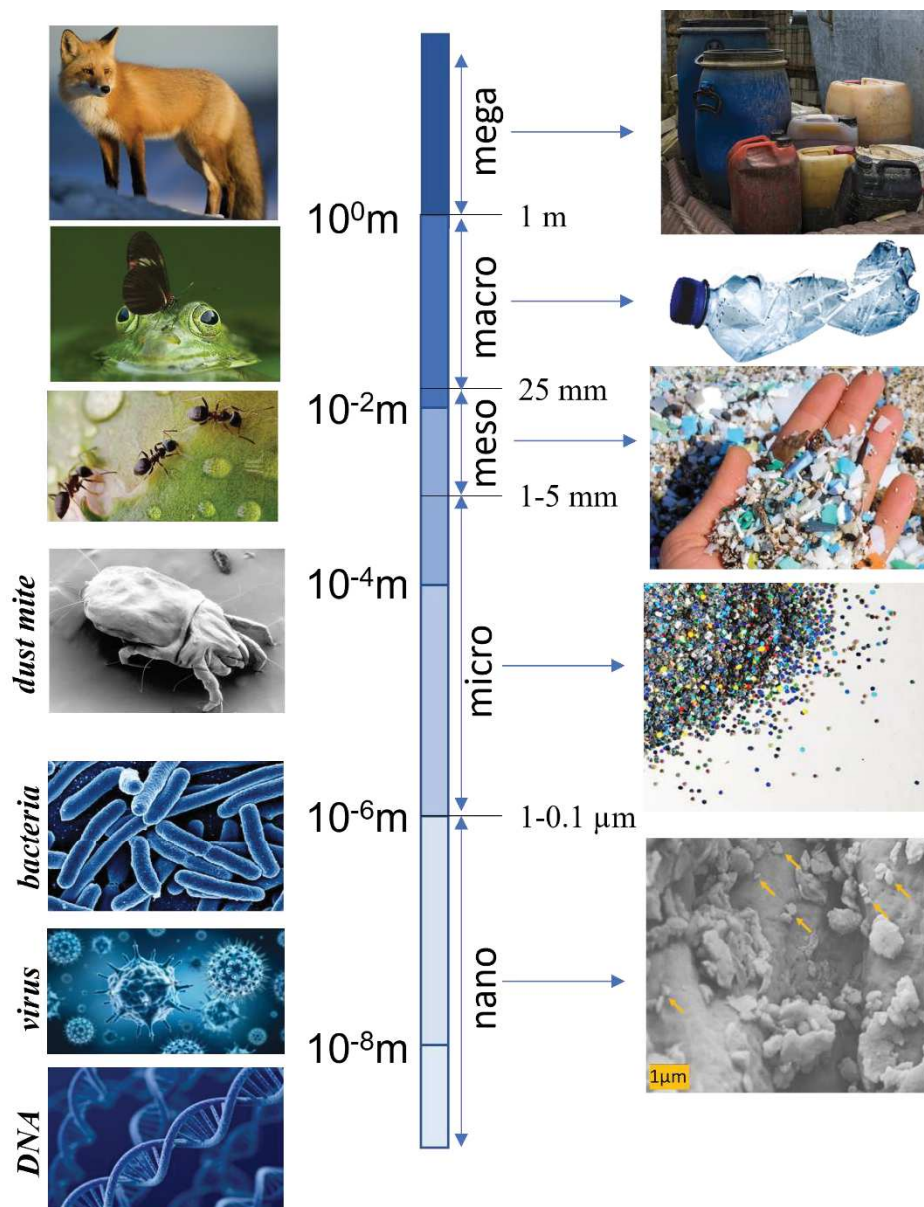


Figure 5: The size range of plastic objects found in the environment, compared with the one of living organisms. Redrawn from (GESAMP, 2015).

In recent decades, much attention has been given to the study of the occurrence and potential negative effects of micro- and nanoplastic. The sizes of these two groups of plastic particles cover the same range as sediments and some planktonic organisms, making them bioavailable for a wide number of living organisms worldwide, which cause a huge concern about the entire trophic chain (Cole *et al.*, 2013).

The upper and lower size limits of these two groups of plastics are still under scientific debate (Hartmann *et al.*, 2019). Based on the most common classifications, “microplastics” (MPs) range from 1 μm to 5 mm (Lindeque *et al.*, 2020), while “nanoplastics” (NPs) are particles less than 1 μm (Gigault *et al.*, 2018). Depending on their origin, MPs and NPs can be



classified as primary or secondary plastic particles. Primary plastic particles are manufactured for specific purposes and have particular chemical and physical properties such as uniform size, regular shape, known composition, etc., (Cole *et al.*, 2011).

For instance, primary MPs are manufactured at the millimetric or submillimetric scale under the form of pellets or microbeads (Dris *et al.*, 2016). MPs pellets are characterized by a rounded shape and diameter sizes from 2 to 5 mm (Costa *et al.*, 2010) and are widely used in the plastics industry as raw materials. Microbeads are plastic particles less than 1 mm size in different shapes (spheres, granules, ellipses, threads, and irregular particles). They are widely used in cosmetics and personal care products such as toothpaste, soap, shampoos, body, and face scrubs (Leslie, 2015; Napper *et al.*, 2015). Primary NPs are also found widely used in industry, particularly in medicine, waterborne paints, adhesives, coatings, 3-D printing, electronics, science, etc. (Koelmans *et al.*, 2015).

On the other side, secondary MPs and NPs are the result of fragmentation of larger plastic debris caused by various degradation processes. These particles are characterized by a wide range of physical and chemical properties including variety of sizes, irregular shapes, chemical composition, etc., (Phuong *et al.*, 2016). Additionally, secondary plastic particles can result from the mechanical wear of the plastic material itself during its lifecycle, as for instance, the release of particles from wearing of car tires, synthetic clothes washing, etc., (Kole *et al.*, 2017; De Falco *et al.*, 2019).

Scientific studies have shown that the whole planet is concerned about the occurrence of these plastic particles in the environment: from one pole to another, from the coast to the abyssal plains (Rochman, 2018).

### **I.3.4. Occurrence and transport of plastic in the environment**

#### ***I.3.4.a. Aquatic environment***

The presence of plastic in the aquatic environment has been actively studied for the last half-century. The aquatic ecosystem is the biggest ecosystem of our planet that became the ultimate sink for plastic waste. Main sources of plastic in the world ocean represent land-based and sea-based sources (EPA US, 2016) (Figure 6).

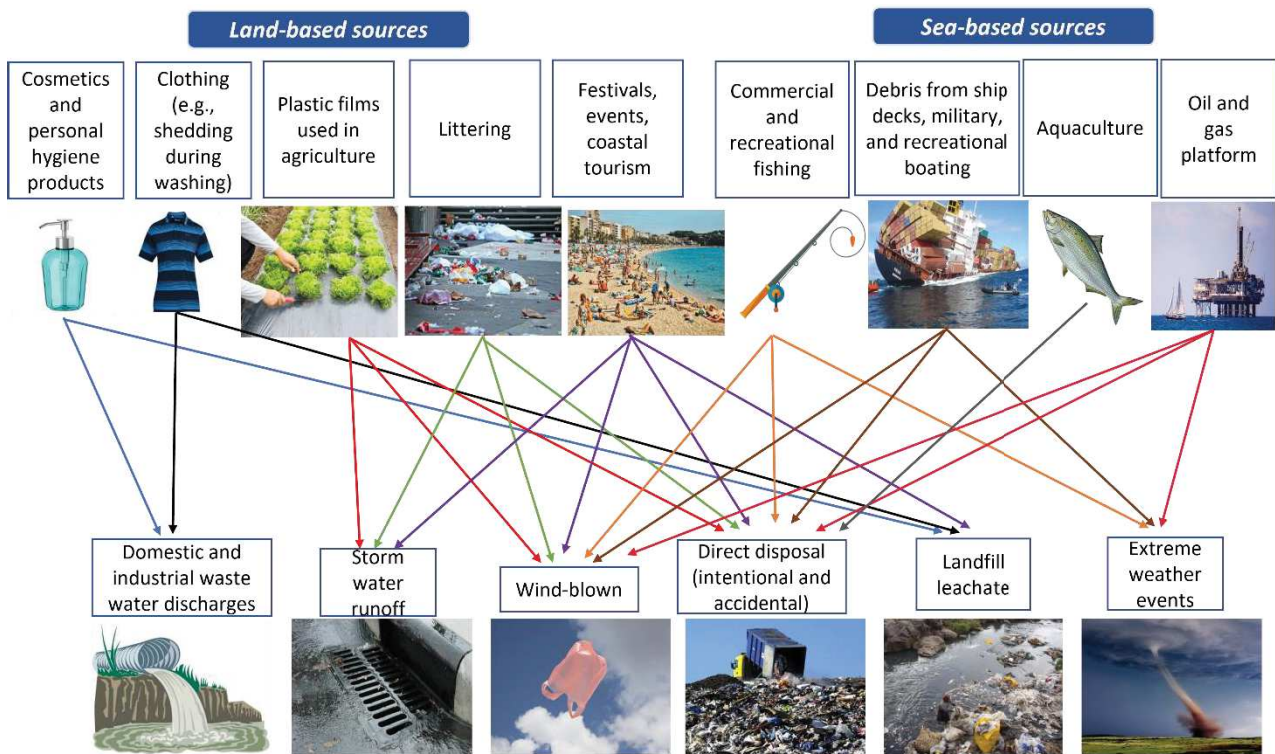


Figure 6: Different sources of plastics and their pathway to the aquatic environment. Redrawn from (EPA US, 2016).

It is estimated that 4.8 to 12.7 million tons of plastic enter the aquatic environment annually (Jambeck *et al.*, 2015). According to the United Nations Organization, 80% of plastic waste in the oceans come from the land surface, while only 20% is linked to direct activity in the aquatic environment (Crawford and Quinn, 2017b). The land-based sources of plastic waste can be introduced into the ocean through several events such as storm water discharge, intentional or accidental dumping, tourism, industrial activities, and accidents during transportation or strong winds. Sources from direct activities in the ocean include fishing, transportation, scientific research, military, tourism, and commercial vehicles (Liffmann and Boogaerts, 1997; European Commission, 2011).

It has been estimated that 60 to 80% of all solid waste presented in the aquatic environment is plastic (Gregory and Ryan, 1997). The number of plastics pieces floating in the aquatic environment is above 5 trillion, for an estimated weight of about 269 000 tons (Eriksen *et al.*, 2014).

The presence of plastic debris in the aquatic environment was first documented in North Pacific and North Atlantic subtropical gyres during 1970s (Carpenter *et al.*, 1972; Venrick *et al.*, 1973; Colton *et al.*, 1974; Wong *et al.*, 1974). In the oceans, plastic tends to accumulate in certain areas such as gyres. Gyres are a large rotating current of water with low water level in

the areas of their centers. They are areas of accumulation of marine debris. There are five main gyres known in the oceans: North and South Pacific Gyre, North and South Atlantic Gyre, and Indian Ocean Gyre, location of which are represented in Figure 7 (Crawford and Quinn, 2017b).

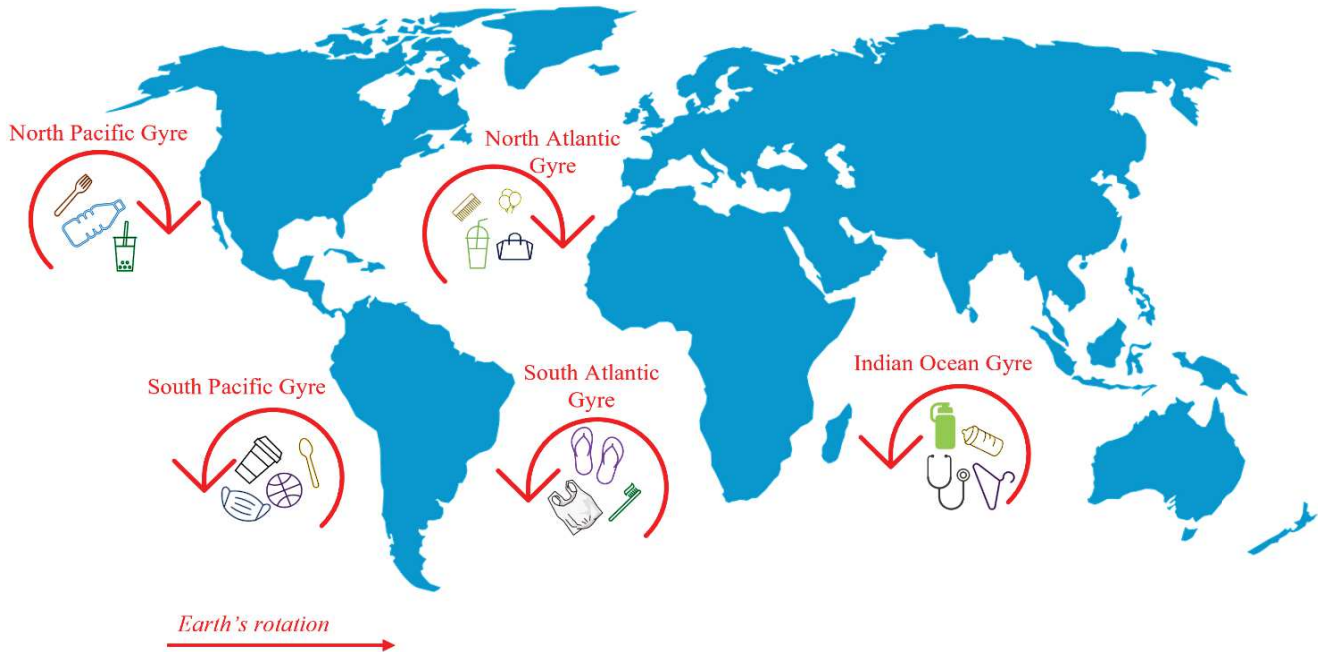


**Figure 7: The world's largest known gyres in the oceans, acting as debris accumulation areas for any type of marine debris.**

The amount of plastic waste in these regions is very high. The highest accumulation of plastic has been registered in the Great Pacific Garbage Patch (GPGP), which is located in North Pacific Gyre, between California and Hawaii. The GPGP has a surface area of around 1.6 million km<sup>2</sup>, three times the one of France. The estimated amount of plastic accumulated here is about 79 000 tons, containing 1.8 trillion pieces of plastic (700 694 particles of different size per km<sup>2</sup>). The majority of these plastic pieces have micrometric size and accounts for 1.1 – 3.6 trillion pieces (Lebreton *et al.*, 2018).

Other studies have reported plastic concentrations in the Pacific Ocean ranging from 26 898 (Eriksen *et al.*, 2013) to 448 000 (Goldstein *et al.*, 2013) particles/km<sup>2</sup> of water. The Atlantic Ocean has considerably lower concentrations with 1534 pieces/km<sup>2</sup> (Law *et al.*, 2010) and 2.46 particles/m<sup>3</sup> (Lusher *et al.*, 2014). Another example of the accumulation of a large number of MPs is the Mediterranean Sea, with 62 000 particles/km<sup>2</sup> (Collignon *et al.*, 2014).

The most commonly found types of MPs on the surface of the Atlantic Ocean and area near Australia are PE and PP which represent 99 % (Law *et al.*, 2010; Poulain *et al.*, 2019) and

98.5 % respectively (Reisser *et al.*, 2013). While the most often in Europe are PE and PS (Phuong *et al.*, 2016).

There is a gap in knowledge about the fate and quantity of NPs in the ocean. Mostly because of the limitations of samples collection techniques and analytical methods available for such small particles. The first evidence of NPs presence in the ocean was reported for the North Atlantic Subtropical gyre (Ter Halle *et al.*, 2017). Currently, more and more attention is paid to the study of the main sources of NPs, their fate and behaviour in all environmental compartments around the globe.

The number and distribution of plastic in the marine environment depend on geographic phenomena such as wind, waves, currents, tides, tsunami etc., (van Sebille *et al.*, 2020). All these phenomena lead to the constant movement, migration and spreading of plastic in aquatic environments. There are also some studies that have shown that the largest amount of plastic is accumulated in places with low-wind conditions (Goldstein *et al.*, 2013).

Plastic is ubiquitous in the aquatic environment and can be found on the surface, in the depths and on the bottom as well as in sediment and sand.

#### **Plastic in sediment/sandy samples**

Sediments are the ultimate compartment where contaminants accumulate in the aquatic environment (Chapman and Wang, 2001). As well as in marine waters, the concentration of plastic in sediment and sand is fluctuating. Considering the concentration of plastics in sediments, it is necessary to pay attention to the coastal zones as they are centers for recreation, tourism, transport, international trade, fishing, and other activity which leads to the plastic distribution.

Reddy *et al.*, published a study of one of the world's largest ship-breaking zones located on the northwest (NW) of the Gulf of Cambay, India, and called Alang-Sosiya ship-breaking yard. The average concentration of plastic fragments in this area reached  $81 \pm 4.03$  mg/kg of sediment. Identified fragments were in PU, PS, polyester (PEST), nylon and glass wool. These materials are widely used in the construction of ships, which explains their presence at this site where occurs ship-breaking activities (Reddy *et al.*, 2006).

Studies of coastal regions have reported different concentrations of plastic particles in sediments. For instance, along Belgian coast, plastic concentration reached  $390.7 \pm 32.6$  particles/kg or 10 mg/kg of dry sediment (Claessens *et al.*, 2011). For the French-

Belgian-Dutch coastline this value was 0.3 particles/kg (Van Cauwenberghe *et al.*, 2015), and for Italy 2 175 particles/kg (Vianello *et al.*, 2013).

The same variety of concentration was observed in sandy samples from 27 particles/m<sup>2</sup> in the Pacific Ocean (Hidalgo-Ruz and Thiel, 2013) to 80 000 particles/m<sup>2</sup> in the Arabian Gulf (Khordagui and Abu- Hilal, 1994).

The most frequently found types of plastic in sediment and sand are PE and PP (Peng *et al.*, 2020; Phuong *et al.*, 2021).

#### ***1.3.4.b. Terrestrial environment***

Terrestrial environment is a main source and dissemination pathway of plastic waste to the world ocean, but little is known about the fate of plastic in soil and freshwater as compared to the marine environment. It has been estimated that the annual release of MPs into the terrestrial environment ranges from 63 000 to 430 000 tons for farmland in Europe and from 44 000 to 300 000 tons for farmland in North America (Nizzetto *et al.*, 2016). Moreover, calculation of total amount of released plastic from European Union to terrestrial ecosystem is 473 000 to 910 000 tonnes, which is 4–23 times above the amount estimated to be in the world ocean (Horton *et al.*, 2017).

Sources of plastic release into the terrestrial environment can be sorted according to the type of plastic particles released, that is, primary or secondary plastic. The main sources of primary plastic pollution in the terrestrial environment are the end products of wastewater treatment plants (WWTPs), which include sewage sludge and water. Sewage sludge is often used as soil fertilizer in agriculture, but it contains primary plastic particles from personal care products as well as synthetic fibers from clothes washing. Sewage water is the source of plastic particles or fibers of low density (LD) which were not retained by sludge. Eventually, they are released into rivers. The quantity of sewage sludge that is used for agriculture depends on the country policy, thus the input of plastic released will significantly vary around the world. For instance, in Spain, sewage sludge is extensively used for agricultural fields as fertilizer. A study by van den Berg *et al.*, on 16 agricultural fields from the east of Spain, confirmed that sewage sludge significantly increases the concentration of plastic in the soil. Soil without application of sewage sludge had an average concentration of LD MPs of  $930 \pm 740$  particles/kg, for a heavy density (HD) MPs of  $1\,100 \pm 570$  particles/kg. Concentrations were much higher for the soil where sewage sludge was used, with LD MPs of  $2\,130 \pm 950$  particles/kg, and HD MPs of  $3\,060 \pm 1\,680$  articles/kg (van den Berg *et al.*, 2020).

Sources of secondary plastic include places of municipal solid waste collection, landfills (He et al., 2019), garbage disposal accidentally or intentionally, tire wearing, paint wearing, compost, use of plastic in agriculture (e.g., mulching film) (Horton *et al.*, 2017).

Recent work by Huang *et al.*, conducted in 19 Chinese provinces across the country, confirms that plastic mulching is a significant source of soil contamination by plastic. The average concentration of macroplastic was 83.6 kg/ha. It was also observed that plots, where plastic mulching had been used for over 24 years, have higher concentrations of MPs than plots where it had been used for 5 years,  $1075.6 \pm 346.8$  vs.  $80.3 \pm 49.3$  pieces/kg of soil (Huang *et al.*, 2020).

High abundances of microplastic 320 – 12 560 items/kg of dry weight, were observed in vegetable farmlands suburb of Wuhan (China), which is the center of economy, culture and education (Chen et al., 2020).

Information on plastic quantity in the soil remains limited due to the lack of a standardized methodology for sampling, plastic extraction from complex environment matrix, and further analysis. Most of the performed studies focusing on macro- and MPs, while information on NPs is limited. Recent work by (Wahl et al., 2021) is the first study that reported NPs presence in the agricultural soil collected from central France. Where, NPs of PE, PS and PVC of 20 to 150 nm were detected (Wahl et al., 2021).

Terrestrial pollution by plastic also occurs through atmospheric depositions. As reported, plastic particles can be transported over long distances and deposited far away from their sources of release to a remote pristine area (Allen et al., 2019).

#### ***1.3.4.c. Atmosphere***

The study of plastic in the atmosphere is a relatively new topic that has caused concern and attracted the attention of scientists in the last decade. But even in such a short period compared to studies of plastic pollution in the aquatic and terrestrial environment, the first studies on plastic pollution in the atmosphere have shown that atmospheric fallout is one potential vector of plastic pollution (Gasperi *et al.*, 2018; Hurley *et al.*, 2020; Zhang *et al.*, 2020). Recent studies show that plastic is present in the atmosphere, as in all other compartments around the world, from high-industry areas to remote mountains, and the open ocean environment.

The presence of MPs in the atmospheric fallout (wet and dry deposition) has been reported in several European cities such as Paris (Dris *et al.*, 2016), Hamburg (Klein and Fischer, 2019), Bremen (Bergmann *et al.*, 2019). In the Paris area, detected concentration of MPs in the air ranged from  $53 \pm 38$  particles/m<sup>2</sup>/day (suburban site) to  $110 \pm 96$  particles/m<sup>2</sup>/day (urban site) (Dris *et al.*, 2016). The average number of MPs in the metropolitan region of Hamburg was 275 plastics/m<sup>2</sup>/day (Klein and Fischer, 2019). Most of the MPs in Paris were fibers made of PET and polyamide (PA) (Dris *et al.*, 2016). While the predominant shape of MPs in Hamburg was fragments made of PE and ethylene-vinyl acetate copolymer (EVA) (Klein and Fischer, 2019).

In the studies reported in China, fibers were also predominant in the atmospheric samples (Cai *et al.*, 2017). In the city of Dongguan, the concentration of MPs identified as PE, PP, PS ranged from  $31 \pm 8$  to  $43 \pm 4$  particles/m<sup>2</sup>/day for atmospheric fallout (Cai *et al.*, 2017). The concentration of suspended atmospheric MPs in Shanghai reached 1.42 particles /m<sup>3</sup>, which were represented by PET, PE, PS, PP, PA, epoxy resin (EP), alkyd resin (ALK), and rayon (RY) (Liu *et al.*, 2019).

All the studies presented above demonstrate the presence of plastic pollution in the air around an urban environment with a high population level and a few possible industrial sources of plastic pollution. However, current research shows the presence of MPs in areas far from any human activity. MPs were found in a remote, pristine mountain (France Pyrenees) that reached  $365 \pm 69$  particles/m<sup>2</sup>/day with size range from 25 to 2 600  $\mu$ m (Allen *et al.*, 2019). Predominant type of plastic founded in this location was PS, PE and PP. Based on this study, it was estimated that MPs were transported through the atmosphere over a distance up to 95 km. MPs have been found even in the last pristine environments on the globe (Arctic) (Bergmann *et al.*, 2019). The study in the Arctic was focused on the investigation of the transport of MPs through atmosphere by analyzing snow samples from ice floes (Frame Strait). The authors also analyzed samples from remote (Swiss Alps) and urbanized (Bremen, Bavaria) European sites. They established concentration for arctic snow between 0 and  $14.4 \times 10^3$  particles/L which is significantly lower than European snow ( $0.19 \times 10^3$  to  $154 \times 10^3$  particles/L). The composition of detected particles was very variable: for European samples highest abundances were registered for PA, varnish, rubber type 3, nitrile rubber, EVA, and PE, whereas PS, PVC, PC, PA and polylactic acid (PLA) have been detected for arctic snow.

Moreover, suspended atmospheric MPs were found in the open ocean environment of South China Sea and East Indian Ocean with concentration  $0.8 \pm 1.3$  items/100 m<sup>3</sup> and

$0.4 \pm 0.6$  items/100 m<sup>3</sup> respectively (Wang *et al.*, 2020). Particles identified were made by PET, PP, poly (ethylene-co-vinyl acetate) (PEVA), poly(ethylene-co-propylene) (PEP), poly(acrylonitrile-co-acrylic acid) (PAN-AA), phenoxy resin (PR). Based on the results of this study plastic particles were found to be transported over 1 000 km from their potential source.

Recent work by Materić *et al.*, reported for the first time NPs occurrences in the snow samples from remote Austrian Alps. These NPs were presented by PET, PVC, and polypropylene carbonate (PPC).

All this evidence of the ubiquitous presence of plastic in the environment raises a huge concern on the exposure of living organisms and possible negative effects.

## **I.4. Interaction of MPs and NPs with living organisms**

### **I.4.1. Inclusion in the trophic chain**

Small size and widespread accumulation of plastic in all environment compartments make them easily bioavailable for ingestion by living organisms. The presence of MPs in living organisms is well studied and show that they are present in a wide variety of organisms and can be found in organisms through ingestion, ranging from zooplankton to marine mammals (Phuong *et al.*, 2016; Peng *et al.*, 2020).

MPs particles were found to be ingested by different types of zooplankton (Cole *et al.*, 2013; Desforges, Galbraith and Ross, 2015; Kosore *et al.*, 2018); benthic organisms such as sea cucumbers (Graham and Thompson, 2009); corals (Hall *et al.*, 2015); bivalves such as blue mussel (Van Cauwenberghe *et al.*, 2015), oysters (Van Cauwenberghe and Janssen, 2014); crustaceans (Murray and Cowie, 2011); shrimp (Devriese *et al.*, 2015); polychaetes (Mathalon and Hill, 2014; Van Cauwenberghe *et al.*, 2015; Revel *et al.*, 2018); fish (Boerger *et al.*, 2010; Lusher *et al.*, 2013). There are many birds from all over the world in the body of which were found plastic fragments (Bond *et al.*, 2014; Wilcox *et al.*, 2015; Nicastro *et al.*, 2018).

Ingestion of MPs has also been reported for mammals, such as seals (Bravo Rebolledo *et al.*, 2013), whale ball (Besseling *et al.*, 2015), whale sharks (Yong *et al.*, 2021).

The uptake of plastic particles by living organisms occurs in two ways: direct and indirect ingestion. The latter occurs as a result of ingestion of contaminated living organisms of a lower trophic level. Information on the transfer of plastic by trophic chain in a wild remains unknown. However, laboratory studies confirm plastic transfer from contaminated prey to



predator along the trophic chain. MPs transfer has been registered from mussels to crabs (Farrell and Nelson, 2013); from copepods to jellyfish (Costa *et al.*, 2020); from mackerel to grey seals (Nelms *et al.*, 2018).

Evidence of the transfer of plastic through the food chain is a great concern for human health. There are many bivalves (oysters, mussels, clams etc.) reported for MPs and NPs ingestion. It has been estimated that annual exposure to MPs through bivalves' consumption for Europeans is above 11 000 microplastics/person (Van Cauwenberghe and Janssen, 2014).

Human exposure to microplastics and nanoplastics can occur in three ways: ingestion, inhalation, and dermal contact (Revel *et al.*, 2018; Prata *et al.*, 2020). Moreover, plastic has been found in the human body, including the lungs (Pauly *et al.*, 1998), digestive system (Smith *et al.*, 2018), and stool (Schwabl *et al.*, 2019).

The impact of MPs and NPs (MNPs) can have two origins: the plastic particles itself or potential chemicals that are related to plastic (additives and pollutant adsorbed from environment).

#### **I.4.2. Toxicity of chemicals related to plastic**

The toxicity of MNPs for aquatic organisms can be related to chemical additives (Bisphenol-A, Phthalates and other) in plastic materials. These chemicals are added to plastics to provide particular properties, such as flexibility, hardness, colour, etc. As additives are not chemically bound to the polymer matrix, they tend to leach from plastic materials to the surrounding environment (water, sediments, soil, living organism). With undergoing degradation processes and losing plastic integrity, the release of plastic additives will be even faster. Eventually additives can cause dangerous disruption of the endocrine system of marine mammals, inhibition of reproduction and reduction of some species (Meeker *et al.*, 2009; Thompson *et al.*, 2009).

Another potential threat is the adsorption of hydrophobic chemicals from water to MPs already present in marine waters (Teuten *et al.*, 2009). The example of such hazardous chemicals is PCBs (Polychlorinated biphenyls), PAHs (polyaromatic hydrocarbons), and DDT (dichlorodiphenyltrichloroethane). These chemicals are a group of Persistent organic pollutants (POPs), which are resistant to environmental degradation and have the ability to bioaccumulate (Laender *et al.*, 2011). They are dangerous toxic compounds with a broad spectrum of activity including endocrine disruption, cancer, and mutations (Rios *et al.*, 2007). Once in the

gastrointestinal tract with pieces of plastic debris, these substances can pass and accumulate in body tissues. Having the ability to bioaccumulation, they represent a high risk in the trophic chain. This means that their concentration increases with every step of the natural food chain. This is a threat not only to marine organisms but also to representatives of terrestrial life, including the human organism (Laender *et al.*, 2011).

#### **I.4.3. Physical effect and toxicity of MPs and NPs**

Getting into the body, MPs and NPs can cause a number of negative physical effects: blockages of the digestive system, which can lead to satiation, starvation and physical deterioration; abrasions (internal or external) and ulcers; blockage of gastric enzyme production; nutrient dilution; reduced growth rates. MPs accumulation in the gastrointestinal tract can cause a feeling of satiety, whereas, in reality, the body is starving (Wright *et al.*, 2013).

Recent studies on the effects of MNPs on marine and freshwater living organisms have shown that the smaller particles easily penetrate living tissue (Browne *et al.*, 2008; Lu *et al.*, 2016) and cells, and cause a higher effect (Rist *et al.*, 2017). Among adverse effects were observed changes in behaviour, feeding activity (Besseling *et al.*, 2013; Kaposi *et al.*, 2014), growth, decrease of reproduction (Lee *et al.*, 2019), and mortality (Lei *et al.*, 2018). MNPs in the organism cause inflammation, oxidative stress (von Moos *et al.*, 2012; Lu *et al.*, 2016; Qiao *et al.*, 2019), changes in energy metabolism (Hall *et al.*, 2015; Van Cauwenberghe *et al.*, 2015).

#### **I.4.4. Particular interaction of MPs and NPs in the aquatic environment**

Microorganisms and small invertebrates can colonize the surface of plastic particles. Such a phenomenon can be a threat since the geographical transfer of microorganisms can lead to the introduction of pathogenic species into new environment where local species are not equipped to defend themselves (Oberbeckmann *et al.*, 2015). Another biological effect is the ability of microorganisms to form a biofilm on the surface of plastic particles. This process can change the physical properties of plastic by reducing the hydrophobicity of its surface. As a result, adsorption of toxic pollutants to the plastic particles surface from the aquatic environment could be increased (Bhagwat *et al.*, 2021). In addition, biofilm contributes to an increase in the density of plastic particles, leading to the sinking of them which may result in sedimentation in benthic regions (Ziajahromi *et al.*, 2018). However, the density of the plastic particles can also rise up due to the biofouling, and particles can move to the surface of the water (Ye and Andrady, 1991; Rummel *et al.*, 2017). Chapter III of this manuscript reveals in

more detail the main aspects of the mechanism of interaction between MPs and microorganisms.

## **I.5. Study of plastic pollution in the environment**

### **I.5.1. Sampling and preparation of MPs and NPs prior to analysis**

Methodology of sample collection depend on the nature of the studies environmental compartment and goal of the sampling. Sampling methods can be divided in three group including selective, volume-reduced, and bulk sampling (Crawford and Quinn, 2017a).

Selective sampling is based on the collection of plastic items directly from surface of water or sediment directly at the sampling site. This method usually applies to plastic particles that are visible to naked eye and have size above 1 mm (Hidalgo-Ruz *et al.*, 2012).

Volume-reduced sampling is applied to water and sediments at sampling stage. For instance, collection of plastic particles from water achieved by different types of net: metal, neuston, plankton, bongo, etc. For sediments is usually used sieves with different mesh aperture.

Unlike the above-described methods, bulk sampling is more reliable because it contains whole volume of the samples without previous separation of particles from it. This method reduces the risk of losing all fractions of plastics present in the samples and limits potential misinterpretation.

After sample collection volume-reduced and bulk samples undergo processing step to extract plastic particles from natural matrix by visual sorting, sieving, density separation, filtration, digestion (Hidalgo-Ruz *et al.*, 2012; Campanale *et al.*, 2020).

Chapter IV of this manuscript reveals the basic approaches and methods used to sample MPs and NPs from the atmosphere.

### **I.5.2. Characterization of MPs and NPs from environment samples**

Many approaches have been used to characterize plastic particles in the environment, from observation with the naked eye to the use of advanced analytical methods.

Naked eye sorting of plastic includes manual separation of plastic particles from the samples and its future analysis by weight, size, shape, and colour. The optimal lower size limit that can be accessed using this approach is 1 mm. This method is cheap, easy to implement but

has limited accuracy, as there is high risk that particles can be mistakenly considered as plastic (Primpke *et al.*, 2020).

Next well-known approach based on the visual observation is microscopy analysis of particles using microscopic (40× to 1000×) or stereoscopic (20× to 50×) magnification. This type of analysis is giving information about the size, shape and colour of particles, but no chemical composition. This method is cheap, easy to use, adopted to remote field trip work (e.g., expeditions) but like the naked eye observation has limited reliability. The size limit of identification is 100 µm (Primpke *et al.*, 2020; Phuong *et al.*, 2021).

These visual observation approaches are a good pre-treatment of the sample and preselection of suspected particles to be a plastic, but they require additional use of more advanced approaches to identify chemical nature of these particles.

Spectroscopic analytical methods such as Fourier transform infrared (FTIR) and Raman spectroscopy, and its versions coupled to microscopy (µFTIR and µRaman) have become the most used in the analysis of microplastic particles. These methods are classified as non-discursive and allow obtaining information on particles morphological characteristic (e.g., size, colour, shape, etc.) and its chemical composition, along with determining the number of particles (Huppertsberg and Knepper, 2018). These techniques are efficient for analyzing particles down to 10-20µm with µFTIR and down to 1 µm using µRaman (Schwaferts *et al.*, 2019). They are therefore not adapted for the nanoscale particles analysis.

Thermoanalytical methods like pyrolysis coupled with gas chromatography-mass spectrometry (Py-GC-MS) and thermal extraction desorption-gas chromatography-mass spectrometry (TED-GC-MS) are destructive methods that are based on the decomposition of solid samples into volatile compounds that are separated by gas chromatography and identified by mass spectrometry (Yakovenko *et al.*, 2020). These methods provide information on the chemical composition of particles and mass (µg/L) of identified compounds in it (polymer, additives, etc.), while information on particles number, size, and colour remain unexplored. However, there is no particles size limitation for this analysis and both micro- and nanoplastic particles can be identified. Another advantage in using thermoanalytical methods it that they can detect several polymer types in a single run, with very little sample preparation.

All these methods have their advantages and disadvantages, but their use as complementary techniques is very encouraging and can provide better understanding of plastics as a pollutant.

### **I.5.3. Relevance of MPs and NPs models in laboratory study**

Scientists around the world are trying to answer questions about the potential negative effects of MPs and NPs on living organisms. Therefore, many studies have been conducted under laboratory conditions to understand uptake, transport and translocation in tissues and organs, as well as excretion of plastic from living organisms (Thomas *et al.*, 2021). Some studies have focused on the bioaccumulation and biomagnification of plastic and its associated chemicals along the trophic chain (Miller *et al.*, 2020). The laboratory study of all these processes raises many questions about the consistency and reliability of laboratory conditions as compared to the environment (Phuong *et al.*, 2016).

There are many factors that have significant influences on the results of such studies. First, these are exposure conditions that include representatives of the habitat of the target living organism. It is very important to reproduce the environmental conditions of the matrix/media in which the experiment is conducted. Such condition includes temperature, illumination, aeration, pH, salinity, duration of exposure, period of organism life cycle (e.g., reproduction), concentration of plastic, etc.

The second key exposure factor is the plastic model used. Morphological, physical, and chemical properties of used plastic model should be as consistent as possible with the characteristics of plastic in the environment. Ensuring a high level of consistency between laboratory exposure and the environment is still a major challenge. Most of the completed works published are based on the use of a commercially manufactured model of micro- and nanoplastic particles in the form of regular spheres or beads (often found as microbeads/microspheres and nanobeads/nanospheres) (Phuong *et al.*, 2016). The most used types of microbeads for exposure are PS and PE, less frequently PP and PVC. Among studies with nanoplastic, PS is the predominant polymer type (Kokalj *et al.*, 2021). These particles have a regular shape, uniform size, and specific physicochemical properties. For example, PS nanobeads are characterized by a variety of functional amino, carboxyl, and hydroxyl groups on their surface that provides particles with positive or negative surface charge as well effecting particles hydrophobicity. All these parameters have a strong influence on particles interaction with living organisms, and what kind of adverse effect they will cause.

In the environment, plastic particles have a variety of sizes, shapes, and very diverse complex physical and chemical properties, which are still not fully understood. Thus, the use

of commercial plastic models for ecotoxicological study has a high risk of false, unreliable, over, or underestimated results on the impact of plastic on living organisms.

It is important to note that even if NPs are the product of MPs fragmentation, they do not possess the same properties. Their behaviour in the environment may be very different from that of MPs or engineered nanomaterials, which are often used in ecotoxicological studies as model NPs (Gigault *et al.*, 2021; Mitrano *et al.*, 2021). Recent work by Gigault *et al.*, highlighted six main characteristics of NPs that distinguish it from MPs, and two characteristic that distinguish it from engineered nanomaterials. These characteristics include: 1) brownian motion, which is characterized by the random movement of NPs in a suspended medium; 2) departure from the geometric/ray approximation between light and matter; 3) a high proportion of molecules adsorbed on the surface resulting in high surface interactions as compared to physical interactions; 4) size compatible with environmental macromolecules that resulting in adsorption and heteroaggregation; 5) extremely small size that allows NPs bio-uptake and translocation in the tissues of living organisms; 6) short length scale that will facilitate release of plastic additives or other not chemically bonded substances; 7) heterogeneity in size, shape; 8) fast fragmentation as a result of influence of environment factors (Gigault *et al.*, 2021).

To overcome this gap in knowledge recent research focuses on the development of relevant environmental model of micro- and especially nanoplastic. A part of this thesis is aimed at producing of such micro- and nanoplastic model (See Chapter II) and at evaluating some of their effects on living organisms (microalgae, see Chapter III).

## **Conclusion**

Plastic is an integral part of almost all the necessary goods of our life and one of the most demanded and produced material of our time. At the end of their lifetime, used plastics form millions of tons of waste that are poorly managed. As a result, plastic accumulates in the environment and disseminates between environmental compartments by means of the winds, rains, surface, and ground waters. Plastic has become a ubiquitous contaminant on our planet, which characterized by a variety of size from mega to nanoscale. Small plastic particles such as MPs and NPs are bioavailable for a wide number of living organisms from zooplankton to mammals, which cause a huge concern about the negative effect of plastic on the entire trophic chain. Thus, a better understanding of the occurrence, fate, and behaviour of plastic in the environment is required.

This PhD work aimed at finding a better understanding of MPs and NPs pollution in the environment. Thee vectors of investigation were combined in this study, including: 1) the development of a methodology of sampling and analysis of MPs and NPs from the atmosphere; 2) the development of an environmentally relevant model of MPs and NPs, which could be used for ecotoxicological studies and 3) the study of its interaction with living microorganisms.

## References

- Akdogan, Z. and Guven, B. (2019) 'Microplastics in the environment: A critical review of current understanding and identification of future research needs', *Environmental Pollution*, 254, p. 113011. doi:10.1016/j.envpol.2019.113011.
- Allen, S. *et al.* (2019) 'Atmospheric transport and deposition of microplastics in a remote mountain catchment', *Nature Geoscience*, 12(5), pp. 339–344. doi:10.1038/s41561-019-0335-5.
- Ammala, A. *et al.* (2011) 'An overview of degradable and biodegradable polyolefins', *Progress in Polymer Science*, 36(8), pp. 1015–1049. doi:10.1016/j.progpolymsci.2010.12.002.
- Andrady, A.L. and Neal, M.A. (2009) 'Applications and societal benefits of plastics', *Philosophical transactions of the Royal Society of London. Series B, Biological sciences*, 364(1526), pp. 1977–1984. doi:10.1098/rstb.2008.0304.
- Bahl, S. *et al.* (2021) 'Biodegradation of plastics: A state of the art review', *International Conference on Advanced Materials and Modern Manufacturing*, 39, pp. 31–34. doi:10.1016/j.matpr.2020.06.096.
- van den Berg, P. *et al.* (2020) 'Sewage sludge application as a vehicle for microplastics in eastern Spanish agricultural soils', *Environmental Pollution*, 261, p. 114198. doi:10.1016/j.envpol.2020.114198.
- Bergmann, M. *et al.* (2019) 'White and wonderful? Microplastics prevail in snow from the Alps to the Arctic', *Science advances*, 5(8), p. eaax1157. doi:10.1126/sciadv.aax1157.
- Besseling, E. *et al.* (2013) 'Effects of Microplastic on Fitness and PCB Bioaccumulation by the Lugworm *Arenicola marina* (L.)', *Environmental Science & Technology*, 47(1), pp. 593–600. doi:10.1021/es302763x.
- Besseling, E. *et al.* (2015) 'Microplastic in a macro filter feeder: Humpback whale *Megaptera novaeangliae*', *Marine Pollution Bulletin*, 95(1), pp. 248–252. doi:10.1016/j.marpolbul.2015.04.007.
- Bhagwat, G. *et al.* (2021) 'Biofilms Enhance the Adsorption of Toxic Contaminants on Plastic Microfibers under Environmentally Relevant Conditions', *Environmental Science & Technology*, 55(13), pp. 8877–8887. doi:10.1021/acs.est.1c02012.
- Boerger, C.M. *et al.* (2010) 'Plastic ingestion by planktivorous fishes in the North Pacific Central Gyre', *Marine Pollution Bulletin*, 60(12), pp. 2275–2278. doi:10.1016/j.marpolbul.2010.08.007.
- Bond, A.L. *et al.* (2014) 'Plastic ingestion by fulmars and shearwaters at Sable Island, Nova Scotia, Canada', *Marine Pollution Bulletin*, 87(1), pp. 68–75. doi:10.1016/j.marpolbul.2014.08.010.
- Bravo Rebolledo, E.L. *et al.* (2013) 'Plastic ingestion by harbour seals (*Phoca vitulina*) in The Netherlands', *Marine Pollution Bulletin*, 67(1), pp. 200–202. doi:10.1016/j.marpolbul.2012.11.035.



- Browne, M.A. *et al.* (2008) 'Ingested Microscopic Plastic Translocates to the Circulatory System of the Mussel, *Mytilus edulis* (L.)', *Environmental Science & Technology*, 42(13), pp. 5026–5031. doi:10.1021/es800249a.
- Cai, L. *et al.* (2017) 'Characteristic of microplastics in the atmospheric fallout from Dongguan city, China: preliminary research and first evidence', *Environmental Science and Pollution Research*, 24(32), pp. 24928–24935. doi:10.1007/s11356-017-0116-x.
- Campanale, C. *et al.* (2020) 'A Practical Overview of Methodologies for Sampling and Analysis of Microplastics in Riverine Environments', *Sustainability*, 12(17). doi:10.3390/su12176755.
- Carpenter, E.J. *et al.* (1972) 'Polystyrene spherules in coastal waters', *Science*, 178(4062), pp. 749–750. doi:10.1126/science.178.4062.749.
- Chalmin, P. (2019) *The history of plastics: from the Capitol to the Tarpeian Rock*. Facts Reports 19. Institut Veolia, pp. 6–11. Available at: <https://journals.openedition.org/factsreports/5071> (Accessed: 27 October 2021).
- Chapman, P.M. and Wang, F. (2001) 'Assessing sediment contamination in estuaries', *Environmental Toxicology and Chemistry: An International Journal*, 20(1), pp. 3–22. doi:10.1002/etc.5620200102.
- Claessens, M. *et al.* (2011) 'Occurrence and distribution of microplastics in marine sediments along the Belgian coast', *Marine Pollution Bulletin*, 62(10), pp. 2199–2204. doi:10.1016/j.marpolbul.2011.06.030.
- Cole, M. *et al.* (2011) 'Microplastics as contaminants in the marine environment: A review', *Marine Pollution Bulletin*, 62(12), pp. 2588–2597. doi:10.1016/j.marpolbul.2011.09.025.
- Cole, M. *et al.* (2013) 'Microplastic Ingestion by Zooplankton', *Environmental Science & Technology*, 47(12), pp. 6646–6655. doi:10.1021/es400663f.
- Collignon, A. *et al.* (2014) 'Annual variation in neustonic micro- and meso-plastic particles and zooplankton in the Bay of Calvi (Mediterranean–Corsica)', *Marine Pollution Bulletin*, 79(1), pp. 293–298. doi:10.1016/j.marpolbul.2013.11.023.
- Colton, J.B., Burns, B.R. and Knapp, F.D. (1974) 'Plastic Particles in Surface Waters of the Northwestern Atlantic', *Science*, 185(4150), pp. 491–497. doi:10.1126/science.185.4150.491.
- Costa, E. *et al.* (2020) 'Trophic Transfer of Microplastics From Copepods to Jellyfish in the Marine Environment', *Frontiers in Environmental Science*, 8, p. 158. doi:10.3389/fenvs.2020.571732.
- Costa, M.F. *et al.* (2010) 'On the importance of size of plastic fragments and pellets on the strandline: a snapshot of a Brazilian beach', *Environmental monitoring and assessment*, 168(1), pp. 299–304. doi:10.1007/s10661-009-1113-4.
- Crawford, C.B. and Quinn, B. (2017a) 'Microplastic collection techniques', in Crawford, C.B. and Quinn, B. (eds) *Microplastic Pollutants*. Elsevier Science: Amsterdam, The Netherland. Elsevier, pp. 179–202. doi:10.1016/B978-0-12-809406-8.00008-6.

Crawford, C.B. and Quinn, B. (2017b) 'Plastic production, waste and legislation', in Crawford, C.B. and Quinn, B. (eds) *Microplastic Pollutants*. Elsevier Science: Amsterdam, The Netherlands. Elsevier, pp. 39–56. doi:10.1016/B978-0-12-809406-8.00003-7.

De Falco, F. *et al.* (2019) 'The contribution of washing processes of synthetic clothes to microplastic pollution', *Scientific Reports*, 9(1), p. 6633. doi:10.1038/s41598-019-43023-x.

Desforges, J.-P.W., Galbraith, M. and Ross, P.S. (2015) 'Ingestion of Microplastics by Zooplankton in the Northeast Pacific Ocean', *Archives of Environmental Contamination and Toxicology*, 69(3), pp. 320–330. doi:10.1007/s00244-015-0172-5.

Devriese, L.I. *et al.* (2015) 'Microplastic contamination in brown shrimp (*Crangon crangon*, Linnaeus 1758) from coastal waters of the Southern North Sea and Channel area', *Marine Pollution Bulletin*, 98(1–2), pp. 179–187. doi:10.1016/j.marpolbul.2015.06.051.

Dris, R. *et al.* (2016) 'Synthetic fibers in atmospheric fallout: A source of microplastics in the environment?', *Marine Pollution Bulletin*, 104(1), pp. 290–293. doi:10.1016/j.marpolbul.2016.01.006.

EPA US (2016) *White Paper: A Summary of the Literature on the Chemical Toxicity of Plastics Pollution on Aquatic Life and Aquatic-Dependent Wildlife*, United State Environmental Protection Agency. Available at: <https://www.epa.gov/wqc/white-paper-summary-literature-chemical-toxicity-plastics-pollution-aquatic-life-and-aquatic> (Accessed: 17 October 2021).

Eriksen, M. *et al.* (2013) 'Plastic pollution in the South Pacific subtropical gyre', *Marine Pollution Bulletin*, 68(1), pp. 71–76. doi:10.1016/j.marpolbul.2012.12.021.

Eriksen, M. *et al.* (2014) 'Plastic pollution in the world's oceans: more than 5 trillion plastic pieces weighing over 250,000 tons afloat at sea', *PLOS ONE*, 9(12), p. e111913. doi:10.1371/journal.pone.0111913.

European Commission (2011) *Plastic waste: Ecological and human health impacts*. Science for environment policy in-Depth Report. Directorate General environment news alert service. Available at: [https://ec.europa.eu/environment/integration/research/newsalert/indepth\\_reports.htm](https://ec.europa.eu/environment/integration/research/newsalert/indepth_reports.htm).

Farrell, P. and Nelson, K. (2013) 'Trophic level transfer of microplastic: *Mytilus edulis* (L.) to *Carcinus maenas* (L.)', *Environmental Pollution*, 177, pp. 1–3. doi:10.1016/j.envpol.2013.01.046.

Fried, J.R. (2014) *Polymer science and technology*. Third Edition. Prentice Hall. Available at: <http://ptgmedia.pearsoncmg.com/images/9780137039555/samplepages/9780137039555.pdf>.

Gasperi, J. *et al.* (2018) 'Microplastics in air: Are we breathing it in?', *Micro and Nanoplastics Edited by Dr. Teresa A.P. Rocha-Santos*, 1, pp. 1–5. doi:10.1016/j.coesh.2017.10.002.

GESAMP (2015) *Sources, fate and effects of microplastics in the marine environment: a global assessment*. 90, p. 98. Available at: <http://www.gesamp.org/publications/reports-and-studies-no-90> (Accessed: 17 October 2021).

Geyer, R., Jambeck, J.R. and Law, K.L. (2017) 'Production, use, and fate of all plastics ever made', *Science Advances*, 3(7), p. e1700782. doi:10.1126/sciadv.1700782.

Ghosh, S.K., Pal, S. and Ray, S. (2013) 'Study of microbes having potentiality for biodegradation of plastics', *Environmental Science and Pollution Research*, 20(7), pp. 4339–4355. doi:10.1007/s11356-013-1706-x.

Gigault, J. *et al.* (2018) 'Current opinion: What is a nanoplastic?', *Environmental Pollution*, 235, pp. 1030–1034. doi:10.1016/j.envpol.2018.01.024.

Gigault, J. *et al.* (2021) 'Nanoplastics are neither microplastics nor engineered nanoparticles', *Nature Nanotechnology*, 16(5), pp. 501–507. doi:10.1038/s41565-021-00886-4.

Goldstein, M.C., Titmus, A.J. and Ford, M. (2013) 'Scales of Spatial Heterogeneity of Plastic Marine Debris in the Northeast Pacific Ocean', *PLOS ONE*, 8(11), p. e80020. doi:10.1371/journal.pone.0080020.

Graham, E.R. and Thompson, J.T. (2009) 'Deposit- and suspension-feeding sea cucumbers (Echinodermata) ingest plastic fragments', *Journal of Experimental Marine Biology and Ecology*, 368(1), pp. 22–29. doi:10.1016/j.jembe.2008.09.007.

Gregory, M.R. and Ryan, P.G. (1997) 'Pelagic Plastics and Other Seaborne Persistent Synthetic Debris: A Review of Southern Hemisphere Perspectives', in Coe, J.M. and Rogers, D.B. (eds) *Marine Debris: Sources, Impacts, and Solutions*. New York, NY: Springer (Springer Series on Environmental Management), pp. 49–66. doi:10.1007/978-1-4613-8486-1\_6.

Hall, N.M. *et al.* (2015) 'Microplastic ingestion by scleractinian corals', *Marine Biology*, 162(3), pp. 725–732. doi:10.1007/s00227-015-2619-7.

Hartmann, N.B. *et al.* (2019) 'Are We Speaking the Same Language? Recommendations for a Definition and Categorization Framework for Plastic Debris', *Environmental Science & Technology*, 53(3), pp. 1039–1047. doi:10.1021/acs.est.8b05297.

Hidalgo-Ruz, V. *et al.* (2012) 'Microplastics in the Marine Environment: A Review of the Methods Used for Identification and Quantification', *Environmental Science & Technology*, 46(6), pp. 3060–3075. doi:10.1021/es2031505.

Hidalgo-Ruz, V. and Thiel, M. (2013) 'Distribution and abundance of small plastic debris on beaches in the SE Pacific (Chile): A study supported by a citizen science project', *Marine Environmental Research*, 87–88, pp. 12–18. doi:10.1016/j.marenvres.2013.02.015.

Hopewell, J., Dvorak, R. and Kosior, E. (2009) 'Plastics recycling: challenges and opportunities', *Philosophical transactions of the Royal Society of London. Series B, Biological sciences*, 364(1526), pp. 2115–2126. doi:10.1098/rstb.2008.0311.

Horton, A.A. *et al.* (2017) 'Microplastics in freshwater and terrestrial environments: Evaluating the current understanding to identify the knowledge gaps and future research priorities', *Science of The Total Environment*, 586, pp. 127–141. doi:10.1016/j.scitotenv.2017.01.190.

Huang, Y. *et al.* (2020) 'Agricultural plastic mulching as a source of microplastics in the terrestrial environment', *Environmental Pollution*, 260, p. 114096. doi:10.1016/j.envpol.2020.114096.

Huppertsberg, S. and Knepper, T.P. (2018) 'Instrumental analysis of microplastics—benefits and challenges', *Analytical and Bioanalytical Chemistry*, 410(25), pp. 6343–6352. doi:10.1007/s00216-018-1210-8.

Hurley, R. *et al.* (2020) 'Plastic waste in the terrestrial environment', in *Plastic Waste and Recycling*, pp. 163–193. doi:10.1016/B978-0-12-817880-5.00007-4.

Industry Canada (2012) 'Understanding green claims: a consumer's guide to common environmental labels and claims in Canada.' Available at: [http://epe.lac-bac.gc.ca/100/201/301/weekly\\_checklist/2012/internet/w12-24-U-E.html/collections/collection\\_2012/ic/Iu23-36-2012-eng.pdf](http://epe.lac-bac.gc.ca/100/201/301/weekly_checklist/2012/internet/w12-24-U-E.html/collections/collection_2012/ic/Iu23-36-2012-eng.pdf) (Accessed: 15 October 2021).

Jambeck, J.R. *et al.* (2015) 'Plastic waste inputs from land into the ocean', *Science*, 347(6223), pp. 768–771. doi:10.1126/science.1260352.

Kaposi, K.L. *et al.* (2014) 'Ingestion of microplastic has limited impact on a marine larva', *Environmental Science & Technology*, 48(3), pp. 1638–1645. doi:10.1021/es404295e.

Kaza, S. *et al.* (2018) *What a Waste 2.0: A Global Snapshot of Solid Waste Management to 2050*. Washington, DC: World Bank. doi:10.1596/978-1-4648-1329-0.

Khordagui, H.K. and Abu-Hilal, A.H. (1994) 'Industrial plastic on the southern beaches of the Arabian Gulf and the western beaches of the Gulf of Oman', *Environmental Pollution*, 84(3), pp. 325–327. doi:10.1016/0269-7491(94)90143-0.

Klein, M. and Fischer, E.K. (2019) 'Microplastic abundance in atmospheric deposition within the Metropolitan area of Hamburg, Germany', *Science of The Total Environment*, 685, pp. 96–103. doi:10.1016/j.scitotenv.2019.05.405.

Koelmans, A.A., Besseling, E. and Shim, W.J. (2015) 'Nanoplastics in the Aquatic Environment. Critical Review', in Bergmann, M., Gutow, L., and Klages, M. (eds) *Marine Anthropogenic Litter*. Cham: Springer International Publishing, pp. 325–340. doi:10.1007/978-3-319-16510-3\_12.

Kokalj, A.J. *et al.* (2021) 'Quality of nanoplastics and microplastics ecotoxicity studies: Refining quality criteria for nanomaterial studies', *Journal of Hazardous Materials*, 415, p. 125751. doi:10.1016/j.jhazmat.2021.125751.

Kole, P.J. *et al.* (2017) 'Wear and tear of tyres: a stealthy source of microplastics in the environment', *International journal of environmental research and public health*, 14(10), p. 1265. doi:10.3390/ijerph14101265.

Kosore, C. *et al.* (2018) 'Occurrence and ingestion of microplastics by zooplankton in Kenya's marine environment: first documented evidence', *African Journal of Marine Science*, 40(3), pp. 225–234. doi:10.2989/1814232X.2018.1492969.

Laender, F.D. *et al.* (2011) 'Combining Monitoring Data and Modeling Identifies PAHs as Emerging Contaminants in the Arctic', *Environmental Science & Technology*, 45(20), pp. 9024–9029. doi:10.1021/es202423f.

Law, K.L. *et al.* (2010) 'Plastic accumulation in the North Atlantic subtropical gyre', *Science (New York, N.Y.)*, 329(5996), pp. 1185–1188. doi:10.1126/science.1192321.

- Lebreton, L. *et al.* (2018) 'Evidence that the Great Pacific Garbage Patch is rapidly accumulating plastic', *Scientific Reports*, 8(1), p. 4666. doi:10.1038/s41598-018-22939-w.
- Lee, W.S. *et al.* (2019) 'Bioaccumulation of polystyrene nanoplastics and their effect on the toxicity of Au ions in zebrafish embryos', *Nanoscale*, 11(7), pp. 3173–3185. doi:10.1039/C8NR09321K.
- Lei, L. *et al.* (2018) 'Microplastic particles cause intestinal damage and other adverse effects in zebrafish *Danio rerio* and nematode *Caenorhabditis elegans*', *The Science of the Total Environment*, 619–620, pp. 1–8. doi:10.1016/j.scitotenv.2017.11.103.
- Leslie, H.A. (2015) *Plastic in Cosmetics: Are we polluting the environment through our personal care? Plastic ingredients that contribute to marine microplastic litter*. United Nations Environment Programme (UNEP), p. 38. Available at: <https://www.openchannels.org/sites/default/files/literature/Plastic%20in%20Cosmetics%20Are%20We%20Polluting%20the%20Environment%20Through%20our%20Personal%20Care%20Plastic%20ingredients%20that%20contribute%20to%20marine%20microplastic%20litter.pdf> (Accessed: 16 October 2021).
- Liffmann, M. and Boogaerts, L. (1997) 'Linkages Between Land-Based Sources of Pollution and Marine Debris', in Coe, J.M. and Rogers, D.B. (eds) *Marine Debris: Sources, Impacts, and Solutions*. New York, NY: Springer (Springer Series on Environmental Management), pp. 359–366. doi:10.1007/978-1-4613-8486-1\_33.
- Lindeque, P.K. *et al.* (2020) 'Are we underestimating microplastic abundance in the marine environment? A comparison of microplastic capture with nets of different mesh-size', *Environmental Pollution*, 265, p. 114721. doi:10.1016/j.envpol.2020.114721.
- Liu, K. *et al.* (2019) 'Accurate quantification and transport estimation of suspended atmospheric microplastics in megacities: Implications for human health', *Environment International*, 132, p. 105127. doi:10.1016/j.envint.2019.105127.
- Lu, Y. *et al.* (2016) 'Uptake and Accumulation of Polystyrene Microplastics in Zebrafish (*Danio rerio*) and Toxic Effects in Liver', *Environmental Science & Technology*, 50(7), pp. 4054–4060. doi:10.1021/acs.est.6b00183.
- Lusher, A.L. *et al.* (2014) 'Microplastic pollution in the Northeast Atlantic Ocean: Validated and opportunistic sampling', *Marine Pollution Bulletin*, 88(1), pp. 325–333. doi:10.1016/j.marpolbul.2014.08.023.
- Lusher, A.L., McHugh, M. and Thompson, R.C. (2013) 'Occurrence of microplastics in the gastrointestinal tract of pelagic and demersal fish from the English Channel', *Marine Pollution Bulletin*, 67(1), pp. 94–99. doi:10.1016/j.marpolbul.2012.11.028.
- Materić, D. *et al.* (2020) 'Micro- and Nanoplastics in Alpine Snow: A New Method for Chemical Identification and (Semi)Quantification in the Nanogram Range', *Environmental Science & Technology*, 54(4), pp. 2353–2359. doi:10.1021/acs.est.9b07540.
- Mathalon, A. and Hill, P. (2014) 'Microplastic fibers in the intertidal ecosystem surrounding Halifax Harbor, Nova Scotia', *Marine Pollution Bulletin*, 81(1), pp. 69–79. doi:10.1016/j.marpolbul.2014.02.018.

- Meeker, J.D., Sathyanarayana, S. and Swan, S.H. (2009) 'Phthalates and other additives in plastics: human exposure and associated health outcomes', *Philosophical transactions of the Royal Society of London. Series B, Biological sciences*, 364(1526), pp. 2097–2113. doi:10.1098/rstb.2008.0268.
- Miller, M.E., Hamann, M. and Kroon, F.J. (2020) 'Bioaccumulation and biomagnification of microplastics in marine organisms: a review and meta-analysis of current data', *PLOS ONE*, 15(10), p. e0240792. doi:10.1371/journal.pone.0240792.
- Millet, H. *et al.* (2018) 'The Nature of Plastics and Their Societal Usage', in *Plastics and the Environment*. Royal Society of Chemistry. Available at: <https://pubs.rsc.org/en/content/chapter/bk9781788013314-00001/978-1-78801-241-6> (Accessed: 16 October 2021).
- Mitrano, D.M., Wick, P. and Nowack, B. (2021) 'Placing nanoplastics in the context of global plastic pollution', *Nature Nanotechnology*, 16(5), pp. 491–500. doi:10.1038/s41565-021-00888-2.
- von Moos, N., Burkhardt-Holm, P. and Köhler, A. (2012) 'Uptake and Effects of Microplastics on Cells and Tissue of the Blue Mussel *Mytilus edulis* L. after an Experimental Exposure', *Environmental Science & Technology*, 46(20), pp. 11327–11335. doi:10.1021/es302332w.
- Murray, F. and Cowie, P.R. (2011) 'Plastic contamination in the decapod crustacean *Nephrops norvegicus* (Linnaeus, 1758)', *Marine pollution bulletin*, 62(6), pp. 1207–1217. doi:10.1016/j.marpolbul.2011.03.032.
- Napper, I.E. *et al.* (2015) 'Characterisation, quantity and sorptive properties of microplastics extracted from cosmetics', *Marine Pollution Bulletin*, 99(1), pp. 178–185. doi:10.1016/j.marpolbul.2015.07.029.
- Nelms, S.E. *et al.* (2018) 'Investigating microplastic trophic transfer in marine top predators', *Environmental Pollution*, 238, pp. 999–1007. doi:10.1016/j.envpol.2018.02.016.
- Nicastro, K.R. *et al.* (2018) 'Plastic ingestion in aquatic-associated bird species in southern Portugal', *Marine Pollution Bulletin*, 126, pp. 413–418. doi:10.1016/j.marpolbul.2017.11.050.
- Nizzetto, L., Futter, M. and Langaas, S. (2016) 'Are Agricultural Soils Dumps for Microplastics of Urban Origin?', *Environmental Science & Technology*, 50(20), pp. 10777–10779. doi:10.1021/acs.est.6b04140.
- Oberbeckmann, S. *et al.* (2015) 'Marine microplastic-associated biofilms – a review', *Environmental Chemistry*, 12(5), pp. 551–562. doi:10.1071/EN15069.
- Pauly, J.L. *et al.* (1998) 'Inhaled cellulosic and plastic fibers found in human lung tissue', *Cancer Epidemiology, Biomarkers & Prevention: A Publication of the American Association for Cancer Research, Cosponsored by the American Society of Preventive Oncology*, 7(5), pp. 419–428.
- Peng, L. *et al.* (2020) 'Micro- and nano-plastics in marine environment: Source, distribution and threats — A review', *Science of The Total Environment*, 698, p. 134254. doi:10.1016/j.scitotenv.2019.134254.

Phuong, N.N. *et al.* (2016) 'Is there any consistency between the microplastics found in the field and those used in laboratory experiments?', *Environmental Pollution*, 211, pp. 111–123. doi:10.1016/j.envpol.2015.12.035.

Phuong, N.N. *et al.* (2021) 'Highlights from a review of microplastics in marine sediments', *Science of The Total Environment*, 777, p. 146225. doi:10.1016/j.scitotenv.2021.146225.

Plastics Europe (2020) *Plastics - the Facts 2020*. Available at: <https://www.plasticseurope.org/en/resources/publications/4312-plastics-facts-2020> (Accessed: 16 October 2021).

Poulain, M. *et al.* (2019) 'Small Microplastics As a Main Contributor to Plastic Mass Balance in the North Atlantic Subtropical Gyre', *Environmental Science & Technology*, 53(3), pp. 1157–1164. doi:10.1021/acs.est.8b05458.

Prata, J.C. *et al.* (2020) 'Environmental exposure to microplastics: An overview on possible human health effects', *The Science of the Total Environment*, 702, p. 134455. doi:10.1016/j.scitotenv.2019.134455.

Primpke, S. *et al.* (2020) 'Critical Assessment of Analytical Methods for the Harmonized and Cost-Efficient Analysis of Microplastics', *Applied Spectroscopy*, 74(9), pp. 1012–1047. doi:10.1177/0003702820921465.

Qiao, R. *et al.* (2019) 'Microplastics induce intestinal inflammation, oxidative stress, and disorders of metabolome and microbiome in zebrafish', *Science of The Total Environment*, 662, pp. 246–253. doi:10.1016/j.scitotenv.2019.01.245.

Reddy, M.S. *et al.* (2006) 'Description of the small plastics fragments in marine sediments along the Alang-Sosiya ship-breaking yard, India', *Ecological and Management Implications on Seagrass Landscapes*, 68(3), pp. 656–660. doi:10.1016/j.ecss.2006.03.018.

Reisser, J. *et al.* (2013) 'Marine plastic pollution in waters around Australia: characteristics, concentrations, and pathways', *PLOS ONE*, 8(11), p. e80466. doi:10.1371/journal.pone.0080466.

Revel, M. *et al.* (2018) 'Accumulation and immunotoxicity of microplastics in the estuarine worm *Hediste diversicolor* in environmentally relevant conditions of exposure', *Environmental Science and Pollution Research*, 27(4), pp. 3574–3583. doi:10.1007/s11356-018-3497-6.

Revel, M., Châtel, A. and Mouneyrac, C. (2018) 'Micro(nano)plastics: A threat to human health?', *Micro and Nanoplastics Edited by Dr. Teresa A.P. Rocha-Santos*, 1, pp. 17–23. doi:10.1016/j.coesh.2017.10.003.

Rios, L.M., Moore, C. and Jones, P.R. (2007) 'Persistent organic pollutants carried by synthetic polymers in the ocean environment', *Marine Pollution Bulletin*, 54(8), pp. 1230–1237. doi:10.1016/j.marpolbul.2007.03.022.

Rist, S., Baun, A. and Hartmann, N.B. (2017) 'Ingestion of micro- and nanoplastics in *Daphnia magna*—Quantification of body burdens and assessment of feeding rates and reproduction', *Environmental pollution*, 228, pp. 398–407. doi:10.1016/j.envpol.2017.05.048.

Rochman, C.M. (2018) 'Microplastics research—from sink to source', *Science*, 360(6384), pp. 28–29. doi:10.1126/science.aar7734.

Rummel, C.D. *et al.* (2017) 'Impacts of Biofilm Formation on the Fate and Potential Effects of Microplastic in the Aquatic Environment', *Environmental Science & Technology Letters*, 4(7), pp. 258–267. doi:10.1021/acs.estlett.7b00164.

Schwabl, P. *et al.* (2019) 'Detection of various microplastics in human stool: a prospective case series', *Annals of internal medicine*, 171(7), pp. 453–457. doi:10.7326/M19-0618.

Schwaferts, C. *et al.* (2019) 'Methods for the analysis of submicrometer- and nanoplastic particles in the environment', *TrAC Trends in Analytical Chemistry*, 112, pp. 52–65. doi:10.1016/j.trac.2018.12.014.

van Sebille, E. *et al.* (2020) 'The physical oceanography of the transport of floating marine debris', *Environmental Research Letters*, 15(2), p. 023003. doi:10.1088/1748-9326/ab6d7d.

Shah, A.A. *et al.* (2008) 'Biological degradation of plastics: A comprehensive review', *Biotechnology Advances*, 26(3), pp. 246–265. doi:10.1016/j.biotechadv.2007.12.005.

Smith, M. *et al.* (2018) 'Microplastics in Seafood and the Implications for Human Health', *Current environmental health reports*, 5(3), pp. 375–386. doi:10.1007/s40572-018-0206-z.

Ter Halle, A. *et al.* (2017) 'Nanoplastic in the North Atlantic Subtropical Gyre', *Environmental Science & Technology*, 51(23), pp. 13689–13697. doi:10.1021/acs.est.7b03667.

Teuten, E.L. *et al.* (2009) 'Transport and release of chemicals from plastics to the environment and to wildlife', *Philosophical transactions of the royal society B, biological sciences*, 364(1526), pp. 2027–2045. doi:10.1098/rstb.2008.0284.

Thomas, P.J. *et al.* (2021) 'Resolving the effects of environmental micro- and nanoplastics exposure in biota: A knowledge gap analysis', *Science of The Total Environment*, 780, p. 146534. doi:10.1016/j.scitotenv.2021.146534.

Thompson, R.C. *et al.* (2009) 'Plastics, the environment and human health: current consensus and future trends', *Philosophical transactions of the royal society B, biological sciences*, 364(1526), pp. 2153–2166. doi:10.1098/rstb.2009.0053.

Van Cauwenberghe, L. *et al.* (2015) 'Microplastics are taken up by mussels (*Mytilus edulis*) and lugworms (*Arenicola marina*) living in natural habitats', *Environmental Pollution*, 199, pp. 10–17. doi:10.1016/j.envpol.2015.01.008.

Van Cauwenberghe, L. and Janssen, C.R. (2014) 'Microplastics in bivalves cultured for human consumption', *Environmental Pollution*, 193, pp. 65–70. doi:10.1016/j.envpol.2014.06.010.

Venrick, E.L. *et al.* (1973) 'Man-made Objects on the Surface of the Central North Pacific Ocean', *Nature*, 241(5387), pp. 271–271. doi:10.1038/241271a0.

Vianello, A. *et al.* (2013) 'Microplastic particles in sediments of Lagoon of Venice, Italy: First observations on occurrence, spatial patterns and identification', *Pressures, Stresses, Shocks and Trends in Estuarine Ecosystems*, 130, pp. 54–61. doi:10.1016/j.ecss.2013.03.022.



Wang, X. *et al.* (2020) 'Atmospheric microplastic over the South China Sea and East Indian Ocean: abundance, distribution and source', *Journal of Hazardous Materials*, 389, p. 121846. doi:10.1016/j.jhazmat.2019.121846.

Wilcox, C., Van Sebille, E. and Hardesty, B.D. (2015) 'Threat of plastic pollution to seabirds is global, pervasive, and increasing', *Proceedings of the national academy of sciences*, 112(38), pp. 11899–11904. doi:10.1073/pnas.1502108112.

Wong, C.S., Green, D.R. and Cretney, W.J. (1974) 'Quantitative Tar and Plastic Waste Distributions in the Pacific Ocean', *Nature*, 247(5435), pp. 30–32. doi:10.1038/247030a0.

Wright, S.L., Thompson, R.C. and Galloway, T.S. (2013) 'The physical impacts of microplastics on marine organisms: A review', *Environmental Pollution*, 178, pp. 483–492. doi:10.1016/j.envpol.2013.02.031.

Yakovenko, N., Carvalho, A. and ter Halle, A. (2020) 'Emerging use thermo-analytical method coupled with mass spectrometry for the quantification of micro(nano)plastics in environmental samples', *TrAC Trends in Analytical Chemistry*, 131, p. 115979. doi:10.1016/j.trac.2020.115979.

Ye, S. and Andrady, A.L. (1991) 'Fouling of floating plastic debris under Biscayne Bay exposure conditions', *Marine Pollution Bulletin*, 22(12), pp. 608–613. doi:10.1016/0025-326X(91)90249-R.

Yong, M.M.H. *et al.* (2021) 'Microplastics in fecal samples of whale sharks (*Rhincodon typus*) and from surface water in the Philippines', *Microplastics and Nanoplastics*, 1(1), p. 17. doi:10.1186/s43591-021-00017-9.

Zhang, Y. *et al.* (2020) 'Atmospheric microplastics: A review on current status and perspectives', *Earth-Science Reviews*, 203, p. 103118. doi:10.1016/j.earscirev.2020.103118.

Ziajahromi, S. *et al.* (2018) 'Environmentally relevant concentrations of polyethylene microplastics negatively impact the survival, growth and emergence of sediment-dwelling invertebrates', *Environmental Pollution*, 236, pp. 425–431. doi:10.1016/j.envpol.2018.01.094.

Chapter II.  
Development of an  
environmentally relevant  
luminescent model of Micro- and  
Nanoplastic for environmental  
assessment



## **Table of content**

II.1. French summary .....	54
II.2. Article .....	59
II.3. Supplementary information .....	78

## **II.1. French summary**

Le travail présenté dans ce chapitre est consacré à la préparation d'un modèle de particules de micro- et nanoplastiques pertinent pour l'environnement, et qui peut être facilement visualisé et suivi, y compris au travers de tissus d'organismes vivants. Ce chapitre est tiré d'une publication qui a été soumise au journal *Environmental Science : Nano*. Le texte principal et les informations complémentaires de cet article sont successivement reportés.

Le polyéthylène, en particulier le polyéthylène haute densité (HDPE), a été utilisé comme polymère modèle pour le développement de micro- et nanoparticules (MPs et NPs), car il est le plus utilisé et l'un des plus couramment retrouvés dans tous les compartiments environnementaux. Cependant, en particulier lorsqu'il est de taille nanométrique, ce matériau est très difficile à détecter dans des échantillons environnementaux par des méthodes non destructives. Ainsi, pour faciliter sa détection tout en utilisant des méthodes non-destructives, nous avons proposé d'incorporer des sondes luminescentes de nanoparticules upconverting à base de lanthanide (Ln-UCNPs) dans le polymère. Ces luminophores récemment développés sont des matériaux inorganiques extrêmement stables et capables de convertir des photons du proche infrarouge de faible énergie en lumière visible. Cela permet leur détection même dans des échantillons épais comme dans un tissu biologique ou un petit animal.

Des particules de  $\text{NaREF}_4$  (RE = 2 % Er ; 30 % Yb ; 68 % Y) recouvertes d'oléate et ayant un diamètre de 20 nm ont été utilisées pour préparer un plastique luminescent vert qui peut être directement observé à l'œil sous une irradiation de 976 nm. L'échantillon brut de plastique marqué (Upcon-PE) a été préparé par incorporation des UCNPs dans la matrice HDPE, en dissolvant le polymère dans de l'o-xylène bouillant, contenant des UCNPs dans un rapport de 10 % en poids (HDPE:UCNPs). Le composite a été séparé du mélange réactionnel par précipitation dans un bain de glace, puis soigneusement rincé avec du cyclohexane pour éliminer les traces d'o-xylène et les UCNPs qui n'auraient pas été incorporées dans la matrice PE. Comme contrôle négatif, un lot de polymère ne contenant pas d'UCNPs (Blank-PE) a été préparé en suivant un protocole similaire.

Pour confirmer l'incorporation réussie des UCNPs, un test qualitatif a été réalisé en irradiant les échantillons avec un laser à onde continue (CW) de 976 nm : alors qu'aucune émission n'a été observée à partir de Blank-PE, une luminescence verte intense, caractéristique de  $\text{Er}^{3+}$  et provenant du phénomène d'upconversion, a été observé pour Upcon-PE (Figure II.1).

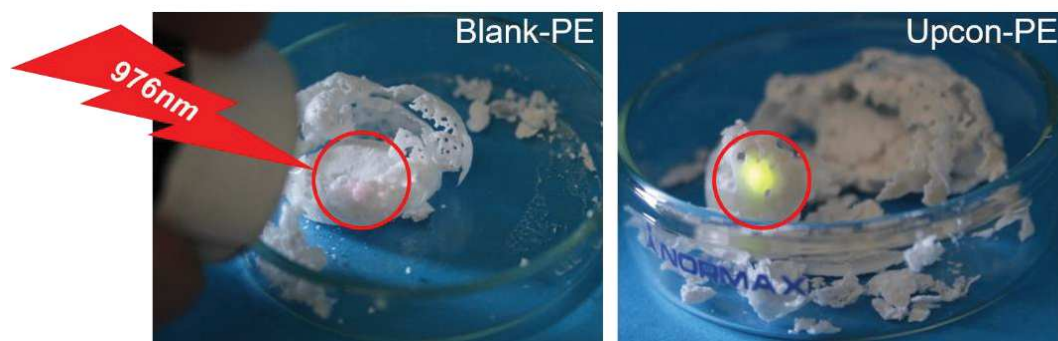


**Figure II. 1 : Matériau HDPE en bulk sous irradiation par un laser continu 976nm (avec un diamètre de faisceau de 1,4 mm). L'échantillon Upcon-PE (droite) montre des propriétés d'émission verte sous irradiation proche infrarouge, alors que le lot contrôle préparé sans UCNP (Blank-PE) demeure non luminescent (gauche).**

Pour préparer les modèles de MPs et NPs (respectivement Model-MPs et Model-NPs), nous avons utilisé une synthèse top-down qui consiste en deux étapes : la préparation des Model-MPs en soumettant le matériau en vrac à un broyage cryogénique, suivie de la préparation des Model-NPs en soumettant les Model-MPs obtenues à un broyage à long terme par des billes de zircone (Figure II.2a). Après le processus de broyage en deux étapes, les particules ont été fractionnées par filtration séquentielle dans l'éthanol (en utilisant des seuils de coupure de 500  $\mu\text{m}$ , 200  $\mu\text{m}$ , 100  $\mu\text{m}$ , 50  $\mu\text{m}$ , 11  $\mu\text{m}$  et 1  $\mu\text{m}$ ). Cette étape nous a permis de séparer les Model-MPs ( $> 1\mu\text{m}$ ) des Model-NPs ( $< 1\mu\text{m}$ ).

Les particules ainsi produites ont ensuite été entièrement caractérisées par des approches analytiques différentes. La distribution de taille des Model-MPs produites a été obtenue par analyse granulométrique (Figure II.2b). Celle-ci a démontré qu'environ 90% des Model-MPs ont une taille inférieure à 15  $\mu\text{m}$ , et n'étaient pas conformes à la coupure du maillage de filtration.

La distribution des particules par NTA a montré qu'environ 90% des nanoparticules étaient respectivement inférieures à 201 nm pour Nano-Blank-PE et 117 nm pour Nano-Upcon-PE. La figure II.2c représente un exemple typique de profil NTA obtenu.

Les Model-MPs et les Model-NPs se sont avérées être chargées négativement avec une valeur de potentiel zêta mesurée autour de -70 mV et -60 mV, respectivement.

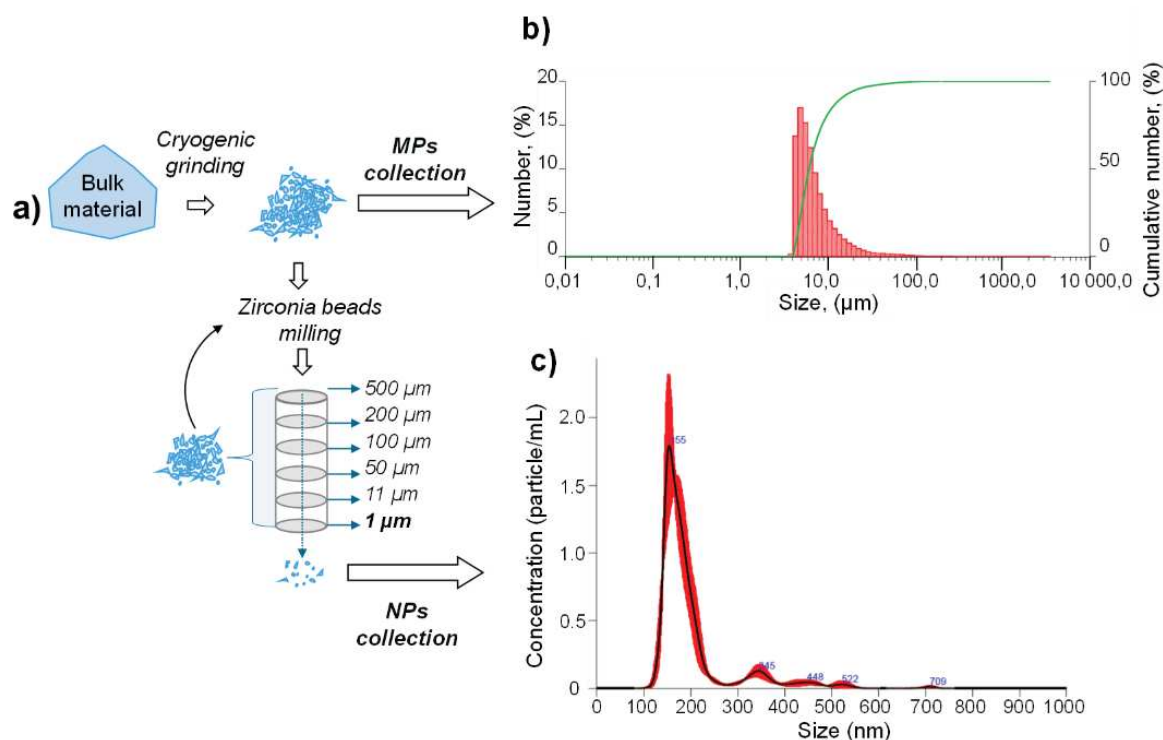


Figure II. 2: a) Schéma général d'un procédé de broyage en deux étapes pour préparer des particules micro et nanométriques ; b) Analyse granulométrique de la fraction micrométrique obtenue après broyage cryogénique, exprimée en pourcentage et en pourcentage cumulé en fonction de la taille ; c) Analyse NTA de la fraction nanométrique obtenue après broyage humide et filtration en cascade.

### *Modèle de microplastiques*

L'analyse par spectroscopie infrarouge à réflexion totale atténuée à transformée de Fourier (ATR-FTIR) démontre que les procédés de synthèse et de broyage ne provoquent aucune modification chimique du PE (voir figure dans la partie Informations Supplémentaire).

Les teneurs en UCNPs (en pourcentage) dans le HDPE ont été obtenues par analyse calorimétrique à balayage différentiel (DSC) et ont été trouvées égales à  $6,4 \pm 1,2$  % en masse dans les  $\mu$ -Upcon-PE. Ce taux de chargement a été confirmé par analyse thermogravimétrique (TGA), qui a donné une valeur de 5,7%.

L'analyse de diffusion des rayons X aux petits angles (SAXS) a confirmé l'incorporation des UCNPs à l'intérieur des matrices de HDPE et a indiqué que cette dernière n'induisait aucune modification des propriétés de surface des particules.

### *Modèle de nanoplastiques*

La forme et la taille des particules nanométriques ont été observées par Microscopie Electronique à Transmission (MET). Cette technique a montré que les particules étaient bien polydisperses, en plus d'être polymorphes. Quelques clichés sont présentés en Figure II.3a.

L'incorporation efficace des UCNPs dans le HDPE a été confirmée, pour les Model-NPs, par TEM haute résolution couplée à une analyse élémentaire aux rayons X à dispersion d'énergie (TEM-EDX) : en effet, l'analyse élémentaire des objets sphériques apparaissant dans les particules de HDPE a montré une distribution homogène de F, Y et Yb, caractéristique des UCNPs (Figure II.3b et figure S6 dans la partie Informations supplémentaires). L'identification des UCNPs a été confirmée par ce résultat et a démontré que l'intégrité chimique et physique des UCNPs avait été maintenue pendant le processus complet de fabrication des Model-NPs (incorporation à chaud et broyage).

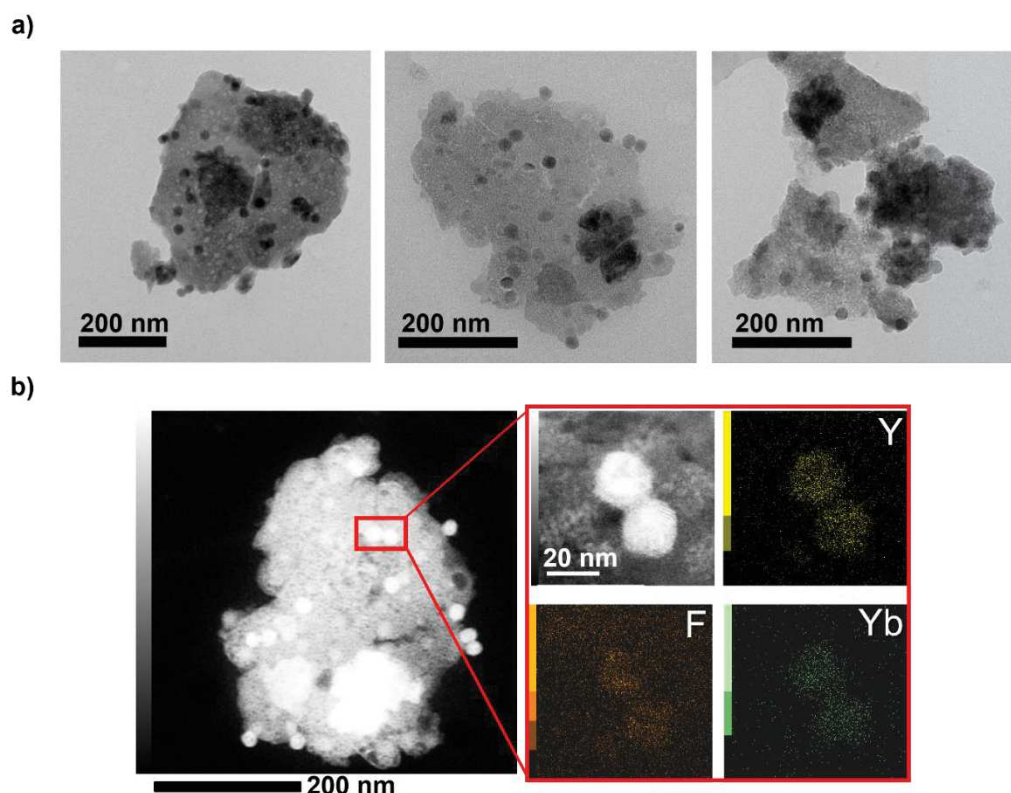


Figure II. 3: a) Images de microscopie électronique à transmission (TEM) de Nano-Upcon-PE. Les trois images illustrent le fait que les particules sont polydisperses et polymorphes. b) Image de TEM à Champ Sombre Annulaire à Grand Angle (HAADF-TEM) sur une particule unique de Nano-Upcon-PE et caractérisation par rayons X à dispersion d'énergie (EDX) des éléments Yttrium (Y), Fluor (F) et Ytterbium (Yb).

### *Propriétés d'émission du modèle de particules marquées*

Les propriétés d'émission des UCNPs une fois incorporées dans le PE ont été étudiées. Les mesures de fluorescence ( $\lambda_{exc} = 980$  nm) des particules dispersées dans l'éthanol n'ont montré aucune émission pour Blank-PE tandis que Upcon-PE montre trois pics d'émission autour de 525, 550 et 655 nm, caractéristiques des transitions de l'ion émetteur erbium  $Er^{3+}$  (Figure II.4a).



La possibilité d'imager et traquer les  $\mu$ -Upcon-PE a été examinée en utilisant une configuration de microscope standard à 2 photons sous excitation à 980 nm (Figure II.4b). Dans ces conditions, les particules non dopées ( $\mu$ -Blank-PE) sont restées non émissives tandis que les particules de  $\mu$ -Upcon-PE ont, comme attendu, émis une luminescence verte et rouge qui a pu être collectée entre 490 et 600 nm et 630 et 710 nm, respectivement. Cette dernière est caractéristique de la présence d'erbium dans les UCNPs. L'absence de toute émission de la particule de PE non marquée indique qu'aucun processus à 2 photons ne se produit dans le PE pur et montre l'intérêt de l'utilisation des UCNPs comme marqueur luminescent sans bruit de fond pour les particules de plastique.

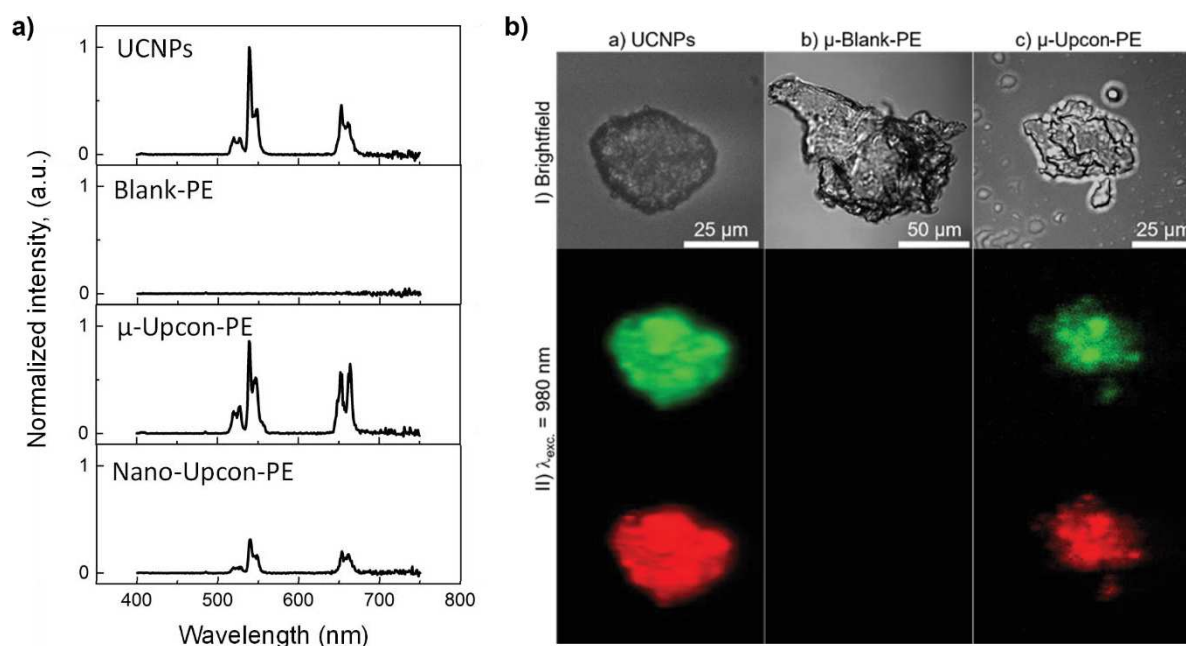


Figure II. 4: a) Spectres d'émission de fluorescence (excitation à 980 nm) des UCNPs, Blank-PE et des micro- et nanoparticules Upcon-PE ; avec l'intensité de fluorescence normalisée. b) I) Image en fond clair d'un agrégat de particules a) UCNPs et d'une particule b)  $\mu$ -Blank-PE et c)  $\mu$ -Upcon-PE. II) Émissions verte et rouge observées sous irradiation proche infrarouge (980 nm) pour les deux a) UCNPs et c)  $\mu$ -Upcon-PE ; b)  $\mu$ -Blank-PE reste non émissif.

Ce chapitre présente un protocole de préparation de modèle de micro- et nano-particules de HDPE marquées qui pourrait être pertinent comme modèle de plastique mimant les particules retrouvées dans l'environnement (hétérogène en forme et en taille). Grâce aux propriétés luminescentes activables par proche infra-rouge du marqueur UCNPs incorporé, ce modèle peut également être bien adapté pour le suivi à long terme de plastique comme polluant persistant ubiquitaire. Ainsi, les stratégies basées sur l'utilisation de ce modèle peuvent ouvrir la voie à des études s'orientant vers une compréhension plus approfondie du devenir des particules plastiques dans la chaîne trophique et peuvent aussi être utilisées dans des champs d'applications au-delà de la portée de ce travail.

## **II.2. Article**

### **Top-Down Synthesis of Luminescent Micro- and Nano-plastics by Incorporation of Upconverting Nanoparticles for Environmental Assessment**

Nadiia Yakovenko<sup>a</sup>, Baptiste Amouroux<sup>a</sup>, Magali Albignac<sup>a</sup>, Fabrice Collin<sup>a</sup>, Clément Roux<sup>a</sup>, Anne-Françoise Mingotaud<sup>a</sup>, Pierre Roblin<sup>c</sup>, Christophe Coudret<sup>a\*</sup>, Alexandra Ter-Halle<sup>a\*</sup>

a : Laboratoire des IMRCP, Université de Toulouse, CNRS UMR 5623, Université Toulouse III - Paul Sabatier, Toulouse 31062, France E-mail: ter-halle@chimie.ups-tlse.fr (A. Ter-Halle), coudret@chimie.ups-tlse.fr (C. Coudret).

b : Laboratoire de Génie Chimique and Fédération de Recherche FERMAT, 31030 Toulouse, France.

**Keywords:** nanoplastic, UCNPs, lanthanide, powdering, milling, top-down synthesis, environmentally relevant, polymer

#### **Abstract**

The occurrence of micro- and nanoplastics is a major environmental problem. Especially for nanoplastics due to their easy bioavailability and unknown impact on living organisms. The monitoring of these extremely small particles during their ingestion, tissue translocation and transfer through the trophic chain remains very challenging. This study aims to develop an environmentally relevant model of luminescent micro- and nanoplastics. First, lanthanide-based upconverting nanophosphors (20 nm) were incorporated in bulk polyethylene without modification of the polymer structure or morphology. Second, micrometric and nanometric particles were obtained after powdering. Two fractions were obtained with cascade filtration with average sizes of 5  $\mu\text{m}$  and 150 nm and characterized in terms of size distribution, morphology and surface charge. The particles are very polydisperse with an irregular shape and a global negative charge; they exhibit morphological characteristics similar to the nanoplastics formed in the environment. Their luminescent properties upon NIR excitation at 980 nm open the possibility to track them in the tissues of organisms. The powdering method is very simple and compatible with many polymers pure or formulated. As a perspective, the use of weathered materials is also possible with the proposed method and will allow the preparation of particles sharing additional properties with environmental micro- and nanoplastics.

## **Introduction**

The scientific community has invested lately very important effort to evaluate plastic impact on ecosystems and this allowed to realize, in addition that all compartments of the earth were concerned, that the pollution reached the nanoscale. Our experience in engineered nanomaterials enables us to envisage that nanoplastics have unique physical and chemical properties (e.g., size, shape, composition, and reactivity). The very nature of nanoplastic (NPs, sizes are below 1  $\mu\text{m}$ )<sup>1-3</sup> being polydisperse, polymorphic, mainly made of C, H, O likewise natural organic matter, further complicates the analysis of NP behavior by traditional colloid science.

In the recent decades, much attention was paid to the study of occurrence and potential negative effects of microplastics (MPs, ranging from 1  $\mu\text{m}$  to 5 mm).<sup>4</sup> MPs were analyzed in organisms ranging from zooplankton<sup>5</sup> to marine mammals.<sup>6</sup> Laboratory studies to investigate MPs bioaccumulation and immunotoxicity in living organisms report their biological impact on organisms (see references <sup>7-9</sup> for review). However, the fate and role of NPs remain poorly understood, due to the lack of suitable analytical methods to monitor their uptake, transport, translocation, and to understand their potential adverse effects on living organisms.<sup>10</sup> To date, most of the evaluation studies were run on model NPs, using commercially available polystyrene (PS) nanospheres.<sup>11,12</sup> The distinction between model NPs and NPs - the nanoscale fraction of plastic debris generated in the environment- is often left aside even if their physico-chemical and biological behavior are drastically different.<sup>10</sup> Model NPs are rather easy to handle and to characterize but, lacking surface chemistry, polydispersity and irregular shape like the one formed in the environment, they are of limited interest for ecotoxicological study.<sup>10</sup>

A few recent studies proposed a top-down approach (i.e. producing smaller particles from bigger objects)<sup>13</sup> to prepare more environmentally relevant model NPs. Magrì et al. described the use of laser ablation in water to obtain polyethylene terephthalate nanoparticles with an average size of 100 nm and a surface chemical composition similar to the plastic exposed to UV-light in the environment.<sup>14</sup> Astner et al. produced model MPs and model NPs (in the range 360 – 390 nm) made of polybutene adipate-co-terephthalate and low-density polyethylene by applying a sequence mimicking environmental weathering.<sup>15</sup> El Hadri et al. produced NPs ranging from 20 nm to 1000 nm by applying blade grinding followed by planetary ball milling.<sup>16</sup> Model NPs production from MPs collected in the environment were also proposed in order to prepare particles with a surface chemistry even closer to native nanoplastic. Their toxicological evaluation demonstrated that their impact on marine organisms was superior to PS

nanospheres.<sup>17</sup> Even if the plastic particles obtained by the top-down methods reproduce the main physico-chemical characteristics as NPs formed in the environment, their tracking remains challenging during biological evaluation tests, rendering difficult to monitor their ingestion, transports, translocation in living organism.

Label model MPs and NPs based on recent synthesis strategies were obtained, such as <sup>13</sup>C-enrichment,<sup>18</sup> rare metals,<sup>19</sup> or simple staining method with fluorescent dyes.<sup>20</sup> Fluorescence labelling is a widely developed strategy, but most of the fluorescent tags operate with UV-blue to green excitation light, showing low tissue penetration, toxicity to living organisms and potentially leading to background autofluorescence, thus preventing their use in deep-tissue imaging. Dyes can also suffer from photobleaching with prolonged exposures<sup>21</sup> or can have solvatochromic properties, making the emission spectra dependent on the polarity of the surrounding environment.<sup>22</sup> Another limitation is the potential co-staining of the organic matter present in the sample under focus, resulting in the false detection. As an alternative to fluorescence labelling, Mitrano et al. proposed the use of heavy metal as tracer and Inductively Coupled Plasma – Mass Spectrometry (ICP-MS) for indirect plastic monitoring. Polyacrylonitrile particles doped with Pd were accurately assessed in a complex matrix (activated sludge from wastewater treatment plant), and no Pd leaching from particles was observed.<sup>19</sup> Such a strategy was found to be very efficient but is not well adapted for monitoring MPs and NPs in living organism because of the use of a destructive analytical technique.

The objective of the present study is to synthesize environmentally relevant models MPs and NPs in terms of polydispersity, shapes and surface properties, that could be easily visualized and tracked in the tissues of living organisms. Polyethylene (PE) was selected as a model polymer as it is the most commonly used polymer and the most frequently found in the environment. However, especially at the nanoscale, this material is very stealthy and poorly detectable using non-destructive methods. For easy imaging, Lanthanide-based upconverting particles (UCNPs) were incorporated into the polymer matrix. Due to the spectroscopic features of the lanthanide family, such nanomaterials are able to accumulate near-infrared (NIR) energy and release it as visible emission as a line spectrum typical of the emitting element, (thus erbium gives rise to a bright green visible emission).<sup>23</sup> They are commonly used as background-free luminophores in imaging or anti-counterfeiting application,<sup>24</sup> or as local sources of light (“nanolamps”)<sup>25</sup> in material or biological applications.<sup>26–29</sup> Moreover, highly photostable (no blinking, no bleaching)<sup>30</sup> and requiring lower power density than 2-photon fluorophores, these background-free persistent fluorophores have become an attractive probe for imaging purposes including into thick samples. Furthermore, UCNPs derived from rare elements salts (NaREF<sub>4</sub>)

can be prepared in a very monodispersed manner depending on the choice of the rare-earths elements and the preparation protocol. We have chosen to develop a top-down approach for the synthesis of labelled PE by incorporating highly monodispersed, hydrophobic and less than 30 nm UCNP into bulk PE material and by using powdering to produce labelled nanometric particles with irregular shapes and variety of sizes. The particles were characterized with many analytical techniques to obtain full information about their physicochemical properties.

## Materials and methods

**Chemicals:** PE pellets (High Density PE, CAS 9002-88-4) were purchased from Sigma Aldrich (Saint Louis, MO, USA). The polymer used was characterized by a melt flow index (MFI) 12 g/10 min, a melting point between 125 and 140°C and a density of 0.952 g/mL at 25°C. Rare Earth (RE) chloride hydrates, ammonium fluoride, oleic acid (OA) and 1-octadecene (ODE) were purchased from Alfa Aesar and used as received. All other organic solvents were of spectroscopic grade and used as received. Water used was deionized water ( $\rho = 18 \text{ M}\Omega \text{ cm}^{-1}$ ) obtained from Aquadem apparatus.

**Upconverting nanoparticles synthesis:** In a three-neck flask, a solution of  $\text{YCl}_3 \cdot 6\text{H}_2\text{O}$  (2.4 g, 7.9 mmol),  $\text{YbCl}_3 \cdot 6\text{H}_2\text{O}$  (1.35 g, 3.5 mmol) and  $\text{ErCl}_3 \cdot 6\text{H}_2\text{O}$  (0.088 g, 0.23 mmol) in water (10 mL) was added to a OA:ODE mixture (35:190 mL:mL) and water was distilled off under Ar-flush. The resulting cloudy suspension was brought to 160°C until clear (*ca* 1 h) then cooled down under Ar-flush.  $\text{NH}_4\text{F}$  (2.37 g, 64 mmol, 80 mL, 0.8 M) and NaOH (1.86 g, 46.6 mmol, 80 mL, 0.58 M) were dissolved separately in MeOH. These two solutions were added simultaneously using syringe pumps at 0.4 mL/min to the vigorously stirred  $\text{RE}(\text{OA})_3$ :OA:ODE solution. Once the addition completed, the methanol was removed under Ar-flush at 100°C. The reaction mixture, after careful degassing, was then brought to 310°C as fast as possible (*ca* 20°C/min) and kept at this temperature for 90 min. After cooling, an equivalent amount of ethanol was added and particles were collected by centrifugation at 9000 g for 10 min. They were purified by repeating twice the sequence: pellet redissolution in cyclohexane / addition of a same volume of ethanol / centrifugation.

Oleate-capped  $\text{NaREF}_4$  (RE = 2% Er; 30% Yb; 68% Y) particles prepared had a diameter of  $21.8 \pm 1.3 \text{ nm}$  and were showing the typical emission peaks of  $\text{Er}^{3+}$  emitter under 980 nm excitation: two intense green emissions (525 and 540 nm) and a red band (650 nm) (Figure 5: UCNP).

**UCNPs incorporation into PE matrix:** PE pellets were previously milled using a RETSCH ZM 200 Ultra Centrifugal Mill. The obtained polymer powder with an average size of 200  $\mu\text{m}$

was dissolved in boiling o-xylene ( $\geq 99.0\%$  (GC grade); Sigma Aldrich, Saint Louis, MO, USA), where UCNPs (10 wt.% of PE) were subsequently introduced. The mixture was homogenized by magnetic stirring at  $146^\circ\text{C}$  for 20 min. Precipitation of the synthesized polymer material was achieved by rapid cooling in an ice bath. UCNPs that were not incorporated into PE were removed by washing the polymer with cyclohexane ( $\geq 99.7\%$  (HPLC grade); Sigma Aldrich, Saint Louis, MO, USA). Before future use, polymer was dried overnight at  $40^\circ\text{C}$ . As a negative control, a second batch of polymer containing only PE (Blank-PE) was prepared following similar protocol.

**Synthesis of the labelled micro- and nanoparticles:** Both bulk material Blank-PE and Upcon-PE were exposed to a cryogenic grinder (SPEX<sup>TM</sup> SamplePrep 6775 Freezer/Mill<sup>TM</sup>, Delta Labo, Avignon, France), first, samples were pre-cooled for 5 min, then the grinding was carried out in 10 cycles of 1 min with cooling between cycles for 2 min in liquid nitrogen. The grinding rate was 10 cycles per second (CPS), which is equal to 20 strokes by impactor per second. The obtained polymer powder was dispersed in Ethanol ( $\geq 99.8\%$  (HPLC grade); Sigma Aldrich, Saint Louis, MO, USA) and sonicated for 15 min at room temperature to avoid particles aggregation. Then particles size separation was performed in 6 sequential filtration steps through a metal mesh with a cutoff of  $500\ \mu\text{m}$  (Retsch, Haan, Germany), and NITEX nylon mesh (Dominique Dutscher SAS, Brumath, France), with pore sizes of  $200\ \mu\text{m}$ ,  $100\ \mu\text{m}$ ,  $50\ \mu\text{m}$ ,  $11\ \mu\text{m}$ , and  $1\ \mu\text{m}$ . Wet milling was performed in a 20 mL glass vial filled with about 50 g of ZY-E (Yttrium stabilized Zirconium Oxide) beads, size of 1.0 – 1.2 mm (Sigmund Lindner GmbH (SiLi), Warmensteinach, Germany), 0.1 to 0.5 g of MPs, and approximately 10 mL of absolute ethanol. Milling process lasted 48, 60, and 120 days under 80 rpm stirring on the horizontal ROLLER 6 digital apparatus (IKA, Staufen, Germany). Eventually, MPs and NPs were separated by the 6 steps of subsequent filtration described above and rinsed with cyclohexane.

**Granulometry analysis:** MPs size distribution was determined using a Mastersizer MS3000 (Malvern Panalytical, UK). The polymer powder was dispersed in ethanol using a HYDRO MV device with stirring at 2500 rpm. The refractive index used for ethanol and for particles was respectively 1.36 and 1.52, with an absorption index for particles of 0.1. Results are presented as a mean number of particles obtained from 5 measurements.

**Differential scanning calorimetry:** DSC was performed with a DSC1 Mettler Toledo apparatus, equipped with an HSS8 sensor. Samples were weighed (between 5 and 7 mg) and sealed in 40 mL aluminium pans. They were heated from  $20^\circ\text{C}$  to  $160^\circ\text{C}$  at  $5^\circ\text{C}/\text{min}$  with an empty aluminum pan as the reference. Dry nitrogen with a flow rate set at  $20\ \text{mL}/\text{min}$  was used

as the purge gas. Each sample was analyzed in triplicates. The first heating cycle was used to erase all processing, thermal, mechanical, crystallization, and shear history of the samples. The melting temperature and the crystallinity were obtained from the second heating cycle. The crystallinity was calculated from the expression:

$$\text{Crystallinity (\%)} = (\Delta H_m / \Delta H_{mref}) * 100 \quad (1)$$

Where  $\Delta H_m$  is melting enthalpy of analyzed samples and  $\Delta H_{mref}$  is a melting enthalpy of 100 % crystalline PE (293 J/g).<sup>31</sup>

**Small-angle X-ray scattering (SAXS) analysis:** SAXS measurements were performed on the XEUSS 2.0 laboratory source equipped with a pixel detector PILATUS 1M (DECTRIS) and an X-rays source provided by a GeniX3D with a fixed wavelength based on Cu K $\alpha$  radiation ( $\lambda = 1.54 \text{ \AA}$ ). The distance between the sample and the detector was fixed at 1216.5 mm, giving a  $q$  range starting from  $0.005 \text{ \AA}^{-1}$  to  $0.5 \text{ \AA}^{-1}$ , assuming that  $q$  is the scattering vector equal to  $4\pi/(\lambda \times \sin \theta)$  with a  $2\theta$  scattering angle. The distance was calibrated in the small angle region using silver behenate ( $d_{001} = 58.34 \text{ \AA}$ ). For solid samples, the dry MPs powder was placed between two Kapton windows with 1 mm of the optical pathway and placed on the motorized sample holder. For liquid samples, particles dispersion was injected into a capillary tube with a diameter of 1.5 mm and then placed under the beam in the conditions. To remove scattering and absorption from air, a primary vacuum has been applied to the entire instrument. To maximize the signal at high angles, 6 acquisitions of 600 seconds were averaged. All scattering curves were corrected for the empty cell contribution or for the solvent, divided by transmission factor, acquisition time and optical path in order to obtain SAXS curves in absolute units ( $\text{cm}^{-1}$ ).

**Transmission electron microscopy energy-dispersive X-ray spectroscopy:** NPs dispersion in ethanol were prepared with polyvinylpyrrolidone (PVP) 0.4% (w/v), to ensure particles adhesion on the top of the formvar/carbon coated copper grid. One drop of 20  $\mu\text{L}$  of sample solution was placed on the top of the grid. After drying, TEM/EDX analysis were performed using a JEOL cold-FEG JEM-ARM200F operated at 200 kV equipped with a probe Cs corrector reaching a spatial resolution of 0.078 nm. EDX spectra were recorded on a JEOL CENTURIO SDD detector.

**Nanoparticle Tracking Analysis:** NTA analyses were performed at 25°C using the NanoSight LM10 (Malvern Instruments, Ltd, UK) instrument equipped with an sCMOS camera. Samples were prepared by NPs dispersion in ultrapure milli-Q water (50 mg/L). Measurement of each sample was performed in triplicate, consisting of three records of 60 s. Results are presented as

a mean size of the particles  $\pm$  SD. NTA is known to provide accurate measurements even for polydisperse nanoparticles, and was thus used without any complementary measurement by Dynamic Light Scattering measurements.

**Fluorescence measurement:** Fluorescence spectra were acquired with a Fluorolog-3-2iHR320 modular spectrofluorimeter (HORIBA Jobin Yvon SAS, Palaiseau, France). The standard light source of the fluorimeter was substituted by a 980 nm Continuous Wave Laser operating at a power of 1.5 W. Emission was collected between 400 nm and 750 nm.

**Two-photon microscopy:** Samples were imaged on a Zeiss LSM-710 two-photon microscope, equipped with a Ti: Sapphire Chameleon Vision II laser (Coherent, Santa Clara, California), operating at 980 nm (4% of max power for UCNPs and 50% for  $\mu$ -Blank-PE and  $\mu$ -Upcon-PE samples, 140 fs pulses, 80 MHz repetition rate), and a Zeiss Plan-Apochromat 63x/1.40 oil immersion lens. Upconverted light was collected between 490 and 600 nm for the green band, and 630 and 710 nm for the red band. Images were processed using ImageJ (Fiji) software.

**Zeta-potential measurements:** Zeta-potential measurements for MPs and NPs were carried out at 25°C on a Zetasizer Nano-ZS (Malvern Instruments, Ltd, UK) equipped with a He-Ne laser ( $\lambda = 633$  nm) at an angle of 173°. Samples were prepared by dispersion of particles in 10 mM NaCl solution, to provide minimum level of conductivity in the samples, following ISO and ASTM standard guides.<sup>32</sup> Before analysis, pH of every sample was measured. Zeta-potential and standard deviation (SD) were obtained from 5 measurements of 11 runs of 10 seconds using the Smoluchowski model.

## Results and discussion

### Large scale monodisperse UCNP synthesis

Using the classical thermal coprecipitation to prepare hydrophobic oleate-coated NaREF<sub>4</sub> UCNPs, we implemented a new protocol to achieve the synthesis of monodisperse 20 nm-UCNPs over a multigram scale. Such an approach allows the use of a single batch of phosphors to be further dispatched in multiple assays, therefore keeping a homogeneous luminescence response over all samples.<sup>33,34</sup> As we noticed that a slow and separate introduction of fluoride and sodium sources using syringe pumps to the rare-earth oleate mixture led to a dramatic size reduction,<sup>35</sup> we decided to adapt this strategy to the efficient protocol described by Zhang et al., known to yield 40 nm NaYF<sub>4</sub>-based UCNPs.<sup>36</sup> To our delight, using this simple protocol modification, we were able to collect regular hexagonal prism shaped Erbium-doped NaYF<sub>4</sub>:Yb30%,Er2% UCNPs (NaREF<sub>4</sub>, where RE= 2% Er; 30% Yb; 68% Y) with an average size of size  $21.8 \pm 1.3$  nm even on a 11.6 mmol scale: up to 3 g of bright green emissive



UCNPs could be obtained this way. XRD analysis was consistent with pure hexagonal phase (Figure 1).

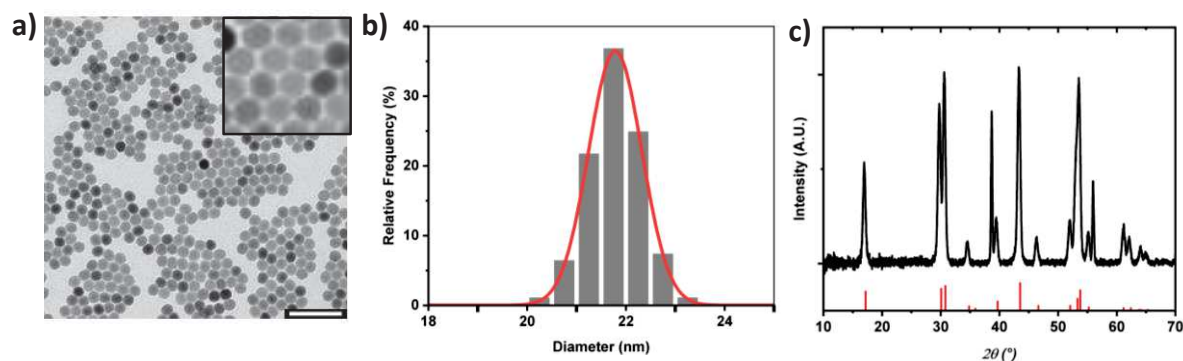


**Figure 1.** Transmission Electron Microscopy (TEM) and X-Ray diffraction characterization of the prepared NaYF<sub>4</sub>:Yb30%, Er2%: a) TEM picture (scale bar is 100 nm); b) Size distribution obtained from analysis of TEM pictures (Gaussian fit in red); c) XRD diffractogram of the particles (red lines show the characteristic peaks of hexagonal NaYF<sub>4</sub> (JCPDS 00-016-0334)).

### Incorporation of UCNP in PE and powdering

We have chosen to incorporate the UCNPs into the polymer using a dissolution/precipitation procedure which allows one to work on smaller quantities compared to melt mixing (Figure 2a). The choice of the UCNP:PE ratio was chosen by comparison with standard nanocomposite formulation involving HDPE.<sup>37</sup> Briefly, PE was solubilized in boiling o-xylene in the presence of UCNPs (10% in weight). Cooling down the colorless solution at 0°C led to the quantitative precipitation of the polymer. Excitation of the collected whitish solid with a 976 nm Continuous Wave (CW) laser induced the bright green luminescence typical of Er<sup>3+</sup> indicating that UCNPs were successfully incorporated in bulk PE (Upcon-PE) A similar test was found negative for the UCNP-free synthesis, Blank-PE.

The powdering process consisted in a first step to cryogenic grinding. We selected this method because it is a process where thermally sensitive and elastic substances are generally successfully processed. The effect of several parameters was considered, including pre-cooling time, grinding time, oscillation frequency. Experiments reveal a non-monotonous effect of these parameters on the abrasion efficiency. At this stage of the powdering process particles at the nanoscale were not detected by nanoparticle tracking analysis (NTA). Both powders, with or without UCNPs were named  $\mu$ -Upcon-PE and  $\mu$ -Blank-PE respectively. The size distribution of the particles obtained by granulometric analysis showed that around 90% of the particles were smaller than 15  $\mu$ m (Figure 2b). The incorporation of the UCNPs did not impact in a significant way the size distribution of the powder (Figure S1).

To reach the nanoscale, we proceeded to further size reduction using a low-energy wet driven milling technique. The method is simple, economical, sustainable and provides the advantage of, like the first step, the preservation of the polymer structure.<sup>38</sup> Ethanol was chosen as solvent because the synthesis in water, which would be more appropriate for future use in toxicological tests, was not possible. PE is very hydrophobic and does not wet in water. Furthermore, PE float in water and the contact with the zirconium beads used for milling was not favored. After the two-stage powdering process, the particles were fractionated by sequential filtration in ethanol (using 6 mesh cut-off: 500  $\mu\text{m}$ , 200  $\mu\text{m}$ , 100  $\mu\text{m}$ , 50  $\mu\text{m}$ , 11  $\mu\text{m}$ , and 1  $\mu\text{m}$ ). This easy-to-implement protocol aimed at preventing rapid clogging of the filter mesh during filtration, without resorting to a more complex process such as tangential flow filtration (TFF).<sup>39</sup> The particles at the nanoscale (Nano-Upcon-PE and Nano-Blank-PE) were produced with a yield of around 6 %. The distribution of the particles by nanoparticle tracking analysis (NTA) showed that around 90 % of the particles were smaller than 201 nm for Nano-Blank-PE and 117 nm for Nano-Upcon-PE respectively (Figure 2c or Figure SI2 for details). The incorporation of UCNPs led to smaller particles; we have no explanation for this.

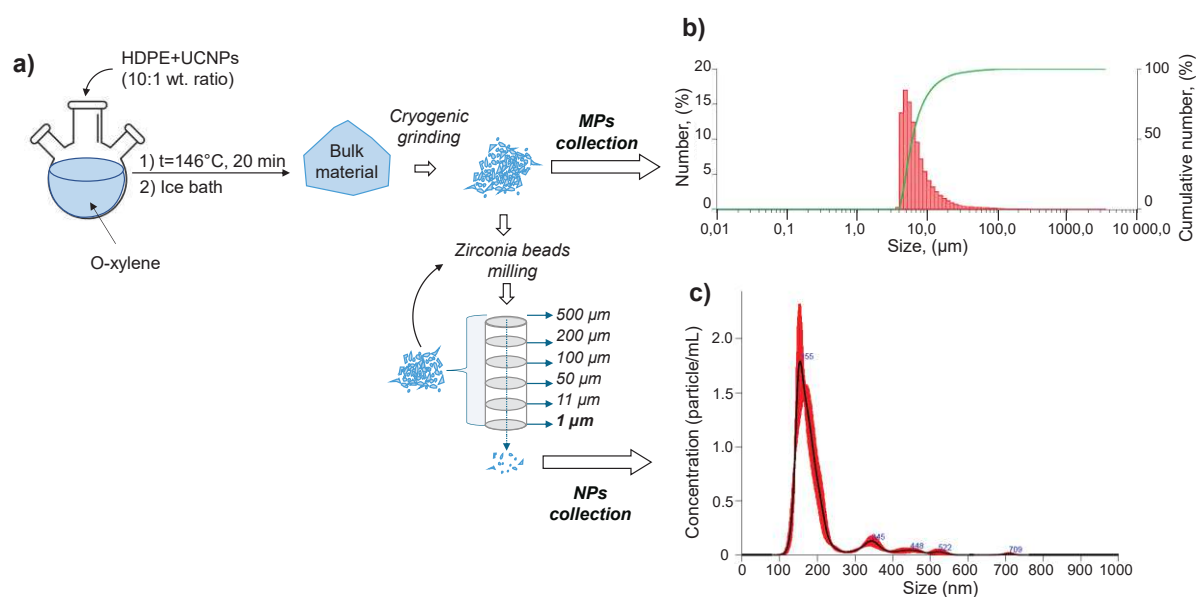


**Figure 2.** a) General scheme of Upconverting Nanoparticles (UCNPs), incorporation into polyethylene (PE) followed by a two-step powdering process to prepare micro- and nano-metric particles; b) Granulometric analysis of micrometric fraction obtained after cryogenic grinding, expressed as a percentage number and percentage cumulative number as a function of the size; c) Nanoparticle Tracking Analysis (NTA) analysis of the nanometric fraction obtained after wet milling and cascade filtration.

## Characterization of labelled micro- and nanoplastics

### Chemical integrity of PE

Attenuated total reflection Fourier Transform Infrared (ATR-FTIR) analysis of the samples (on bulk and micrometric particles) was performed to determine if there was any PE degradation during synthesis or powdering. An important side-reaction could be PE oxidation leading, in particular, to the formation of carbonyl moieties, easily detected by an intense absorption band in the region 1650-1850  $\text{cm}^{-1}$ .<sup>40</sup> FTIR spectra were registered after each processing step and compared to the spectra of raw PE pellets. No absorption band due to the presence of oxidation was detected (Figure S3). This indicates that synthesis and grinding processes do not cause any chemical modification of PE.

### Effectiveness of UCNPs incorporation in PE

During the synthesis of the bulk material, the dissolution/precipitation procedure does not allow to control the UCNPs rate of incorporation. This amount was measured by two distinct techniques: Differential Scanning Calorimetry (DSC) and thermogravimetric analysis (TGA). DSC was used to accurately determine the PE crystallinity at each stage of the preparation. The melting enthalpy ( $\Delta H_m$ ), the onset temperature ( $T_{\text{onset}}$ ), and the exothermic peak temperature ( $T_{\text{peak}}$ ) of crystallization were obtained from second heating cycle (Table 1). If a polymer is mixed with a material that does not melt in the same range of temperature, DSC is a way to record in what proportion it is added.<sup>37</sup> We selected the second cycle because this measurement does not record the history of the material, for example the way it was cooled down (the use of the enthalpy recorded at the first cycle gave anyway the same proportion of incorporated UCNPs, data not shown).

The melting points were similar whatever the stage of the process; this confirms the absence of PE chemical modification after the incorporation of UCNPs or powdering. The two samples before engagement in the dissolution/precipitation step, PE raw pellet and raw powder, had similar melting enthalpy. After cryogenic grinding, the enthalpy of  $\mu$ -Blank-PE was slightly superior, that is to say that the polymer was slightly more crystalline at this stage (85% of crystallinity compared to 83% initially). Knowing that UCNPs are thermodynamically stable in the hexagonal phase up to 700 °C,<sup>41</sup> their presence did not contribute to the enthalpy recorded between 20 °C to 160 °C. This led us UCNPs-content in  $\mu$ Upcon-PE at  $6.4 \pm 1.2$  wt.%. This rate was confirmed by thermogravimetric analysis which gave a value of 5.7% (Table S1).

**Table 1.** DSC analysis of raw PE pellets,  $\mu$ -Blank-PE and  $\mu$ -Upcon-PE. Melting enthalpy, onset temperature and exothermic peak temperature were obtained from the second heating cycle (average values  $\pm$  SD). The corresponding degrees of crystallinity ( $X_c$ ) were calculated as the ratio between  $\Delta H_m$  of the sample and the reference  $\Delta H_{mref}$  value for a 100% crystalline form of PE (293 J/g).<sup>31</sup>

Sample	$\Delta H_m$ , (J g <sup>-1</sup> )	$T_{onset}$ , (°C)	$T_m$ , (°C)	$X_c$ , (%)
PE raw pellet	-243.7 $\pm$ 1.4	122.4 $\pm$ 0.1	128.3 $\pm$ 0.4	83.2 $\pm$ 0.5
PE raw powder	-244.2 $\pm$ 3.4	122.8 $\pm$ 0.2	128.5 $\pm$ 0.3	83.3 $\pm$ 1.2
$\mu$ -Blank-PE	-250.6 $\pm$ 2.9	122.2 $\pm$ 0.1	128.9 $\pm$ 0.2	85.5 $\pm$ 1.0
$\mu$ -Upcon-PE	-234.5 $\pm$ 1.5	122.4 $\pm$ 0.3	129.2 $\pm$ 0.3	

### Study of UCNPs dispersion within PE

The way UCNPs were incorporated in PE was investigated in details with particles at the microscale by Small-Angle X-ray Scattering (SAXS). Details of the applied models for SAXS are given in Supporting Information. The SAXS curve of  $\mu$ -Blank-PE (Figure 3a and Figure S4) shows a constant decay with a small inflexion around 0.05 Å<sup>-1</sup>, reflecting the correlation distance between crystalline parts present in the PE matrix. The SAXS curve of  $\mu$ -Upcon-PE follows the same decay as the SAXS curve of  $\mu$ -Blank-PE plus the contribution of UCNPs (Figure 3a). The first result confirms that the UCNPs do not alter the organization of PE. The contribution of UCNPs was investigated in order to depict if the UCNPs were fully incorporated inside PE or adsorbed on the surface (partially incorporated) of PE. To discriminate the last case, a simulated SAXS curve was obtained by linear combination of the two contributions and compared to the experimental curve (Figure 3b). Data were plotted in  $\text{Log } I(q) \times q^4$  as a function of  $\text{Log } q$ , in order to magnify the differences. No linear combination of the SAXS curves of PE and UCNPs was found to fit the experimental SAXS data of Upcon-PE. The difference observed between the curves suggests that another term contributes to the SAXS curves. In the case where UCNPs are distributed in the PE matrix, it is necessary to consider the scattering cross terms, which reflect the interactions between atoms of UCNPs and PE. A simplified model was applied to describe  $\mu$ -Upcon-PE and a two-component one to describe the organization at large distances (see Applied models for SAXS analysis and Figure S5, in Supporting Information, for more details). The state of the surface of  $\mu$ -Blank-PE and  $\mu$ -Upcon-PE was found to be similar, indicating that the incorporation of UCNPs does not induce any

modification of the surface particle properties. This suggests that UCNPs are not adsorbed onto the surface of PE but rather fully incorporated inside the PE matrix. This result is interesting since PE is not prone to easily accept the incorporation of other material, fabrication of PE composites generally requiring more complex process than a simple dissolution/precipitation procedure like the one proposed here.<sup>42,43</sup> The effective incorporation of UCNPs into the PE prevents UCNPs from leaching and enables their detectability whatever the treatments or experiments done with them (washing, purification, use *in vivo*, etc.).

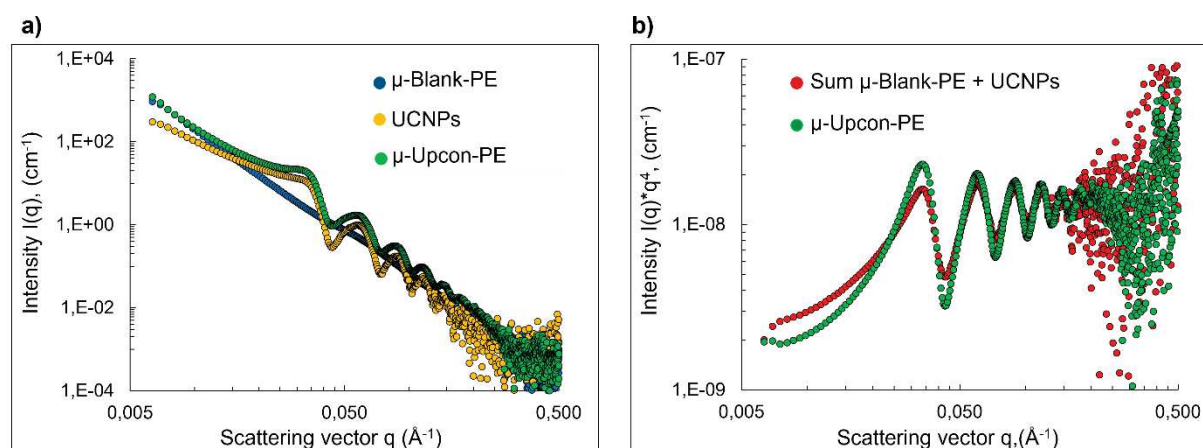


**Figure 3.** Small-Angle X-ray Scattering (SAXS) analysis of a) of  $\mu$ -Blank-PE (blue curve),  $\mu$ -Upcon-PE (green curve) and UCNPs alone (yellow curve), where  $\text{Log } I(q)$  is plotted as a function of  $\text{Log } q$ ; b) of  $\mu$ -Upcon-PE and simulated spectrum of a linear combination of the scattering curves of  $\mu$ -Blank-PE and UCNPs, considered as two independent contributions;  $\text{Log } I(q) \times q^4$  is plotted as a function of  $\text{Log } q$ .

## Colloidal properties of labelled nanoplastics

### Electron microscopy

As discussed earlier, NTA allowed to conclude that the particles prepared at the nanoscale were very polydisperse and mostly smaller than 200 nm. The shape of the particles was assessed by Transmission Electron Microscopy (TEM) and showed that the particles were indeed polydisperse and in addition polymorphic (Figure 4a). The incorporation of UCNP did not modify their shapes (data not shown). The heterogeneous shapes obtained by this top-down process is in accordance with a recent study.<sup>44</sup> The darker dots in the particles were supposed to be UCNP because they were expected to be highly dense and their size were around 20 nm (Figure 4a). The images showed that the UCNP were rather well dispersed within PE particles. The identification of UCNPs was confirmed by High Resolution TEM coupled to energy-

dispersive X-ray elemental analysis (TEM-EDX) as the dark dots showed the homogeneous distribution of F, Y and Yb (Figure 4 b and Figure S6 for more details). This result showed that the chemical integrity of UCNPs was maintained during the powdering process as well as their sizes and shapes.

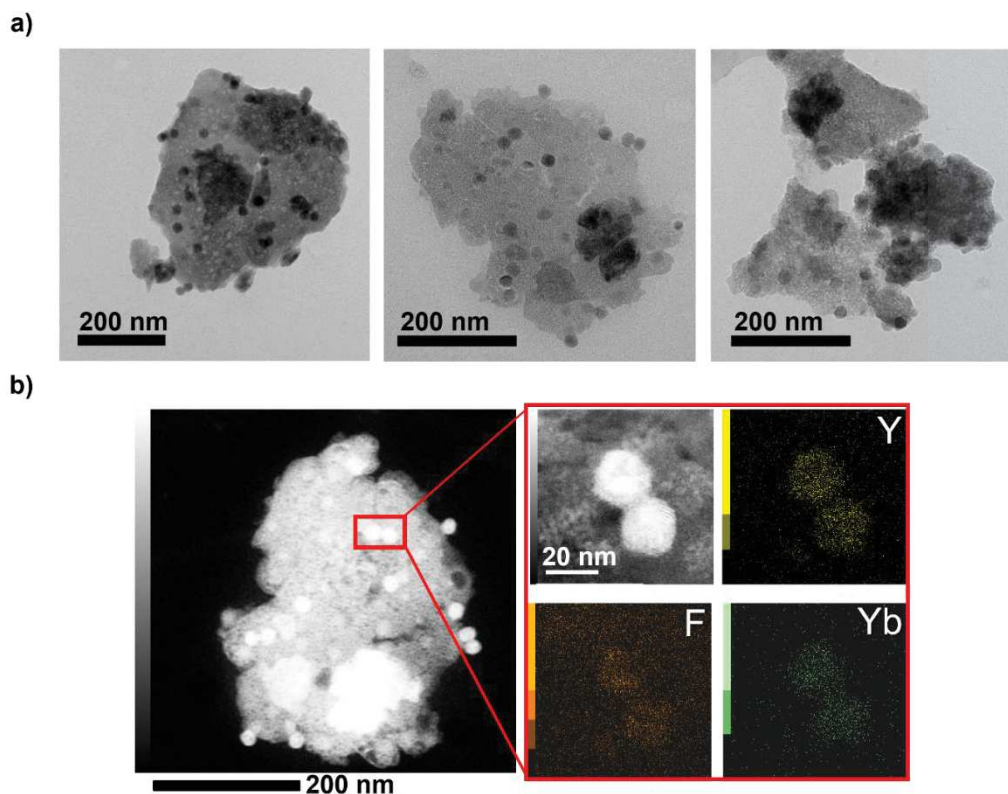


**Figure 4.** a) Transmission Electron Microscopy (TEM) bright field images of Nano-Upcon-PE. The three images illustrate the fact that the particles were polydisperse and polymorphic. b) High-Angle Annular Dark Field (HAADF) TEM of a single Nano-Upcon-PE along with Energy-Dispersive X-ray characterization of Yttrium (Y), Fluorine (F) and Ytterbium (Yb).

### Zeta potential

The surface charge of the produced micro- and nanometric particles was obtained by zeta-potential ( $\zeta$ -potential) measurements. Both at the micro- and nanoscale, the particles were found to be negatively charged (Table S2). The presence of incorporated UCNP did not significantly modify the particle charges. The zeta potential for the micro- and nano-metric particles were around -70 mV and -60 mV, respectively. These values were in accordance with a recent study using the top-down process, all the model NPs were negatively charged and the ones in PE had a zeta potential of  $-38 \pm 2.4$  mV at similar pH.<sup>44</sup>

It is expected that most NPs surfaces would bear functional groups like carboxylic acid or hydroxyl resulting from the oxidation of the polymer, consequently at neutral pH they are

expected to be negatively charged. The model NPs prepared are also negatively charged. This is an important parameter as the surface charge of nanoparticles dramatically affects their behavior in the environment or *in vivo*.<sup>45</sup>

### Emission properties of the labelled micro- and nanoplastic model

The emission properties of the UCNPs once incorporated in PE were investigated. Fluorescence measurements ( $\lambda_{\text{exc.}} = 980 \text{ nm}$ ) of the dispersed particles in ethanol showed no emission for Blank-PE while Upcon-PE show three emission peaks around 525, 550 and 655 nm, attributed to the  $\text{Er}^{3+}$  transitions  ${}^2\text{H}_{11/2} \rightarrow {}^4\text{I}_{15/2}$ ,  ${}^4\text{S}_{3/2} \rightarrow {}^4\text{I}_{15/2}$  and  ${}^4\text{F}_{9/2} \rightarrow {}^4\text{I}_{15/2}$ .<sup>36</sup> These specific emission peaks were observed with both  $\mu$ -Upcon-PE and Nano-Upcon-PE (Figure 5).

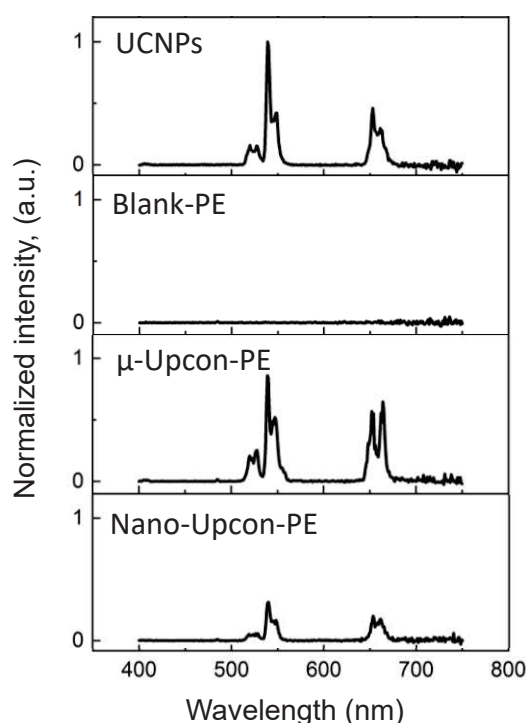


**Figure 5.** Upconversion emission spectra of UCNPs, Blank-PE, and Upcon-PE micro- and nanoparticles; normalized fluorescence intensity as a function of the wavelength ( $\lambda_{\text{exc.}} = 980 \text{ nm}$ ).

To check whether the UCNPs maintained their functionality once encapsulated in PE, the emission properties of all the prepared particles were investigated under upconversion conditions. Under continuous-wave laser irradiation at 980 nm, the pristine Er-UCNPs displayed a typical green visible luminescence. The recorded spectrum of the dispersed UCNPs in cyclohexane showed three emission peaks around 525, 550 (green) and 655 nm (red), attributed to the  $\text{Er}^{3+}$  transitions  ${}^2\text{H}_{11/2} \rightarrow {}^4\text{I}_{15/2}$ ,  ${}^4\text{S}_{3/2} \rightarrow {}^4\text{I}_{15/2}$  and  ${}^4\text{F}_{9/2} \rightarrow {}^4\text{I}_{15/2}$ .<sup>[33]</sup> (Figure 5). As expected, blank PE particles dispersed in ethanol did not show any signal in this spectral

range upon excitation under similar conditions. However, Upcon-PE (micro and nano) displayed an emission spectrum similar to the UCNPs' one: the upconversion property has not been lost in the PE-incorporation/grinding and milling process.

The suitability of such labelled PE particles for imaging purposes was then examined. UCNPs are known to be able to produce an upconversion spectrum under a large range of laser fluence, therefore a standard 2-photon emission microscope setup was employed. To achieve our goal the particles were spread over a microscope blade and examined under standard 2-photon microscopy conditions using 980 nm laser source. Images showed Z-projection in a maximum intensity (Figure 6). Under such conditions, control particles ( $\mu$ -Blank-PE) remained non-emissive while particles of  $\mu$ -Upcon-PE gave rise to green (G) and red (R) upconverted light that could be collected between 490 and 600 nm, and 630 and 710 nm, respectively. The absence of any emission from the  $\mu$ -Blank-PE particle indicates that no 2-photon processes occur in pure PE and justifies the use of UCNPs as background-free luminescent tag for plastic particles. The band ratio G/R was found to be different from the one recorded at lower fluence. It is known that the power dependence of the emission lines is rather non-linear, therefore the band ratio typically observed at very low fluence such as with a CW 980nm laser can be different when using a more intense pulse laser as what is commonly used to trigger 2-photon fluorescence emission. This spectral alteration is also a signature of the presence of the UCNPs and can be used to identify the tagged particles in more complex environments.

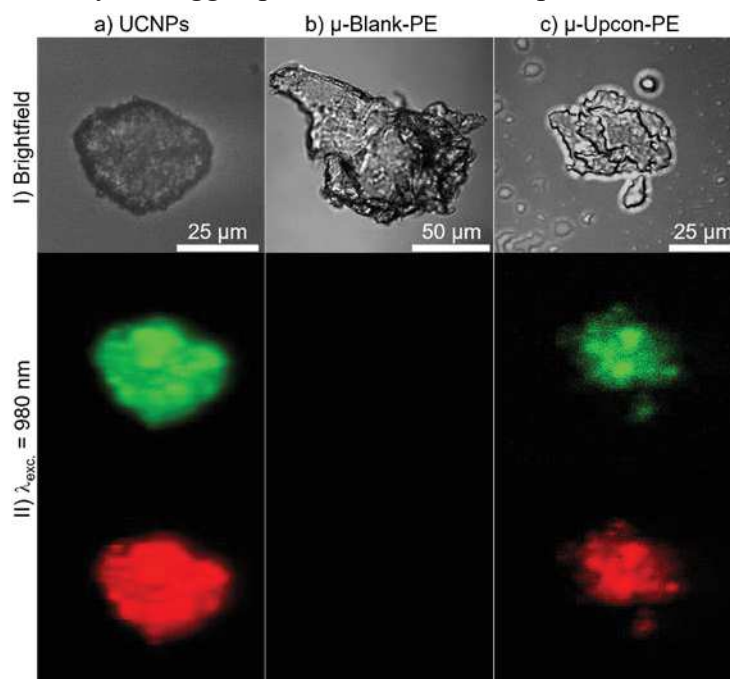


**Figure 6.** I) Brightfield image of particles aggregate: a) UCNPs; b)  $\mu$ -Blank-PE; c)  $\mu$ UCNPs-PE. II) Green and red emission under NIR irradiation observer for both a) UCNPs and c)  $\mu$ UCNPs-PE; b)  $\mu$ -Blank-PE remains non-emissive.



## Conclusion

This top-down synthesis allows to produce model plastic particles within the micro- and nanometric range which present a heterogeneity in size and shape that is absent for most of the particles formed by the bottom-up approaches. This method does not allow to control the amount of UCNPs incorporated in the polymer as the parameters of precipitation process are difficult to control, but the UCNPs content reach 6 % in weight. Using a series of physico-chemical characterization we evidenced that the UCNPs were incorporated within the polymer, not localised at its surface (SAXS) and well dispersed (TEM-EDX). The powdering process does not alter the chemical structure nor the morphology of the polymer (ATR-FTIR and DSC). The mixture of micro- and nano-metric objects formed can easily be separated by filtration; it is thus possible to select a range of size for a given application. The nanometric particles were formed in a small proportion (6% yield), but the remaining micrometric particles can be engaged in another long process of wet milling for further production of smaller particles.

The incorporation of the UCNPs did not alter their luminescent properties and the labelled PE particles can be easily monitored with a standard two-photon microscope. This offers the possibility to easily detect these model MPs and NPs in complex organic matrices while the detection of plastic itself is always difficult.

The method proposed is compatible with a large variety of polymers while the UCNPs rate of incorporation in the polymer matrix is not easily controllable and is certainly depending on the polarity and affinity of the UCNPs for the polymer. But this method also offers the possibility to use formulated polymers, like commercialized plastic in order to produce plastic particles even closer to the ones present in the environment. This process is also compatible with weathered polymers.

The polydispersity and heterogeneity of the particles prepared make them very good environmentally relevant models. These two properties are very scarcely considered in the actual toxicological evaluation studies because most of the particles used are produced with a bottom-up method.<sup>[10]</sup> Thanks to its extreme photostable and NIR-activable luminescent properties, strategies based on its use can pave the way for a deeper understanding of the fate of plastic particles in the trophic chain.

## Acknowledgements

The authors acknowledge the Université Paul Sabatier and CNRS for financial support. C. C., B. A. and A.-F. M. gratefully acknowledge the Agence Nationale de la Recherche (Grant ANR-15-CE09-0020 BLINK) for financial support. We would like to thank Teresa *Hungria* (The

Raimond Castaing (Micro-characterisation Centre) for the TEM/EDX images, Corinne Routaboul (The infrared spectroscopy service, Institute of Chemistry of Toulouse (ICT)), for the help with ATR-FTIR analysis, Rodica Chiriac (Thermal Analysis Platform (PLAT)) at the Laboratory of Multimaterials and Interfaces (LMI), for the TGA analysis, and Christine Rey-Rouch (Service Analyse et Procédés - SAP, Chemical Engineering Laboratory (LGC)) for granulometry analysis. Antonio Peixoto (IPBS) for two-photon microscopy images.

## References

- 1 O. S. Alimi, J. Farner Budarz, L. M. Hernandez and N. Tufenkji, Microplastics and Nanoplastics in Aquatic Environments: Aggregation, Deposition, and Enhanced Contaminant Transport, *Environ Sci Technol*, 2018, **52**, 1704–1724.
- 2 J. Gigault, A. ter Halle, M. Baudrimont, P.-Y. Pascal, F. Gauffre, T.-L. Phi, H. El Hadri, B. Grassl and S. Reynaud, Current opinion: What is a nanoplastic?, *Environmental Pollution*, 2018, **235**, 1030–1034.
- 3 A. Ter Halle, L. Jeanneau, M. Martignac, E. Jardé, B. Pedrono, L. Brach and J. Gigault, Nanoplastic in the North Atlantic Subtropical Gyre, *Environ. Sci. Technol.*, 2017, **51**, 13689–13697.
- 4 A. A. Horton, A. Walton, D. J. Spurgeon, E. Lahive and C. Svendsen, Microplastics in freshwater and terrestrial environments: Evaluating the current understanding to identify the knowledge gaps and future research priorities, *Science of The Total Environment*, 2017, **586**, 127–141.
- 5 M. Cole, P. Lindeque, E. Fileman, C. Halsband, R. Goodhead, J. Moger and T. S. Galloway, Microplastic Ingestion by Zooplankton, *Environ. Sci. Technol.*, 2013, **47**, 6646–6655.
- 6 L. J. Zantis, E. L. Carroll, S. E. Nelms and T. Bosker, Marine mammals and microplastics: A systematic review and call for standardisation, *Environmental Pollution*, 2021, **269**, 116142.
- 7 S. Anbumani and P. Kakkar, Ecotoxicological effects of microplastics on biota: a review, *Environ Sci Pollut Res*, 2018, **25**, 14373–14396.
- 8 C. G. Alimba and C. Faggio, Microplastics in the marine environment: Current trends in environmental pollution and mechanisms of toxicological profile, *Environmental Toxicology and Pharmacology*, 2019, **68**, 61–74.
- 9 T. S. Galloway, M. Cole and C. Lewis, Interactions of microplastic debris throughout the marine ecosystem, *Nat Ecol Evol*, 2017, **1**, 116.
- 10 J. Gigault, H. El Hadri, B. Nguyen, B. Grassl, L. Roweczyk, N. Tufenkji, S. Feng and M. Wiesner, Nanoplastics are neither microplastics nor engineered nanoparticles, *Nat. Nanotechnol.*, 2021, **16**, 501–507.
- 11 C. Larue, G. Sarret, H. Castillo-Michel and A. E. Pradas del Real, A Critical Review on the Impacts of Nanoplastics and Microplastics on Aquatic and Terrestrial Photosynthetic Organisms, *Small*, 2021, **17**, 2005834.
- 12 L. C. de Sá, M. Oliveira, F. Ribeiro, T. L. Rocha and M. N. Futter, Studies of the effects of microplastics on aquatic organisms: What do we know and where should we focus our efforts in the future?, *Science of The Total Environment*, 2018, **645**, 1029–1039.
- 13 A. Reverberi, M. Vocciante, E. Lunghi, L. Pietrelli and B. Fabiano, New Trends in the Synthesis of Nanoparticles by Green Methods, *Chemical Engineering Transactions*, 2017, **61**, 667–672.

- 14 D. Magri, P. Sánchez-Moreno, G. Caputo, F. Gatto, M. Veronesi, G. Bardi, T. Catelani, D. Guarnieri, A. Athanassiou, P. P. Pompa and D. Fragouli, Laser Ablation as a Versatile Tool To Mimic Polyethylene Terephthalate Nanoplastic Pollutants: Characterization and Toxicology Assessment, *ACS Nano*, 2018, **12**, 7690–7700.
- 15 A. F. Astner, D. G. Hayes, H. O’Neill, B. R. Evans, S. V. Pingali, V. S. Urban and T. M. Young, Mechanical formation of micro- and nano-plastic materials for environmental studies in agricultural ecosystems, *Science of The Total Environment*, 2019, **685**, 1097–1106.
- 16 H. El Hadri, J. M. Lisa, J. Gigault, S. Reynaud and B. Grassl, Fate of nanoplastics in the environment: Implication of the cigarette butts, *Environmental Pollution*, 2021, **268**, 115170.
- 17 M. Baudrimont, A. Arini, C. Guégan, Z. Venel, J. Gigault, B. Pedrono, J. Prunier, L. Maurice, A. Ter Halle and A. Feurtet-Mazel, Ecotoxicity of polyethylene nanoplastics from the North Atlantic oceanic gyre on freshwater and marine organisms (microalgae and filter-feeding bivalves), *Environ Sci Pollut Res*, 2020, **27**, 3746–3755.
- 18 M. Sander, H.-P. E. Kohler and K. McNeill, Assessing the environmental transformation of nanoplastic through <sup>13</sup>C-labelled polymers, *Nat. Nanotechnol.*, 2019, **14**, 301–303.
- 19 D. M. Mitrano, A. Beltzung, S. Frehland, M. Schmiedgruber, A. Cingolani and F. Schmidt, Synthesis of metal-doped nanoplastics and their utility to investigate fate and behaviour in complex environmental systems, *Nat. Nanotechnol.*, 2019, **14**, 362–368.
- 20 T. Maes, R. Jessop, N. Wellner, K. Haupt and A. G. Mayes, A rapid-screening approach to detect and quantify microplastics based on fluorescent tagging with Nile Red, *Sci Rep*, 2017, **7**, 44501.
- 21 A. Paganin-Gioanni, E. Bellard, L. Paquereau, V. Ecochard, M. Golzio and J. Teissié, Fluorescence imaging agents in cancerology, *Radiology and Oncology*, 2010, **44**, 142–148.
- 22 P. Greenspan and S. D. Fowler, Spectrofluorometric studies of the lipid probe, Nile Red, *J Lipid Res*, 1985, **26**, 781–789.
- 23 S. F. Himmelstoß and T. Hirsch, A critical comparison of lanthanide based upconversion nanoparticles to fluorescent proteins, semiconductor quantum dots, and carbon dots for use in optical sensing and imaging, *Methods Appl Fluoresc*, 2019, **7**, 022002.
- 24 M. Kermorgant, J. Ben Salem, J. Santelli, D. Calise, A.-C. Oster, O. Lairez, C. Coudret, M. Verelst, C. Gales, J.-M. Sénard, F. Beaudry, A. Pavy-Le Traon, C. Roux, R. Mauricot and D. N. Arvanitis, Evaluation of upconverting nanoparticles towards heart theranostics, *PLoS One*, 2019, **14**, e0225729.
- 25 B. Amouroux, C. Roux, J.-C. Micheau, F. Gauffre and C. Coudret, A photochemical determination of luminescence efficiency of upconverting nanoparticles, *Beilstein J. Org. Chem.*, 2019, **15**, 2671–2677.
- 26 M. V. DaCosta, S. Doughan, Y. Han and U. J. Krull, Lanthanide upconversion nanoparticles and applications in bioassays and bioimaging: a review, *Anal Chim Acta*, 2014, **832**, 1–33.
- 27 Y. I. Park, K. T. Lee, Y. D. Suh and T. Hyeon, Upconverting nanoparticles: a versatile platform for wide-field two-photon microscopy and multi-modal in vivo imaging, *Chem Soc Rev*, 2015, **44**, 1302–1317.
- 28 R. Yang, Ed., *Principles and Applications of Up-converting Phosphor Technology*, Springer Singapore, 2019.
- 29 D. Kang, E. Jeon, S. Kim and J. Lee, Lanthanide-Doped Upconversion Nanomaterials: Recent Advances and Applications, *BioChip J*, 2020, **14**, 124–135.

- 30 S. Wu, G. Han, D. J. Milliron, S. Aloni, V. Altoe, D. V. Talapin, B. E. Cohen and P. J. Schuck, Non-blinking and photostable upconverted luminescence from single lanthanide-doped nanocrystals, *Proc Natl Acad Sci U S A*, 2009, **106**, 10917–10921.
- 31 T. Ahmed and O. Mamat, The development and characterization of HDPE-silica sand nanoparticles composites, *2011 IEEE Colloquium on Humanities, Science and Engineering*, 2011, 6–11.
- 32 ASTM E2865-12, *Guide for Measurement of Electrophoretic Mobility and Zeta Potential of Nanosized Biological Materials*, ASTM International, West Conshohocken, PA, 2018.
- 33 S. Wilhelm, M. Kaiser, C. Würth, J. Heiland, C. Carrillo-Carrion, V. Muhr, O. S. Wolfbeis, W. J. Parak, U. Resch-Genger and T. Hirsch, Water dispersible upconverting nanoparticles: effects of surface modification on their luminescence and colloidal stability, *Nanoscale*, 2015, **7**, 1403–1410.
- 34 Y. Jiao, C. Ling, J.-X. Wang, H. Amanico, J. Saczek, H. Wang, S. Sridhar, B. B. Xu, S. Wang and D. Wang, Controllable Synthesis of Upconversion Nanophosphors toward Scale-Up Productions, *Particle & Particle Systems Characterization*, 2020, **37**, 2000129.
- 35 B. Amouroux, C. Roux, J.-D. Marty, M. Pasturel, A. Bouchet, M. Sliwa, O. Leroux, F. Gauffre and C. Coudret, Importance of the Mixing and High-Temperature Heating Steps in the Controlled Thermal Coprecipitation Synthesis of Sub-5-nm Na(Gd-Yb)F<sub>4</sub>:Tm, *Inorg Chem*, 2019, **58**, 5082–5088.
- 36 Z. Li and Y. Zhang, An efficient and user-friendly method for the synthesis of hexagonal-phase NaYF<sub>4</sub>:Yb, Er/Tm nanocrystals with controllable shape and upconversion fluorescence, *Nanotechnology*, 2008, **19**, 345606.
- 37 J. L. Gao, Y. H. Liu and S. D. Wei, Preparation and Properties of High-Density Polyethylene/Silica Composites, *Advanced Materials Research*, 2011, **279**, 115–119.
- 38 M. Trofa, G. D'Avino, B. Fabiano and M. Vocciante, Nanoparticles Synthesis in Wet-Operating Stirred Media: Investigation on the Grinding Efficiency, *Materials (Basel)*, 2020, **13**, E4281.
- 39 M. Dehghani, K. Lucas, J. Flax, J. McGrath and T. Gaborski, Tangential flow microfluidics for the capture and release of nanoparticles and extracellular vesicles on conventional and ultrathin membranes, *Adv Mater Technol*, 2019, **4**, 1900539.
- 40 E. Chiellini, A. Corti, S. D'Antone and R. Baciú, Oxo-biodegradable carbon backbone polymers – Oxidative degradation of polyethylene under accelerated test conditions, *Polymer Degradation and Stability*, 2006, **91**, 2739–2747.
- 41 R. E. Thoma, H. Insley and G. M. Hebert, The Sodium Fluoride-Lanthanide Trifluoride Systems, *Inorg. Chem.*, 1966, **5**, 1222–1229.
- 42 W.-H. Xu, Y. He, H. Xie, S. Qin, L.-C. Tan, T. Wu and J.-P. Qu, Ultrafast Fabrication of Graphene-Reinforced Nanocomposites via Synergy of Steam Explosion and Alternating Convergent-Divergent Flow, *Small*, 2021, **17**, e2100017.
- 43 C. Hu, X. Liao, Q.-H. Qin and G. Wang, The fabrication and characterization of high density polyethylene composites reinforced by carbon nanotube coated carbon fibers, *Composites Part A: Applied Science and Manufacturing*, 2019, **121**, 149–156.
- 44 H. El Hadri, J. Gigault, B. Maxit, B. Grassl and S. Reynaud, Nanoplastic from mechanically degraded primary and secondary microplastics for environmental assessments, *NanoImpact*, 2020, **17**, 100206.
- 45 E. M. Hotze, T. Phenrat and G. V. Lowry, Nanoparticle aggregation: challenges to understanding transport and reactivity in the environment, *J Environ Qual*, 2010, **39**, 1909–1924.

## II.3. Supplementary information

### Top-Down Synthesis of Luminescent Micro- and Nano-plastics by Incorporation of Upconverting Nanoparticles for Environmental Assessment

Nadiia Yakovenko<sup>a</sup>, Baptiste Amouroux<sup>a</sup>, Magali Albignac<sup>a</sup>, Fabrice Collin<sup>a</sup>, Clément Roux<sup>a</sup>, Anne-Françoise Mingotaud<sup>a</sup>, Pierre Roblin<sup>c</sup>, Christophe Coudret<sup>a\*</sup>, Alexandra Ter-Halle<sup>a\*</sup>

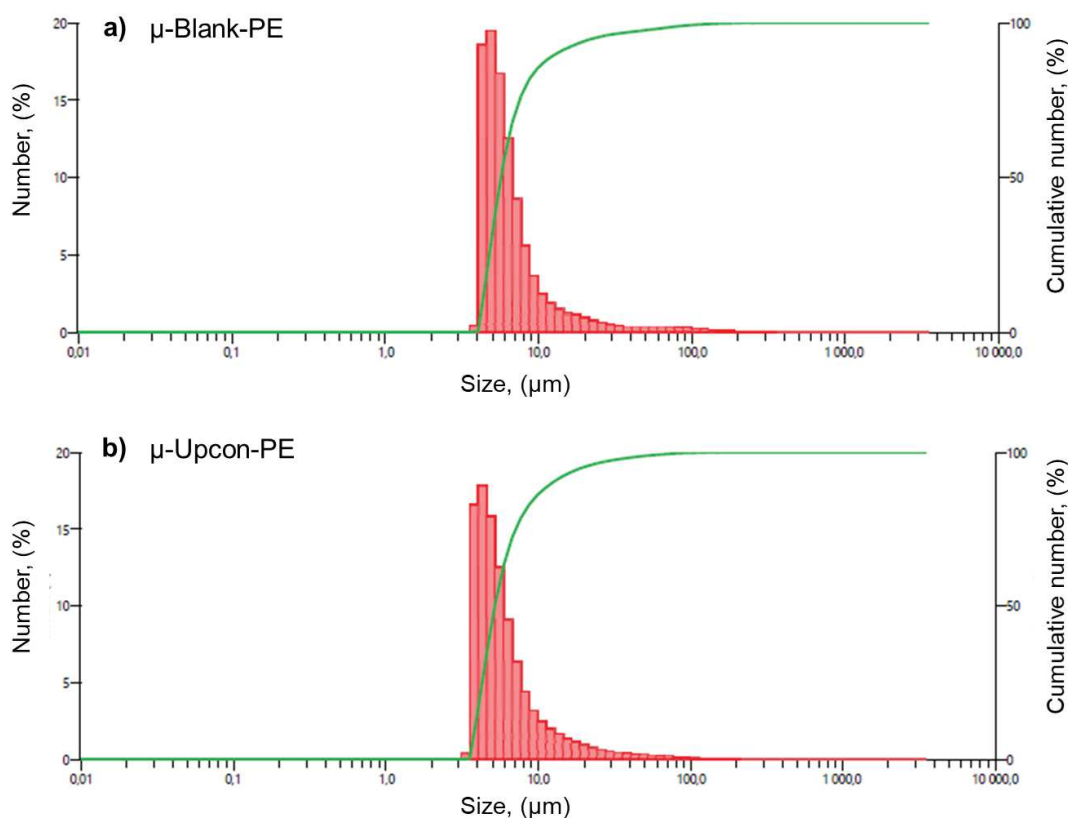


**Figure S1.** Granulometric analysis after cryogenic grinding, expressed as a percentage number and percentage cumulative number as a function of the size of a) the blank where  $D_n(10) = 4.31 \mu\text{m}$ ,  $D_n(50) = 5.69 \mu\text{m}$  and  $D_n(90) = 13 \mu\text{m}$  and b) the UCNPs doped particle where  $D_n(10) = 3.82 \mu\text{m}$ ,  $D_n(50) = 5.18 \mu\text{m}$  and  $D_n(90) = 12.3 \mu\text{m}$ . The distribution of the particles is not significantly different with or without incorporation of UCNP. The parameter  $D_n(x)$  is the value in size distribution, up to and including which,  $x\%$  of the total number of particles in the sample. Acronyms: Upconverting Nanoparticles (UCNPs).

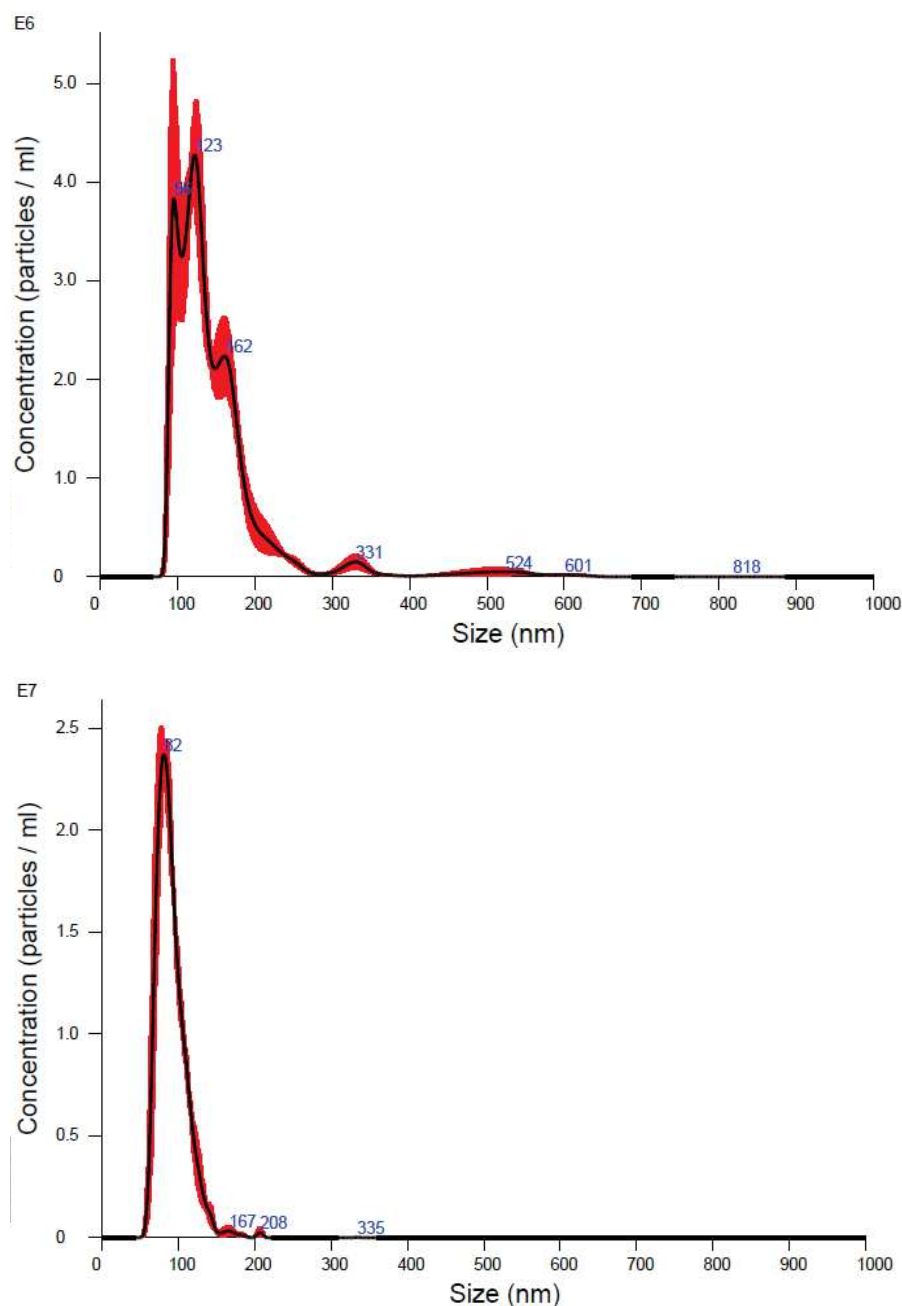


**Figure S2.** Size distributions of Blank-Upcon-PE and Nano-Upcon-PE obtained by Nanoparticle Tracking Analysis (NTA). Data are presented as average concentration per size over three measurements. For the Blank-Upcon-PE the values obtained were  $D_n(10) = 96.9$  nm,  $D_n(50) = 130.9$  nm,  $D_n(90) = 201.4$  nm and b) for Nano-Upcon-PE  $D_n(10) = 70.8$  nm,  $D_n(50) = 87.9$  nm and  $D_n(90) = 117.3$  nm. The distribution of the particles is not significantly different with or without incorporation of UCNPs. The parameter  $D_n(x)$  is the value in size distribution, up to and including which,  $x\%$  of the total number of particles in the sample. Acronyms: Upconverting Nanoparticles (UCNPs).

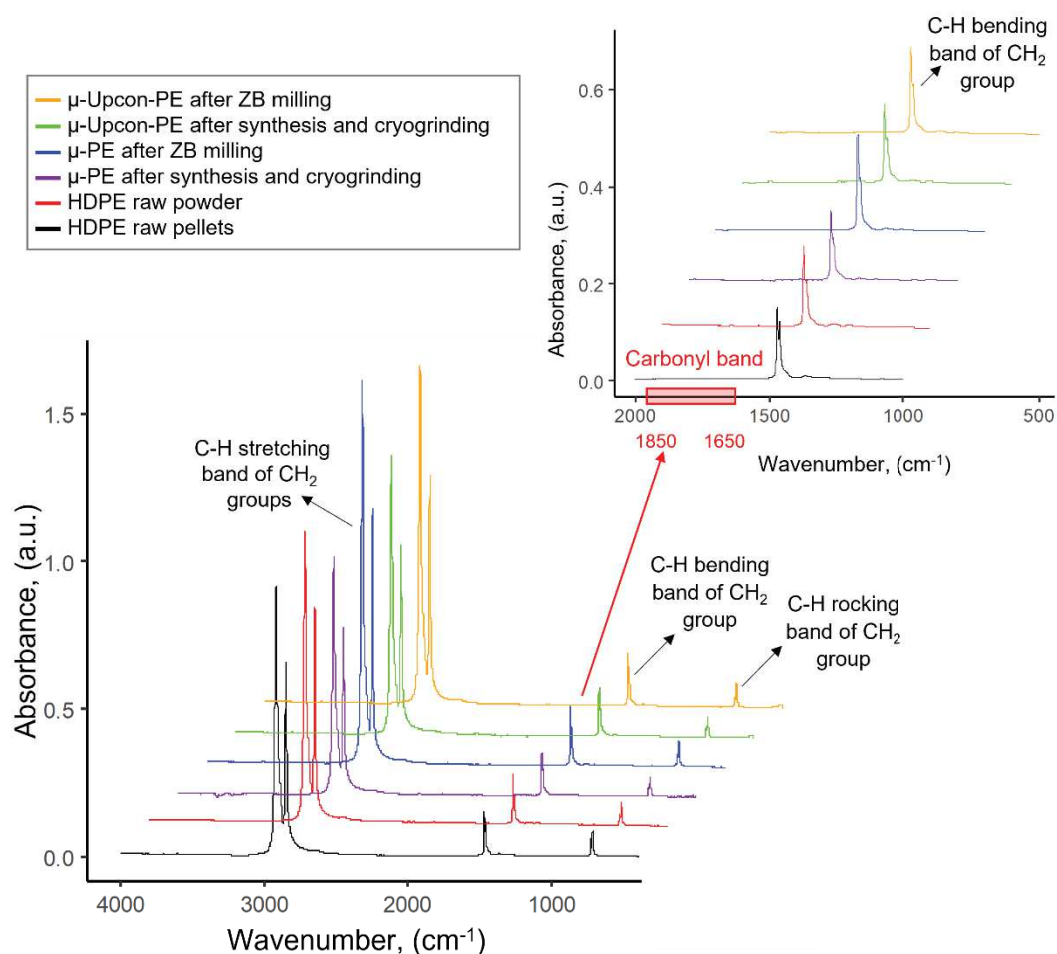


**Figure S3.** Attenuated Total Reflectance Fourier Transform Infrared Spectroscopy (ATR-FTIR) of raw PE and at different stage of the particle synthesis were recorded using a Thermo Nicolet 6700 spectrometer equipped with a diamond crystal attenuated total reflectance accessory and a deuterated triglycine sulfate (DTGS) detector. Background and sample spectra were recorded as the average of 16 scans in the spectral range of 650-4000 cm<sup>-1</sup> at a resolution of 4 cm<sup>-1</sup>. Recorded data were corrected to obtain transmission-like spectra using the ATR Thermo correction (the refractive index considered as 1.5). The carbonyl signal for all analysed samples was integrated in the 1650-1850 cm<sup>-1</sup> region. a) FTIR spectra of raw PE material and both Blank-PE and Upcon-PE samples recorded after every processing step of MPs synthesis (synthesis of bulk material, cryogenic grinding, ZB milling); b) Zoom around the carbonyl region, showing absence of carbonyl band, that signify that no oxidation occurs for PE during synthesis of MPs.

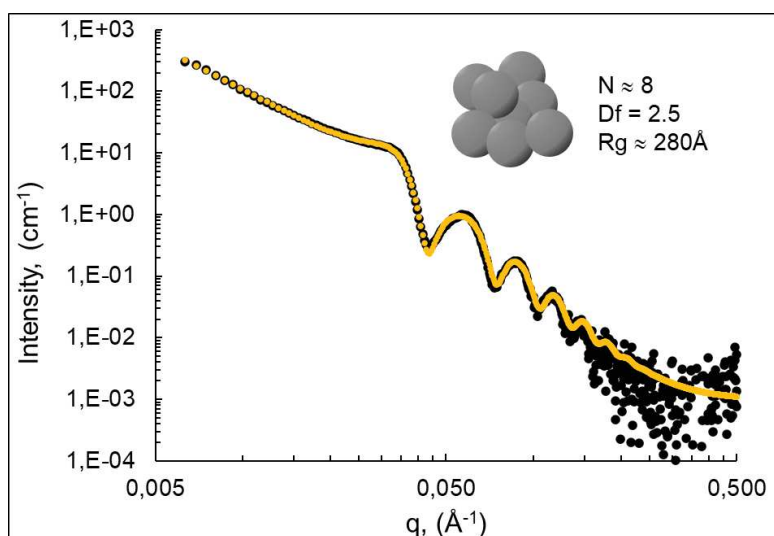


**Figure S4:** SAXS spectrum of UCNPs in solution. The experimental SAXS curve is plotted in  $\text{Log } I(q)$  as a function of  $\text{Log } q$  (black dots). The scattering curve can be described as the scattering of an aggregate object containing hard spheres. The fitting curve corresponding to the modeled SAXS curve is plotted in red dots, for a model compatible to the SAXS data that was found to have the following physical parameters: number of nanosphere per cluster  $N = 8$ , fractal dimension  $Df = 2.5$  and gyration radius  $Rg = 280 \pm 10 \text{ \AA}$ .



### Applied models for SAXS analysis

The SAXS curves can be described by the following equation written with SASView program (SasView, <http://www.sasview.org/>):

$$I(q)_{global} = I(q)_{powerlaw} + I(q)_{sphere} * S(q)_{hardsphere} \quad (1)$$

$$I(q)_{global} = Aq^{-P} + \frac{B}{V} \left[ \frac{3V(\Delta\rho)(\sin(qr) - qr\cos(qr))}{(qr)^3} \right]^2 * S(q)$$

where the  $A$  and  $B$  are factor scaling and the sphere is described by the volume  $V$ , the radius  $r$  and the contrast  $\Delta\rho$ . The nanospheres interact each other and the conditions where  $S(q) = 1$  at small angles was not verified. The form factor  $S(q)$  is described here with an “hard sphere interaction model” described by Percus-Yevick (J.K. Percus, J. Yevick, J. Phys. Rev., 1958, 110, 1).

In the case UCNPs are distributed in the PE matrix, it is necessary to consider the scattering cross terms that reflect the interactions between the atoms of UCNPs and PE. However, we can apply the simplified model proposed in equation (1) to describe Upcon-PE and a two-component model to describe the organization of PE MPs at large distances as following:

$$I(q) = Aq^{-P} + \frac{C}{(1+|q_0-q|\xi)^m} \quad (3)$$

Where the second term represents a Lorentzian function to describe the interaction between the crystalline cluters inside the plastic matrix.  $q_0$  is the position of the peak corresponding to the averaged distance separating the clusters ( $q_0 = 0.05 \text{ \AA}^{-1} \Leftrightarrow d = 125 \text{ \AA}$ ).

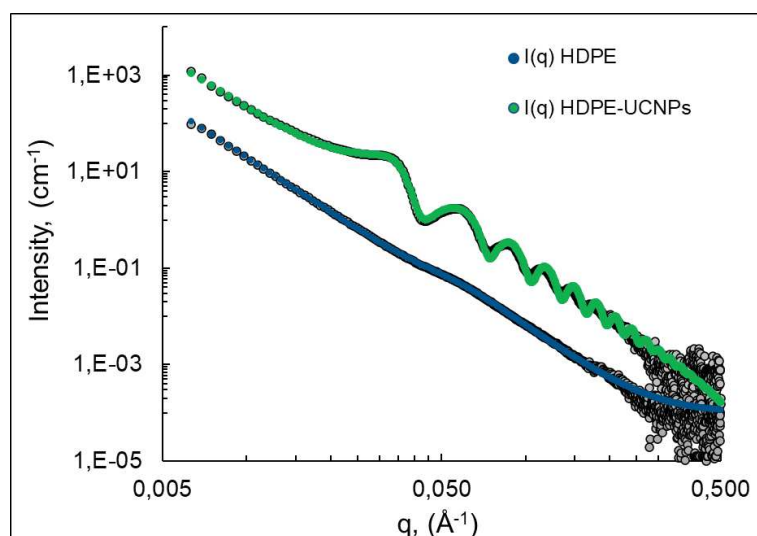


**Figure S5.** SAXS spectra of  $\mu$ -Blank-PE (blue) and  $\mu$ -Upcon-PE (green), along with superimposed fitting curves (blue and green, respectively). The experimental SAXS curves are plotted in Log  $I(q)$  as a function of Log  $q$ .

The most interesting term is the exponent parameter  $P$  in eq. (1) and (3), which describes the state of the particle surface. For both curves, the value is close to 3.7 corresponding to a slightly rough surface. The absence of difference in value of  $P$  suggests that the presence of UCNPs does not modify the state of PE MPs surface. Thus, these results suggest that UCNPs are absorbed inside the PE matrix.

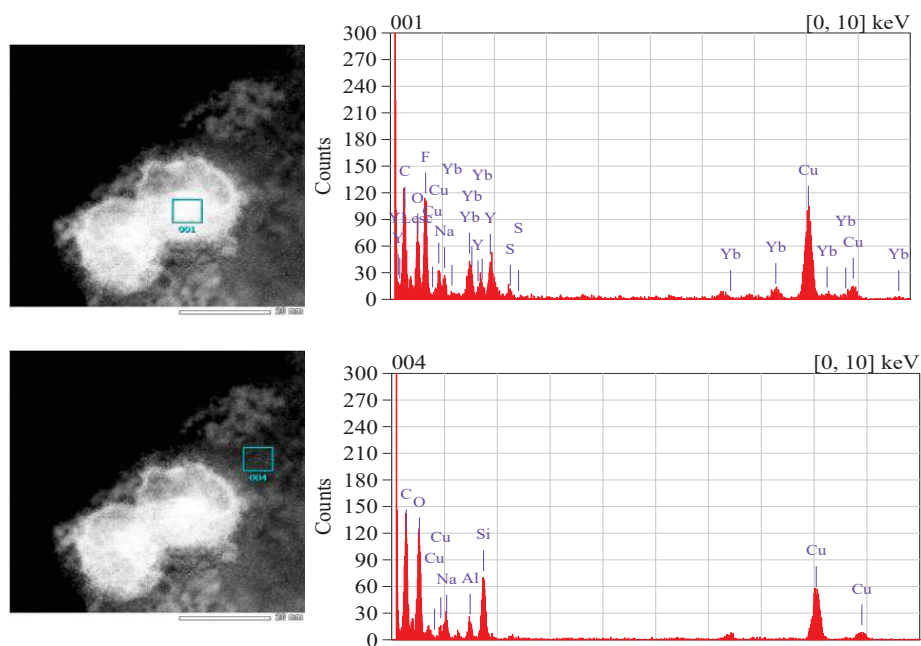


**Figure S6.** TEM image and energy-dispersive X-ray spectra of Upcon-PE nanoparticles. The box indicates where the measurement was taken on UCNP (top) and on the PE matrix (bottom). Fluorine, yttrium, and ytterbium are detected in UCNP, while not present in PE matrix.

**Table S1.** The thermal stability of the samples was analysed using Thermogravimetric analysis (TGA). The apparatus was a TGA/SDTA 851 Mettler Toledo device. Around 15 mg of each sample were placed in 150  $\mu$ L aluminium pans with a pierced cover. The analysis was performed from 30 to 900  $^{\circ}$ C, at a heating rate of 10 $^{\circ}$ C/min under a nitrogen atmosphere with a rated flow of 40 mL/min. For each sample, a blank (analysis with empty crucible) was carried out under the same conditions as for the sample. All samples were analysed in duplicate.

Sample	Mass, (mg)	T <sub>peak</sub> , ( $^{\circ}$ C)	Mass loss, (%)	Residue, (%)
PE raw powder	15.31	483	100.8	-0.8
$\mu$ -Blank-PE	15.45	483	100.7	-0.7
$\mu$ -Upcon-PE	15.84	481	94.3	5.7

**Table S2.** Average zeta-potential were measured at 10 mM NaCl at native pH of 7.8 for the micrometric particles and at pH of 7.5 for the nanometric particles.

Sample	Zeta potential, (mV)
$\mu$ -Blank-PE	-71 $\pm$ 7
$\mu$ -Upcon-PE	-73 $\pm$ 8
Nano-Blank-PE	-56 $\pm$ 11
Nano-Upcon-PE	-62 $\pm$ 10



## Chapter III.

Study of the mechanism of  
interaction between microplastic  
and microalgae



## **Table of content**

III.1. French summary .....	90
III.2. Article .....	98



### III.1. French summary

Ce chapitre présente les résultats obtenus lors de l'étude de l'interaction entre MPs et cellules de microalgues, et leur rôle dans l'agrégation de ces dernières. Cette étude a été réalisée en menant principalement des expériences à l'échelle nanométrique et moléculaire par microscopie à force atomique (AFM). Les microparticules de HDPE préparées précédemment ont été utilisées comme modèle de MPs qui sera noté Model-MPs (voir chapitre II). Le modèle de microalgues était constitué par la microalgue verte d'eau douce *Chlorella vulgaris*. Les travaux réalisés vont donner lieu à un article intitulé "The role of microplastics in microalgae cells aggregation: a study at the molecular scale using AFM", qui sera prochainement soumis pour publication.

Dans la première partie de cette étude, le Model-MPs a été caractérisé à l'aide d'un AFM et d'un microscope à force fluide (Fluid FM) pour visualiser les particules et obtenir des informations sur leur rugosité. Le caractère hydrophobe de leur surface a également été étudié, et vient en complément de la caractérisation physico-chimique exposée dans le chapitre II.

Tout d'abord, les  $\mu$ -PE (modèle de MPs de HDPE) et les  $\mu$ -Upcon-PE (modèle de MPs de HDPE marqué par des UCNPs) immobilisés sur des substrats en PolyDiMethylSiloxane (PDMS) ont été imagés par AFM en mode contact (Figure III.1). Les images AFM 3D enregistrées en hauteur (Figures III.1a et b) et en déviation verticale (Figures III.1c et d) montrent que les deux types de Model-MPs ( $\mu$ -PE et  $\mu$ -Upcon-PE) ont une forme et une surface irrégulières. Ils se trouvent principalement sous forme d'agrégats de particules et ne sont pas présents en tant qu'entités uniques. Ceci est confirmé par la coupe transversale prise le long des côtés les plus longs des particules dans les figures III.1c et 1d, qui montre clairement cette irrégularité, avec des variations de hauteur de plus de 6 nm (figures 1e et f). Nous avons ensuite acquis des images haute résolution sur de petites zones ( $5\mu\text{m} \times 5\mu\text{m}$ ) sur le dessus des particules, en utilisant la figure d'imagerie quantitative (QI) en mode avancé (Figures III.1g et h). De cette façon, nous avons pu obtenir des images haute résolution de la surface des particules (Figures III.1i et j), et quantifier leur rugosité (Figure III.1k). Les  $\mu$ -PE ont une rugosité moyenne de  $3,7 \pm 1,1$  nm, qui augmente à  $7,6 \pm 5,4$  nm lorsque les UCNPs sont incorporées dans les particules. Ce résultat montre donc que l'incorporation d'UCNPs peut affecter la structure des Model-MPs, en modifiant leur morphologie de surface. Cependant, l'hétérogénéité des mesures effectuées sur les  $\mu$ -Upcon-PE reflète l'incorporation non contrôlée des UCNPs sur les particules présentes dans l'échantillon.

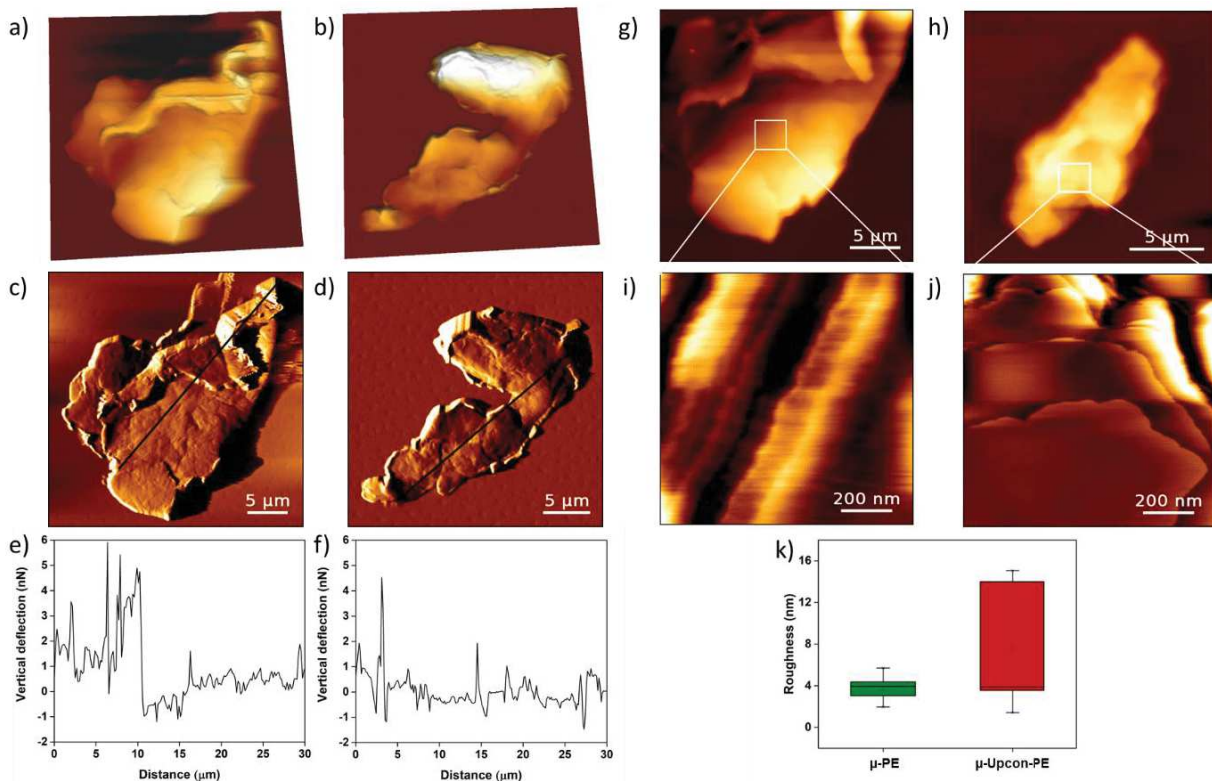


**Figure III. 1: Imagerie et caractérisation de la surface du  $\mu$ -PE avec ou sans incorporation d'UCNPs :** a) Image AFM 3D en hauteur du  $\mu$ -PE ; b) Image AFM 3D en hauteur du  $\mu$ -Upcon-PE ; c) Images en déviation verticale du  $\mu$ -PE ; d) Images en déviation verticale du  $\mu$ -Upcon-PE ; e) et f) Déflexion verticale en fonction de la distance, selon l'axe transversal pris le long du côté le plus large dans l'image c) et d) ; g) Images AFM en hauteur du  $\mu$ -PE et h) Images AFM en hauteur des  $\mu$ -Upcon-PE ; i) Images AFM en hauteur de la surface du  $\mu$ -PE en haute résolution ( $5\mu\text{m} \times 5\mu\text{m}$ ) et j) Images AFM de la hauteur de la surface des  $\mu$ -Upcon-PE en haute résolution ( $5\mu\text{m} \times 5\mu\text{m}$ ) ; k) Mesure de rugosité des  $\mu$ -PE et  $\mu$ -Upcon-PE représentée dans une boîte à moustaches (box plot).

Les propriétés d'hydrophobicité des Model-MPs ont été obtenues en sondant les interactions de surface des particules avec les bulles d'air produites en utilisant la technologie FluidFM. Les Model-MPs ont été immobilisés sur un substrat PDMS et leur interaction avec les bulles a été mesurée dans un tampon PBS à pH 7.4 (Figure III.2a). Des interactions hydrophobes, avec une force moyenne de  $10,1 \pm 6,2$  nN et  $13,7 \pm 15,3$  nN ont été obtenues respectivement pour les  $\mu$ -PE et les  $\mu$ -Upcon-PE. Après avoir incubé les  $\mu$ -(Upcon)-PE (soit  $\mu$ -PE et  $\mu$ -Upcon-PE) avec des cellules en culture pendant 7 jours, les interactions hydrophobes ont été enregistrées, avec une force d'adhésion moyenne de  $16,4 \pm 8,0$  nN. Ce point est important car il signifie que les Model-MPs ont leur surface modifiée après sept jours d'exposition aux cellules. Une hypothèse plausible pourrait être que les cellules produisent de la matière organique algale (AOM) dans le milieu de culture, qui pourrait alors être présente à la surface des particules.

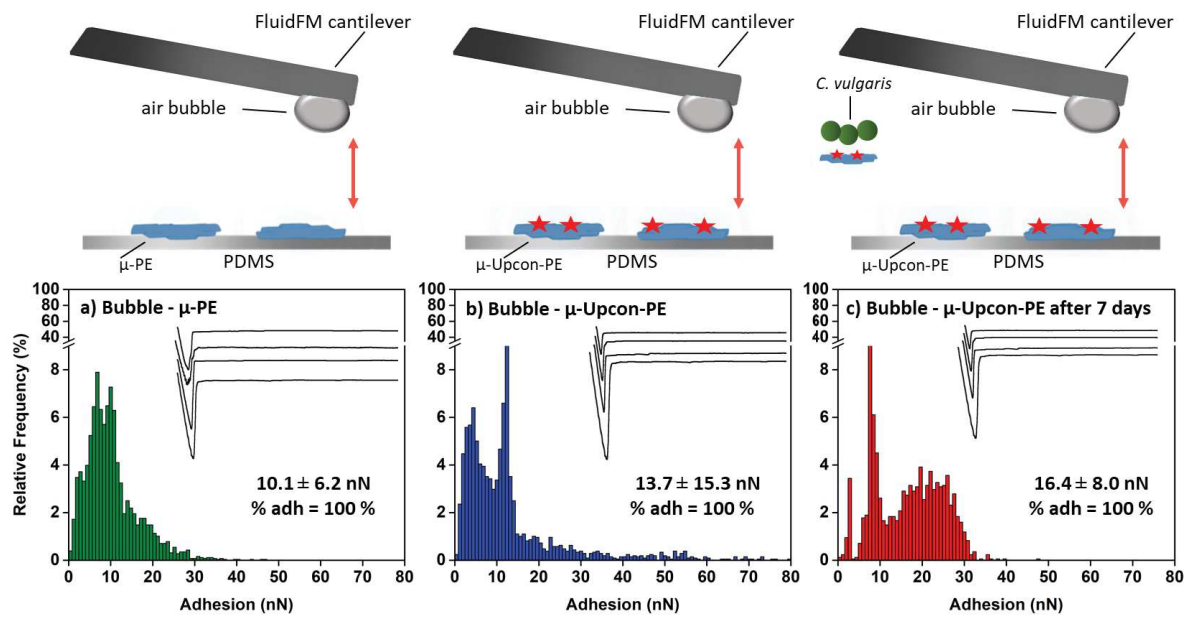


Figure III. 2: Evaluation de l'hydrophobicité des Model-MPs. Histogrammes de la force d'adhésion obtenue pour l'interaction entre une bulle d'air et a) les  $\mu$ -PE, b) les  $\mu$ -Upcon-PE, et c) les  $\mu$ -Upcon-PE après une incubation de 7 jours avec des cellules de *C. vulgaris*. Les inserts en a, b et c montrent les courbes de force représentatives obtenues pendant les expériences de spectroscopie de force.

Suite à ces premiers résultats, montrant un changement de l'état de surface des Model-MPs en présence des microalgues, nous avons voulu savoir si ces dernières pouvaient influencer la croissance des microalgues. Après une période d'incubation de 7 jours avec des  $\mu$ -(Upcon)-PE à des concentrations de 0, 5, 10 et 40 mg/L, aucun effet des Model-MPs sur la croissance cellulaire n'a été observé. De plus, nous avons également constaté que les Model-MPs n'avaient aucun effet sur la morphologie (rugosité) des cellules. Il nous a cependant paru important d'évaluer un possible effet des Model-MPs sur l'agrégation cellulaire.

Pour cela, nous avons d'abord réalisé une imagerie par microscopie optique après 7 jours de culture, et sans ou avec incubation de Model-MPs (Figure III.3). De grands agrégats de cellules sont visibles autour des particules de Model-MPs, uniquement lorsque les cellules ont été incubées à 40 mg/L en présence de ces dernières (de façon similaire, que ce soit des  $\mu$ -PE ou des  $\mu$ -Upcon-PE). Ces premiers résultats semblent indiquer que les Model-MPs peuvent déclencher l'agrégation des microalgues.

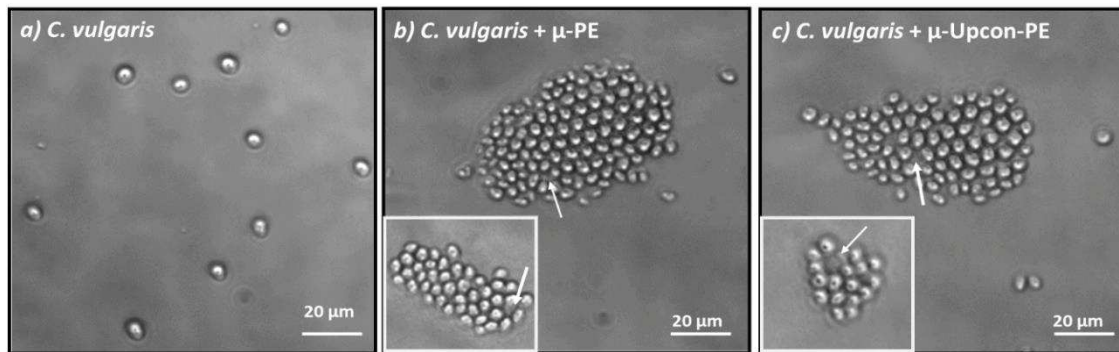


Figure III. 3: Imagerie optique de cellules de *C. vulgaris* après incubation pendant 7 jours a) seul ; b) avec  $\mu$ -PE; c) avec  $\mu$ -Upcon-PE. La flèche indique les Model-MPs.

Afin de quantifier plus précisément l'effet des Model-MPs sur l'agrégation cellulaire, nous avons réalisé des expériences de floculation/flottation avec différentes concentrations de  $\mu$ -PE (concentration finale de 0, 5, 10 et 40 mg/L) incubées pendant 7 jours avec des cellules de *C. vulgaris*. Aucune floculation des cellules n'a été observée lorsque les Model-MPs ont été utilisés à des concentrations de 5 mg/L et 10 mg/L. En revanche, à une concentration de 40 mg/L, l'agrégation des cellules se produit. La principale hypothèse est que lorsque les Model-MPs sont présents dans le milieu, les cellules ont tendance à les coloniser pour former un biofilm, ce qui déclenche la production de substances polymériques extracellulaires (EPS).

Pour tester cette hypothèse, des expériences de floculation/flottation ont été répétées à des concentrations de 40 mg/L en Model-MPs, et ce dans différentes conditions (Figure III.4). Tout d'abord, les Model-MPs ont été incubés pendant 7 jours avec les cellules de *C. vulgaris* avant de réaliser les expériences. Ensuite, les cellules en culture n'ont pas été exposées aux Model-MPs, mais ces derniers ont été ajoutés à la fin de la période de culture, pendant 15 minutes avant les expériences de floculation/flottation. La comparaison des résultats obtenus dans ces deux conditions avait pour but de comprendre si l'AOM interagit avec les Model-MPs et de quelle manière ; et si les cellules sécrètent plus d'AOM lorsqu'elles sont cultivées en présence de MPs. Dans la troisième condition, à la fin de la culture, les cellules ont été lavées dans du PBS pour éliminer l'AOM qu'elles ont pu produire, puis seuls des Model-MPs ont été ajoutés pendant 15 minutes avant les expériences de floculation/flottation.

Les résultats obtenus dans chaque cas sont présentés dans la Figure III.4. Même si les cellules ne sont pas cultivées en présence de Model-MPs (condition 2), l'agrégation cellulaire peut toujours se produire, et a lieu rapidement puisque 15 minutes seulement sont suffisantes pour obtenir une efficacité de séparation similaire à celle obtenue après 7 jours d'incubation (condition 1). Cependant, lorsque l'AOM est éliminé (condition 3), l'efficacité de séparation

devient comparable à ce qui est obtenu dans les expériences de contrôle avec des cellules sans Model-MPs, lavées ou non.

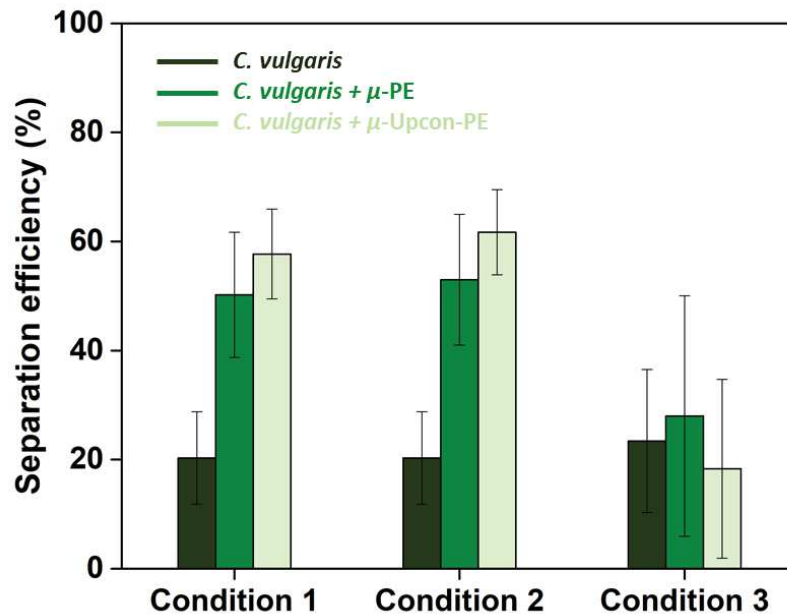
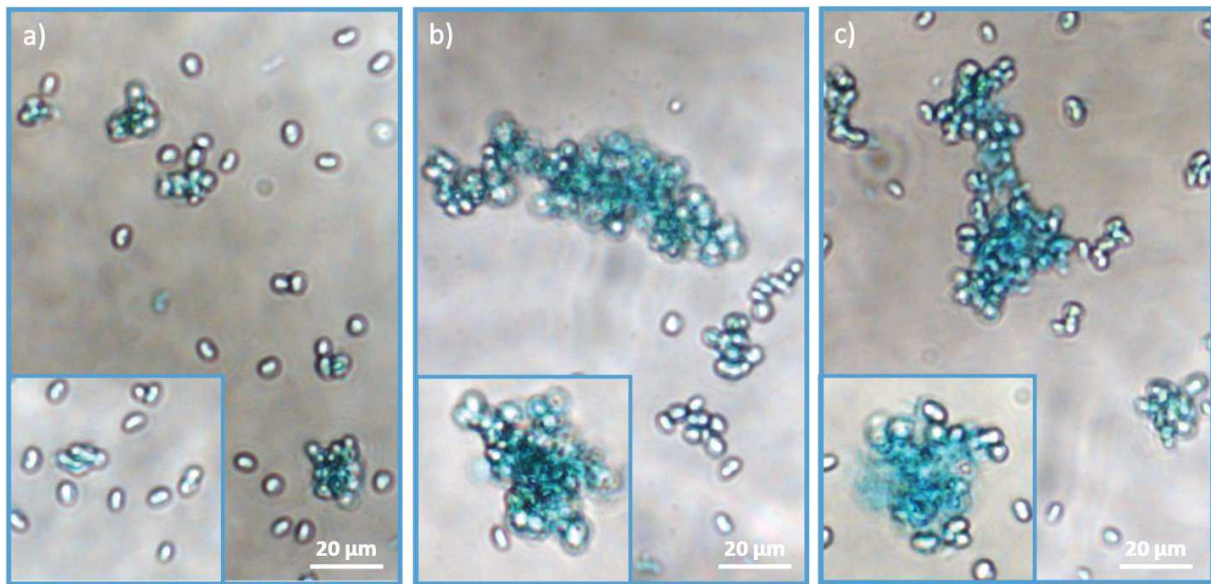


Figure III. 4: Expériences de floculation des cellules de *C. vulgaris*. Efficacité de flottation de *C. vulgaris* avec  $\mu$ -PE et  $\mu$ -Upcon-PE à une concentration de 40 mg/L dans différentes conditions. Condition 1, Model-MPs ( $\mu$ -PE et  $\mu$ -Upcon-PE) + cellules après 7 jours d'incubation ensemble. Condition 2, Model-MPs directement ajoutés aux cellules après 7 jours de culture. Condition 3, Model-MPs directement ajoutés aux cellules après 7 jours de culture et lavage au PBS.

Ces expériences suggèrent donc que l'AOM joue un rôle important dans l'agrégation des cellules en présence de MPs. De plus, un point important à noter est que la modification des Model-MPs marqués avec des UCNP n'a pas d'effet sur l'efficacité de floculation/flottation.

Pour comprendre si la présence d'AOM est effectivement un facteur important dans l'agrégation des cellules en présence de MPs, nous avons effectué des tests supplémentaires en microscopie optique en utilisant la coloration au bleu Alcian. Ce colorant est spécifiquement connu pour réagir avec les polysaccharides acides présents dans l'AOM excrétée par les cellules de microalgues. Nous avons donc choisi cette technique pour évaluer qualitativement la présence d'AOM dans les cellules cultivées en présence de Model-MPs. Les résultats obtenus sont présentés dans la figure III.5.

Ainsi, nous avons pu observer que lorsque les cellules sont cultivées sans Model-MPs, elles sont légèrement tachées, ce qui reflète la présence de polysaccharides à leur surface (Figure III.5a). Lorsqu'elles ont été cultivées pendant 7 jours en présence de Model-MPs ( $\mu$ -PE et  $\mu$ -Upcon-PE), les agrégats visibles de cellules montrent une couleur bleue bien plus intense que lorsque les cellules sont cultivées seules (Figures III.5b et c).



**Figure III. 5:** Imagerie optique de l'AOM, après réaction au bleu Alcian, produite par *C. vulgaris* après incubation pendant 7 jours : a) seul ; en présence de b)  $\mu$ -PE ou de c)  $\mu$ -Upcon-PE.

Cette expérience montre que la présence de Model-MPs a tendance à stimuler la production d'AOM. En outre, elle suggère également que l'AOM pourrait être partie prenante de l'agrégation des cellules, car sa production est bien plus faible dans les conditions de contrôle (cellules non agrégées). Les Model-MPs présents dans le milieu semblent donc être en mesure de déclencher la production d'AOM, les cellules ayant tendance à former des biofilms autour d'elles. Le point intéressant est qu'aux concentrations en Model-MPs de 5 et 10 mg/L, nous n'observons pas de floculation/flottation. Cela signifie qu'il pourrait y avoir une concentration seuil de MPs dans le milieu pour déclencher la production d'AOM, donc la formation de biofilm autour des cellules.

Cependant, l'agrégation des cellules se produit également si les Model-MPs sont ajoutés aux cellules au dernier moment (Figure III.4, Condition 2).

Ainsi, pour comprendre si une interaction entre les MPs et les cellules est possible, nous avons réalisé des expériences de spectroscopie de force pour sonder les interactions entre une cellule unique de *C. vulgaris* et des  $\mu$ -(Upcon)-PE. Pour cela, nous avons utilisé la technologie FluidFM, où des cellules uniques de *C. vulgaris* ont été aspirées au niveau de l'ouverture des sondes FluidFM en exerçant une pression négative à l'intérieur du cantilever microfluidique (Figure III.6). En accord avec les expériences précédentes de floculation/flottation, ces expériences ont pu démontrer que bien que l'incorporation d'UCNPs au  $\mu$ -PE modifie l'architecture et la rugosité de surface des particules, elle n'affecte pas leur interaction avec les cellules de *C. vulgaris*.

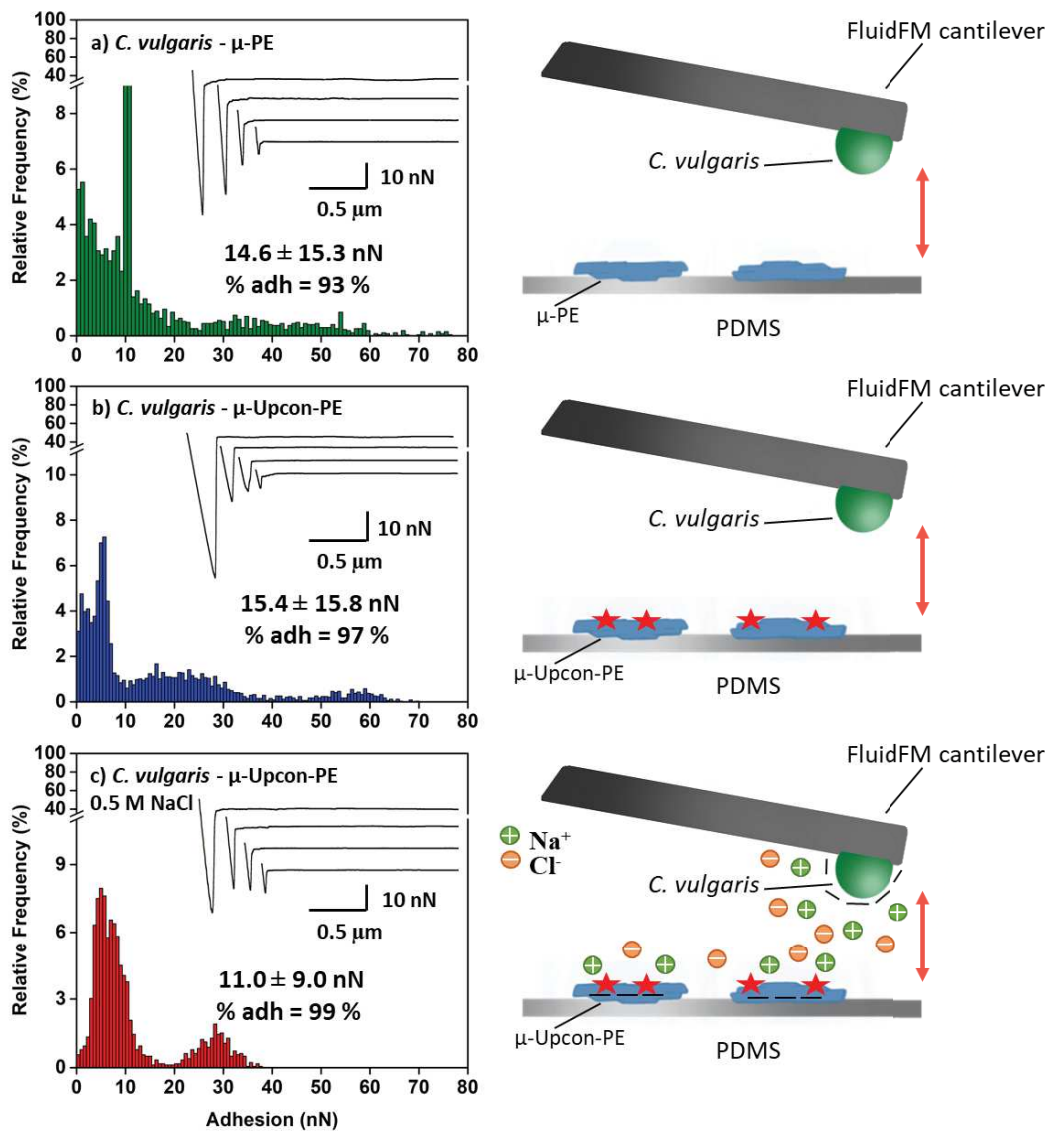


Figure III. 6: Étude de l'interaction entre les cellules de *C. vulgaris* et les Model-MPs. Histogrammes de force d'adhésion obtenues pour l'interaction entre les cellules de *C. vulgaris* et a) les  $\mu$ -PE, b) les  $\mu$ -Upcon-PE, et c) les  $\mu$ -Upcon-PE après ajout de NaCl 0,5 M. Les inserts en a, b et c montrent les courbes de force représentatives obtenues pendant les expériences de spectroscopie de force.

Pour la première fois nous avons pu mettre en évidence, par l'analyse des courbes de force de rétraction qu'il existe bien une interaction entre les cellules et les  $\mu$ -(Upcon)-PE, et que ces interactions sont non spécifiques et hydrophobes (Figures III.6 a et b). L'interaction hydrophobe semble l'emporter sur la répulsion électrostatique entre *C. vulgaris* négatif et les Model-MPs chargés négativement, donnant une force d'adhésion moyenne d'environ 15 nN, c'est-à-dire presque 3,6 fois plus élevée que l'interaction entre *C. vulgaris* et une bulle d'air.

Des expériences supplémentaires de spectroscopie de force à des concentrations de sel plus élevées (Figure III.6c, en présence de 0,5 M NaCl) ont ensuite été menées pour confirmer ce point et exclure la contribution possible d'autres types d'interactions entre les cellules de *C. vulgaris* et les  $\mu$ -(Upcon)-PE, telles que les interactions électrostatiques. En effet, même si

la charge globale de *C. vulgaris* est négative, il pourrait y avoir des molécules chargées positivement sur la paroi cellulaire de *C. vulgaris* qui pourraient interagir de façon électrostatique avec les  $\mu$ -(Upcon)-PE chargées négativement. Lorsque nous augmentons la concentration en sel en ajoutant 0,5 M de NaCl dans un tampon PBS (à 0,137 M de NaCl) à pH 7,4, les charges présentes sur les cellules de *C. vulgaris* et les Model-MPs sont masquées par la présence des ions sodium. Les résultats obtenus dans ces conditions (0,5 M NaCl) sont significativement différents, et ont tendance à montrer que les interactions électrostatiques jouent un rôle non négligeable (même si moins important que les interactions hydrophobes).

En fin de compte, cette étude a démontré que l'agrégation des cellules induite par les MPs est un processus en deux étapes. D'abord, une interaction hydrophobe initiale a lieu entre les MPs et les microalgues. Elle déclencherait la production d'AOM par les cellules. Ces substances favoriseraient ensuite l'agrégation de davantage de cellules et de MPs.



## III.2. Article

### **The role of microplastics in microalgae cells aggregation: a study at the molecular scale using AFM**

**Irem Demir-Yilmaz,<sup>1,2</sup> Nadiia Yakovenko,<sup>3</sup> Clément Roux,<sup>3</sup> Pascal Guiraud,<sup>1,4</sup> Fabrice Collin,<sup>3</sup> Christophe Coudret,<sup>3</sup> Alexandra ter Halle,<sup>3</sup> and Cécile Formosa-Dague,<sup>1,4\*</sup>**

<sup>1</sup> TBI, Université de Toulouse, INSA, INRAE, CNRS, Toulouse, France.

<sup>2</sup> LAAS, Université de Toulouse, CNRS, Toulouse, France.

<sup>3</sup> UMR 5623 IMRCP, CNRS, Toulouse, France.

<sup>4</sup> Fédération de Recherche Fermat, CNRS, Toulouse, France.

\*corresponding author: Cécile Formosa-Dague, [formosa@insa-toulouse.fr](mailto:formosa@insa-toulouse.fr)

## **INTRODUCTION**

Plastic is a revolutionary discovery of the early twentieth century that changed our way of life forever. It has become an integral part of all consumer goods such as packaging, clothing, electronic devices, medicine, etc., (Andrady & Neal, 2009). However, high demand, massive production, extensive use, and poor plastic waste management contributes to plastic release and accumulation in the environment, which has become one of the most pressing environmental problems of our time (Geyer et al., 2017). Plastic waste accounts for 60 to 80% of all solid waste present in the aquatic environment (Gregory & Ryan, 1997), most of them being microplastics particles (MPs) (EPA US, 2016). MPs are plastic particles ranging in size from 1  $\mu\text{m}$  to 5 mm (Horton et al., 2017), which are characterized by a variety of physical, chemical, and morphological properties such as different types of polymers and composition, size, shape, density, colour, etc. In the environment, MPs represent a group of persistent synthetic pollutants, consisting of primary particles, manufactured at the millimetric or sub-millimetric scale under the form of pellets or microbeads, and secondary particles, resulting from the fragmentation of larger plastic debris through thermal, photo-oxidative, mechanical, and biological degradation processes (Cole et al., 2011). Because of their small size and ubiquitous distribution in all environmental compartments (Horton et al., 2017; Peng et al., 2020; Y. Zhang et al., 2020), MPs are of great concern with respect to their bioavailability, toxicity and potential adverse effect on living organisms and ecosystem as a whole. Ingestion of MPs by aquatic living organisms from zooplankton (Cole et al., 2013) to mammals (Zantis et al., 2021), and the wide range of possible negative effects of plastic particles uptake are well documented. (EPA US, 2016; GESAMP, 2016; Peng et al., 2020).

However, there is a gap of knowledge on the interaction and the effects of MPs on the basic organisms of the trophic chain, such as microalgae. Microalgae are photosynthetic microorganisms that are the most numerous primary producers in the entire aquatic ecosystem (Barbosa, 2009; Beardall & Raven, 2004). They are key organisms in a wide range of ecosystem functions, where they have an impact on ocean's carbon sequestration (Singh & Ahluwalia, 2013), oxygen production, nutrient cycling, etc., (Hopes & Mock, 2015). Being ubiquitous, sensitive to environmental disturbances, and easy to cultivate in laboratory, microalgae are an ideal model to study the effects of different pollutants in the environment including MPs (Cid et al., 2012). The interaction between MPs and microalgae is a complex process that leads to a multitude of effects acting on the further fate and behaviour of both MPs and microalgae, and thus potentially affecting the entire ecosystem (Nava & Leoni, 2021). For instance, in the

environment, microalgae tend to colonize plastic surfaces, using them as an abiotic substrate to grow in a biofouling process (Bravo M et al., 2011; Carson et al., 2013; Jorissen, 2014; Reisser et al., 2014). While colonising plastic surfaces, microalgae cells secrete extracellular polymeric substances (EPS), which play an important role in biofilm formation. EPS consist of polysaccharides, lipids, nucleic acids, proteins, and other polymeric compounds (Wingender et al., 1999a; Xiao and Zheng, 2016), which favours cells cohesion and future adhesion to the substrate' surface (Wingender et al., 1999b). In addition, biofouling changes the density of plastic particles, affecting their buoyancy (Nava & Leoni, 2021; Oberbeckmann et al., 2015; Rummel et al., 2017) and thus leading to the dissemination of plastic particles through the water column by sinking to the bottom or moving to the surface. This widespread abundance of MPs particles consequently increases their bioavailability for various living organisms. Another effect of biofouling is a decrease in the hydrophobicity of the particle surface (Lobelle & Cunliffe, 2011). As a result, adsorption of toxic pollutants from the aquatic environment to the surface of the plastic particles can be enhanced (Bhagwat et al., 2021; Dong et al., 2017), which can amplify the toxicity of MPs. Moreover, extracellular polymeric substances (EPS) produced by microalgae promote the heteroaggregation of MPs and microalgae. The resulting aggregates become easy food for the aquatic organisms and are also more prone to sediment, thus here also affecting their dissemination through the water column as mentioned above (Lagarde et al., 2016; Long et al., 2015; Rummel et al., 2017). Finally, MPs were also found to have a number of adverse effects on microalgae, including inhibition of growth (Sjollema et al., 2016; Zhang et al., 2017; Liu et al., 2020; Song et al., 2020), decrease in chlorophyll content (Tunali et al., 2020; Wu et al., 2019) and photosynthetic activity (C. Zhang et al., 2017), physical and morphological damages (Mao et al., 2018), oxydative stress (Y. Xiao et al., 2020). In addition, due to constant movement in the aquatic environment, plastic is a potential vector of geographic transport for the migration of microalgae. This phenomenon creates a risk of introducing pathogenic species (e.g. harmful algal blooms) into a new environment where native species are not adapted to defend themselves (Masó et al., 2003; Glibert et al., 2014; Oberbeckmann et al., 2015).

For all these reasons, scientists are making increasing efforts to study the mechanism of MPs and microalgae interaction, to better understand its negative impact on a global scale. Most of the ecotoxicological studies under laboratory conditions are using commercially manufactured models of MPs, in the vast majority of the studies the model plastic are polystyrene micro- or nano- spheres, which which are not representative of plastic particles found in the environment

(Kokalj et al., 2021; Phuong et al., 2016). Thus, there is a need for research based on the use of an environmentally relevant model of plastic particles in terms of polydispersity, irregular shapes, and surface properties. In this study, we investigated the interaction between model of MPs (Model-MPs) of HDPE (with and without UCNPs luminescent label) developed in Chapter II, and microalgae cells and their further role in the aggregation of cells using atomic force microscopy (AFM) nano- and molecular scale experiments.

AFM, first developed in 1986 (Binnig et al., 1986), has proven over the years to be a powerful tool for surface characterization at the nanoscale (Pillet et al., 2014; Xiao & Dufrêne, 2016). In addition to high-resolution imaging capacities, down to the nanometer scale, AFM is also a sensitive force machine able to record piconewton level forces, thus making it possible to access the nanomechanical and adhesive properties of samples, as well as their interactions with their environment (Formosa-Dague et al., 2018). In the particular context of microalgae, AFM has been used to understand the morphology, nanostructure, nanomechanics and adhesive behavior of cells (Demir-Yilmaz et al., 2021), but most importantly their interactions with particles or molecules present in their environment (Besson et al., 2019; Demir et al., 2020; Demir-Yilmaz et al., 2021). In the first part of this study, Model-MPs were characterized using an atomic force AFM and a Fluidic force microscopy (Fluid FM) to visualize the particles and obtain information about their roughness and the hydrophobic character of their surface. Then AFM was used to probe the interaction between Model-MPs and *C. vulgaris* cells. Finally, the mechanism of microalgae flocculation induced by Model-MPs under different conditions and concentrations was investigated.

## **MATERIALS and METHODS**

**Microalgae strain and culture.** The green freshwater microalgae *Chlorella vulgaris* strain CCAP 211/11B (Culture Collection of Algae and Protozoa) was cultivated in sterile conditions in Wright's cryptophyte (WC) medium prepared with deionized water (Guillard & Lorenzen, 1972). Cells were cultivated at 20°C, under 120 rpm agitation, in an incubator equipped with white neon light tubes providing illumination of approximately 40  $\mu\text{mol photons m}^{-2} \text{s}^{-1}$ , with a photoperiod of 18h light: 6h dark. All experiments were carried out with 7 days exponential phase batch cultures. Cells were first harvested by centrifugation (3000 rpm, 3 min), washed two times in phosphate buffered saline (PBS) at pH 7.4 and directly used for the experiments.

**Microparticles model.** The synthesis and full characterization of the HDPE microparticle model, are described elsewhere (Chapter II). Briefly, two bulk polymeric materials were

prepared, including UCNPs-labelled HDPE (Upcon-PE) and UCNPs-free HDPE (Blank-PE). The oleate-capped NaREF<sub>4</sub> (RE= 2% Er; 30% Yb; 68% Y) with a diameter of 20 nm were used to provide a green luminescent plastic that can be directly observed by eye under 976 nm irradiation. UCNPs were incorporated into the HDPE (CAS 9002-88-4, Sigma Aldrich, Saint Louis, MO, USA) matrix by dissolving the polymer in boiling o-xylene ( $\geq 99.0\%$  (GC grade); Sigma Aldrich, Saint Louis, MO, USA), containing UCNPs in a 10 wt.% HDPE:UCNPs ratio. The composite was separated from the reaction mixture by precipitation in the ice bath. The Blank-PE batch of polymer containing only HDPE was prepared following the same protocol. Microparticles model was obtained by exposing each bulk material to a cryogenic grinder (SPEX™ SamplePrep 6775 Freezer/Mill™, Delta Labo, France). The resulting polymer particles were dispersed in ethanol and fractionated by subsequent cascade filtration to micro- and nanosized particles. The collected Model-MPs were named as  $\mu$ -PE (HDPE microparticles), and  $\mu$ -Upcon-PE (HDPE labelled with the inclusion of UCNPs as a luminescent tag). The full characterization of the Model-MPs of particle size, shape, crystallinity, chemical composition, surface charge, and luminescence properties, are described elsewhere (Chapter II).

**Zeta potential measurements.** Zeta-potential measurements for Model-MPs were carried out at 25°C on a Zetasizer Nano-ZS (Malvern Instruments, Ltd, UK) equipped with a He-Ne laser ( $\lambda = 633$  nm) at an angle of 173°. Samples were prepared by dispersion of particles in 10 mM NaCl solution, to provide minimum level of conductivity in the samples, following ISO and ASTM standard guides (ASTM E2865-12, 2018). Before analysis, pH of every sample was measured. Zeta-potential and standard deviation (SD) were obtained from 5 measurements of 11 runs of 10 seconds using the Smoluchowski model (Chapter II).

**Flocculation/flotation experiments.** Flocculation/flotation separation of *C. vulgaris* was performed in dissolved air flotation (DAF) experiments in a homebuilt flotation device, shown in Figure 1. The depressurization at atmospheric pressure of water saturated by air at 6 bars induced the formation of bubbles. Water free of algae was pressurized for 30 min before injection into the jars. The injection was controlled by a solenoid valve and 20 mL of pressurized water was added to each beaker sample.

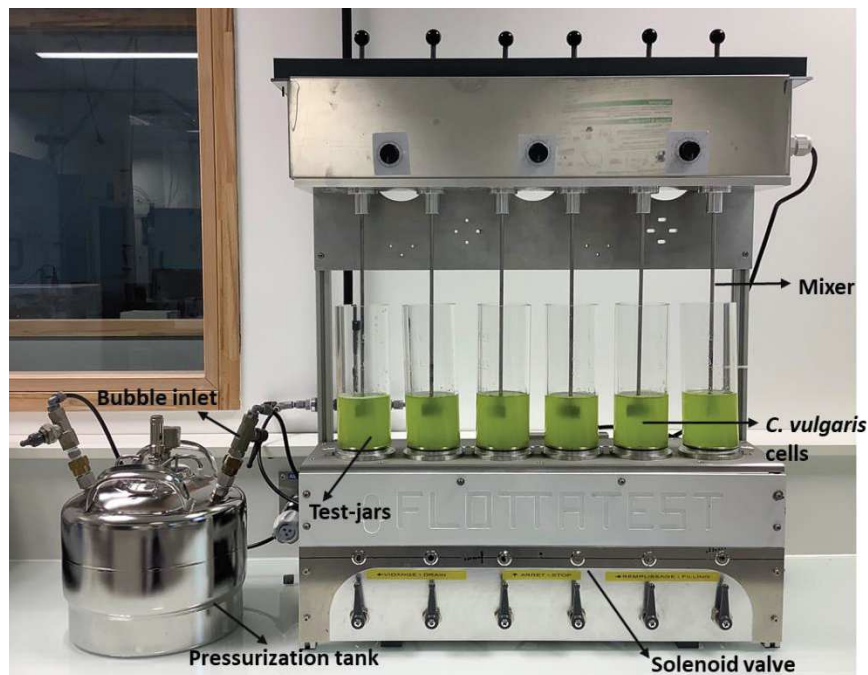


**Figure 1: Image of Flotation device.**

The flotation tests were conducted in three different conditions;

**Condition 1:** *C. vulgaris* cells were inoculated 7 days together with different concentrations of  $\mu$ -PE and  $\mu$ -Upcon-PE (final concentrations of 0, 5, 10 and 40 mg/L for  $\mu$ -PE and 40 mg/L for  $\mu$ -Upcon-PE) until they reached mid-exponential phase. Then 100 mL of cell suspension was directly poured into the test-jars with an initial OD<sub>750</sub> nm of 1.

**Condition 2:** *C. vulgaris* cells were grown for 7 days until they reached mid-exponential phase. After that, 100 mL of cell suspension was directly poured into the test-jars with an initial OD<sub>750</sub> nm of 1. Then  $\mu$ -PE and  $\mu$ -Upcon-PE were added (final concentration of 40 mg/L) to the suspensions, which were stirred at 100 rpm for 15 min to homogenize the suspension before introduction of the bubbles.

**Condition 3:** *C. vulgaris* cells were grown for 7 days until they reached mid-exponential phase. After that, cells were harvested by centrifugation at 3000 rpm for 3 min, then washed two times with phosphate buffered saline (PBS) at pH 7.4. After that, 100 mL of cell suspension was directly poured into the test-jars with an initial OD<sub>750</sub> nm of 1. Particles of  $\mu$ -PE and  $\mu$ -Upcon-PE were directly added (final concentration of 40 mg/L) to the suspensions, which were stirred at 100 rpm for 15 min to homogenize the suspension before introducing bubbles.

For all condition, after bubbles were introduced, the algal suspension was retrieved from the bottom of the test-jars: the first 5 mL of treated phase were discarded, the next 20 mL were used

for quantifying flocculation/flotation efficiency. For that, the optical density of the withdrawn algal suspension was measured and compared to the optical density of the microalgae suspension measured before the experiments. The flotation efficiency ( $E$ ) was calculated according to the following equation 1.

$$E = \frac{OD_i \cdot V_i - OD_f \cdot V_f}{OD_i \cdot V_i} \quad (1)$$

**Optical imaging experiments.** Flocculation was directly observed after resuspension of the cells in PBS at a pH 7.4 containing  $\mu$ -PE or  $\mu$ -Upcon-PE at a concentration of 40 mg/L. Flocculation levels were observed using an Axio Observer Z1 microscope (Zeiss, Germany) at high magnification (50 $\times$ ).

**Force spectroscopy experiments using FluidFM technology.** Force spectroscopy experiments were conducted using a NanoWizard III AFM (Bruker, USA), equipped with FluidFM technology (Cytosurge AG, Switzerland). In each case, experiments were performed in PBS, using micropipette probes with an aperture of 2  $\mu$ m (spring constant of 0.3, and 4 N/m, Cytosurge AG, Switzerland). First, PBS at a pH of 7.4 was used to fill the probe reservoir (5  $\mu$ L); by applying an overpressure (100 mBar) the PBS then filled the entire cantilever microchannel. The probe was then immersed in PBS and calibrated using the thermal noise method prior to measurement (Hutter & Bechhoefer, 1993). A single *C. vulgaris* cell was then aspirated from the surface of the Petri dish by approaching the FluidFM probe and applying a negative pressure (-200 mBar). The presence of the cell on the probe was verified by optical microscopy. The cell probe was then used to measure the interactions with Model-MPs. For that,  $\mu$ -PE and  $\mu$ -Upcon-PE solutions at a concentration of 40 mg/L were deposited on polydimethylsiloxane (PDMS) surfaces and left for 30 min. After that, the PDMS surfaces were rinsed using PBS and directly used. Interactions between single *C. vulgaris* cells aspirated at the aperture of FluidFM cantilevers and  $\mu$ -(Upcon)-PE were recorded at a constant applied force of 2 nN, force curves were recorded with a z-range of up to 2  $\mu$ m and a constant retraction speed of 2.0  $\mu$ m/s to 20  $\mu$ m/s. Data were analyzed using the Data Processing software from Bruker. Adhesion forces were obtained by calculating the maximum adhesion force for each retract curves. Experiments were repeated three times with ten different cells coming from at least three different cultures.

**AFM imaging.** AFM images of *C. vulgaris* were recorded with cells immobilized on positively charged glass slides (Superfrost<sup>TM</sup> Plus adhesion, Epreidia, USA). For  $\mu$ -PE and  $\mu$ -Upcon-PE, particles were immobilized on PDMS. In both cases, images were then recorded in PBS at

pH 7.4, using the Quantitative Imaging mode available on the Nanowizard III AFM (Bruker, USA), with MSCT cantilevers (Bruker, nominal spring constant of 0.01 N/m). Images were recorded with a resolution of 256 pixels  $\times$  256 pixels, at an applied force of  $<1.0$  nN and a constant approach/retract speed of 90  $\mu\text{m/s}$  (z-range of 3  $\mu\text{m}$ ). In all cases the cantilevers spring constants were determined by the thermal noise method prior to imaging (Hutter & Bechhoefer, 1993).

**Roughness analyses.** Roughness analyses were performed on  $\mu\text{-PE}$  and  $\mu\text{-Upcon-PE}$  immobilized on PDMS and on cells after incubation with and without Model-MPs for 7 days, immobilized on positively charged glass slides (Superfrost<sup>TM</sup> Plus adhesion, Epremedia, USA). Individual  $\mu\text{-PE}$  and  $\mu\text{-Upcon-PE}$  images were recorded in PBS whereas for cells, after incubation with Model-MPs, samples were directly imaged in culture medium using contact mode with a Nanowizard III AFM (Bruker, USA), using MSCT cantilevers (Bruker, nominal spring constant of 0.01 N/m). Images were recorded in contact mode using an applied force of  $<1$  nN for Model-MPs and of  $<0.5$  for cells and the cantilever spring constants were determined thermal noise method prior to imaging (Hutter & Bechhoefer, 1993).

## RESULTS and DISCUSSION

### Model-MPs have a rough and hydrophobic surface

The Model-MPs immobilized on PDMS substrates were first characterized by AFM in contact mode to image both  $\mu\text{-PE}$  and  $\mu\text{-Upcon-PE}$ . The images obtained are presented in Figure 2. The 3D AFM height images (Figure 2a and b) and vertical deflection (Figure 2c and d) images recorded show that both types of Model-MPs have an irregular shape and a heterogeneous surface. They are found mostly as aggregates of particles and are not present as a single particle. This is confirmed by the cross-section taken along the longer sides of the particles in Figure 2c and d, which clearly show this irregularity, with height variations over 6 nm in Figure 2e and f.

We then acquired high resolution images on small areas ( $5\mu\text{m} \times 5\mu\text{m}$ ) on top of the particles, using QI advanced imaging mode; the resulting images are shown in Figure 2g-h. In this case, QI mode was used instead of contact mode because of the complexity of Model-MPs surfaces. QI being a force spectroscopy based imaging mode, there is no lateral forces exerted by the tip as there are in contact mode, which can damage the sample (Chopinnet et al., 2013). This way we could obtain high-resolution images of the particles surface (Figure 2i and j) and quantify their roughness. Roughness measurements were performed on 9 different particles in each case; the results of these analysis are presented in the boxplot Figure 2k. They show that  $\mu\text{-PE}$  have



an average roughness of  $3.7 \pm 1.1$  nm, which increases to  $7.6 \pm 5.4$  nm when UCNPs are incorporated in the particles ( $\mu$ -Upcon-PE). Although there is an important heterogeneity in the measurements in this last case, the difference with the  $\mu$ -PE is not significantly different at 0.05 level (non-parametric Mann and Whitney test). This result thus shows that the incorporation of UCNPs may affect the structure of Model-MPs, by modifying their surface morphology; however, the heterogeneity of the measurements performed on  $\mu$ -Upcon-PE reflects the uncontrolled incorporation of the UCNPs over the particles present in the sample.

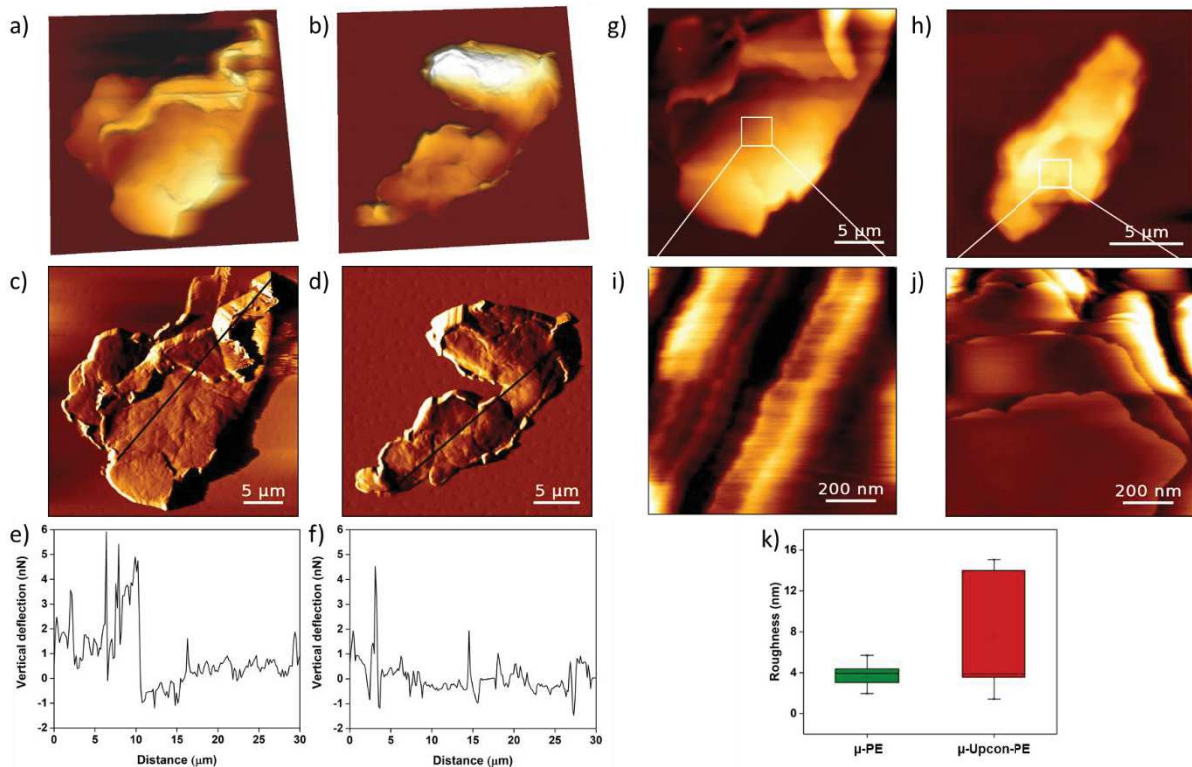


**Figure 2: Imaging and characterization of  $\mu$ -PE surface before and after incorporation of UCNPs:** a) 3-D AFM height image of  $\mu$ -PE; b) 3-D AFM height image of  $\mu$ -Upcon-PE. c) Vertical deflection images of  $\mu$ -PE; d) Vertical deflection images of  $\mu$ -Upcon-PE; e) Cross section taken along the larger side in panel c and f) Cross section taken along the larger side in panel d; g) AFM height images of  $\mu$ -PE and h) AFM height images of  $\mu$ -Upcon-PE; i) AFM height images of  $\mu$ -PE surface ( $5\mu\text{m} \times 5\mu\text{m}$ ) and j) AFM height images of  $\mu$ -Upcon-PE surface ( $5\mu\text{m} \times 5\mu\text{m}$ ); k) Quantification of  $\mu$ -PE and  $\mu$ -Upcon-PE surface roughness in a box plot.

In the next step we then assessed the hydrophobic properties of the Model-MPs, which are an important physico-chemical factor that could greatly influence their interactions with microalgae. To this end, we used a recently developed method that consists in probing the interactions of samples with bubbles produced using FluidFM technology (Demir et al., 2021), which is a combination of AFM with microfluidics (Meister et al., 2009). Air bubbles in water behave like hydrophobic surfaces. By producing them using FluidFM, it is then possible to

probe their interactions with complex abiotic surfaces such as the MPs, and measure the hydrophobicity with accuracy, avoiding the issues related to other tests like water contact angle measurement (WCA) that are not adapted to the sample we have here. To perform these experiments, Model-MPs were immobilized on a PDMS substrate and their interaction with bubbles were measured in PBS buffer at pH 7.4 (Figure 3a). For both  $\mu$ -PE and  $\mu$ -Upcon-PE, 5 different particles were probed. In the case of  $\mu$ -PE, the retract force curves obtained (inset in Figure 3a) show a single peak occurring at the contact point, typical of a hydrophobic interaction (Dague et al., 2007), with an average force of  $10.1 \pm 6.2$  nN (Figure 3a,  $n = 2558$  force curves obtained from 5 different particles). This force corresponds to the height of the adhesion peak, and thus to the force needed to break the interaction between the bubble and the sample. As a hydrophobic interface like bubbles interact with hydrophobic surfaces, then this force reflects the degree of hydrophobicity of the sample, the stronger the adhesion, the higher the hydrophobicity. Similarly, in case of  $\mu$ -Upcon-PE a single peak occurring at a contact point is visible (inset in Figure 3b); retract adhesion forces in this case were on average of  $13.7 \pm 15.3$  nN (Figure 3b,  $n = 2107$  force curves obtained from 5 different particles). The large distribution of the adhesion values obtained in these experiments reflect the irregularities of the Model-MPs used that were visible in the AFM experiments in terms of nanostructure, but they are not significantly different from the first condition. These experiments were then repeated with  $\mu$ -Upcon-PE that were incubated with cells during their culture (7 days, Figure 3c). In this case also, hydrophobic interactions are recorded, with an average adhesion force of  $16.4 \pm 8.0$  nN ( $n = 1685$  force curves obtained from 4 different particles), a value that is significantly different from the two first conditions (p-value of 0.05, unpaired student test). Thus, the incubation of Model-MPs with cells change their hydrophobic properties. This is an important point because it means that our Model-MPs, after seven days exposed to the cells, have their surface modified; a plausible hypothesis could be that cells produce AOM in the culture medium, which then could coat the surface of the particles. Finally, in order to confirm that the forces recorded are due only to the interactions between Model-MPs and bubbles, we also probed the interactions between bubbles and the PDMS surface. An average adhesion force of  $1.5 \pm 0.1$   $\mu$ N ( $n = 2500$  force curves) was obtained. This adhesion force is much higher than the ones obtained with Model-MPs (maximum around 50 nN), thus meaning that we could precisely measure the interaction between bubbles and the particles without interfering with the surface where they are immobilized.

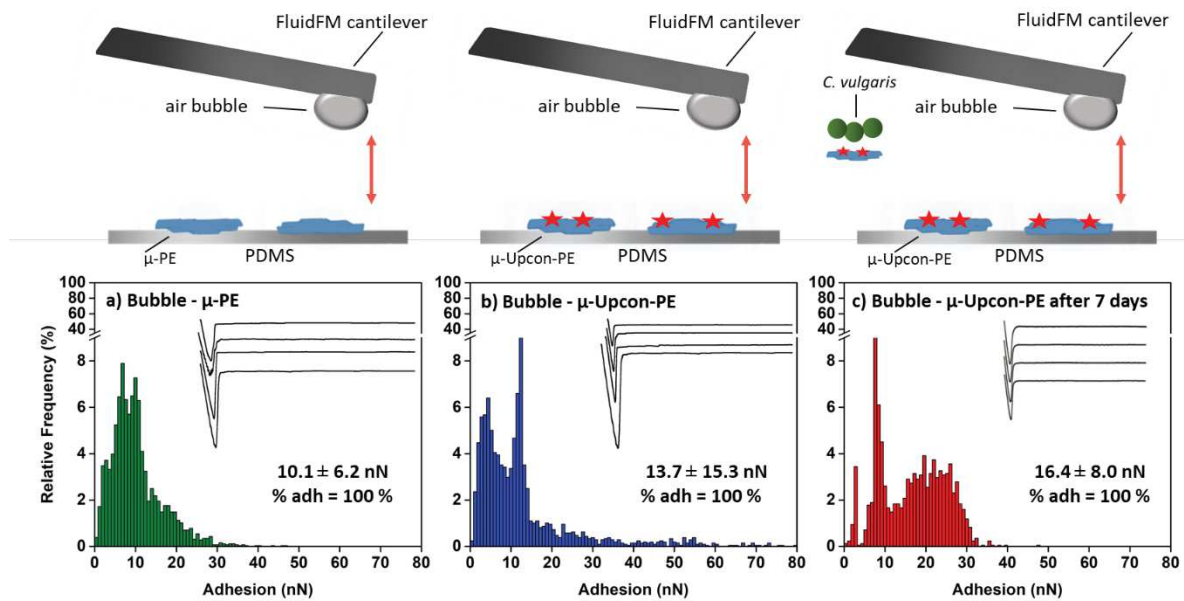


**Figure 3: Probing the interaction between bubble and MPs:** Adhesion force histogram obtained for the interaction between bubbles and a)  $\mu$ -PE, b)  $\mu$ -Upcon-PE, and c)  $\mu$ -Upcon-PE after incubation for 7 days with *C. vulgaris* cells. Insets in a, b and c shows the representative force curves obtained during force spectroscopy experiments.

### **Model-MPs do not affect cell growth or morphology but have a positive effect on their aggregation.**

In a second part of the study, we then evaluated the effects of Model-MPs on cell growth. In the literature, studies state that MPs have no toxic effect up to 50 mg/L (Bergami et al., 2017; Yan et al., 2021). To verify whether it is the case for our microalgae strain, we monitored the cell growth of *C. vulgaris*, incubated or not with Model-MPs at a concentration of 40 mg/L, which is the maximum concentration that we will use throughout this study. The growth curves obtained are presented in Figure 4a; they show that in each case cell growth is similar, thereby showing that neither  $\mu$ -PE nor  $\mu$ -Upcon-PE affect *C. vulgaris* cell growth. This confirms the data from the literature, and in addition, this also shows that UCNPs are not toxic, as  $\mu$ -Upcon-PE do not have an effect on cell growth. Moreover, incubation with Model-MPs do not prolong the exponential phase, meaning that *C. vulgaris* cells and Model-MPs do not have a symbiotic relation either, as it was shown for other species. Indeed, as Kang *et al.*, observed that, organic intermediates resulting from MPs degradation can serve as a carbon source for algae (Kang et al., 2019). Also in some cases, cell growth can be modified resulting from the EPS production (Casabianca et al., 2020; Cunha et al., 2019; Long et al., 2017).

We then went down to the nanometer scale to evaluate if the presence of Model-MPs in the culture medium had an effect on cell morphology. For that, we incubated *C. vulgaris* for 7 days together with  $\mu$ -PE, and took a close look at the cell surface and measured the roughness on small areas ( $0.3 \mu\text{m} \times 0.3 \mu\text{m}$ ) on top of the cells in contact mode, as shown in Figure 4b and c in normal conditions or incubated with  $\mu$ -PE for 7 days, respectively. Measurements were performed on 10 different *C. vulgaris* cells coming from at least 2 independent cultures in each case; the results of these analysis are presented in the boxplot Figure 4d. They show that *C. vulgaris* cells have an average roughness of  $0.8 \pm 0.2 \text{ nm}$ , and  $0.6 \pm 0.2 \text{ nm}$  when cells incubated with  $\mu$ -PE. Roughness of *C. vulgaris* has been determined before by using AFM in study by Demir et al. (Demir et al., 2020) and were in the same range at pH 6 and pH 8. Note that our experiments performed in PBS buffer at pH 7.4 and pH change affect the cell surface roughness (Demir et al., 2020). Roughness measurements are in line with the growth curve experiments. Altogether, these data show that Model-MPs do not affect neither the cell growth, nor the nanostructure of cells.

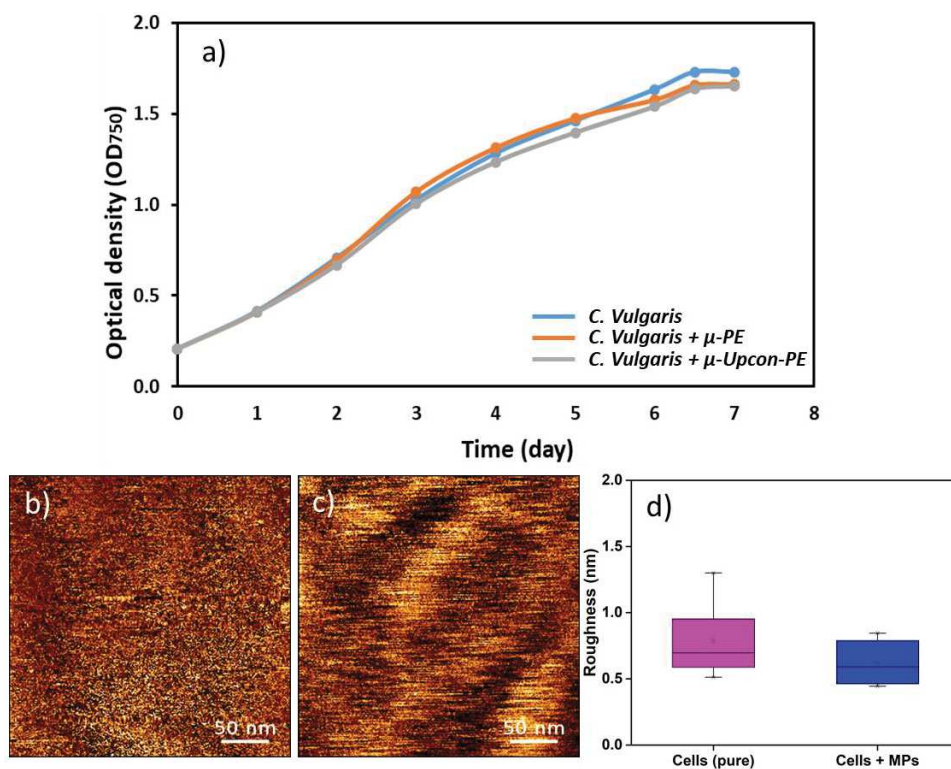


**Figure 4: Characterization of *C. vulgaris* cells:** a) Variations in cell concentration of *C. vulgaris* cells before and after incubated with Model-MPs ( $\mu$ -PE and  $\mu$ -Upcon-PE); b) AFM height images of *C. vulgaris* cell surface ( $0.3 \mu\text{m} \times 0.3 \mu\text{m}$ ) in contact mode and c) AFM height images of *C. vulgaris* cell surface ( $0.3 \mu\text{m} \times 0.3 \mu\text{m}$ ) after incubated 7 days together with MPs in contact mode; d) Quantification roughness values of *C. vulgaris* cell before and after incubation with Model-MPs for 7 days in a box plot.

Although our Model-MPs do not have an effect on *C. vulgaris* cell growth nor its (nano)structure, we then wanted to evaluate if the addition of Model-MPs in the culture medium would have an influence on the aggregation of cells. For that we first performed optical microscopy imaging (Figure 5). In these experiments, cells were incubated 7 days with  $\mu$ -PE and  $\mu$ -Upcon-PE at the concentration of 40 mg/L. In the control case (Figure 5a, without Model-MPs), we can see that cells are randomly distributed over the surface and no cell aggregation is observed. In the cases cells were incubated with  $\mu$ -PE and  $\mu$ -Upcon-PE (Figure 5b and c), large aggregates of cells are visible around Model-MPs particles, which are indicated by the arrows on the images. Moreover, through its small size, it is hard to observe these particles just using an optical microscope. Thus, taking advantage of the fluorescence properties of our labelled Model-MPs ( $\mu$ -Upcon-PE), they can be easily observed with a standard two-photon microscope under 980 nm excitation (as presented in Chapter II). We further plan to image the *C. vulgaris* cell aggregates with Model-MPs to clearly distinguish the presence of the latter in these aggregates.

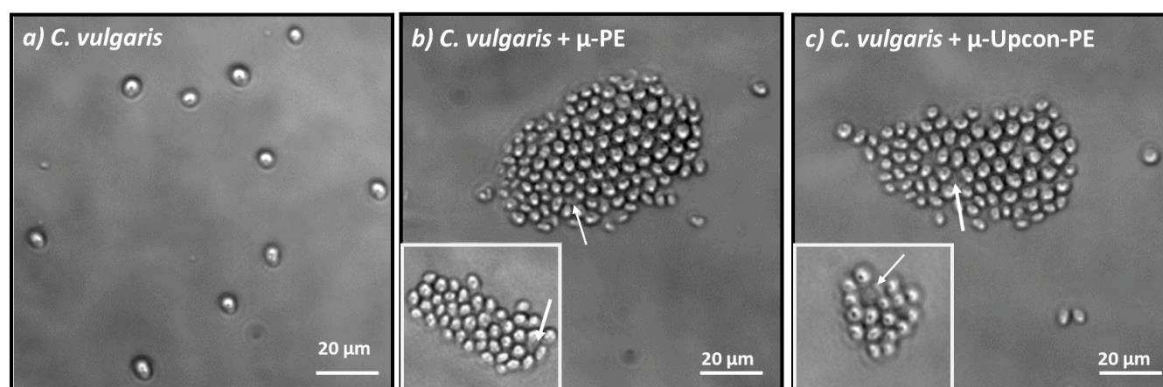


**Figure 5: Optical imaging of *C. vulgaris* cells** after incubated 7 days with a) nothing b)  $\mu$ -PE c)  $\mu$ -Upcon-PE. The arrow indicated particles of the Model-MPs.

Then, in order to quantify the effect of Model-MPs on cell aggregation, we performed flocculation/flotation experiments with different  $\mu$ -PE concentrations (final concentration of 0, 5, 10 and 40 mg/L) incubated 7 days together with *C. vulgaris* cells. In such experiments, cells can be separated from the water by bubbles only if they are aggregated into flocs that are easily captured by the rising bubbles. Thus, the flotation step allows us to separate the aggregated cells from the suspension, and thus to quantify the influence of Model-MPs on cell aggregation, which is reflected by the separation efficiency percentage that we further use. In the absence of Model-MPs, the separation efficiency obtained is of 20 %; in this case, cells should not be flocculated, thus this number reflect the fact that individual cells can be caught by the bubbles, with low efficiency. When adding Model-MPs at a concentration of 5 mg/L and 10 mg/L into

the culture medium for the 7 days of the culture, the separation efficiencies are even lower, indicating that in these cases neither, no flocculation takes place. This is an interesting point because it means that to obtain aggregation, the concentration of MPs must be important in the environment. Then, this absence of flocculation at these concentrations could be explained by the fact that both *C. vulgaris* cells and  $\mu$ -PE have a negative surface potential, of -21.9 mV (Demir et al., 2020) and of -70 mV respectively. For instance, in the literature, it was shown that MPs bearing positive charges could interact with cells through electrostatic interactions (Bhattacharya et al., 2010; Nolte et al., 2017), leading to an aggregation of cells increased compared to negatively charged MPs (Wang et al., 2021). Then, as we expected from the optical microscopy assays, when cells are incubated with  $\mu$ -PE at a concentration of 40 mg/L, the separation efficiency increases to 50 %. Different hypothesis could explain the fact that at this concentration only, cell aggregation occurs. The principal one is that when MPs are present in the medium, cells tend to colonize them to form biofilm, which triggers the production of EPS, as it has been showed already in the literature (Harrison et al., 2014; Lagarde et al., 2016; Yan et al., 2021).

To test this hypothesis, flocculation/flotation experiments were repeated at 40 mg/L concentration in different conditions (Figure 6). In the first condition, Model-MPs were incubated for 7 days together with *C. vulgaris* cells before conducting the experiments. In the second condition, the cells in culture were not exposed to the Model-MPs, instead particles were added at the end of the culture, for 15 minutes before flocculation/flotation experiments. The comparison of the results obtained in these two conditions will help understanding if and how AOM interacts with Model-MPs, or if cells secret more AOM when they are cultured in the presence of these particles. Finally in the third condition, at the end of the cultures cells were washed in PBS to remove the AOM they may have produced, and then only Model-MPs were added for 15 minutes before flocculation/flotation experiments. The results obtained in each case are presented in Figure 6, they show that there is no difference between condition 1 (flocculation efficiency of  $50 \pm 11$  %) and condition 2 (flocculation efficiency of  $53 \pm 12$  %), meaning that even if cells are not grown in the presence of Model-MPs, cell aggregation can still occur, and takes place rapidly as 15 minutes only are sufficient to obtain a separation efficiency similar to the one obtained in the condition 1. However, in condition 3, when AOM is removed by centrifugation, the separation efficiency decreases to  $28 \pm 22$  %, similar to what is obtained in control experiments with cells without particles, washed or not (dark green bars on Figure 6). These experiments thus suggest that AOM plays an important role in the

aggregation of cells in the presence of MPs. In addition, an important point to note is that the modification of the Model-MPs used with UCNPs does not have an effect on the flocculation/flotation efficiency, as similar efficiencies are observed with both types of microplastics in the different conditions tested.

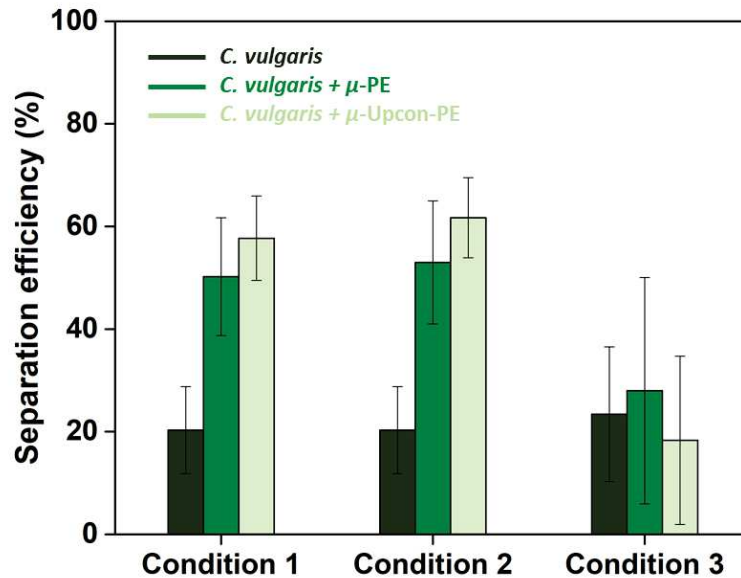


**Figure 6:** Flocculation experiments of *C. vulgaris* cell flotation efficiency with  $\mu$ -PE and  $\mu$ -Upcon-PE at 40 mg/L concentration under different conditions. Condition 1, Model-MPs + cells ( $\mu$ -PE and  $\mu$ -Upcon-PE) after 7 days incubation together (no washing). Condition 2, Model-MPs directly added to the cells ( $\mu$ -PE and  $\mu$ -Upcon-PE) (no washing). Condition 3, Model-MPs directly added to the cells ( $\mu$ -PE and  $\mu$ -Upcon-PE) (washing PBS).

### Model MPs-induced aggregation of cells is a two-factor process

To understand if indeed the presence of AOM is an important factor in the aggregation of cells in the presence of Model-MPs, we performed additional optical microscopy assays using Alcian blue staining. This dye is specifically known to react with acidic polysaccharides (Reddy et al., 1996; Shiraishi, 2015; Vergnes et al., 2019) present in the AOM excreted by microalgae cells, thus we selected this technique to qualitatively evaluate the presence of AOM in cells grown in presence of Model-MPs. The images obtained are presented in Figure 7. They show that when cells are grown without Model-MPs shown in Figure 7a, cells are lightly tainted, which reflects the presence of polysaccharides on their surface. However, when cells have grown for 7 days in the presence of Model-MPs ( $\mu$ -PE and  $\mu$ -Upcon-PE), the visible aggregates of cells show also aggregates of blue staining (Figure 7b and c). This experiment proves the presence in this case of AOM, which is produced only if cells are incubated with Model-MPs. In addition, it also suggests that AOM is responsible for the aggregation of cells, as cells in control conditions (not aggregated) do not produce them. This is thus in line with the flocculation/flotation

experiments performed earlier, which showed that removal of AOM by centrifugation resulted in a decrease in the aggregation of cells (Figure 6). MPs are known to provide the sides for colonization and biofilm formation for different microorganisms like bacteria (Harrison et al., 2014). Moreover, in the literature, increased production and composition change of AOM have been highlighted for nanoparticles (NPs) (Pletikapić et al., 2012; Taylor et al., 2016). For example, the biofilm formation thickness of *Chlorella pyrenoidosa* is increased 4-fold in response to CuO NPs exposure (Chen et al., 2019). In our case, while keeping these examples in mind, MPs present in the medium may trigger the AOM production as cells tend to form biofilm around themselves. The interesting point is that up to a specific concentration, we do not observe any aggregation. At Model-MPs concentrations of 5 and 10 mg/L, we do not see flocculation/flotation, meaning there could be a threshold concentration for MPs in the medium to trigger the AOM production, thus the biofilm formation around the cells. Moreover, it is known that higher MPs concentration has a toxic effect, growth inhibition, or oxidative stress, or decreased photosynthetic capacity on algae cells. For example, both micro- and nano-sized polystyrene (PS) microbeads (concentration range of 50 to 500 mg/L) had adverse effects on algae *C. reinhardtii* by reducing its biomass and photosynthetic pigments (Yan et al., 2021). It may mean that the composition and concentration of AOM could be enhanced to resist the adverse effect caused by Model-MPs ( $\mu$ -PE and  $\mu$ -Upcon-PE). Consequently, we could not observe any aggregation at 5 and 10 mg/L. This hypothesis could be supported by recent study by Yan et al. (2021). EPS content in *C. reinhardtii* increased with the increase of PS-MPs concentration which suggests that microalgae under PS-MPs secrete more EPS to resist the toxic effect of MPs (Yan et al., 2021).

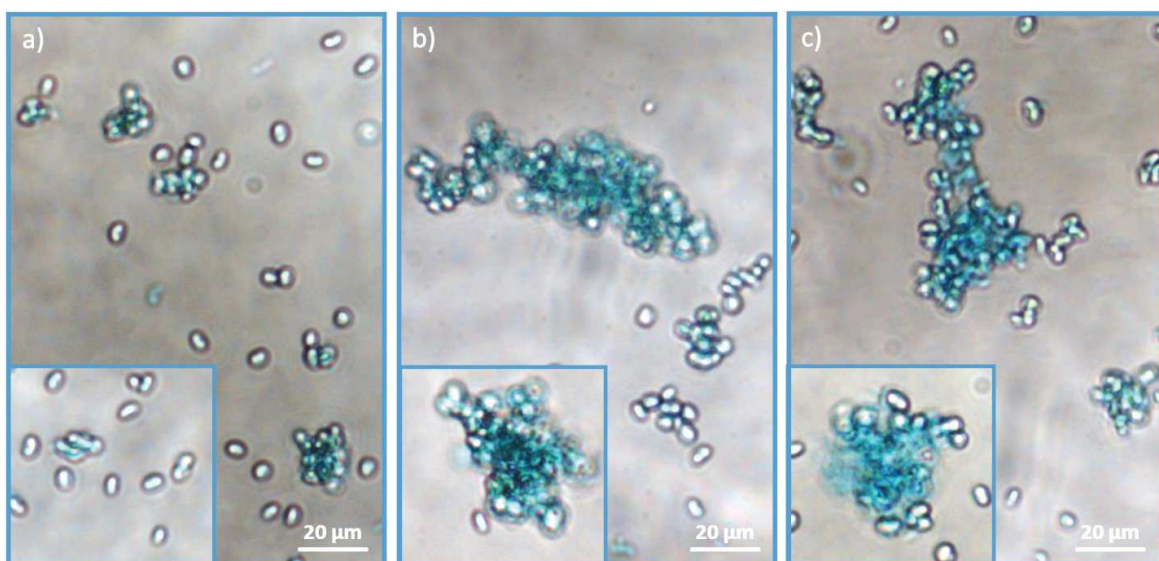


**Figure 7: Optical imaging of AOM produced by *C. vulgaris* after incubated 7 days with a) nothing, b)  $\mu$ -PE and c)  $\mu$ -Upcon-PE.**



However, the presence of AOM when cells are incubated with Model-MPs might not be the only factor resulting in the aggregation of cells. Indeed, as we showed using the flocculation/flotation experiment, the aggregation of cells occurs also if Model-MPs are added at the last moment to the cells (Figure 6, condition 2). In this condition, cells have not grown with the particles and thus do not produce AOM as it was showed with the Alcian blue staining (Figure 7a). But in this case, the aggregation still occurs, which means that particles at some point might be able to interact with cells. Thus, to understand if an interaction between Model-MPs and cells is possible, we performed force-spectroscopy experiments to probe the interactions between single *C. vulgaris* cell and  $\mu$ -(Upcon)-PE. For that, we used FluidFM technology, where single *C. vulgaris* cells were aspirated at the aperture of FluidFM probes by exerting a negative pressure inside the microfluidic cantilever. This negative pressure, compared to classic single-cell force spectroscopy methods using AFM, has the advantage to keep the cells stable on the cantilever even when in contact with a strongly adhesive surface (Demir et al., 2020). The results of these experiments are presented in Figure 8. In the case of  $\mu$ -PE (Figure 8a), the retract force curves obtained present a single retract peak happening at the contact, similar to what was observed with bubbles, with an average force of  $14.6 \pm 15.3$  nN ( $n = 2713$  force curves with 8 cells and particles coming from 2 different cultures). As for the interactions with bubbles, this force signature is typical of non-specific interactions, and most likely reflect a hydrophobic interaction between *C. vulgaris* cells and  $\mu$ -PE. Similar force curves were obtained for  $\mu$ -Upcon-PE with a similar average adhesion force of  $15.4 \pm 15.8$  nN ( $n = 3470$  force curves with 10 cells and particles coming from 2 different cultures) shown in Figure 8b. The adhesion forces are not significantly different at p-value of 0.05 (unpaired student test). This is an interesting point, in line with the previous flocculation/flotation experiments: although incorporating UCNPs to the  $\mu$ -PE changes the architecture and surface roughness of the particles, it does not affect their interaction with *C. vulgaris* cells. Thus, these results first show that there is indeed an interaction between cells and Model-MPs, and that these interactions are nonspecific and hydrophobic. Recently, we evaluated the hydrophobicity of *C. vulgaris* by measuring the interaction between air bubble and single *C. vulgaris* cells (Demir et al., 2021). The forces recorded between negatively charged bubbles (Yang et al., 2001) and negatively charged *C. vulgaris* at considered pH (Demir et al., 2020) result from a balance between electrostatic repulsion and hydrophobic interaction. Once hydrophobic interactions are dominant than electrostatic repulsion, we record an interaction. In the case of *C. vulgaris* and bubble, the average interaction was recorded as 4.2 nN (Demir et al., 2021). Most probably, this is the case for *C. vulgaris* and Model-MPs interaction. Hydrophobic

interaction could overcome the electrostatic repulsion between negative *C. vulgaris* and negatively charged Model-MPs giving an average adhesion force around 15 nN, almost 3.6 - fold higher than the interaction between *C. vulgaris* and bubble. This increase is logical when we consider the contact area as in bubble-*C. vulgaris* case, two spherical shape (almost) bodies interact, whereas, in the *C. vulgaris*-particles case, spherical and flat (almost flat compared to bubble) bodies interact, leading to an increase in contact area; thus, higher adhesion forces are obtained. Another possibility is the contribution of other types of non-specific interaction like electrostatic as in bubble-*C. vulgaris* interaction case only attractive interaction taking place is hydrophobic interaction.

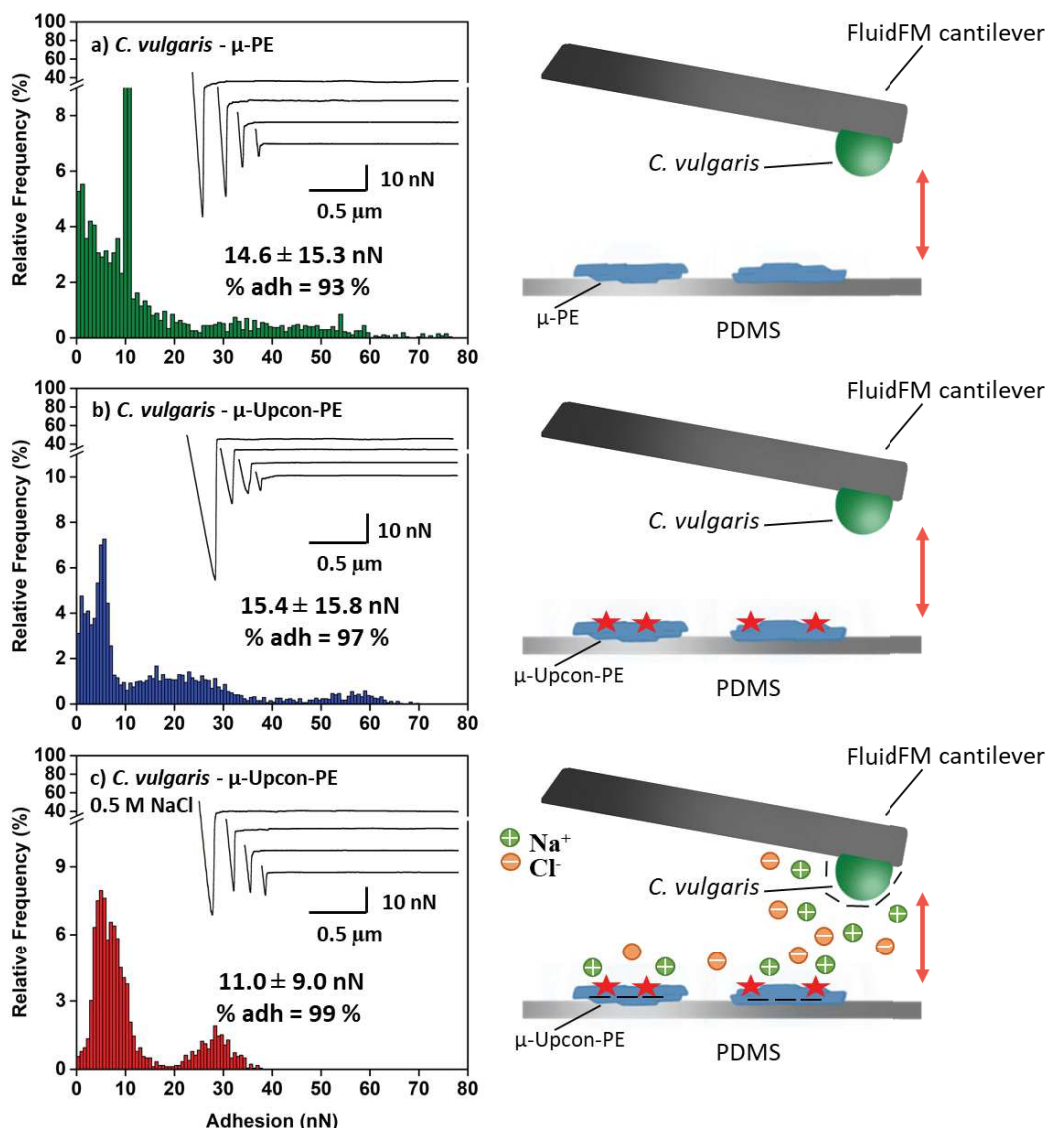


**Figure 8: Probing the interaction between *C. vulgaris* cells and Model-MPs.** Adhesion force histogram obtained for the interaction between *C. vulgaris* cells and a)  $\mu$ -PE, b)  $\mu$ -Upcon-PE, and c)  $\mu$ -Upcon-PE after 0.5 M NaCl addition. Insets in a, b and c shows the representative force curves obtained during force spectroscopy experiments.

Additional experiments were then carried out to further prove this point and exclude the possible contribution of other types of interactions between Model-MPs and *C. vulgaris* cells like for instance electrostatic interactions. Indeed, even though the global charge of the *C. vulgaris* is negative, there might be positively charged molecules on the cell wall of *C. vulgaris* which could interact electrostatically with negatively charged Model-MPs. For that, force spectroscopy experiments were performed between *C. vulgaris* and Model-MPs at higher salt concentrations (Figure 8c). When we increase the salt concentration by adding 500 mM of NaCl in PBS buffer (0.137 M of NaCl) at pH 7.4, the charges present on *C. vulgaris* cells and Model-MPs are shielded. Although the adhesion forces recorded is  $11.0 \pm 9.0$  nN ( $n = 1785$  force curves with 6 cells and particles coming from 2 different cultures), given the wide distribution of the values obtained, it is in the same range as for cells without salt addition. But still the difference is significant (unpaired t-test, p-value of 0.05), meaning that electrostatic interactions are involved, but are not dominant. An interesting point to note concerns the wide distribution of the adhesion values obtained in each case. This heterogeneity can be explained by the fact that in each case we aspirated a different cell. As we have no control over the cell sizes, the contact area in each case is different, resulting in different adhesion values. Also, this heterogeneity in the results may be associated with the surface structure of the Model-MPs which is irregular, perhaps modifying the contact area and the adhesion force recorded. Indeed, when we look at the adhesion forces obtained throughout the surface of the particles scanned, we can see that as the cantilever moves on the surface, the Model-MPs adhesion force does not stay constant over consecutive measurements (data not shown). Finally, to confirm that the forces recorded are due to only interactions of cells with Model-MPs, we probed the interactions between *C. vulgaris* cells and PDMS surface. The results showed that neither *C. vulgaris* - PDMS nor FluidFM cantilever - Model-MPs interaction occurs, confirming that the interactions described here take place between cells and Model-MPs. Understanding the interaction between cells and MPs has many implications in different fields such as the medical field, marine, or industrial biofouling process. The most common form of biofouling can be found in the marine environment. To illustrate, a ship's waterline, propeller, and rudder blade experience the highest amount of fouling (Lebret et al., 2009). In the normal biofouling process, cells produce AOM to form a biofilm on the particle, further contributing to the cell aggregation on these particles. When we remove the AOM, we most probably remove the particles, and we do not observe aggregation. Understanding the parameters that influence this interaction allows to modulate the MPs properties, achieve accumulation in certain territories, or attain tunable cellular interaction.

## Conclusions

Revealing the interaction between MPs and cells is a crucial step to understanding the biofouling process to the end, as these interactions are involved in the initial step to chain effects on the behavior of both cells and MPs. In order to understand these interactions, it is essential to look at the interface between them, AOM, and how AOM affects these interactions. For that, we have chosen the freshwater green species, *C. vulgaris*, and studied at nanoscale its interaction with Model-MPs and their further role in aggregation of cells using AFM. Moreover, we also investigated the role of AOM in these aggregation processes. In combination with population-scale flocculation experiments, these data obtained from AFM allow us to understand the mechanism behind these interactions. In the end, our study demonstrated that the aggregation of cells induced by MPs is a two-step process; first, an initial hydrophobic interaction takes place that triggers the production of AOM by cells. These AOM then allow the aggregation of more cells and more MPs.

## Acknowledgements

C. F.-D. is a researcher at CNRS. C. F.-D. acknowledges financial support for this work from the Agence Nationale de la Recherche, JCJC project FLOTALG (ANR-18-CE43-0001-01).

## References

- Andrady, A., & Neal, M. (2009). Applications and Societal Benefits of Plastics. *Philosophical transactions of the Royal Society of London. Series B, Biological sciences*, 364, 1977-1984. <https://doi.org/10.1098/rstb.2008.0304>
- ASTM E2865-12. (2018). *Guide for Measurement of Electrophoretic Mobility and Zeta Potential of Nanosized Biological Materials*. ASTM International, West Conshohocken, PA. <https://doi.org/10.1520/E2865-12R18>
- Barbosa, A. B. (2009). Dynamics of living phytoplankton : Implications for paleoenvironmental reconstructions. *IOP Conference Series: Earth and Environmental Science*, 5(1), 012001. <https://doi.org/10.1088/1755-1307/5/1/012001>
- Beardall, J., & Raven, J. A. (2004). The potential effects of global climate change on microalgal photosynthesis, growth and ecology. *Phycologia*, 43(1), 26-40. <https://doi.org/10.2216/i0031-8884-43-1-26.1>
- Bergami, E., Pugnali, S., Vannuccini, M. L., Manfra, L., Faleri, C., Savorelli, F., Dawson, K. A., & Corsi, I. (2017). Long-term toxicity of surface-charged polystyrene nanoplastics to marine planktonic species *Dunaliella tertiolecta* and *Artemia franciscana*. *Aquatic Toxicology*, 189, 159-169. <https://doi.org/10.1016/j.aquatox.2017.06.008>
- Besson, A., Formosa-Dague, C., & Guiraud, P. (2019). Flocculation-flotation harvesting mechanism of *Dunaliella salina*: From nanoscale interpretation to industrial optimization. *Water Research*, 155, 352-361. <https://doi.org/10.1016/j.watres.2019.02.043>
- Bhagwat, G., Tran, T. K. A., Lamb, D., Senathirajah, K., Grainge, I., O'Connor, W., Juhasz, A., & Palanisami, T. (2021). Biofilms Enhance the Adsorption of Toxic Contaminants

- on Plastic Microfibers under Environmentally Relevant Conditions. *Environmental Science & Technology*, 55(13), 8877-8887. <https://doi.org/10.1021/acs.est.1c02012>
- Bhattacharya, P., Lin, S., Turner, J. P., & Ke, P. C. (2010). Physical Adsorption of Charged Plastic Nanoparticles Affects Algal Photosynthesis. *The Journal of Physical Chemistry C*, 114(39), 16556-16561. <https://doi.org/10.1021/jp1054759>
- Binnig, G., Quate, C. F., & Gerber, Ch. (1986). Atomic Force Microscope. *Physical Review Letters*, 56(9), 930-933. <https://doi.org/10.1103/PhysRevLett.56.930>
- Bravo M, Astudillo JC, Lancellotti D, Luna-Jorquera G, Valdivia N, & Thiel M. (2011). Rafting on abiotic substrata : Properties of floating items and their influence on community succession. *Marine Ecology Progress Series*, 439, 1-17. <https://doi.org/10.3354/meps09344>
- Carson, H. S., Nerheim, M. S., Carroll, K. A., & Eriksen, M. (2013). The plastic-associated microorganisms of the North Pacific Gyre. *Marine Pollution Bulletin*, 75(1), 126-132. <https://doi.org/10.1016/j.marpolbul.2013.07.054>
- Casabianca, S., Capellacci, S., Penna, A., Cangiotti, M., Fattori, A., Corsi, I., Ottaviani, M. F., & Carloni, R. (2020). Physical interactions between marine phytoplankton and PET plastics in seawater. *Chemosphere*, 238, 124560. <https://doi.org/10.1016/j.chemosphere.2019.124560>
- Chen, F., Xiao, Z., Yue, L., Wang, J., Feng, Y., Zhu, X., Wang, Z., & Xing, B. (2019). Algae response to engineered nanoparticles : Current understanding, mechanisms and implications. *Environmental Science: Nano*, 6(4), 1026-1042. <https://doi.org/10.1039/C8EN01368C>
- Chopin, L., Formosa, C., Rols, M. P., Duval, R. E., & Dague, E. (2013). Imaging living cells surface and quantifying its properties at high resolution using AFM in QI™ mode. *Micron*, 48, 26-33. <https://doi.org/10.1016/j.micron.2013.02.003>
- Cid, Á., Prado, R., Rioboo, C., Suarez-Bregua, P., & Herrero, C. (2012). *Use of microalgae as biological indicators of pollution : Looking for new relevant cytotoxicity endpoints*. 311-323.
- Cole, M., Lindeque, P., Fileman, E., Halsband, C., Goodhead, R., Moger, J., & Galloway, T. S. (2013). Microplastic Ingestion by Zooplankton. *Environmental Science & Technology*, 47(12), 6646-6655. <https://doi.org/10.1021/es400663f>
- Cole, M., Lindeque, P., Halsband, C., & Galloway, T. S. (2011). Microplastics as contaminants in the marine environment : A review. *Marine Pollution Bulletin*, 62(12), 2588-2597. <https://doi.org/10.1016/j.marpolbul.2011.09.025>
- Cunha, C., Faria, M., Nogueira, N., Ferreira, A., & Cordeiro, N. (2019). Marine vs freshwater microalgae exopolymers as biosolutions to microplastics pollution. *Environmental Pollution*, 249, 372-380. <https://doi.org/10.1016/j.envpol.2019.03.046>
- Dague, E., Alsteens, D., Latgé, J.-P., Verbelen, C., Raze, D., Baulard, A. R., & Dufrêne, Y. F. (2007). Chemical Force Microscopy of Single Live Cells. *Nano Letters*, 7(10), 3026-3030. <https://doi.org/10.1021/nl071476k>
- Demir, I., Blockx, J., Dague, E., Guiraud, P., Thielemans, W., Muylaert, K., & Formosa-Dague, C. (2020). Nanoscale Evidence Unravels Microalgae Flocculation Mechanism Induced by Chitosan. *ACS Applied Bio Materials*, 3(12), 8446-8459. <https://doi.org/10.1021/acsabm.0c00772>
- Demir, I., Luchtefeld, I., Lemen, C., Dague, E., Guiraud, P., Zambelli, T., & Formosa-Dague, C. (2021). Probing the interactions between air bubbles and (bio)interfaces at the nanoscale using FluidFM technology. *Journal of Colloid and Interface Science*, 604, 785-797. <https://doi.org/10.1016/j.jcis.2021.07.036>

- Demir-Yilmaz, I., Guiraud, P., & Formosa-Dague, C. (2021). The contribution of Atomic Force Microscopy (AFM) in microalgae studies : A review. *Algal Research*, 60, 102506. <https://doi.org/10.1016/j.algal.2021.102506>
- Dong, D., Zhang, L., Guo, Z., & Hua, X. (2017). The role of extracellular polymeric substances on the sorption of pentachlorophenol onto natural biofilms in different incubation times : A fluorescence study. *Chemistry and Ecology*, 33(2), 131-142. <https://doi.org/10.1080/02757540.2017.1281253>
- EPA US. (2016, décembre 20). *White Paper : A Summary of the Literature on the Chemical Toxicity of Plastics Pollution on Aquatic Life and Aquatic-Dependent Wildlife* [Overviews and Factsheets]. United State Environmental Protection Agency. <https://www.epa.gov/wqc/white-paper-summary-literature-chemical-toxicity-plastics-pollution-aquatic-life-and-aquatic>
- Formosa-Dague, C., Duval, R. E., & Dague, E. (2018). Cell biology of microbes and pharmacology of antimicrobial drugs explored by Atomic Force Microscopy. *Seminars in Cell & Developmental Biology*, 73, 165-176. <https://doi.org/10.1016/j.semcdb.2017.06.022>
- GESAMP. (2016). *Sources, Fate and Effects of Microplastics in the Marine Environment (Part 2)* (Journal Series GESAMP Reports and Studies GESAMP Reports and Studies N° 93; p. 220). <http://www.gesamp.org/publications/microplastics-in-the-marine-environment-part-2>
- Geyer, R., Jambeck, J. R., & Law, K. L. (2017). Production, use, and fate of all plastics ever made. *Science advances*, 3(7), e1700782. <https://doi.org/10.1126/sciadv.1700782>
- Glibert, P. M., Icarus Allen, J., Artioli, Y., Beusen, A., Bouwman, L., Harle, J., Holmes, R., & Holt, J. (2014). Vulnerability of coastal ecosystems to changes in harmful algal bloom distribution in response to climate change : Projections based on model analysis. *Global change biology*, 20(12), 3845-3858. <https://doi.org/10.1111/gcb.12662>
- Gregory, M. R., & Ryan, P. G. (1997). Pelagic plastics and other seaborne persistent synthetic debris : A review of Southern Hemisphere perspectives. *Marine debris*, 49-66. [https://doi.org/10.1007/978-1-4613-8486-1\\_6](https://doi.org/10.1007/978-1-4613-8486-1_6)
- Guillard, R. R. L., & Lorenzen, C. J. (1972). Yellow-green algae with chlorophyllide C2. *Journal of Phycology*, 8(1), 10-14.
- Harrison, J. P., Schratzberger, M., Sapp, M., & Osborn, A. M. (2014). Rapid bacterial colonization of low-density polyethylene microplastics in coastal sediment microcosms. *BMC Microbiology*, 14(1), 232. <https://doi.org/10.1186/s12866-014-0232-4>
- Hopes, A., & Mock, T. (2015). Evolution of microalgae and their adaptations in different marine ecosystems. *eLS*, 1-9. <https://doi.org/10.1002/9780470015902.a0023744>
- Horton, A. A., Walton, A., Spurgeon, D. J., Lahive, E., & Svendsen, C. (2017). Microplastics in freshwater and terrestrial environments : Evaluating the current understanding to identify the knowledge gaps and future research priorities. *Science of the total environment*, 586, 127-141. <https://doi.org/10.1016/j.scitotenv.2017.01.190>
- Hutter, J. L., & Bechhoefer, J. (1993). Calibration of atomic-force microscope tips. *Review of Scientific Instruments*, 64(7), 1868-1873. <https://doi.org/10.1063/1.1143970>
- Jorissen, F. (2014). Colonization by the benthic foraminifer *Rosalina* (*Tretomphalus*) *concinna* of Mediterranean drifting plastics. In *Marine litter in the Mediterranean and Black Seas* (p. 87-95). [https://ciesm.org/online/monographs/46/CIESM\\_Monograph\\_46\\_Marine\\_Plastic\\_Litter\\_87\\_95.pdf](https://ciesm.org/online/monographs/46/CIESM_Monograph_46_Marine_Plastic_Litter_87_95.pdf)
- Kang, J., Zhou, L., Duan, X., Sun, H., Ao, Z., & Wang, S. (2019). Degradation of Cosmetic Microplastics via Functionalized Carbon Nanosprings. *Matter*, 1(3), 745-758. <https://doi.org/10.1016/j.matt.2019.06.004>

- Kokalj, A. J., Hartmann, N. B., Drobne, D., Potthoff, A., & Kühnel, D. (2021). Quality of nanoplastics and microplastics ecotoxicity studies: Refining quality criteria for nanomaterial studies. *Journal of Hazardous Materials*, 415, 125751. <https://doi.org/10.1016/j.jhazmat.2021.125751>
- Lagarde, F., Olivier, O., Zanella, M., Daniel, P., Hiard, S., & Caruso, A. (2016). Microplastic interactions with freshwater microalgae: Hetero-aggregation and changes in plastic density appear strongly dependent on polymer type. *Environmental Pollution*, 215, 331-339. <https://doi.org/10.1016/j.envpol.2016.05.006>
- Lebret, K., Thabard, M., & Hellio, C. (2009). 4 - Algae as marine fouling organisms: Adhesion damage and prevention. In C. Hellio & D. Yebra (Éds.), *Advances in Marine Antifouling Coatings and Technologies* (p. 80-112). Woodhead Publishing. <https://doi.org/10.1533/9781845696313.1.80>
- Liu, G., Jiang, R., You, J., Muir, D. C. G., & Zeng, E. Y. (2020). Microplastic Impacts on Microalgae Growth: Effects of Size and Humic Acid. *Environmental Science & Technology*, 54(3), 1782-1789. <https://doi.org/10.1021/acs.est.9b06187>
- Lobelle, D., & Cunliffe, M. (2011). Early microbial biofilm formation on marine plastic debris. *Marine Pollution Bulletin*, 62(1), 197-200. <https://doi.org/10.1016/j.marpolbul.2010.10.013>
- Long, M., Moriceau, B., Gallinari, M., Lambert, C., Huvet, A., Raffray, J., & Soudant, P. (2015). Interactions between microplastics and phytoplankton aggregates: Impact on their respective fates. *Marine Chemistry*, 175, 39-46. <https://doi.org/10.1016/j.marchem.2015.04.003>
- Long, M., Paul-Pont, I., Hégaret, H., Moriceau, B., Lambert, C., Huvet, A., & Soudant, P. (2017). Interactions between polystyrene microplastics and marine phytoplankton lead to species-specific hetero-aggregation. *Environmental Pollution*, 228, 454-463. <https://doi.org/10.1016/j.envpol.2017.05.047>
- Mao, Y., Ai, H., Chen, Y., Zhang, Z., Zeng, P., Kang, L., Li, W., Gu, W., He, Q., & Li, H. (2018). Phytoplankton response to polystyrene microplastics: Perspective from an entire growth period. *Chemosphere*, 208, 59-68. <https://doi.org/10.1016/j.chemosphere.2018.05.170>
- Masó, M., Garcés, E., Pagès, F., & Camp, J. (2003). Drifting plastic debris as a potential vector for dispersing Harmful Algal Bloom (HAB) species. *Scientia Marina*, 67(1), 107-111. <https://doi.org/10.3989/scimar.2003.67n1107>
- Meister, A., Gabi, M., Behr, P., Studer, P., Vörös, J., Niedermann, P., Bitterli, J., Polesel-Maris, J., Liley, M., Heinzelmann, H., & Zambelli, T. (2009). FluidFM: Combining Atomic Force Microscopy and Nanofluidics in a Universal Liquid Delivery System for Single Cell Applications and Beyond. *Nano Letters*, 9(6), 2501-2507. <https://doi.org/10.1021/nl901384x>
- Nava, V., & Leoni, B. (2021). A critical review of interactions between microplastics, microalgae and aquatic ecosystem function. *Water Research*, 188, 116476. <https://doi.org/10.1016/j.watres.2020.116476>
- Nolte, T. M., Hartmann, N. B., Kleijn, J. M., Garnæs, J., van de Meent, D., Jan Hendriks, A., & Baun, A. (2017). The toxicity of plastic nanoparticles to green algae as influenced by surface modification, medium hardness and cellular adsorption. *Aquatic Toxicology*, 183, 11-20. <https://doi.org/10.1016/j.aquatox.2016.12.005>
- Oberbeckmann, S., Löder, M. G., & Labrenz, M. (2015). Marine microplastic-associated biofilms—a review. *Environmental chemistry*, 12(5), 551-562. <https://doi.org/10.1071/EN15069>

- Peng, L., Fu, D., Qi, H., Lan, C. Q., Yu, H., & Ge, C. (2020). Micro- and nano-plastics in marine environment : Source, distribution and threats—A review. *Science of The Total Environment*, 698, 134254. <https://doi.org/10.1016/j.scitotenv.2019.134254>
- Phuong, N. N., Zalouk-Vergnoux, A., Poirier, L., Kamari, A., Châtel, A., Mouneyrac, C., & Lagarde, F. (2016). Is there any consistency between the microplastics found in the field and those used in laboratory experiments? *Environmental Pollution*, 211, 111-123. <https://doi.org/10.1016/j.envpol.2015.12.035>
- Pletikapić, G., Žutić, V., Vinković Vrček, I., & Svetličić, V. (2012). Atomic force microscopy characterization of silver nanoparticles interactions with marine diatom cells and extracellular polymeric substance. *Journal of Molecular Recognition*, 25(5), 309-317. <https://doi.org/10.1002/jmr.2177>
- Reddy, K. J., Soper, B. W., Tang, J., & Bradley, R. L. (1996). Phenotypic variation in exopolysaccharide production in the marine, aerobic nitrogen-fixing unicellular cyanobacterium *Cyanothece* sp. *World Journal of Microbiology and Biotechnology*, 12(4), 311-318. <https://doi.org/10.1007/BF00340206>
- Reisser, J., Shaw, J., Hallegraeff, G., Proietti, M., Barnes, D. K. A., Thums, M., Wilcox, C., Hardesty, B. D., & Pattiaratchi, C. (2014). Millimeter-Sized Marine Plastics : A New Pelagic Habitat for Microorganisms and Invertebrates. *PLOS ONE*, 9(6), e100289. <https://doi.org/10.1371/journal.pone.0100289>
- Rummel, C. D., Jahnke, A., Gorokhova, E., Kühnel, D., & Schmitt-Jansen, M. (2017). Impacts of Biofilm Formation on the Fate and Potential Effects of Microplastic in the Aquatic Environment. *Environmental Science & Technology Letters*, 4(7), 258-267. <https://doi.org/10.1021/acs.estlett.7b00164>
- Shiraishi, H. (2015). Association of heterotrophic bacteria with aggregated *Arthrospira platensis* exopolysaccharides : Implications in the induction of axenic cultures. *Bioscience, Biotechnology, and Biochemistry*, 79(2), 331-341. <https://doi.org/10.1080/09168451.2014.972333>
- Singh, U. B., & Ahluwalia, A. S. (2013). Microalgae : A promising tool for carbon sequestration. *Mitigation and Adaptation Strategies for Global Change*, 18(1), 73-95. <https://doi.org/10.1007/s11027-012-9393-3>
- Sjollema, S. B., Redondo-Hasselerharm, P., Leslie, H. A., Kraak, M. H. S., & Vethaak, A. D. (2016). Do plastic particles affect microalgal photosynthesis and growth? *Aquatic Toxicology (Amsterdam, Netherlands)*, 170, 259-261. <https://doi.org/10.1016/j.aquatox.2015.12.002>
- Song, C., Liu, Z., Wang, C., Li, S., & Kitamura, Y. (2020). Different interaction performance between microplastics and microalgae : The bio-elimination potential of *Chlorella* sp. L38 and *Phaeodactylum tricornutum* MASCC-0025. *The Science of the Total Environment*, 723, 138146. <https://doi.org/10.1016/j.scitotenv.2020.138146>
- Taylor, C., Matzke, M., Kroll, A., Read, D. S., Svendsen, C., & Crossley, A. (2016). Toxic interactions of different silver forms with freshwater green algae and cyanobacteria and their effects on mechanistic endpoints and the production of extracellular polymeric substances. *Environmental Science: Nano*, 3(2), 396-408. <https://doi.org/10.1039/C5EN00183H>
- Tunali, M., Uzoefuna, E. N., Tunali, M. M., & Yenigun, O. (2020). Effect of microplastics and microplastic-metal combinations on growth and chlorophyll a concentration of *Chlorella vulgaris*. *Science of The Total Environment*, 743, 140479. <https://doi.org/10.1016/j.scitotenv.2020.140479>
- Vergnes, J. B., Gernigon, V., Guiraud, P., & Formosa-Dague, C. (2019). Bicarbonate Concentration Induces Production of Exopolysaccharides by *Arthrospira platensis* That Mediate Bioflocculation and Enhance Flotation Harvesting Efficiency. *ACS Sustainable*



- Chemistry & Engineering*, 7(16), 13796-13804.  
<https://doi.org/10.1021/acssuschemeng.9b01591>
- Wang, Y., Li, Y., Tian, L., Ju, L., & Liu, Y. (2021). The removal efficiency and mechanism of microplastic enhancement by positive modification dissolved air flotation. *Water Environment Research*, 93(5), 693-702. <https://doi.org/10.1002/wer.1352>
- Wingender, J., Neu, T. R., & Flemming, H.-C. (Éds.). (1999a). *Microbial Extracellular Polymeric Substances : Characterization, Structure and Function*. Springer-Verlag. <https://doi.org/10.1007/978-3-642-60147-7>
- Wingender, J., Neu, T. R., & Flemming, H.-C. (1999b). What are Bacterial Extracellular Polymeric Substances? In J. Wingender, T. R. Neu, & H.-C. Flemming (Éds.), *Microbial Extracellular Polymeric Substances : Characterization, Structure and Function* (p. 1-19). Springer. [https://doi.org/10.1007/978-3-642-60147-7\\_1](https://doi.org/10.1007/978-3-642-60147-7_1)
- Wu, Y., Guo, P., Zhang, X., Zhang, Y., Xie, S., & Deng, J. (2019). Effect of microplastics exposure on the photosynthesis system of freshwater algae. *Journal of Hazardous Materials*, 374, 219-227. <https://doi.org/10.1016/j.jhazmat.2019.04.039>
- Xiao, R., & Zheng, Y. (2016). Overview of microalgal extracellular polymeric substances (EPS) and their applications. *Biotechnology Advances*, 34(7), 1225-1244. <https://doi.org/10.1016/j.biotechadv.2016.08.004>
- Xiao, Y., Jiang, X., Liao, Y., Zhao, W., Zhao, P., & Li, M. (2020). Adverse physiological and molecular level effects of polystyrene microplastics on freshwater microalgae. *Chemosphere*, 255, 126914. <https://doi.org/10.1016/j.chemosphere.2020.126914>
- Yan, Z., Xu, L., Zhang, W., Yang, G., Zhao, Z., Wang, Y., & Li, X. (2021). Comparative toxic effects of microplastics and nanoplastics on *Chlamydomonas reinhardtii*: Growth inhibition, oxidative stress, and cell morphology. *Journal of Water Process Engineering*, 43, 102291. <https://doi.org/10.1016/j.jwpe.2021.102291>
- Yang, C., Dabros, T., Li, D., Czarnecki, J., & Masliyah, J. H. (2001). Measurement of the Zeta Potential of Gas Bubbles in Aqueous Solutions by Microelectrophoresis Method. *Journal of Colloid and Interface Science*, 243(1), 128-135. <https://doi.org/10.1006/jcis.2001.7842>
- Zantis, L. J., Carroll, E. L., Nelms, S. E., & Bosker, T. (2021). Marine mammals and microplastics: A systematic review and call for standardisation. *Environmental Pollution*, 269, 116142. <https://doi.org/10.1016/j.envpol.2020.116142>
- Zhang, C., Chen, X., Wang, J., & Tan, L. (2017). Toxic effects of microplastic on marine microalgae *Skeletonema costatum*: Interactions between microplastic and algae. *Environmental Pollution*, 220, 1282-1288. <https://doi.org/10.1016/j.envpol.2016.11.005>
- Zhang, Y., Kang, S., Allen, S., Allen, D., Gao, T., & Sillanpää, M. (2020). Atmospheric microplastics: A review on current status and perspectives. *Earth-Science Reviews*, 203, 103118. <https://doi.org/10.1016/j.earscirev.2020.103118>

Chapter IV.  
Development of a sampling and  
preparation protocol for  
atmospheric Micro- and  
Nanoplastics



## Table of content

IV.1. French summary.....	126
IV.2. Introduction.....	131
IV.2.1. Scientific problematic .....	131
IV.2.2. Context and objectives of the study .....	132
IV.3. Materials and methods .....	135
IV.3.1. Areas of investigation .....	135
IV.3.2. Sampling of the atmosphere.....	137
IV.3.3. Sampling campaigns .....	141
IV.4. GF/F samples .....	144
IV.5. Samples of aqueous dispersion .....	144
IV.5.1. Protocol 1 (2019) .....	144
IV.5.2. Protocol 2 (2020) .....	152
Conclusions and perspectives.....	160
References .....	161

## **IV.1. French summary**

Des études récentes confirment la présence de particules de microplastique dans l'atmosphère, dont les formes, les tailles et les types sont divers. Cependant, en raison de l'absence d'un protocole opérationnel universel pour la collecte et l'analyse des échantillons de plastique dans l'atmosphère, il est difficile de comparer les résultats des différentes études et d'obtenir des informations fiables quant à la distribution en taille et la concentration des microparticules de plastique, par exemple. Il n'existe que peu d'informations quantitatives sur la présence de nanoplastiques dans l'atmosphère, et il est par conséquent difficile d'évaluer leur biodisponibilité et leur impact sur les organismes vivants. La recherche d'un protocole d'échantillonnage standardisé et d'outils permettant la détection, la caractérisation et la quantification des particules de plastique micro- et nanométriques dans l'atmosphère revêt donc un intérêt particulier. Il peut aider à comprendre le transfert des particules entre les écosystèmes, et à accéder à une connaissance plus globale de l'impact potentiel de cette pollution sur l'environnement et la santé humaine.

Ce chapitre est consacré au développement de méthodes d'échantillonnage, de préparation et de caractérisation des particules de plastique collectées dans l'atmosphère. L'étude a été réalisée en prenant en compte des zones présentant différents niveaux d'activité humaine : d'une zone séparée des activités humaines (activité humaine minimale) à une zone fortement industrialisée. Ces deux zones d'échantillonnage sélectionnées pour cette étude ont été la mer Méditerranée ouverte et la région Auvergne en France (Figure IV.1).

La mer Méditerranée est un environnement océanique éloigné des sources directes de pollution et de l'activité humaine continue. L'objectif principal d'une campagne d'échantillonnage atmosphérique en mer est d'évaluer la probabilité de transfert de microplastique sur de longues distances depuis l'environnement terrestre vers le milieu océanique ouvert, et d'étudier un possible transfert des particules dans l'air depuis la surface de l'eau de mer. L'échantillonnage en mer a eu lieu lors d'une campagne de l'Expédition 7<sup>ème</sup> Continent en septembre-octobre 2019. La zone d'échantillonnage était située entre l'Espagne et les îles Baléares, à l'intersection des courants d'eau froide et d'eau chaude. Ces sites sont caractérisés par des niveaux élevés d'accumulation de plastique à la surface de l'eau de mer.

Dans la région Auvergne, nous avons sélectionné 4 sites d'échantillonnage :

- Le premier site est le Puy-de-Dôme (PDD), situé à 1465 m au-dessus du niveau de la mer (a.s.l. : above sea level). Cette zone d'étude est caractéristique de la troposphère

libre, située loin des sources directes de pollution et présentant des niveaux limités d'activité humaine dans ses environs.

- Le deuxième site est une zone rurale nommée Opme (684 m a.s.l.). Ce site est situé à 10 km de Clermont-Ferrand et du Puy-de-Dôme. Cette station peut être considérée comme une zone à niveau modéré d'activité anthropique.
- Le troisième site de prélèvement est le campus des Cézeaux (410 m a.s.l.), situé en zone péri-urbaine de la ville de Clermont-Ferrand.
- Le quatrième point d'échantillonnage est un site industriel de l'agglomération de Clermont-Ferrand (328 m d'altitude). Ce lieu est spécialisé dans le tri et le traitement des déchets plastiques et caractérisé par une forte activité anthropique et industrielle.

Les premières étapes de la mise en œuvre de ce projet ont été l'établissement d'un protocole d'échantillonnage qui puisse être standardisé et le développement d'outils pour la collecte d'échantillons. Pour réduire le risque de contamination croisée, tous les outils d'échantillonnage ont été conçus en verre et en métal pour éviter que les échantillons ne soient en contact avec un matériau polymère. La conception, la fabrication et l'acquisition des outils d'échantillonnage ont été réalisées en collaboration avec l'équipe BIOMETA (Biocatalyse et Métabolisme) de l'Institut de Chimie de Clermont-Ferrand (ICCF) de l'université Clermont Auvergne (UCA).

Deux types d'échantillons atmosphériques ont été collectés : les aérosols atmosphériques (particules en suspension dans l'air) et les dépôts (pluie et neige). Le Tableau IV.1 montre les principales techniques qui ont été utilisées pour l'échantillonnage et décrit le principe de base de leur fonctionnement.

**Tableau IV.1: Outils utilisés pour l'échantillonnage.**

Type d'échantillon	Outils de prélèvement	Principe de l'échantillonnage
Pluie	Echantillonneur automatisé de précipitations (Eigenbrodt NSA 181/KHS)	L'échantillonneur a une surface d'échantillonnage de 1765 cm <sup>2</sup> et est équipé d'un capteur permettant d'ouvrir un couvercle en polytétrafluoroéthylène (PTFE) uniquement lorsqu'il y a des précipitations, empêchant ainsi la contamination par les dépôts secs entre les événements de précipitation.
Neige	Bocaux en verre de 1,5 L et cuillères stériles en acier inoxydable.	Les premiers centimètres de neige ont été enlevés et la neige a été recueillie dans des bocaux en verre avec des cuillères.
Aérosols	Systèmes de collecte d'aérosols à bas débit (BD)	Il s'agit d'un porte-filtre en acier inoxydable de haute qualité, dédié à la collecte des aérosols de l'air sur des filtres en fibre de verre (GF/F) (Ø= 47 mm ; porosité 0,7 µm), et connecté à une pompe 12V DC fonctionnant à 30 L/min.
	Systèmes de collecte d'aérosols à haut débit (HD)	Il fonctionne sur le principe d'un impacteur à haut volume. L'air est pompé à un débit élevé (2000 L/min) et les particules d'aérosol sont collectées dans de l'eau ultrapure.

Des campagnes d'échantillonnage ont eu lieu en 2019 et en 2020. Le type et la quantité d'échantillons collectés pour chaque site d'étude sont présentés dans la Figure IV.1.

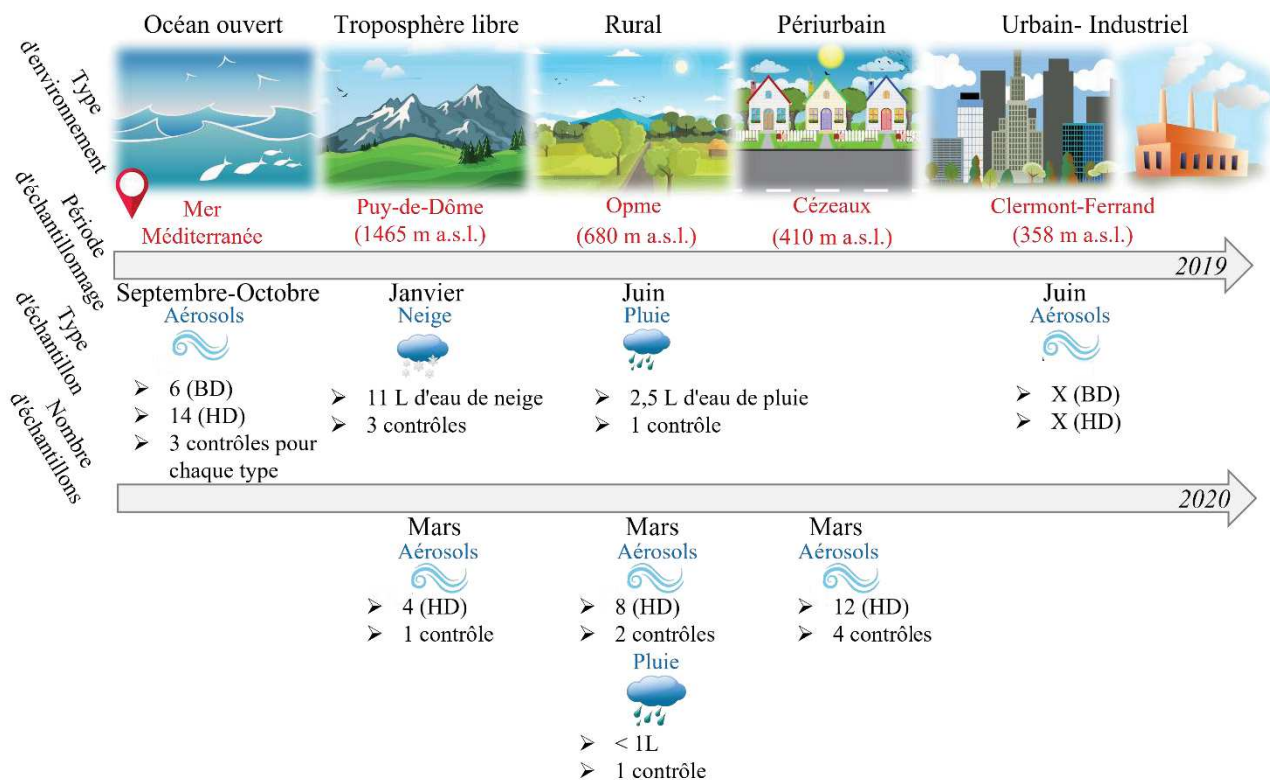


**Figure IV 1: Résumé des campagnes d'échantillonnage atmosphérique.**

Deux types d'échantillons ont pu être obtenus à l'issue de ces campagnes : soit un dépôt de particules sur filtre GF/F (aérosols), soit une suspension de particules dans l'eau (neige, pluie, aérosol). Pour chaque type d'échantillon, plusieurs protocoles ont été développés et améliorés au cours de cette étude, les plus efficaces étant présentés ci-dessous.

Les filtres GF/F obtenus à partir de l'unité de collecte d'aérosols BD ont été observés par microscopie optique. Ensuite, chaque filtre a été soumis à un broyage cryogénique afin de garantir l'homogénéité des échantillons. Enfin, l'analyse quantitative et qualitative de ces échantillons a été réalisée par pyrolyse couplée à la chromatographie en phase gazeuse-spectrométrie de masse (Py-GC-MS).

Le protocole pour les échantillons aqueux est basé sur 4 étapes de filtration séquentielles. La filtration en cascade permet de séparer les microparticules en deux groupes : les particules supérieures à 50  $\mu\text{m}$  et les particules comprises entre 1 et 50  $\mu\text{m}$ . Cette séparation est réalisée par une filtration en cascade à travers une maille métallique (taille des pores 50  $\mu\text{m}$ ) et une maille en nylon Nitex (1  $\mu\text{m}$ ). Les particules collectées par ces deux types de filtres sont transférées sur des filtres d'analyse GF/F pour la microscopie optique et la caractérisation Py-GC-MS/MS. Après filtration à 1  $\mu\text{m}$ , le filtrat a été analysé par analyse de suivi de nanoparticules (NTA) et de diffusion dynamique de la lumière (DLS), afin de détecter la présence de particules sub-micrométriques et de déterminer la distribution de taille des particules présentes. Enfin, la dernière étape de filtration visait à recueillir les particules submicrométriques sur des filtres en fibre de verre (GF/F, 0,7  $\mu\text{m}$ ) ou des filtres en fibre de quartz (QMA, 0,3  $\mu\text{m}$ ). Les filtres avec les NPs collectés ont été homogénéisés et analysés par Py-GC-MS/MS. Le filtrat restant après les filtrations successives en cascade à travers la membrane d'ultrafiltration (UB, 50 kDa) a été analysé, à l'Institut de Chimie de Clermont-Ferrand (ICCF), par chromatographie en phase liquide couplée à la spectrométrie de masse (LC-MS) pour détecter la présence d'oligomères.

Pour éviter toute contamination croisée, toutes les étapes du traitement des échantillons ont été réalisées sous une hotte à flux laminaire. Les opérateurs étaient obligatoirement équipés de blouses de laboratoire (100 % coton) et de gants en nitrile. Tous les outils en verre et les filtres GF/F ont été calcinés avant utilisation, pendant une nuit à 500°C. Les équipements d'échantillonnage ont été rincés à l'éthanol et à l'eau ultrapure avant d'être utilisés. En outre, des contrôles négatifs ont été effectués pendant l'échantillonnage et les étapes de traitement ultérieures afin d'examiner les contaminations potentielles.



Des résultats préliminaires ont été obtenus sur des échantillons de neige qui ont été préparés et analysés selon le protocole que nous avons développé. Les premiers résultats qualitatifs préliminaires obtenus par Py-GC-MS/MS nous ont permis de détecter trois types de polymères dans les échantillons de neige, notamment le polyéthylène téréphtalate (PET), le polypropylène (PP) et le polystyrène (PS). Il a également été trouvé que la fraction 1-50  $\mu\text{m}$  contenait plus de particules atmosphériques que la fraction supérieure à 50  $\mu\text{m}$ . Le signal du PS et du PP était également plus intense pour cette même fraction.

## IV.2. Introduction

### IV.2.1. Scientific problematic

For the last seven years study of plastic pollution in the atmosphere gains more and more attention from the scientific world. Recent studies have confirmed the presence of plastic in the atmosphere from highly developed industrial areas to remote pristine regions (see Chapter I) (Zhang *et al.*, 2020). Thus, the atmosphere began to be seen as an important vector and pathway of plastic particles transport across the planet (Gasperi *et al.*, 2018).

Until now, almost all research has focused on the study of the sources of micro-metric plastic particles in the atmosphere, their fate, behaviour, transport, and data on nano-metric size are practically absent. This is due to the limitations of the standard protocol for samples collection and preparation prior to analysis, as well as limitations of analytical methods for its characterization.

Table 1 provides an overview of current strategies and methodological approaches that people use to study plastic pollution in the air. The type of samples, the period and duration of collection, the type of investigated area, the preparation of samples and along with the methods of analysis are presented (Huang *et al.*, 2020; Zhang *et al.*, 2020). Depending on the study, two types of atmospheric samples are collected: aerosols and depositions. Aerosols are a suspension of fine solid particles or liquid droplets, in the air (dust, clouds, etc). Depositions includes all kinds of atmospheric precipitation (rain, snow, sleet, etc). Sampling duration varies from few days (González-Pleiter *et al.*, 2021) to 1 year (Dris *et al.*, 2016). Depending on the samples type, two sampling approaches are used: passive and active. Both sampling approaches are not standardized and depend on the specific study. Passive sampling are used for the collection of both wet and dry depositions, by the means of funnels with a determined surface area, which are connected to some reservoir (bottle, box, etc.) to collect precipitations (Dris *et al.*, 2016; Cai *et al.*, 2017; Klein and Fischer, 2019), special rain samplers, and particulate fallout collectors (e.g., NILU, which are considered by the International Organization for Standardization (ISO) as an international reference collector (ISO4222.2)) (Allen *et al.*, 2019). Dust are reported to be collected by brush and pan (Abbasi *et al.*, 2019), while snow by using mug, spoon, soup ladle, etc., (Bergmann *et al.*, 2019).

Active sampling is applied to the collection of aerosol samples by pumping air at different flow rate through filter (the type of filter depends on the study) (Liu *et al.*, 2019; Trainic *et al.*, 2020; Wang *et al.*, 2020; González-Pleiter *et al.*, 2021).

The methodology of sample preparation also differs among published studies. Some used only samples filtration, others added density separation and digestion steps. Microscopy (e.g., stereomicroscope, fluorescence microscope, digital microscope) and spectroscopy (e.g.,  $\mu$ FTIR,  $\mu$ Raman) have been the most used techniques for airborne microplastics characterization.

Not much is known about NPs collection and characterization from the atmosphere. Very recent work by Materić *et al.*, demonstrate a new approach on how NPs can be accessed and characterized from snow samples using Thermal Desorption - Proton Transfer Reaction - Mass Spectrometry (TD-PTR-MS). The use of the thermo-analytical method coupled with mass spectrometry is a promising tool that can help to manage this gap in knowledge of nanoplastic pollution in the atmosphere and other environmental compartments (Yakovenko *et al.*, 2020).

Due to the lack of a standard operating protocol for the collection and analysis of plastic samples in the atmosphere, it is hard to compare the results and determine the main size distribution and concentration of plastic for example. To address these issues, a standard sampling protocol and tools are needed to be developed to detect and quantify micro- and nano-metric plastic particles in the atmosphere and to understand how these particles can be transferred between ecosystems. These are important steps for a comprehensive understanding of the potential impact of this pollution on the environment and human health.

#### **IV.2.2. Context and objectives of the study**

The global goal of this project is to detect the presence of MPs and NPs in the atmosphere and conduct their qualitative and quantitative analysis. For this, areas with different levels of human activity were selected for the study: from the area with limited human activity to highly industrialized territory. The study of these areas involves the collection of meteorological data and atmospheric samples of both types: aerosols and depositions. This chapter will focus on the development of tools and methods for samples collection, preparation, and analysis to evaluate the presence of MPs and NPs in the atmosphere.

**Table 1: Bibliographic analysis of the methodology of sample collection, preparation, and analysis used in recent studies related to plastic pollution in the atmosphere**

Reference	Sampling location / type of area	Nature of samples	Period / duration	Plastic size MPs/NPs	Methodology		
					Sampling	Samples preparation (filtration / digestion / density separation)	Analysis
(Dris <i>et al.</i> , 2016)	Paris, France: • urban • sub-urban	Atmospheric fallout: (dry and wet deposition)	Urban area: 1 year (February 2014 - March 2015) Sub-urban: 5 months (October 2014 - March 2015)	MPs	Stainless steel funnel: (surface area = 0,325 m <sup>2</sup> ) connected to 20 L glass bottle	Glass fiber filter GF/A (pore size: 1,6 μm)	Stereomicroscope μFTIR - ATR
(Cai <i>et al.</i> , 2017)	Dongguan, China: • urban	Atmospheric fallout: (dry and wet deposition)	3 months October - December 2016	MPs	Stainless steel funnel: (surface area = 0,0177 m <sup>2</sup> ) connected to bottle 5,31 L	Glass microfiber filter GF/B (pore size: 1,0 μm)	Digital microscope μFTIR SEM analysis
(Abbasi <i>et al.</i> , 2019)	Asaluyeh, Iran. • urban industrial	Street dust Suspended dust	Dry season August 2017	MPs	Dust: metallic pan, wooden brush, polyethylene bags;  ECHO PM ambient filter sampler (TECOR) equipped with PTFE filter (ø = 46,2 mm; pore size: 2 μm)	• Sieve; • Digestion: 30% H <sub>2</sub> O <sub>2</sub> ; • Density separation: NaI (1,6 g cm <sup>-1</sup> );	Fluorescence microscopy Polarized light microscope SEM/EDX
(Allen <i>et al.</i> , 2019)	French Pyrenees: • remote pristine mountain catchment	Atmospheric fallout: (dry and wet deposition)	November 2017 - March 2018	MPs	Palmex Rain Sampler funnel: (surface area = 0.014 m <sup>2</sup> )  NILU Particulate Fallout Collector (p.no. 9721): (surface area = 0.03 m <sup>2</sup> )	• Filtration: PTFE filter (ø = 47 mm; pore size: 0,45 μm); • Digestion: 30% H <sub>2</sub> O <sub>2</sub> ; • Density separation: ZnCl <sub>2</sub> (1,6 g cm <sup>-1</sup> ); • Filtration: Anodisc (ø = 25 mm; pore size: 0,2 μm);	Stereomicroscopy μRaman
(Bergmann <i>et al.</i> , 2019)	Arctic and Swiss Alps: • remote Bremen, Bavaria • populated European sites	Surface snow	2015 – 2017	MPs	Mug, steel spoon, soup ladle	Filtration: Anodisc (ø = 25 mm; pore size: 0,2 μm);	Stereomicroscope μFTIR
(Klein and Fischer, 2019)	Hamburg, Germany • urban • sub-urban	Atmospheric fallout: • depositions	December 2017 to February 2018	MPs	PE funnel: (surface area = 0,0113 m <sup>2</sup> ) connected to PE bottle	• Digestion: 6-14% NaClO • Filtration: cellulose filter (ø = 55 mm; pore size: 5-13 μm );	Nile red staining Fluorescence microscope μRaman

Reference	Sampling location / type of area	Nature of samples	Period / duration	Plastic size MPs/NPs	Methodology		
					Sampling	Samples preparation (filtration / digestion / density separation)	Analysis
(Liu <i>et al.</i> , 2019)	Shanghai, East China • urban industrial	Aerosols	May - June 2019	MPs	KB-120F particulate sampler	Glass microfiber filter GF/A ( $\phi = 90$ mm; pore size: 1,6 $\mu$ m)	Stereomicroscopy $\mu$ FTIR
(Wang <i>et al.</i> , 2020)	South China Sea and East Indian Ocean	Suspended particulate matter	March - April 2019 (EIO voyage)	MPs	KB-120F middle flow total suspended atmospheric particulate sampler with sampling flow rate: $100 \pm 0.1$ L/min	Glass microfiber filter GF/A ( $\phi = 90$ mm; pore size: 1,6 $\mu$ m)	Stereomicroscope $\mu$ FTIR
(Trainic <i>et al.</i> , 2020)	North Atlantic Ocean Open ocean	Aerosols	Tara pacific expedition 2016–2018	MPs	Auto sampler: flow rate $\sim 20$ L/min	Polycarbonate membrane (pore size: 0,8 $\mu$ m)	$\mu$ Raman
(González-Pleiter <i>et al.</i> , 2021)	Madrid, Spain: • urban high-density; Guadalajara, Spain: • urban low-density; Central Spain: • rural and sub-rural	Aerosols High altitude: (701 - 3496 m a.s.l.)		MPs	Pumping system	Stainless steel meshes (pore size: 25 $\mu$ m)	$\mu$ FTIR
(Materić <i>et al.</i> , 2020)	Austrian Alps: • remote area (high-altitude) (3106 m a.s.l.)	Surface snow	1.5 month campaign in late winter 2017	NPs	Scooped by polypropylene vials	PTFE syringe filters (pore size: 200 nm)	TD-PTR-MS

Acronyms: Micro-Fourier Transform Infrared spectroscopy coupled with an Attenuated Total Reflectance accessory ( $\mu$ FTIR -ATR); Micro-Raman spectroscopy ( $\mu$ Raman); Scanning electron microscopy (SEM) and energy dispersive X-ray spectroscopy (EDS); Thermal Desorption - Proton Transfer Reaction - Mass Spectrometry (TD-PTR-MS); Polytetrafluoroethylene (PTFE); Polyethylene (PE); Microplastic (MPs); Nanoplastic (NPs).

## IV.3. Materials and methods

### IV.3.1. Areas of investigation

Two sampling areas were selected for this study: the open Mediterranean Sea and the Auvergne region in France. The Mediterranean Sea is an oceanic environment remote from direct sources of pollution and continuous human activity. The main goal of the atmospheric sampling campaign in the sea is to detect the probability of plastic transfer by long distance from terrestrial zone to open oceanic environmental or to investigate if particles can be transferred to the air from the surface of the seawater. The sampling at sea occurred during a 7<sup>th</sup> Continent Expedition campaign in September-October 2019. The area of interest was located between Spain and the Balearic Islands at the intersection of cold and warm water currents (Figure 1). These sites are characterized by high levels of plastic accumulation at the sea water surface.

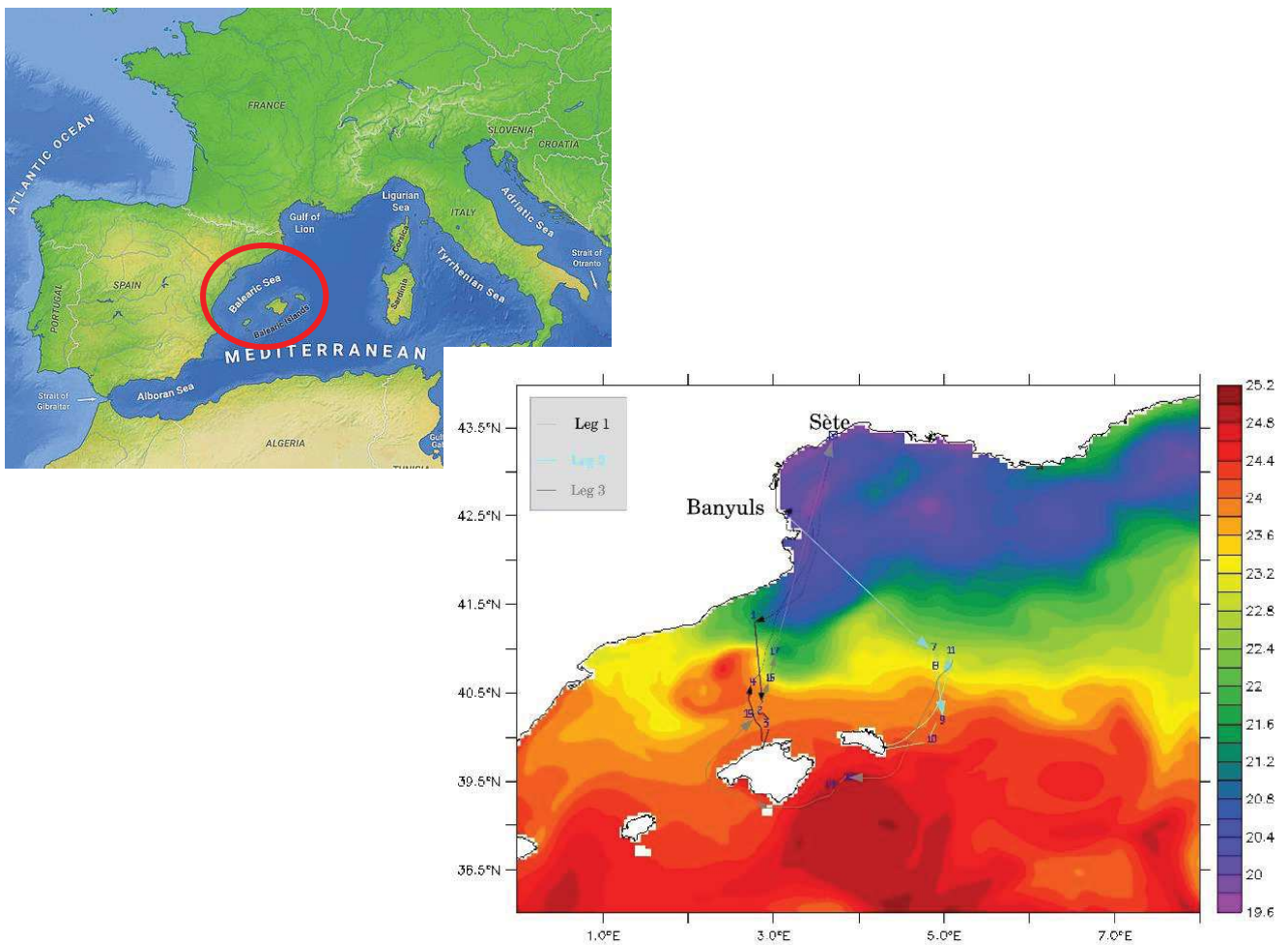


Figure 1: Sampling sites of the 7<sup>th</sup> Continent Expedition mission in the Mediterranean Sea during September-October 2019.

In the Auvergne area we selected 4 sites of sampling (Figure 2). The first site is the Puy-de-Dôme (PDD), located at 1465 m above sea level (a.s.l.). This area of study is a free troposphere, located far from direct sources of pollution and has limited levels of human activity around. The second site is a rural area called “Opme” (684 m a.s.l.). This site is associated with PDD and located 10 km from Clermont-Ferrand. Opme can be considered as a zone with a moderate level of anthropogenic activity. The third sampling point is Cézeaux (410 m a.s.l.), located in peri-urban area, above the city of Clermont-Ferrand.

These three sites constitute the atmospheric monitoring station Cézeaux-Opme-Puy de Dôme (CO-PDD). The research carried out on these sites aims to document the evolution of the composition of the troposphere, by studying:

- 1) the properties of gases, aerosols, and clouds in the medium and long term and their vertical distribution in the troposphere;
- 2) the impact of anthropogenic modifications on the composition of the troposphere, and their consequences in terms of climate (cloud, radiation) and weather (precipitation).

Finally, the fourth sampling point is an Industrial site in the Clermont-Ferrand agglomeration (328 m a.s.l.). This place is specializing in sorting and processing of plastic waste and characterized by a high level of anthropogenic and industrial activity.

Atmospheric monitoring station Cézeaux-Opme-Puy de Dôme (CO-PDD)

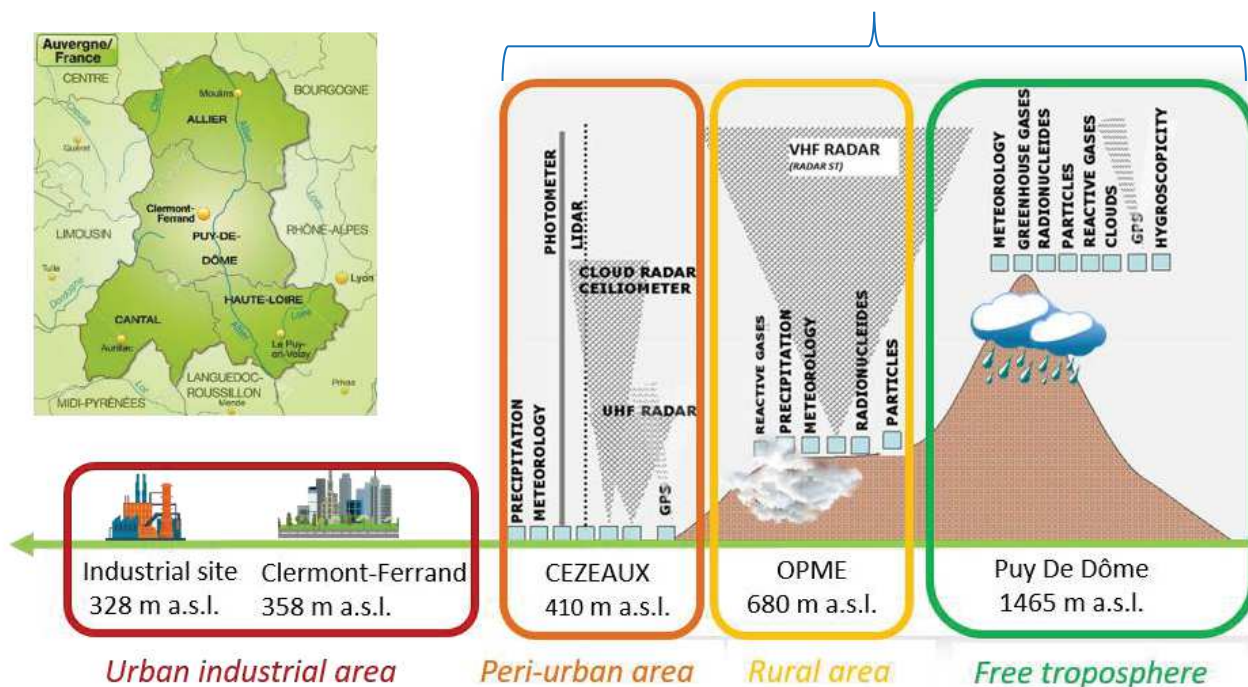


Figure 2: General scheme of sampling sites in the Auvergne region.

### IV.3.2. Sampling of the atmosphere

One of the first steps in the implementation of the current project is the establishment of a standard operational sampling protocol and development tools for sample collection. Two types of atmospheric samples were collected: atmospheric aerosols and depositions.

#### IV.3.2.a. Collection of aerosol samples

Two types of sampling systems have been used for aerosol samplings: low flow (LF) and high flow (HF) aerosol collection units.

The LF aerosol collection system consists of a high-quality stainless-steel filter holder, with which aerosols from air are collected on glass fiber (GF/F) filters ( $\text{Ø} = 47 \text{ mm}$ ; pore size  $0.7 \text{ }\mu\text{m}$ ), (Figure 3), and connected to 12V DC pumps operating at 30 L/min.

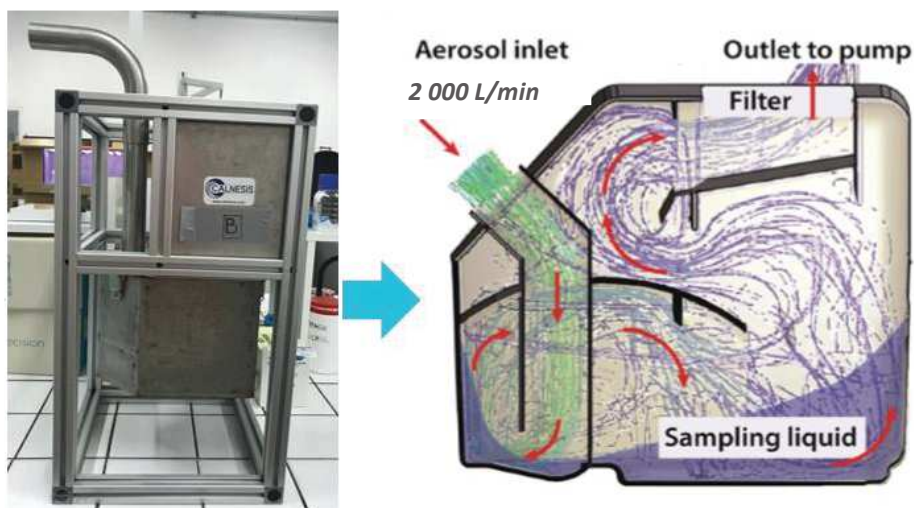


Figure 3: Filter holder for the LF aerosol sampling.

Before each sampling procedure, filter holder and tweezers were rinsed with Milli-Q water and Ethanol. GF/F filters were calcined overnight at  $500^{\circ}\text{C}$  before use. After sample collection, all GF/F filters were individually placed in aluminium foil with a label and stored in an aluminium box in the freezer. For the negative control (blank), the GF/F filter was placed in the filter holder for 2 hours without pumping. After what the blank sample was processed by the same methodology as the rest of the samples.

HF aerosol collection system operates on the principle of a high volume impinger. Air is pumped at a high flow rate ( $2\ 000 \text{ L/min}$ ) through ultrapure water retaining aerosol particles (Santl-Temkiv *et al.*, 2017). This device specially conceived for this study is made of stainless steel and has no plastic parts that come into direct contact with the sample (Figure 4).





**Figure 4:** High flow aerosol collection system developed for the project; Impinger principle from (Santl-Temkiv et al., 2017).

The sampling procedure used only Milli-Q water as the collection liquid. The Milli-Q water was prefiltered through mixed cellulose ester membrane filter (MCE, Ø 47 mm; pore size 0.22 µm) and sterilized by autoclaved (30 min at 121°C) before use. Before each sampling procedure, the system was first rinsed with 500 mL of sterile filtered water. Then the collection cuve was emptied and re-filled with 1 L of sterile filtered water for sampling, and the pumping was started. At the end of the sampling procedure (1 h), water was transferred back to the 1 L glass bottle. To recover the particles that could have sedimented in the cuve, the cuve was finally rinsed with 100 mL additional sterile filtered water which was added to the 1 L collection liquid of the sample. To prevent bacteria growth in the samples, we added sodium azide (NaN<sub>3</sub>) 0.01% (w/v). Field blank corresponded to filling the system with 1 L of sterile filtered water, waiting for 2 hours without pumping. Then blank is collected and processed according to the same procedure as the samples.

#### ***IV.3.2.b. Collection of deposition samples***

Fresh snow samples were collected during a strong snowfall event (31.01.2019) from the snow cover at Puy-de-Dôme mountain summit (1465 m a.s.l.). Visually large untouched snow areas were selected for sampling, and the covers sampled corresponded to one single snowfall of several centimetres (cm) deep (Figure 5).



**Figure 5: Snow collection at Puy-de-Dôme summit during winter 2019.**

The top cm of snow was removed, and snow was collected into 1.5 L glass jars using stainless steel sterile spoons. Before use, the glass jars were rinsed 3 times with sterile Milli-Q water and autoclaved (121°C). During sampling, the operator collected the snow by positioning himself directly in front of the wind direction. In this way, possible cross-contamination from the clothes of the operator is estimated to be minimalized. All snow water samples were melted and added with sodium azide ( $\text{NaN}_3$ ) 0.01% (w/v). Procedural blank was performed by filling the same clean glass jar with 1 L of Milli-Q water, with the following treatment as the samples.

Precipitation samples were collected at about 1.5 m above ground at Opme meteorological station in Central France (680 m a.s.l), in a rural area at about 7 km from Clermont-Ferrand city and 13 km from the top of Puy-de-Dôme. The station is operated by the Observatory of the Globe of Clermont-Ferrand (OPGC) and part of several national and international atmospheric observation networks. An automated wet-deposition sampler (Eigenbrodt NSA 181/KHS) was used (Figure 6); it is equipped with a sensor to open a polytetrafluoroethylene (PTFE) lid only when precipitation occurs, thus preventing contamination by dry deposition between precipitation events. The water collected by the glass funnel ( $r = 23.7$  cm) of the sampler was immediately transferred by gravity into sterile (autoclaved) 1 L glass bottles through sterile silicone tubing. The carousel holding 8 collection bottles was maintained at 4°C, and it was set to switch every 24 h at midnight to a new bottle. Tubing and collection bottles were all (even if empty) collected every week or less and replaced by new (Milli-Q water-rinsed and autoclaved) sets of tubing and bottles, after careful rinsing of the collection funnel with ethanol 70% and sterile Milli-Q water.



Figure 6: Wet-deposition sampler (Eigenbrodt NSA 181/KHS), Opme summer 2019.

#### IV.3.2.c. Sampling strategy

Based on the locations and types of atmospheric samples we would like to investigate, a sampling strategy was developed (Table 2).

Table 2: Sampling strategy for the current project.

Areas of investigation	Sampling sites	Type of samples		
		Aerosols	Rain	Snow
Mediterranean Sea	The intersection of cold and warm water currents (sea level)	X	X	
Auvergne, France	Puy-de-Dôme (1465 m a.s.l.)	X	X	X
	Opme (680 m a.s.l.)	X	X	
	Cézeaux (410 m a.s.l.)	X	X	
	Industrial site, Clermont-Ferrand agglomeration (328 m a.s.l.)	X	X	

Sampling tools and methodologies have been developed for each type of sample. To reduce the risk of cross-contamination by plastic, all sampling tools were conceived to be made of glass and metal to prevent samples to be in contact with a polymer material. The first year of this study was partly dedicated to the conception, manufacturing, and acquisition of the sampling tools.

#### IV.3.2.d. Types of generated samples

Our sampling strategy is generating two types of samples: particles deposition on GF/F filter and particles suspension in water (Table 3).

**Table 3: Types of samples according to the sampling method.**

<i>Type of sample</i>		<i>Material containing samples</i>	<i>Sample preparation</i>
Aerosols	LF	GF/F	Cryogenic grinding
	HF	Aqueous dispersion	Successive cascade filtration
Precipitation	Rain		
	Snow		

Using the LF aerosol collection systems we are collecting the particles on GF/F filter. HF aerosol collection system traps the particles from the air to ultrapure water. Samples of snow and rain are water containing particles from the atmosphere. All samples representing the suspension of particles in water will be treated according to the same sample preparation protocol. With the development of sample preparation, we came to two separate procedures, the first protocol was developed in 2019. Then we improved the protocol in 2020.

#### IV.3.3. Sampling campaigns

##### IV.3.3.a Sampling campaigns 2019

During 2019, several atmospheric sampling campaigns were conducted in the Auvergne region and the Mediterranean Sea (Table 4).

**Table 4: Sampling campaign 2019.**

<i>Areas of investigation</i>	<i>Sampling sites</i>	<i>Type of samples collected</i>			
		<i>Aerosols</i>		<i>Rain</i>	<i>Snow</i>
		<i>LF</i>	<i>HF</i>		
Auvergne, France	Puy-de-Dôme				X
	Opme			X	
	Cézeaux		X		
	Industrial site, Clermont-Ferrand agglomeration		X		
Mediterranean Sea	The intersection of cold and warm water currents	X	X		

In January 2019, snow samples were collected at the Puy-de-Dôme Mountain's summit (Figure 7). In total were collected 22 glass jars of snow (Site 1 = 16 jars; Site 2 = 6 jars) that contained in total about 11 L of snow water, and 3 processing blanks.



Figure 7: Snow collection points at Puy de Dome.

In June was performed a collection of rainwater samples at Opme. In total 2.5 L of rain water were collected. At the same period, a collection of aerosol samples at an Industrial site was performed. We performed a sampling campaign in the Mediterranean Sea in September-October 2019 (Figure 8). Aerosol samples were collected using LF and HF devices; 6 and 14 samples and their corresponding controls were collected, respectively.

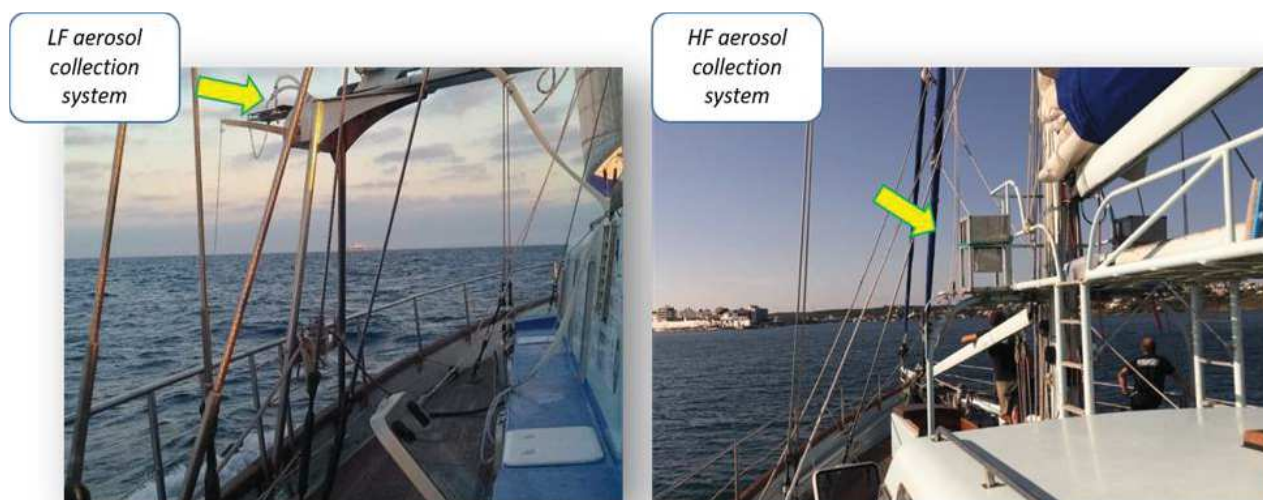


Figure 8: Aerosol sampling at Mediterranean Sea during autumn 2019

#### IV.3.3.b. Sampling campaigns 2020

Atmospheric sampling campaigns in 2020 was aimed at supplementing the samples already collected in 2019. In March 2020, an aerosols sampling campaign was organized in the

Auvergne region. The aerosol collection was performed at three sampling sites (Puy-de-Dôme, Opme, and Cézeaux) using the HF aerosol collection system. Each sample consisted of a pool of 4 individual samples and one negative control. One individual sample represents 120 m<sup>3</sup> of collected air. A total of 12 samples and 3 negative controls were collected in Cézeaux, representing 1440 m<sup>3</sup> of collected air. At Opme were collected 8 samples and 2 negative controls (960 m<sup>3</sup> of air). And at Puy-de-Dôme were collected pool of 4 individual samples and one negative control (480 m<sup>3</sup> of air). Rainwater was constantly collected at Opme site over different seasons.

An LF aerosol collection system was installed in the room where all the sampling equipment was prepared (Figure 9).

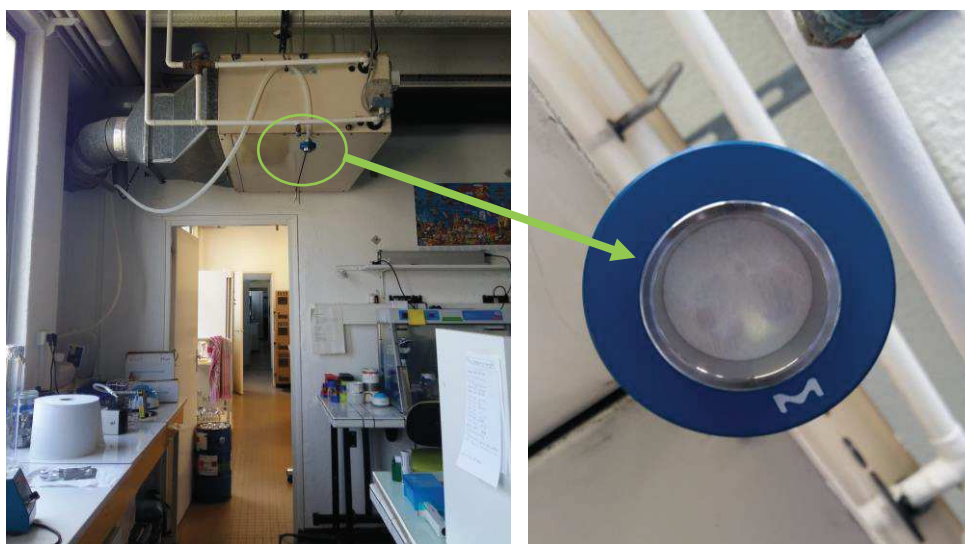


**Figure 9: Indoor aerosol collection (laboratory ICCF).**

The collection took 4 days and allowed to collect 52 m<sup>3</sup> of indoor air. This sample aimed at investigating possible cross-contamination of collected environmental samples during equipment preparation and sample processing.

To avoid cross-contamination, all sampling processing steps were performed under a laminar flow hood. Operators were equipped with lab coats (100 % cotton) and nitrile gloves. In addition, negative controls (blanks) were performed during sampling and its further processing steps to examine potential contaminations.

## IV.4. GF/F samples

GF/F filters obtained from LF aerosol collection system (Figure 10).

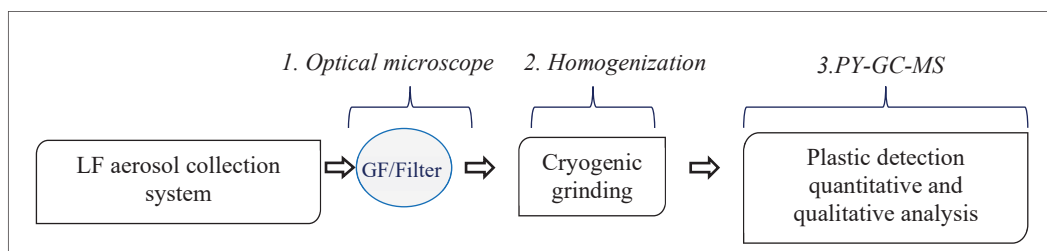


Figure 10: Scheme of preparation and analysis of sample deposited on GF/Filters.

Each filter is observed under an optical microscope (OM). Then each filter is subjected to cryogenic grinding (SPEX™ SamplePrep 6775 Freezer/Mill™) to ensure the homogeneity of the samples. Finally, quantitative, and qualitative analysis of these samples are performed by pyrolysis coupled with gas chromatography-mass spectrometry (Py-GC-MS).

## IV.5. Samples of aqueous dispersion

### IV.5.1. Protocol 1 (2019)

#### IV.5.1.a. Sample preparation

The first protocol was aimed at dividing the potential plastic presented in the samples into three categories: the small microplastic (SMPs, below 1 mm), the nanoplastic (NPs, < 1 μm) (Gigault *et al.*, 2018), and the oligomers (Eyheraguibel *et al.*, 2017). After fractionation each size category is analyzed by appropriate analytical methods (Figure 11).

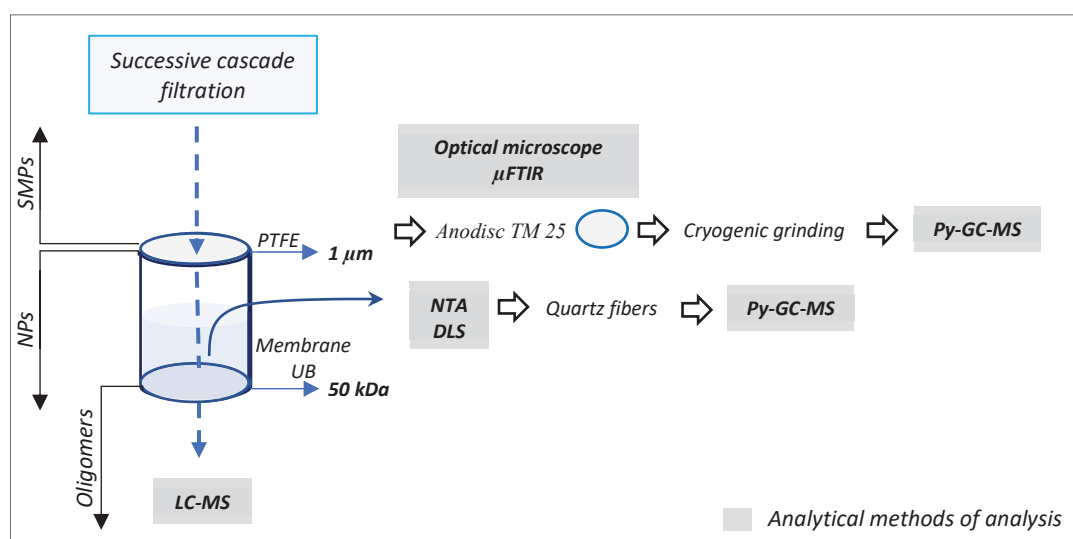


Figure 11: Protocol 1 (2019): Scheme of preparation and analysis of aqueous samples.

### Step 1: Extraction of the SMPs

SMPs fraction is separated from samples by vacuum filtration through PTFE filtration membrane ( $\varnothing=47$  mm; pore size 1  $\mu\text{m}$ ). Then each filter is observed under an optical microscope (OM). The second step of processing includes preparation of the sample for the Fourier transform infrared microscopy ( $\mu\text{FTIR}$ ) analysis. For this step, the PTFE filter is sonicated in 99.9 % ethanol for 15 min, with subsequent filtration through Anodisc TM 25 ( $\varnothing= 25$  mm; pore size 0.2  $\mu\text{m}$ ). After  $\mu\text{FTIR}$  analysis, Anodisc membrane with the sample is carefully detached from the annular polypropylene ring that is used as a support for this kind of membrane. Finally, Anodisc membrane is homogenized with a mortar and pestle and sample is analyzed by Py-GC-MS.

### Step 2: Extraction of the NPs

The NPs fractions were concentrated by frontal ultrafiltration through UB 50 kDa membrane. Samples were concentrated down to 10 mL and collected in a glass vial. Concentrate was analyzed by Dynamic Light Scattering (DLS) and Nanoparticle Tracking Analysis (NTA) analysis to detect the presence of sub-micrometric particles and to determine the size distribution of presented particles in the samples. Thereafter, a small amount of quartz fiber within average length of 5 mm was added to each vial, after which the sample was completely dried by lyophilization. This procedure allows us to perform maximum level of samples concentration by deposition of nanoparticles on quartz fibers for analysis by Py-GC-MS.

#### IV.5.1.b. Sample analysis

Physical and chemical characterization of the particles in the samples will be performed by several analytical methods (Table 5).

**Table 5: Methods of characterization of plastic particles in atmospheric samples.**

<i>Particles size category</i>	<i>Analytical methods of analysis</i>	<i>The type of information being investigated for the plastic characterization</i>
Small microplastic	Optical microscopy (OM)	Number, size, shape, color
	$\mu\text{FTIR}$	Number, size, chemical nature
	Py-GC-MS	Chemical nature, concentration
Nanoplastic	DLS and NTA	Size distribution
	Py-GC-MS	Chemical nature, concentration



## Characterization of the SMPs

### *Optical microscopy*

PTFE filters with SMPs were observed under an optical microscope (OM). Optical images were recorded using an Olympus BX53 microscope with a PLN X10 lens, and the images were processed with the Stream Basic software (Olympus Inc.).

### *$\mu$ -FTIR*

Anodisc filters with SMPs were analyzed by a Thermo Scientific Nicolet iN10 infrared microscope equipped with a liquid nitrogen cooled MCT detector. The spectra were recorded as the average of 16 scans in the spectral range of 1200–3600  $\text{cm}^{-1}$  at a resolution of 8  $\text{cm}^{-1}$ . Particles with size more than 50  $\mu\text{m}$  were chosen for analysis because of the limit of resolution of  $\mu$ -FTIR. The particles were identified if the match with the library was over 70 %. All data processing was performed using Thermo Scientific™ OMNIC™ Picta software.

### *Py-GC-MS*

To complete the  $\mu$ FTIR analysis, the Anodisc filter was analyzed by pyrolysis coupled Py-GC-MS. Currently, the Py-GC-MS evaluation method is under active development. However, the initial method (2019) was applied for sample evaluation (Table 6).

**Table 6: Conditions for preliminary Py-GC-MS evaluation method 2019.**

<b>Pyrolyzer: CDS 6150</b>	
Pyrolyzing temperature	700°C
Pyrolyzing time	30 s
Carrier gas	Helium
Transfer line temperature	280°C
<b>Gas chromatograph: Trase 1310</b>	
Injection mode	Splitless
Column	ZB-50; 30m × 0.25 mm ID, film thickness 0.25 $\mu\text{m}$
Flow	1.25 mL/min
Temperature program	40°C (1 min)→320°C at 10°C/min
<b>Mass spectrometer: TSQ900 Thermo</b>	
Ionization energy	70 eV
Scan range	45-600 amu
<b>Software: Chromeleon 7.2</b>	

Samples were analyzed in the full scan acquisition mode and total ion current (TIC) chromatograms were plotted. Identification of the molecules was made by searching against the National Institute of Science and Technology (NIST05 and NIST05s) library. Blank runs were performed between each analysis to avoid cross-contamination.

## **Characterization of the NPs**

### *DLS*

DLS measurements were carried out at 25°C on a Malvern (Orsay, France) Zetasizer NanoZS equipped with a He-Ne laser ( $\lambda = 633$  nm) at an angle of 173°. The correlation function was analyzed according to the general purpose of the non-negative least-squares (NNLS) method to obtain the distribution of the diffusion coefficients (D) of the particles in solutions. The hydrodynamic diameter was calculated according to the Stokes-Einstein equation. Number-weighted hydrodynamic size distribution and standard deviation (SD) were obtained from 5 measurements of 11 runs of 10 seconds.

### *NTA*

NTA analysis were performed at 22°C using the NanoSight LM10 instrument equipped with an sCMOS camera. Samples were prepared by 1:100 dilution in ultrapure water. Measurement of each sample was performed in triplicate, consisting of three records of 60 s. Results are presented as a mean size of the particles  $\pm$  SD.

### IV.5.1.c. Results

#### SMPs analysis

Figure 12 presents some images obtained by optical microscopy for the snow samples from Puy-de-Dôme (PDD). As compared to the blank samples, several fibers and particles are detected in both snow sites 1 and 2, whose sizes seem to vary from few to several dozen of  $\mu\text{m}$ .

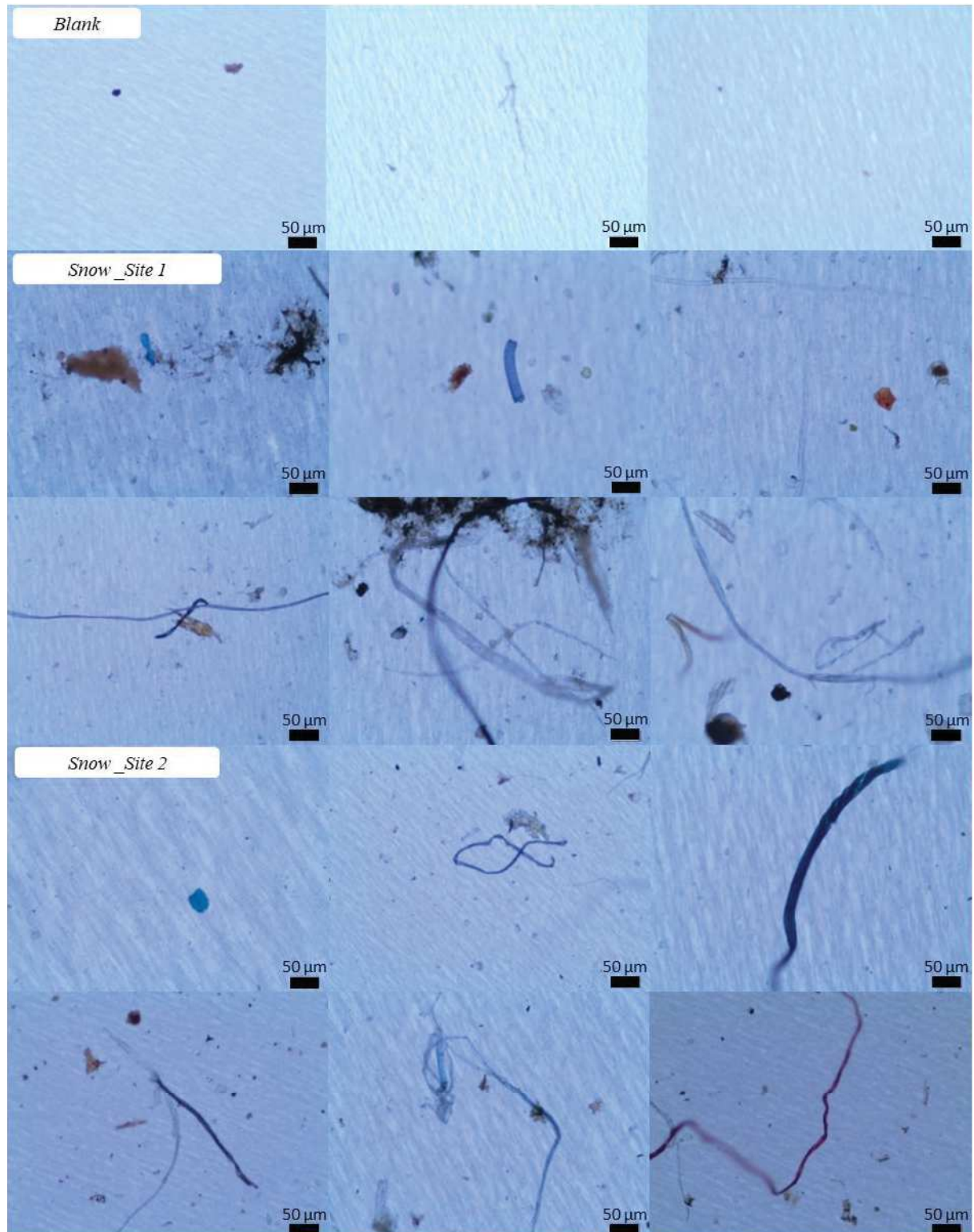


Figure 12: Optical microscopy of the SMPs fraction presented in snow samples from the PPD study site.

Analysis by  $\mu$ FTIR allowed us to determine and analyze particles larger than 50  $\mu\text{m}$  (Table 7).

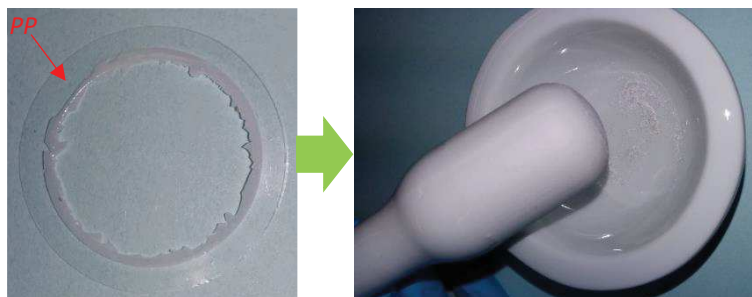
**Table 7: Preliminary results of snow water analysis by  $\mu$ FTIR.**

Samples	Blank	Site 1	Site 2
Total area of filter, $\text{mm}^2$	133		
Total area analysed, $\text{mm}^2$	42	32	52
<b>% of the filter area analyzed</b>	<b>32</b>	<b>24</b>	<b>39</b>
Total number of particles found	73	659	427
<b>Number of identified particles</b>	<b>4</b>	<b>51</b>	<b>36</b>

A fraction of the total surface area of each filter was analyzed. In the control filter, only 73 particles were detected over 32% of the total surface area analyzed. We could identify 4 of them as natural compounds: cellulose (75%) and proteins (25%). As no plastic was detected in the procedural blank  $\mu$ -FTIR, this attest of a satisfactory sample handling strategy.

In the atmospheric sample, particles and fibers were characterized by different shapes, sizes, and colors. The predominant color observed for all fragments and fibers was represented by different shades of blue, some orange and red fragments were observed also. For the snow sample from Site 1, 659 particles were detected over 24% of the surface of the filter of which 7.7% were identified. Most (98%) were related to natural compounds, while 2% were synthetic material (Nylon 6 polymer). Conversely, the sample from Site 2 contained 427 particles over 39% of the surface area of the filter, 8.4% of which were identified. All identified particles were natural compounds (cellulose and proteins).

After  $\mu$ FTIR analysis, Anodisc membrane with each sample was carefully detached from the annular polypropylene ring that is used as support for this kind of membrane (Figure 13). Finally, Anodisc membrane was homogenized with a mortar and pestle and sample is analyzed by Py-GC-MS (Table 8).

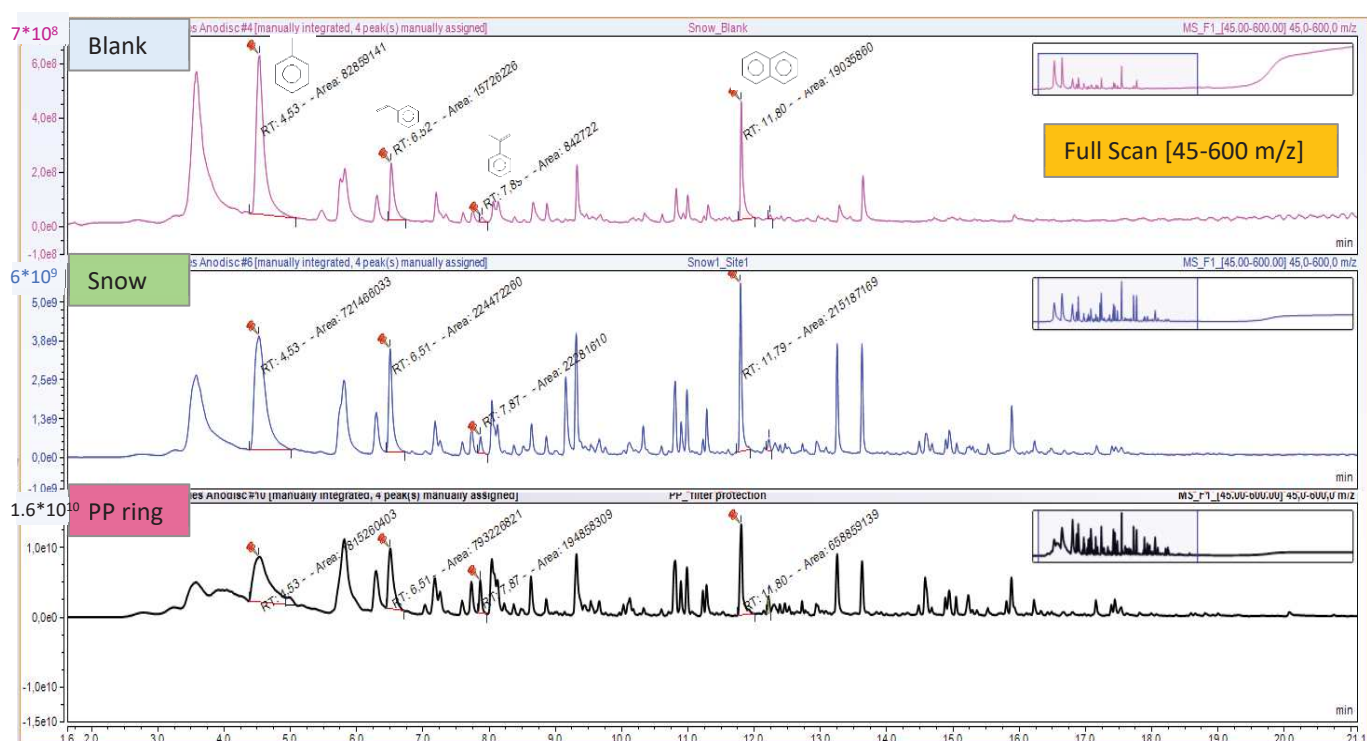


**Figure 13: Homogenization of Anodisc filter before Py-GC-MS analysis**

**Table 8: Part of the filter that was analyzed.**

Sample	Mass of Anodisc filter injected, (mg)	% of filter analysed
Anodisc new (negative control)	2.74	21
Blank	2.82	21
Snow	7.00	59

The new Anodisc filter and pieces of the PP ring were analyzed to determine possible cross-contamination of our samples with PP. Samples were analyzed in the full scan mode ( $m/z$  45-600). As we can see from the obtained Total ion chromatogram, the peak profiles of blank, snow samples and PP ring look similar (Figure 14).

**Figure 14: Total ion chromatogram (TIC) of analyzed snow samples.**

The blank contains many peaks, found also in PP, indication a contamination of the whole Anodisc filter, which could result from the process of fabrication. Even if some new peaks appear in the snow sample (e.g., around 9.2 or 10.3 min), the contamination is too high to make possible a reliable identification of the species present in the snow sample. The best will be to use inorganic based filter membrane to avoid any contamination by organic compounds, and to develop a MS-based targeted approach by working in the Selected Reaction Monitoring (SRM) mode, for increasing selectivity and thus sensitivity.

## NP analysis

Nanoparticle tracking analysis was performed to measure the size distribution of NP presented in the snow samples from the Puy-de-Dôme site (Figure 15).

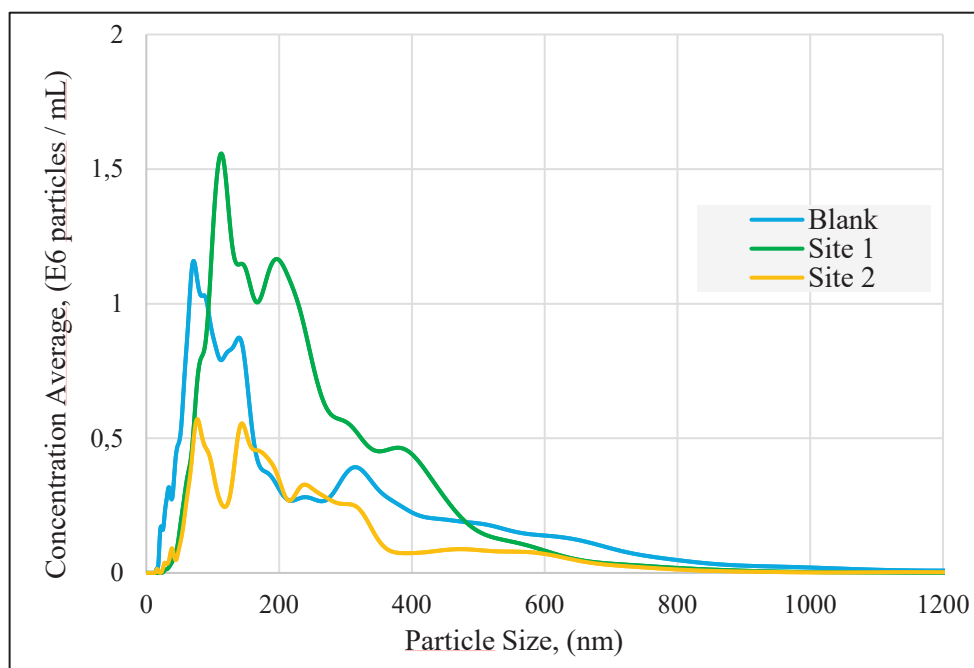


Figure 15: NTA analysis of NP size distribution at snow samples from PDD site.

The analysis confirmed the presence of nanoparticles for both samples and blank. All samples were characterized by high polydispersity with particle size distribution ranging from 50 to 400 nm. Py-GC-MS analysis was used to identify the chemical nature of these nanoparticles, in the full scan mode. However, we were unable to detect any characteristic polymers decomposition products. We also have not observed significant differences between the blank and the snow samples. Two conclusions can be drawn: 1) we have no nanosize polymers in the snow samples; 2) the concentration is below the detection limit. To improve our sensitivity, we decided to:

- 1) Analyze higher volumes of samples;
- 2) In order to improve the limit of detection we will perform tandem mass spectrometry MS/MS doing selected-reaction monitoring (SRM).

## IV.5.2. Protocol 2 (2020)

### IV.5.2.a. Sample preparation

The second version of our protocol is based on 4 sequential filtration steps (Figure 16). The cascade filtration allows to separate the SMPs into two groups: the particles larger than 50  $\mu\text{m}$  and particles ranging from 1 to 50  $\mu\text{m}$ . This separation is achieved by cascade filtration through a metal mesh (pore size 50  $\mu\text{m}$ ) and a nylon Nitex mesh (1  $\mu\text{m}$ ). The particles collected by these two types of filters are transferred on GF/F filters which are analysed by optical microscopy and Py-GC-MS/MS. Particles transfer on the GF/F filter was achieved in two steps. First, to detach particles from metal or nylon mesh, the filtration unit was turned upside down and rinsed with Milli-Q water, the flow of water thus collecting the particles. After that, the suspension obtained was filtered through the GF/F filter.

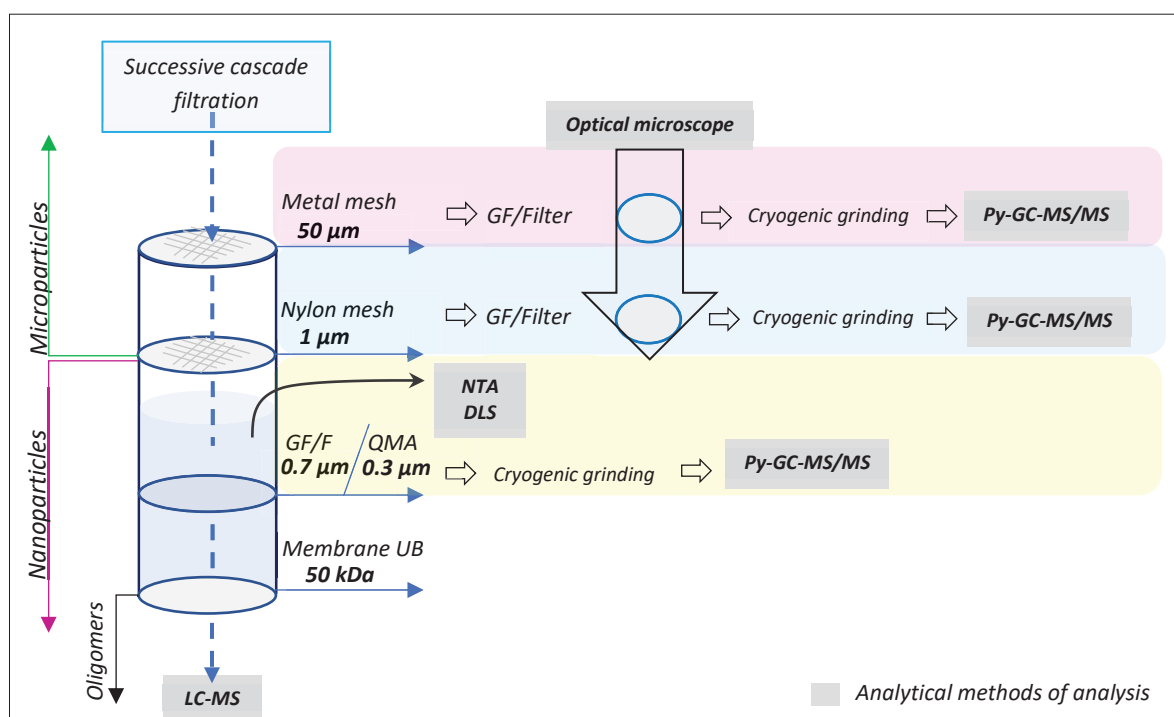


**Figure 16: Protocol 2 (2020): Scheme of preparation and analysis of aqueous samples.**

After filtration on 1  $\mu\text{m}$ , the filtrate was analyzed by DLS and NTA, in order to detect the presence of sub-micrometric particles and to determine the size distribution of presented particles in the samples.

Finally, the last step of filtration is directed at collecting the sub-micrometric particles on glass fiber filters (GF/F, 0.7  $\mu\text{m}$ ) or quartz fiber filters (QMA, 0.3  $\mu\text{m}$ ). A quantitative study on model latex polystyrene nanospheres reveals that the particle retention on these filters does not actually correspond to the pore size specified by the manufacturer (Figure 17).

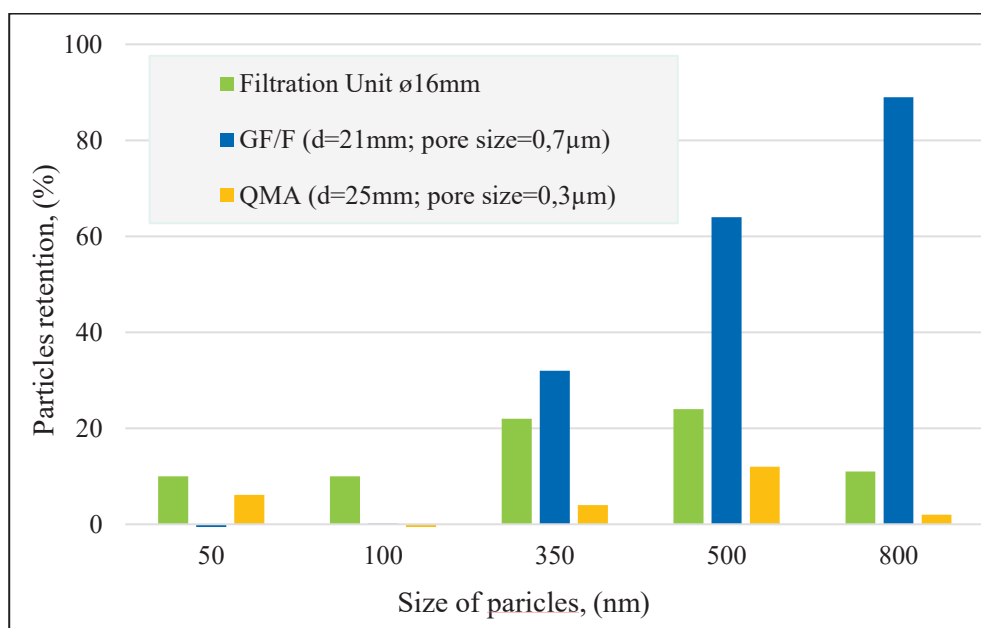


**Figure 17: Percentage of particle retention by: green→filtration unit; blue→GF/F filter (d=21mm; pore size=0.7 µm), and yellow→QMA filter (d=25mm; pore size=0.3 µm).**

Even though the specified pore size of GF/F filter is 0.7 µm, it is able to capture particles much smaller than the mentioned size (down to 0.1 µm). While the QMA filter with a pore size of 0.3 µm shows a very low retention capacity for 0.8 µm particles. The filtering device used can also affect future results by trapping particles and limiting the reliability of quantitative analysis.

Thus, it is important to quantify the retention capacity of the used type of filter prior samples preparation, as this might affect the results interpretation in future. For example, based only on the characteristics of the filter purchased by the manufacturer we may refer all detected plastic particles for a specific size range, missing smaller particles than the filter cut-off.

The filters with the collected NPs will be homogenized and analyzed by Py-GC-MS/MS. Remaining filtrate after successive cascade filtration through ultrafiltration membrane UB (50 kDa) will be analyzed by LC-MS for the presence of oligomers at the ICCF.

#### ***IV.5.2.b. Sample analysis***

As mentioned above, the detection of plastic and its quantitative and qualitative analysis are performed using Py-GC-MS/MS. To improve our sensitivity and increase the limit of detection (LOD), we improved our method by implementing Selected ion monitoring (SIM) and SRM approaches. Target analysis limits the pre-treatment of the sample from organic matter.



### IV.5.2.c. Preliminary results

#### Snow samples (Puy-de-Dôme), Protocole 2

Using Protocol 1 for sample preparation and analysis, we were probably below the limit of detection (LOD) of our analytical method by Py-GC-MS. To solve this, we increased the volume of the sample by pooling 5 snow samples with a total volume of 6 756 mL (4 times higher as compared to Protocol 1). SMPs with a size above 50  $\mu\text{m}$  were collected using metal mesh and were transferred on QMA ( $\text{Ø} = 12 \text{ mm}$ ; pore size 0.3  $\mu\text{m}$ ) calcinated filter.

Particles less than 50  $\mu\text{m}$  were filtrated directly through QMA filters. It was observed that most of the particles in sample have size from 1 to 50  $\mu\text{m}$  (Figure 18).

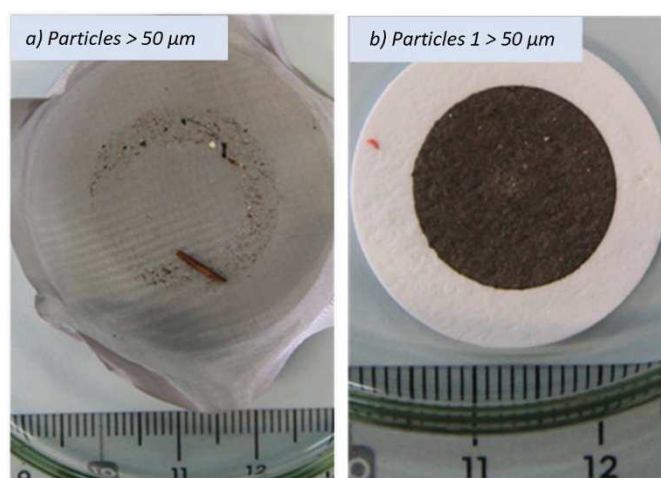


**Figure 18:** Extraction of SMPs from snow samples: a) Particles with size above 50 $\mu\text{m}$ ; b) Particles with size between 1 and 50  $\mu\text{m}$ .

Small amount of filters (representing around 5% of the total surface area) with both particle fractions above and below 50  $\mu\text{m}$  were analyzed by Py-GC-MS/MS working with both SIM and SRM approaches (Table 9).

**Table 9:** Selected characteristic decomposition products of polymers for sample analysis, along with the MS transitions (SRM) or ions (SIM) under focus

Polymer type	Characteristic decomposition product	RT, (min)	SRM		SIM	
			Quantification transition, ( $T_q$ )	Confirmation transition, ( $T_c$ )	Quantification Ion, ( $I_q$ )	Confirmation Ion, ( $I_c$ )
PS	2,4-Diphenyl-1-butene (Styrene dimer)	17.70	91 $\rightarrow$ 65	130 $\rightarrow$ 115		
	2,4,6-Triphenyl-1-hexene (Styrene trimer)	24.50	117 $\rightarrow$ 91	91 $\rightarrow$ 65		
PP	2,4 Dimethyl-hept-1-ene	5.22	70 $\rightarrow$ 55	126 $\rightarrow$ 83		
PET	Dimethyl tetraphenylphthalate	15.2			163	135 and 179

Preliminary results are presented as the intensity of decomposition product peaks. Two decomposition product characteristics for PS were detected in the snow samples: styrene dimer and styrene trimer, for each both quantification and confirmation transition were analyzed.

Figure 19 represents the results obtained for styrene dimer, in the SRM mode, where the two transitions under focus were  $m/z$  91 $\rightarrow$ 65 and  $m/z$  130 $\rightarrow$ 115. First, empty pyrolysis tube without sample was analyzed as a Blank of Py-GC-MS/MS system. No trace of styrene dimer was detected. A similar result was obtained for the Blank of QMA filter (Figure 19b). Styrene dimer was detected in the processing blanks, which were prepared by the same protocol than snow sample and called as “Processing blank > 50 $\mu$ m” (Figure 19c) and “Processing blank 1 < 50 $\mu$ m” (Figure 19d).

This may indicate a possible contamination during sample preparation and requires additional analysis. Snow sample with particles less than 50  $\mu$ m shows a peak intensity twice higher than the corresponding processing blank. This indicates the presence of PS in these samples. The intensity of the styrene dimer signal is much higher in the sample containing the particles between 1 and 50  $\mu$ m (Figure 19f) as compared to the particles above 50  $\mu$ m (Figure 19e).

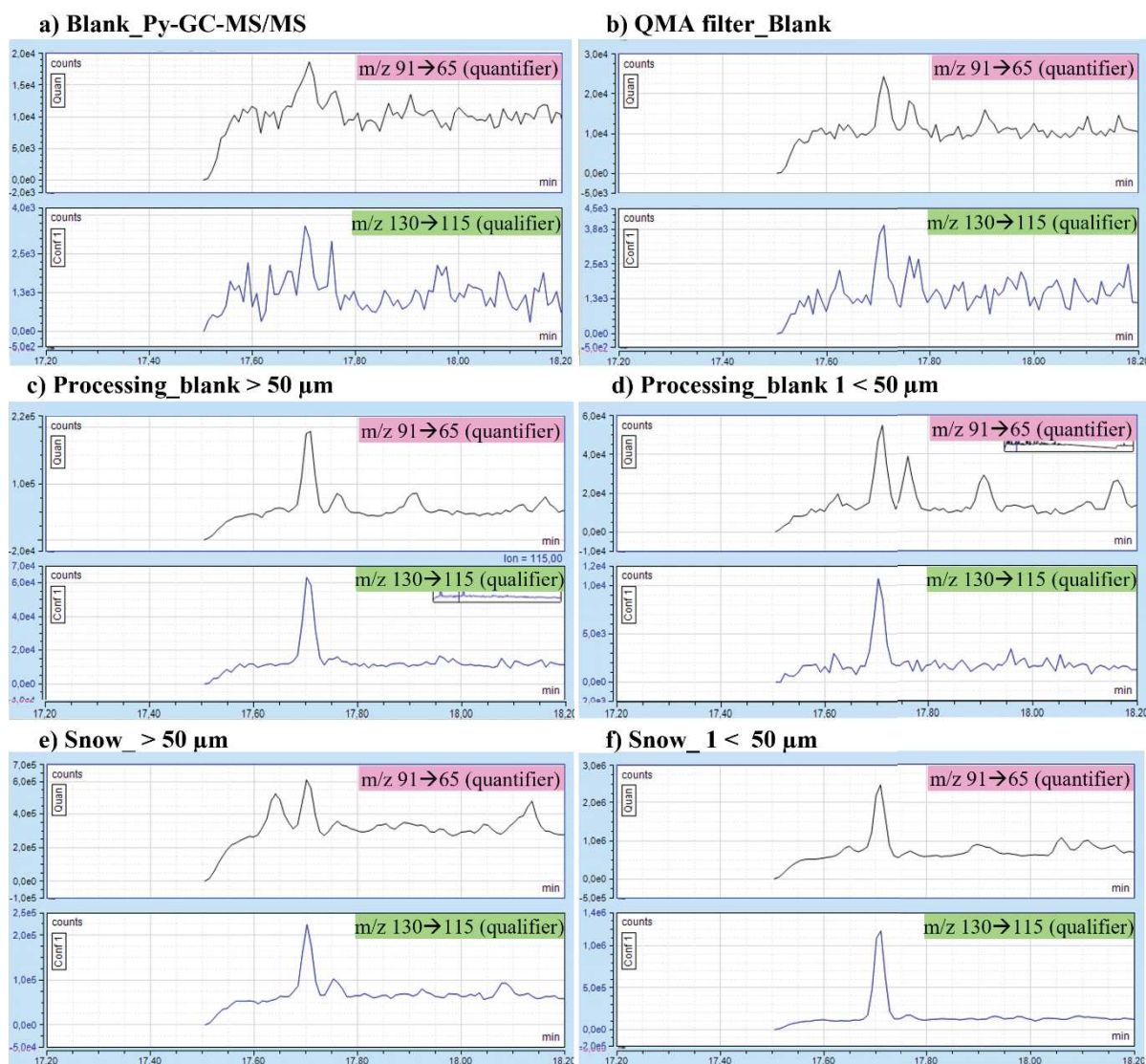


Figure 19: SRM trace chromatograms obtained for styrene dimer; transitions under focus are  $m/z\ 91 \rightarrow 65$  and  $m/z\ 130 \rightarrow 115$ .

Similar results were observed for the styrene trimer (Figure 20). Sample with particles above and less 50  $\mu\text{m}$  were characterized respectively by a peak intensity of one and two orders of magnitude higher than the corresponding processing blanks. These results are based on one single injection and require additional tests to investigate the source of contamination in the sample and have more reliable data. In addition, the Py-GC-MS/MS method used for the analysis was in development and required more optimization.

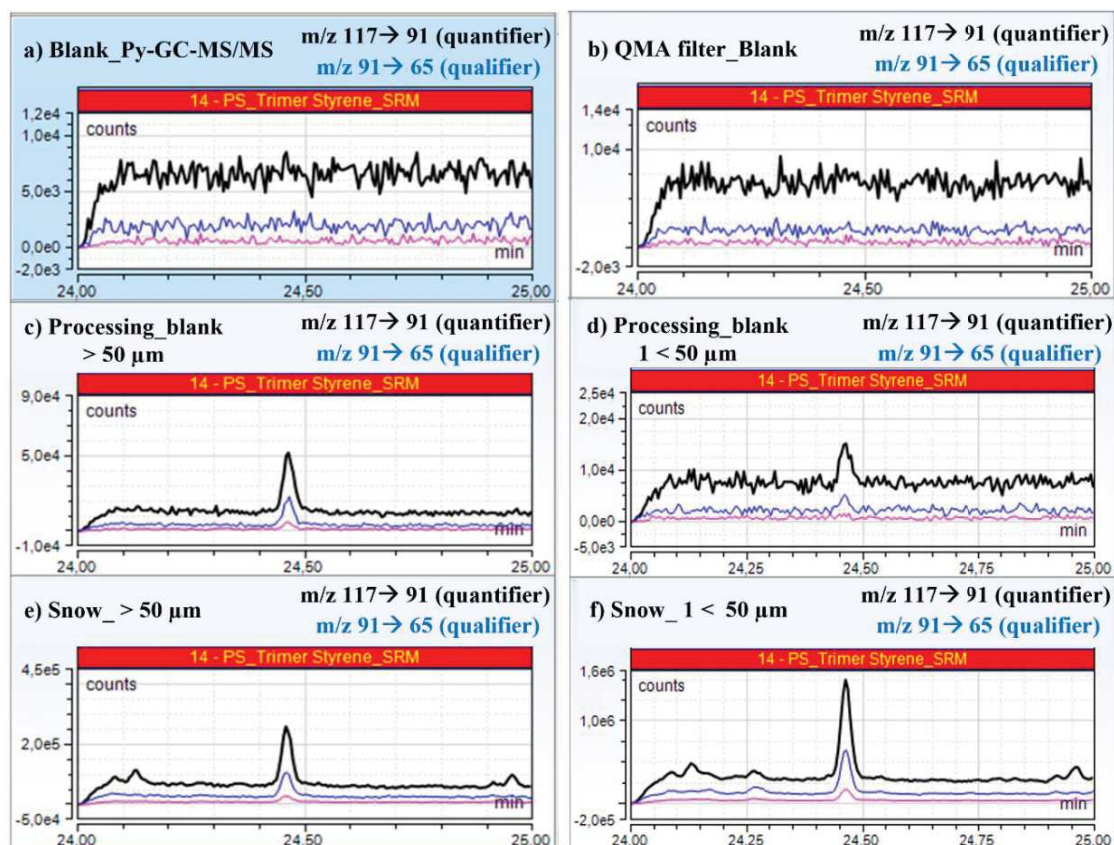
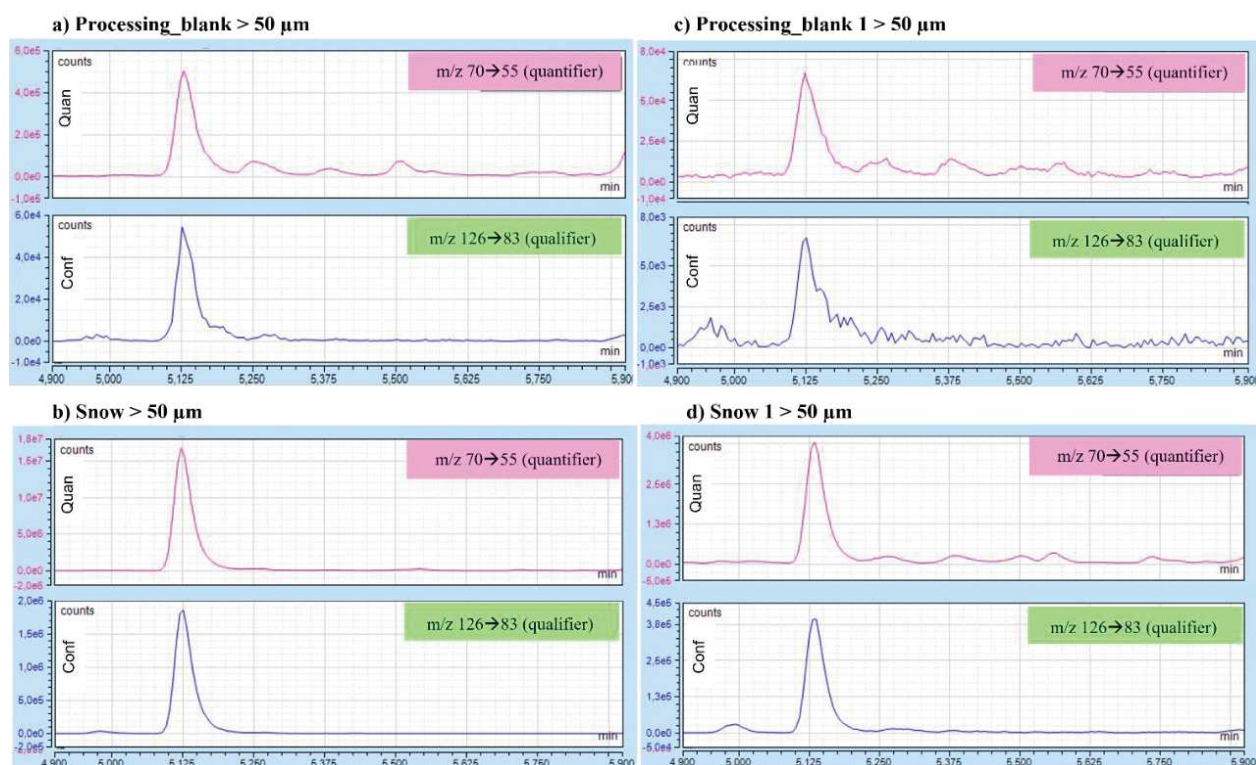


Figure 20: SRM trace chromatograms obtained for styrene trimer; transitions under focus are m/z 117 → 91 and m/z 91 → 65.

The same tendency was observed for the PP decomposition product (2,4 Dimethyl-hept-1-ene). A small contamination was observed for the processing blanks. But the peak intensity of the sample was two orders of magnitude higher than processing blank. For PP, signal is more intense in the sample containing the particle above 50 μm as compared to the particles from 1 to 50 μm (Figure 21).



**Figure 21: SRM trace chromatograms obtained for 2,4 dimethyl-hept-1-ene; transitions under focus are  $m/z$  70→55 and  $m/z$  126→83.**

PET was detected by reactive pyrolysis using tetramethylammonium hydroxide (TMAH) as the derivatization agent (Dimitrov *et al.*, 2013; Fischer and Scholz-Böttcher, 2017; He *et al.*, 2020). In presence of TMAH, terephthalate derivatives of PET are converted into dimethyl terephthalate. Detection of the latter can be achieved with a way higher sensitivity than the PET decomposition products observed in absence of TMAH. Dimethyl terephthalate presence in the snow samples was confirmed by SRM of quantification ion 163 and two confirmation ion: 135 and 179 (Figure 22). No comparison is presented with processing blanks, as blank were analyzed without TMAH. Thus, these results should be confirmed by additional analysis of the representative processing blanks and rest of the sample.

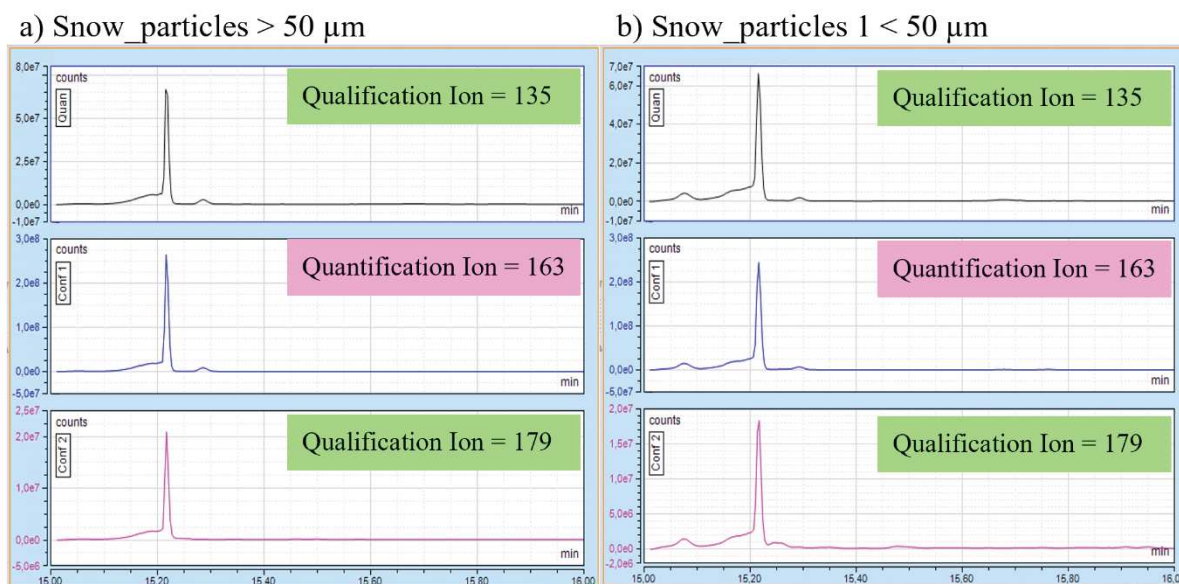


Figure 22: Selected ion monitoring of the PET decomposition product, quantification ion 163 and qualification ions 135 and 179.

Obtained results are promising, as we were able to detect 3 types of polymers in the two range of particles size above and below 50 $\mu\text{m}$ . However, to valorize these results it is important to analyze bigger area of the filter to provide some reliable data and investigate better the possible sources of samples contamination.

These preliminary results will be supplemented by the complete analysis of all extracted particles from snow samples. Obtained data will be analyzed by the area integration of all peaks detected. Finally, quantitative analysis will be performed to determine the concentration of detected plastics type.

## **Conclusions and perspectives**

During 2019, the main tasks and vectors of work were identified. A sampling methodology was developed, and several research tools were developed like the LF and HF aerosol collection systems for investigating the presence of micro- and nanoplastics in the outdoor atmosphere. Samples of aerosols, precipitation and fresh snow were collected at remote mountain sites and over the Mediterranean Sea, and aerosol samples were taken from a highly contaminated environment for being used as references. The first series of analyses led on fresh snow samples gave encouraging preliminary results about the detection and quantification of plastic particles in remote atmospheric samples. These also provided hints for future improvements regarding the analysis of the samples that have been collected and archived.

During the first months of 2020 we proceeded to a second field campaign in the Auvergne region. We also implemented the sample preparation and analysis protocol. This allowed us to increase the limit of detection and selectivity of our analytical method. We have detected three types of plastic in the snow samples: PS, PP, and PET. The fraction 1-50  $\mu\text{m}$  contains more atmospheric particles than the fraction above 50  $\mu\text{m}$ . The signal of PS and PP is also more intense for the fraction 1-50  $\mu\text{m}$ .

The following work on this study will be completed by other members of the project. Collected atmospheric samples will be prepared in accordance with the developed sample preparation protocol. Detection of plastic and its quantitative and qualitative analysis will be performed by Py-GC-MS/MS. This is the first study that focuses on the study of micro- and nanoplastic as two separate fractions of plastic present in the atmosphere.

## References

- Abbasi, S. *et al.* (2019) ‘Distribution and potential health impacts of microplastics and microrubbers in air and street dusts from Asaluyeh County, Iran’, *Environmental pollution*, 244, pp. 153–164. doi:10.1016/j.envpol.2018.10.039.
- Allen, S. *et al.* (2019) ‘Atmospheric transport and deposition of microplastics in a remote mountain catchment’, *Nature Geoscience*, 12(5), pp. 339–344. doi:10.1038/s41561-019-0335-5.
- Bergmann, M. *et al.* (2019) ‘White and wonderful? Microplastics prevail in snow from the Alps to the Arctic’, *Science advances*, 5(8), p. eaax1157. doi:10.1126/sciadv.aax1157.
- Cai, L. *et al.* (2017) ‘Characteristic of microplastics in the atmospheric fallout from Dongguan city, China: preliminary research and first evidence’, *Environmental Science and Pollution Research*, 24(32), pp. 24928–24935. doi:10.1007/s11356-017-0116-x.
- Dimitrov, N. *et al.* (2013) ‘Analysis of recycled PET bottles products by pyrolysis-gas chromatography’, *Polymer Degradation and Stability*, 98(5), pp. 972–979. doi:10.1016/j.polymdegradstab.2013.02.013.
- Dris, R. *et al.* (2016) ‘Synthetic fibers in atmospheric fallout: A source of microplastics in the environment?’, *Marine Pollution Bulletin*, 104(1), pp. 290–293. doi:10.1016/j.marpolbul.2016.01.006.
- Eyheraguibel, B. *et al.* (2017) ‘Characterization of oxidized oligomers from polyethylene films by mass spectrometry and NMR spectroscopy before and after biodegradation by a *Rhodococcus rhodochrous* strain’, *Chemosphere*, 184, pp. 366–374. doi:10.1016/j.chemosphere.2017.05.137.
- Fischer, M. and Scholz-Böttcher, B.M. (2017) ‘Simultaneous Trace Identification and Quantification of Common Types of Microplastics in Environmental Samples by Pyrolysis-Gas Chromatography–Mass Spectrometry’, *Environmental Science & Technology*, 51(9), pp. 5052–5060. doi:10.1021/acs.est.6b06362.
- Gasperi, J. *et al.* (2018) ‘Microplastics in air: Are we breathing it in?’, *Current Opinion in Environmental Science & Health*, Volume 1, February 2018, pp. 1–5. doi:10.1016/j.coesh.2017.10.002.
- Gigault, J. *et al.* (2018) ‘Current opinion: What is a nanoplastic?’, *Environmental Pollution*, 235, pp. 1030–1034. doi:10.1016/j.envpol.2018.01.024.
- González-Pleiter, M. *et al.* (2021) ‘Occurrence and transport of microplastics sampled within and above the planetary boundary layer’, *Science of The Total Environment*, 761, p. 143213. doi:10.1016/j.scitotenv.2020.143213.
- He, Y. *et al.* (2020) ‘The search for organic compounds with TMAH thermochemolysis: From Earth analyses to space exploration experiments’, *TrAC Trends in Analytical Chemistry*, 127, p. 115896. doi:10.1016/j.trac.2020.115896.



Huang, Y. *et al.* (2020) ‘Mini-review on current studies of airborne microplastics: Analytical methods, occurrence, sources, fate and potential risk to human beings’, *TrAC Trends in Analytical Chemistry*, 125, p. 115821. doi:10.1016/j.trac.2020.115821.

Klein, M. and Fischer, E.K. (2019) ‘Microplastic abundance in atmospheric deposition within the Metropolitan area of Hamburg, Germany’, *Science of The Total Environment*, 685, pp. 96–103. doi:10.1016/j.scitotenv.2019.05.405.

Liu, K. *et al.* (2019) ‘Accurate quantification and transport estimation of suspended atmospheric microplastics in megacities: Implications for human health’, *Environment International*, 132, p. 105127. doi:10.1016/j.envint.2019.105127.

Materić, D. *et al.* (2020) ‘Micro- and Nanoplastics in Alpine Snow: A New Method for Chemical Identification and (Semi)Quantification in the Nanogram Range’, *Environmental Science & Technology*, 54(4), pp. 2353–2359. doi:10.1021/acs.est.9b07540.

Santl-Temkiv, T. *et al.* (2017) ‘High-flow-rate impinger for the study of concentration, viability, metabolic activity, and ice-nucleation activity of airborne bacteria’, *Environmental science & technology*, 51(19), pp. 11224–11234. doi:10.1021/acs.est.7b01480.

Trainic, M. *et al.* (2020) ‘Airborne microplastic particles detected in the remote marine atmosphere’, *Communications Earth & Environment*, 1(1), pp. 1–9. doi:10.1038/s43247-020-00061-y.

Wang, X. *et al.* (2020) ‘Atmospheric microplastic over the South China Sea and East Indian Ocean: abundance, distribution and source’, *Journal of Hazardous Materials*, 389, p. 121846. doi:10.1016/j.jhazmat.2019.121846.

Yakovenko, N., Carvalho, A. and ter Halle, A. (2020) ‘Emerging use thermo-analytical method coupled with mass spectrometry for the quantification of micro(nano)plastics in environmental samples’, *TrAC Trends in Analytical Chemistry*, 131, p. 115979. doi:10.1016/j.trac.2020.115979.

Zhang, Y. *et al.* (2020) ‘Atmospheric microplastics: A review on current status and perspectives’, *Earth-Science Reviews*, 203, p. 103118. doi:10.1016/j.earscirev.2020.103118.

# General Conclusion



Depuis plusieurs années, la pollution plastique et son impact sur l'environnement connaissent l'intérêt croissant d'une part de la communauté scientifique. Leurs rejets, leur devenir dans l'environnement, leur dégradation et leur interaction avec des organismes vivants font ainsi l'objet d'études scientifiques qui visent à accroître la connaissance générale sur ce type particulier de pollution. On entend beaucoup parler du 7<sup>e</sup> continent, ce « monstre de plastique » qui a pris ses quartiers et s'étend en plein cœur du Pacifique, sur une surface équivalente à trois fois celle de la France. Outre les déchets plastiques de grande taille qu'on y trouve, une partie non négligeable de ce matériel flottant est constitué de micro- et nanoparticules de plastique, qui proviennent en particulier de la dégradation de matériaux plus gros. De quoi sont constituées ces particules de plastique ? Comment interagissent-elles avec leur environnement immédiat, avec les organismes vivants ? Comment leur structure chimique évolue-t-elle au cours du temps ? Il est encore bien difficile de répondre à toutes ces questions, tant la variabilité de telles microparticules est grande, aussi bien en ce qui concerne leurs caractéristiques (taille, forme, type de polymère, rugosité, ...) que l'état de leur surface, qui dépend à la fois du processus ayant conduit à leur génération et de leur durée de résidence dans l'environnement. Tous ces paramètres ne peuvent être pris en compte simultanément. Il est nécessaire, pour mener à bien des études scientifiques visant à accroître les connaissances dans ce domaine, de construire des modèles pertinents qui répondent à certaines des questions posées. En particulier, le développement de modèles particuliers de plastique, facilement traçables et suffisamment représentatifs des particules présentes dans l'environnement, est un enjeu important car il permettrait de mieux comprendre le devenir des particules de plastique dans l'environnement et leur interaction avec les organismes vivants.

Dans ce contexte, le travail réalisé visait à développer un modèle, environnementalement pertinent, de micro- et de nanoparticules de plastique qui soient facilement détectables et traçables par des techniques analytiques non destructrices. Le polymère choisi a été le polyéthylène haute densité (HDPE), l'un des matériaux les plus présents dans les plastiques du quotidien. Nous y avons incorporé des nanoparticules upconverting (UCNPs) à base d'ions lanthanides de manière à pouvoir détecter les micro- et nanoplastiques par des techniques de fluorescence, non-destructrices et habituellement très sensibles. Nous avons développé une approche top-down de production de ces particules, c'est-à-dire en les générant de façon mécanique à partir d'un pool macroscopique de matière brute, comme cela se produit dans l'environnement. Le résultat est l'obtention de particules polydisperses, de surfaces rugueuses, et ayant une grande diversité de formes, telles que celles

que l'on trouve dans l'environnement. La caractérisation physico-chimique de ces particules a été réalisée au moyen de nombreuses techniques analytiques. Nous avons pu montrer que les particules upconverting, incorporées dans la matrice polymérique (6% en masse), permettait la détection efficace des particules de plastique sous irradiation infrarouge (excitation à 980 nm).

Le modèle ainsi développé et caractérisé a été utilisé pour étudier son interaction avec des organismes vivants. Nous avons choisi de travailler avec un modèle de microalgues de *C. vulgaris*, car elles sont des organismes-clés dans un large éventail de fonctions de l'écosystème, sont ubiquitaires, sensibles aux perturbations environnementales et sont facilement cultivables en laboratoire. Les résultats obtenus par microscopie à force atomique et à force fluïdique ont montré qu'il existait bel et bien une interaction entre les microparticules de plastique et les microalgues. Nous avons mis en évidence qu'une interaction hydrophobe entre les algues et les microplastiques était à l'origine de la production de matière organique par les algues, et que cette dernière jouait un rôle important dans les phénomènes d'agrégation des microalgues et des microplastiques.

Ces hétéroagrégats de microplastiques et de microalgues constituent une nourriture facile pour les organismes aquatiques, des herbivores aux prédateurs supérieurs, ce qui suscite des inquiétudes quant à la bioaccumulation du plastique et à la bioamplification pour l'ensemble de la chaîne trophique. Le modèle de micro et nanoplastiques marqués que nous avons développé permet d'envisager une suite axée sur des études écotoxicologiques. Il s'agirait notamment d'étudier l'absorption de ces hétéroagrégats par des organismes vivants et leur transfert, leur translocation et leur accumulation dans les tissus des organismes vivants. On pourrait pour cela marquer les particules plastiques avec d'autres types d'UCNPs. En fonction de la nature de l'émetteur choisi lors du design des UCNPs, ce type de sonde peut montrer des émissions bleues, rouges, et infrarouges (émetteur Tm) ou encore vertes et rouges (émetteur Er) en utilisant la même longueur d'onde d'excitation (980nm). Il serait ainsi possible de suivre simultanément deux cibles par la détection de 2 longueurs d'onde d'émission de fluorescence.

La première idée serait d'exposer simultanément un modèle d'organisme vivant à des micro- et nanoparticules marquées chacune avec des étiquettes différentes. Cela permettrait de suivre spécifiquement leur absorption, leur transport et leur translocation dans les tissus d'un organisme vivant, simultanément, dans les mêmes conditions et dans le même organisme. Il serait ainsi possible de mettre en lumière les différences existantes entre les MPs et les NPs quant à leurs interactions avec des organismes vivants. Il serait également envisageable

d'étudier certaines étapes du transfert des particules plastiques le long de la chaîne trophique, en travaillant simultanément avec des organismes vivants proies et prédateurs.

La méthodologie que nous avons développée pour le marquage et la synthèse top-down des micro- et nanoparticules de PE pourrait être appliquée à d'autres types de polymères (PVC, PS, PP, ...). Un panel de modèles particuliers serait alors disponible et permettrait de mener des études visant à mieux comprendre le comportement dans l'environnement et les interactions spécifiques de chacun de ces polymères avec des organismes vivants. Dans le cadre des collectes en milieu atmosphérique, auxquelles nous nous sommes également intéressés dans ce travail, de tels modèles pourraient également être utilisés pour aider à la recherche de méthodes de collecte et d'analyses standardisées, qui font défaut actuellement, ou à l'étude des transports à longue distance. C'est une perspective à bien plus long terme... et une nouvelle histoire à imaginer !







## Abstract

The management and monitoring of plastic waste have become a major issue for our society. However, there is no single optimal method for the effective study and monitoring of plastic pollution. The objective of this thesis work was to explore new approaches to study the occurrences, fate, and behavior of micro- and nanoplastics in the environment. Three vectors of investigation were combined in this work, including: i) the development of a methodology of sampling and analysis of MPs and NPs from the atmosphere; ii) the development of an environmentally relevant model of MPs and NPs, which could be used for ecotoxicological studies and iii) the study of its interaction with living microorganisms.

Environmentally relevant models of micro- and nanoplastics of HDPE were obtained by top-down approach, by exposing bulk polymer material to mechanical grinding. Particles were labelled with background-free persistent luminescent probes such as UCNPs that allows their detection even in thick samples such as in a tissue or a small animal.

Further, we used a developed model of plastic to study the interaction mechanism between MPs and green freshwater microalgae *Chlorella vulgaris* using atomic force microscopy (AFM) nano- and molecular scale experiments. This work revealed that a hydrophobic interaction between algae and microplastics was at the origin of the production of organic matter by algae, and that the latter played an important role in the aggregation phenomena of microalgae and microplastics.

Otherwise, MPs and NPs from the atmosphere were collected on areas with different levels of human activity: from an area separated from human activities to a highly industrialized. Investigation of those areas included the collection of meteorological data and sampling of atmospheric samples including aerosols (suspended particles in the atmosphere) and deposition (rain, snow, sleet, etc.). As a result, we proposed a methodology for samples collection, preparation, qualitative and quantitative analysis performed by the combination of analytical methods including  $\mu$ -FTIR (Fourier transform-infrared microscopy), Py-GC-MS (pyrolysis coupled with gas chromatography and mass spectrometry), DLS (Dynamic Light Scattering), NTA (Nanoparticle Tracking Analysis), etc.

## Résumé

Le suivi et la gestion des déchets plastiques sont devenus un enjeu important pour nos sociétés. Cependant, il n'existe pas de méthode optimale unique pour l'étude et la surveillance efficaces de la contamination plastique. L'objectif de ce projet était d'explorer de nouvelles approches pour étudier l'origine, le devenir et le comportement de la matière plastique présente dans l'environnement. Trois axes d'investigation ont été combinés dans ce travail : i) le développement d'une méthodologie de collecte, d'échantillonnage et d'analyse de micro (MPs) et nanoparticules (NPs) de plastique provenant de l'atmosphère ; ii) le développement d'un modèle de MPs et de NPs pertinent pour l'environnement, qui pourrait être utilisé pour des études écotoxicologiques et iii) l'étude de son interaction avec les micro-organismes vivants.

Un modèle pertinent de micro- et nanoplastiques de HDPE a ainsi été obtenu par une approche top-down, en exposant du matériau polymère brut à un broyage mécanique. Les particules ont été marquées avec des sondes luminescentes constituées de particules upconverting, qui permettent leur détection même dans des échantillons épais, comme dans un tissu ou un petit animal.

Ce modèle de plastique a été ensuite utilisé pour étudier le mécanisme d'interaction entre les MPs et la microalgue verte d'eau douce *Chlorella vulgaris* en utilisant des expériences à l'échelle nanométrique et moléculaire par microscopie à force atomique (AFM). Ces travaux ont révélé qu'une interaction hydrophobe entre les algues et les microplastiques était à l'origine de la production de matière organique par les algues, et que cette dernière jouait un rôle important dans les phénomènes d'agrégation des microalgues et des microplastiques.

Par ailleurs, des MPs et NPs de l'atmosphère ont été collectées sur des zones présentant différents niveaux d'activité humaine : d'une zone éloignée des activités humaines à une zone fortement industrialisée. L'étude de ces zones comprenait la collecte de données météorologiques et l'échantillonnage d'échantillons atmosphériques, y compris les aérosols (particules en suspension dans l'atmosphère) et les dépôts (pluie, neige, grésil, etc.). À la suite de ce travail, nous avons proposé une méthodologie de collecte d'échantillons, de préparation, d'analyse qualitative et quantitative effectuée par la combinaison de méthodes analytiques, notamment la  $\mu$ -FTIR (microscopie infrarouge à transformée de Fourier), la Py-GC-MS (pyrolyse couplée à la chromatographie en phase gazeuse et à la spectrométrie de masse), la DLS (diffusion dynamique de la lumière) ou encore la NTA (analyse de suivi des nanoparticules), etc...